Mono- and bimetallic nanoparticles for the metallization of microvias using an innovative process in ionic liquids

Philippe Arquillière

N° d'ordre 196 Année 2012

THESE DE L'UNIVERSITE DE LYON

Délivrée par

L'UNIVERSITE CLAUDE BERNARD LYON 1

ECOLE DOCTORALE DE CHIMIE, SPECIALITE CHIMIE

DIPLOME DE DOCTORAT

(arrêté du 7 août 2006)

soutenue publiquement le 24 Octobre 2012

par

M. ARQUILLIERE Philippe

NANOPARTICULES MONO- ET BIMETALLIQUES POUR LA METALLISATION DE MICROVIAS PAR UN PROCEDE INNOVANT UTILISANT LES LIQUIDES IONIQUES

Directeur de thèse : Catherine SANTINI

Co-encadrant : Paul-Henri HAUMESSER

JURY :

Mr Yves Chauvin

Mr Agílio PADUA

Mr Stéphane DANIELE

Mr Emmanuel COTTANCIN

RAPPORTEURS :

Mme Carmen CLAVER

Mme Suzanne GIORGIO

UNIVERSITE CLAUDE BERNARD - LYON 1

Président de l'Université	**M. François-Noël GILLY**
Vice-président du Conseil d'Administration	M. le Professeur Hamda BEN HADID
Vice-président du Conseil des Etudes et de	M. le Professeur Philippe LALLE
Vice-président du Conseil Scientifique	M. le Professeur Germain GILLET
Secrétaire Général	M. Alain HELLEU

COMPOSANTES SANTE

Faculté de Médecine Lyon Est – Claude Bernard	Directeur : M. le Professeur J. ETIENNE
Faculté de Médecine et de Maïeutique Lyon Sud – Charles Mérieux UFR d'Odontologie	Administrateur provisoire : M. le Professeur G. KIRKORIAN
Institut des Sciences Pharmaceutiques et Biologiques	Directeur : M. le Professeur D. BOURGEOIS
Institut des Sciences et Techniques de la Réadaptation	Directeur : Mme la Professeure C. VINCIGUERRA.
Département de formation et Centre de Recherche en Biologie Humaine	Directeur : M. le Professeur Y. MATILLON
	Directeur : M. le Professeur P. FARGE

COMPOSANTES ET DEPARTEMENTS DE SCIENCES ET TECHNOLOGIE

Faculté des Sciences et Technologies	Directeur : M. le Professeur F. De MARCHI
Département Biologie	Directeur : M. le Professeur F. FLEURY
Département Chimie Biochimie	Directeur : Mme le Professeur H. PARROT
Département GEP	Directeur : M. N. SIAUVE
Département Informatique	Directeur : M. le Professeur S. AKKOUCHE
Département Mathématiques	Directeur : M. le Professeur A. GOLDMAN
Département Mécanique	Directeur : M. le Professeur H. BEN HADID
Département Physique	Directeur : Mme S. FLECK
Département Sciences de	Directeur : Mme la Professeure I. DANIEL
UFR Sciences et Techniques des Activités Physiques et Sportives	Directeur : M. C. COLLIGNON
Observatoire de Lyon	Directeur : M. B. GUIDERDONI
Polytech Lyon	Directeur : M. P. FOURNIER
Ecole Supérieure de Chimie Physique Electronique	Directeur : M. G. PIGNAULT
Institut Universitaire de Technologie de Lyon 1	Directeur : M. C. VITON
Institut Universitaire de Formation des Maîtres	Directeur : M. R. BERNARD
Institut de Science Financière et d'Assurances	Directeur : Mme la Professeure V. MAUME-DESCHAMPS

Les travaux exposés dans ce mémoire ont été réalisés entre novembre 2009 et octobre 2012 au laboratoire de Chimie, Catalyse, Polymérisation et Procédé dans l'équipe de Chimie Organométallique de Surface, unité mixte CNRS-CPE Lyon. Je remercie Monsieur Gérard Pignault, directeur de CPE Lyon, pour m'avoir accueilli dans ses locaux.

Ce travail étant codirigé avec le CEA de Grenoble, 6 mois ont été effectués dans cette institution et je remercie Sylvain Maitrejean de m'avoir accueilli à Minatec dans le laboratoire LDJ, département DTSi du LETI.

Que Madame Bernadette Charleux soit remerciée de m'avoir accueilli au sein de son laboratoire.

J'adresse mes plus vifs remerciements à Madame Catherine Santini ainsi qu'à Monsieur Paul-Henri Haumesser pour leurs encadrements, leurs aides et leurs soutiens qu'ils m'ont accordés pendant ces trois années de thèse.

Que Mesdames ; Carmen Claver, Professeur à l'Université Rovira I Virgili Tarragona, Suzanne Giorgio, Professeur à l'Université d'Aix Marseille, et Messieurs; Yves Chauvin, Prix Nobel de Chimie, Agílio Pádua, Professeur à l'Université Blaise Pascal Clermont-Ferrand, Stéphane Daniele, Professeur à l'Université Claude Bernard Lyon 1, Emmanuel Cottancin, Maître de conférences à l'Université Claude Bernard Lyon 1, soient vivement remerciés de l'honneur qu'ils m'ont fait en acceptant de juger ce mémoire.

Je remercie la Région Rhône-Alpes pour le financement de ce travail ainsi que des locaux où il a été effectué. Ce travail a permis d'établir de nombreuses collaborations. Je remercie particulièrement Jean-Luc Rousset et Laurence Massin pour leur expertise dans les analyses XPS, Mimoun Aouine pour les nombreuses analyses HRTEM et leurs interprétations, et Patrice Gergaud pour les futures analyses SAXS qui seront effectuées par mes successeurs. Je remercie en outre Karim Yckache, Jean Guerrero (RTP), Maryline Cordeau (AFM), Sylvie Favier (GIXRD), Dominique Lafond (HRTEM) Céline Ribière et Olivier Kim-Hak pour leur aide au CEA Grenoble. De même, je remercie Kai Szeto (DRIFT), Sebastien Norsic, Christine Lucas (RMN), Olivier Boyron (DSC), François Bayard (modélisation) ainsi que Bastien Doumèche (AFM, Profilométrie) pour leur aide à CPE Lyon.

Je souhaite également remercier tout les étudiants du groupe « Liquide Ionique » dirigée par Catherine Santini, Inga S. Hegadottir, Hassan Srour, Leila Moura, Paul S. Campbell, Gorka Salas, Léa Chancelier, Jérome Pradelok, Pablo Brea, Maria Fuentes, Wallid Darwich, Christopher Schikaneder, Cherif Larabi, Wallid Alkmasoud, Anthony Garron pour m'avoir aidés dans mon travail durant ces trois années. Je remercie mes collègues thésards C2P2/CEA pour leurs remarques et leur disponibilité, notamment Arthur Roussey, Laurent Mathey et Pierre Laurent qui finissent en même temps leur thèse.

Que le personnel du laboratoire LDJ au CEA et du laboratoire COMS trouvent dans ces quelques lignes l'expression de ma plus profonde gratitude. Je remercie également toute les personnes de l'open space G328 pour la bonne ambiance dans laquelle s'est déroulée ma thèse, ainsi que la rédaction de celle-ci.

Abbreviations and acronyms

Units

h: hour	min: minute	M: $mol.L^{-1}$	g: gram
°C: degree Celsius	rpm: round per min		

Techniques

TEM: transmission electron microscopy
SEM: scanning electron microscopy
EDX: electron dispersive X-Ray analysis
HRTEM: high resolution TEM
XPS: X-Ray photoelectron spectroscopy
GC: gas chromatography
MS: mass spectrometry
EELS: electron energy loss spectroscopy
NMR: nuclear magnetic resonance
DRIFT: diffuse reflectance infrared Fourier transform
RTP: rapid thermal process
XRR: X-Ray reflectometry
SAXS: small angle X-Ray scattering
GIXRD: grazing incidence X-Ray diffraction
XAES: X-Ray Auger electron spectroscopy

Chemicals

IL: ionic liquid
NP: nanoparticle
OM: organometallic precursor
Im: imidazolium
C_1: methyl, C_2: ethyl, C_4: butyl, C_6: hexyl, C_8: octyl
$C_1C_4Im^+$: 1-butyl-3-methylimidazolium cation
NTf_2^-: bis(trifluoromethanesulphonyl)imide anion

COD: cyclooctadiene, COT: cyclooctatriene, COA: cyclooctane, COE: cyclooctene
CHD: cyclohexadiene, CHE: cyclohexene, CHA: cyclohexane
Mes-H: mesitylene, Np: neopentyl, Np-H: neopentane

Ru(COD)(COT): (1,5-cyclooctadiene)(1,3,5-cyclooctatriene)ruthenium
$Ni(COD)_2$: bis(1,5-cyclooctadiene) nickel
Mes-Cu: mesitylcopper
$Pt(COD)Me_2$: (1,5-cyclooctadiene) dimethylplatinum
$Np_3Ta{=}CHCMe_3$: tris(neopentyl)(neopentylidene) tantalum
$MnNp_2$: bis(neopentyl)manganese
(η^5-$MeCpMn(CO)_3$): methylcyclopentadienyl manganese tricarbonyl
$(EtCp)_2Mn$: bis(ethylcyclopentadienyl) manganese

Résumé : Nanoparticules mono- et bimétalliques pour la métallisation de microvias par un procédé innovant utilisant les liquides ioniques

De nos jours, nous sommes entourés de dispositifs microélectroniques de plus en plus petits et performants. Pour poursuivre cette évolution, une nouvelle technologie est en cours de développement qui consiste à empiler plusieurs circuits intégrés. L'une des clefs pour aboutir à ce type d'architecture est la formation de microvias entre les différentes couches. Ce travail s'inscrit dans un à objectif à long terme qui vise à la mise au point d'un procédé innovant à coût réduit pour la métallisation de ces microvias, à partir de nanoparticules (NPs) métalliques de taille parfaitement calibrée. En particulier, des NPs bimétalliques de Mn et Cu pourraient être des précurseurs intéressants pour l'élaboration de barrières dites auto-formées et de couches d'accroches dans les microvias. Les liquides ioniques sont des milieux intéressants pour la synthèse de telles NPs, notamment à partir de précurseurs organométalliques. Il a été démontré que leur structure tridimensionnelle spécifique « guide » la croissance de NPs de Ru et les stabilise tout en les laissant libres de toute contamination de surface. Dans ce travail, ce concept a été enrichi par la synthèse de NPs d'autres métaux tels que Cu et Mn, et étendu à la formation de NPs constituées de deux métaux (M-M'NPs bimétalliques). De façon remarquable, les M-M'NPs obtenues ont toujours une taille inférieure aux MNPs et M'NPs prises séparément. Ces suspensions homogènes, très stables dans le temps, ont été directement déposées et frittées sur des substrats technologiques dans le but de former des films métalliques uniformes et adhérents.

Abstract: Mono- and bimetallic nanoparticles for the metallization of microvias using an innovative process in ionic liquids

Nowadays, microelectronic devices are omnipresent in our everyday life. To make them smaller and smaller as well as smarter and smarter, a new process which consists in stacking integrated circuits is being studied. In order to build this type of structures, the fabrication of microvias between layers is key. This work ultimately aims at developing an innovative process with reduced cost for the efficient metallization of these microvias. This can be achieved using perfectly calibrated metallic nanoparticles (NPs). In particular, bimetallic Mn-CuNPs could be interesting precursors to grow "self-formed" barriers and seed layers in microvias. Ionic liquids (ILs) are extremely well adapted media for the synthesis of such nano-objects, especially when organometallic precursors are used. It has been shown that their specific 3D structure provides a template to grow RuNPs of controlled size. The IL also acts as stabilizer, eliminating the need to use ligands that contaminate the metallic surface. In this work, this concept have been extended to the synthesis of other metallic NPs, such as Cu and Mn, as well as synthesis of NPs containing the two metals (bimetallic M-M'NPs). Remarkably, these M-M'NPs always exhibit a smaller size than the MNPs and M'NPs separately. These homogeneous and stable suspensions have been directly applied and sintered onto technological substrates in order to form uniform and adherent metallic layers.

Table of Contents

Introduction

Pursuing miniaturization of integrated circuits is a constant challenge in the microelectronics industry. Nowadays, multi-core processors are used in order to improve the performances. Several strategies are currently developed, among which the so-called 3D chip stacking is particularly promising. To achieve this architecture, Through Silicon Vias (TSVs) must be fabricated to interconnect adjacent levels. Usually, these structures are first drilled in the substrate then filled with metal. Copper is the best candidate as a conducting material for this application. However, its integration requires the deposition of thin metal liners, namely a barrier and a seed layer. Recently, the synthesis of these two layers in one step has been proposed through annealing of manganese-doped copper layers.

The aim of this thesis was to synthesize mono- and bimetallic nanoparticles in ionic liquid and use the resulting suspensions as precursor for the formation of barrier and seed layers. Manganese and copper were selected for this study: Copper is the metal of choice to form seed layers, and manganese is the best candidate to form barriers, without addition of further additives. Indeed, organometallic decomposition or reduction under H_2 allows formation of relatively small NPs with narrow size distribution without surface contaminants since by-products can be easily removed from solution under primary vacuum.

For this purpose, the synthesis of mono- and bimetallic nanoparticles through chemical route in ionic liquids has been optimized. Indeed, the specific physicochemical properties of ionic liquids such large liquidus range and high thermal stability simplify the process since synthesis and annealing of nanoparticles can be performed in the same medium.

In the first chapter, the current tendencies in microelectronic are presented, with focus on the so-called 3D chip stacking technology. Also, a brief survey of the literature concerning the synthesis of mono- and bimetallic nanoparticles in ionic liquids will be proposed.

The second chapter deals with the synthesis and characterization by high resolution transmission electron microscopy and X-Ray photoelectron microscopy of copper and manganese monometallic nanoparticles synthesized from hydrogenolysis of mesitylcopper (I) and bis(neopentyl) manganese (II) in 1-butyl-3-methylimidazolium bis(trifluoromethanesulfonyl) imide.

In the third chapter, the formation of bimetallic nanoparticles by simultaneous hydrogenolysis of two organometallic precursors is reported. Their characteristics (size distribution, structure, oxidation state of both metals, …) are studied. Several bimetallic couples based on copper are investigated.

In chapter fourth, the elaboration of films by annealing of nanoparticles in suspension in ionic liquids is described. The effect of different experimental conditions (temperature, concentration of nanoparticles, nature of wafer, gas atmosphere) is investigated in order to improve the quality of the resulting deposits. Contact angle measurements, *in-situ* diffuse reflectance infrared Fourier transform annealing, atomic force microscopy and rapid thermal process annealing experiments are performed for this purpose.

Finally, all experimental techniques used throughout this study are detailed in Chapter V.

Chapter I

Breakthrough in Microelectronic, Trough Silicon Vias as Key for 3D Architecture Development

Chapter I

Breakthrough in Microelectronic,

Trough Silicon Vias as Key for 3D Architecture Development

I. Introduction

Integrated circuits (ICs) are omnipresent in our everyday life (cell phones, cameras, computers, tablets, automotive …). They become smaller and smaller as well as smarter and smarter.

Fig. 1| Example of devices which contain microprocessors.

Miniaturization is the most challenging part of microelectronic. Nowadays, multi-core processors are used in order to improve the performance. The use of 3-D architecture allows reaching this goal and even going further than Moore's law.[1] Several strategies are currently developed to achieve this 3-D structure. One of the simplest ways consists in the superimposition of two or more microprocessors, connected with Through Silicon Vias (TSVs).

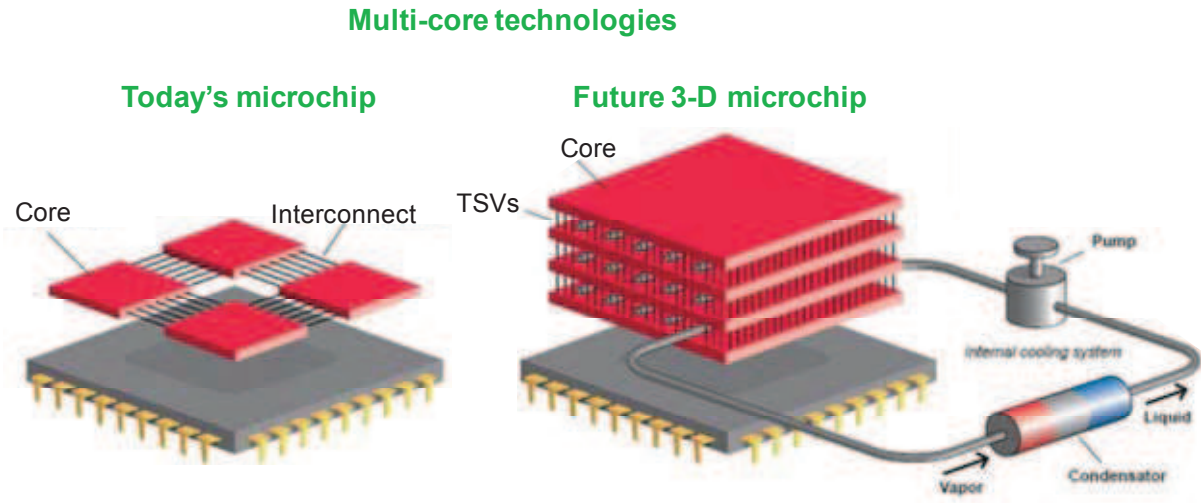

Fig. 2| Scheme presenting the difference between today's multicores technology and future developing architecture. Adapted from EPFL.LTCM, John R. Thome; infograph: Pascal Coderay.

These new approaches have been detailed in this chapter. Currently, processes are mainly based on PVD (physical vapor deposition: metal evaporation under high vacuum), CVD (chemical vapor deposition: evaporation of organometallic precursors (OM) and decomposition / reduction) or ALD (atomic layer deposition: chemical vapor deposition split-up in three parts: adsorption of one monolayer of OM, remove excess, and insertion of second precursors for reaction).[2, 3] However, these high vacuum techniques do not seem economically adapted for 3-D technologies. Consequently, the research on new, low cost and efficient silica surface metallization (layer of metal deposited to substrate surface to provide electrical contact) process is still a scientific and an economic challenge.

II. Current researches in microelectronics

II.1 Approaches to 3-D technologies

The superimposition of two or more microprocessors is a way to obtain faster and more reliable processors. Moreover, this induces a decrease of the interconnection (Through Silicon Vias: TSVs) length between devices. The dimensions of TSVs are for instance a diameter of 10 µm and 100 µm in length. Other processes which allow increasing of performance is the superimposition of several transistor strata on the same chip, or the connection of two processors front side with front side, Figure 3

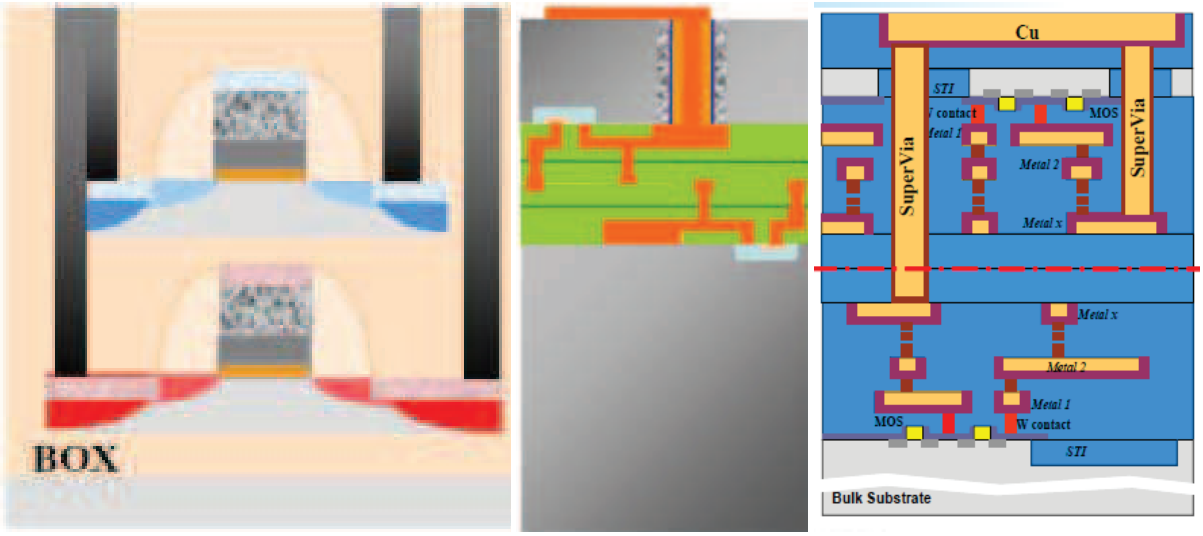

Fig. 3| Scheme presenting kinds of 3D architecture. Left: superimposition of transistors on one chip; middle: processor link front side with front side; right: superimposition of thin processors.

II.2. 2-D process applied for synthesis 3-D structures

3-D technologies have been developed on the basis of 2-D one. A 3-D package contains two or more chips (integrated circuits) stacked vertically so that they occupy less space and/or have faster connectivity. Currently, copper (Cu) is used as interconnect materials, replacing aluminum (Al), due to its higher electrical conductivity and good resistance to electromigration (atoms displacement under electrical flux). In spite of Al, directly patterned and isolated by dielectric deposition, Cu patterning in a controlled way is difficult. Thus, to

overcome this difficulty, currently silica was first patterned followed by Cu filling of the trench.[4]

However, Cu can easily diffuse in silica, which could lead to damage of the device.[5] To prevent this effect, a barrier layer is deposited onto the dielectric. A barrier layer is a film deposited between the silicide layer (which is formed over the silicon substrate as an interconnection path or contact) and the metallization layer. Moreover, the high diffusivity of silicon through silicide layers can be a problem under heat treatment; these can exhibit excessive interdiffusion between the metal and the silicon through the silicide layer. This silicon-metal interdiffusion can result in loss of system integrity. Barrier layers are therefore used for preventing this interdiffusion problem. Aside from excellent interdiffusion barrier properties, films used as a barrier layer between the metal layer and the silicide/silicon layers must exhibit excellent adhesion to both the metal layer and the silicide layer. They are composed of metals such as currently PVD deposited Ta/TaN.

Onto the barrier layer, a PVD seed layer of Cu is plated. Before bulk copper deposition on a dielectric layer, it is always necessary to deposit a thin seed layer. This provides nucleation sites for the bulk copper grain and film formations. With this conducting surface, copper atoms will stick very well to the wafer when the copper atoms migrate to the surface during electrochemical plating, Figure 4.

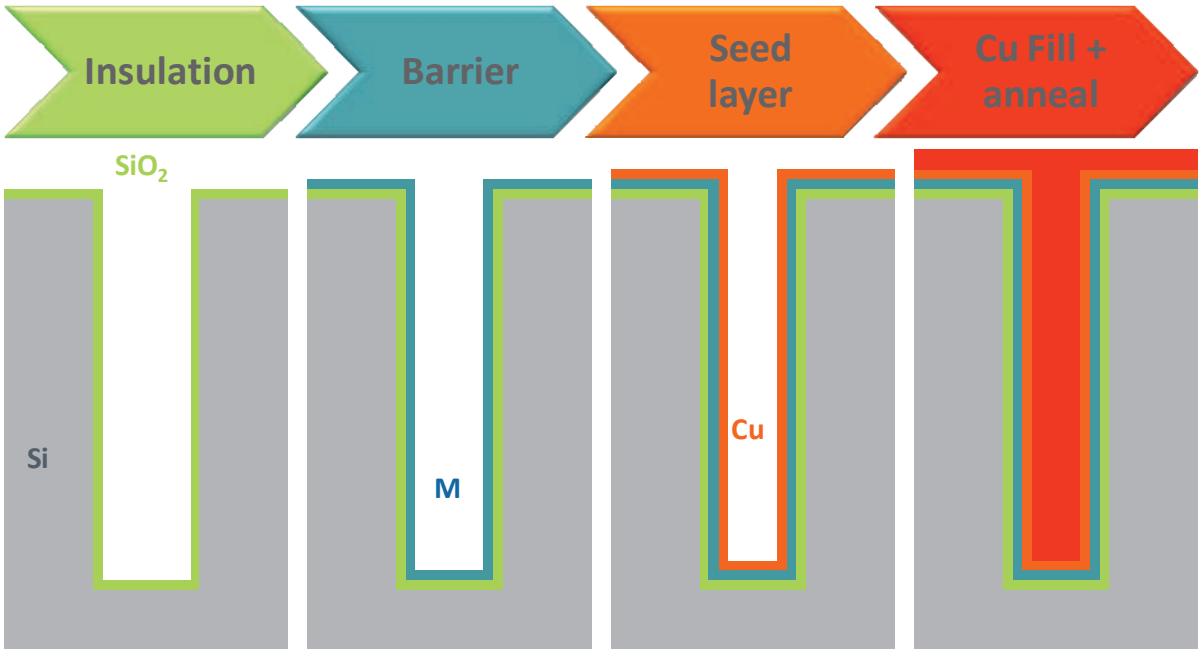

Fig. 4| Scheme of TSVs fabrication.

Then, on the seed layers, playing the role of an electrode (cathode), the Cu filling of the interconnects is performed by electroplating from a Cu ions aqueous solution. These two layers have to be very thin to have largest Cu interconnects, and uniform in order to avoid hole formation during Cu electroplating (Figure 5).

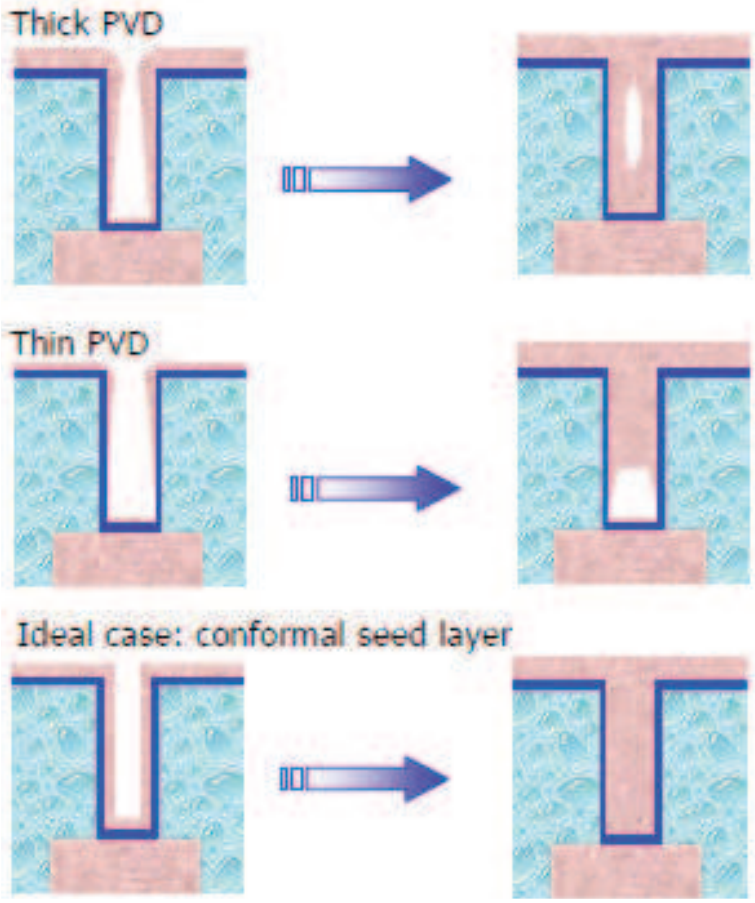

Fig. 5| Why seed layer has to be conformal?

II.3. Improvement on barrier formation: self-formed barrier

In order to improve the uniformity of the barrier, a new approach consisting in the deposition of copper based alloy has been recently reported.[6] The barrier layer formation has become increasingly difficult as the technology node is reduced from 90 to 65 and to 45 nm. An alternative to the conventional barrier process is a "self-forming" barrier process. This process involved the deposition of a Cu alloy thin film directly onto SiO_2, followed by heat treatment to migrate the alloying element to the alloy / SiO_2 interface and to form a thin barrier layer through reaction with SiO_2. This reduces to one step the two PVD steps, Figure 6.

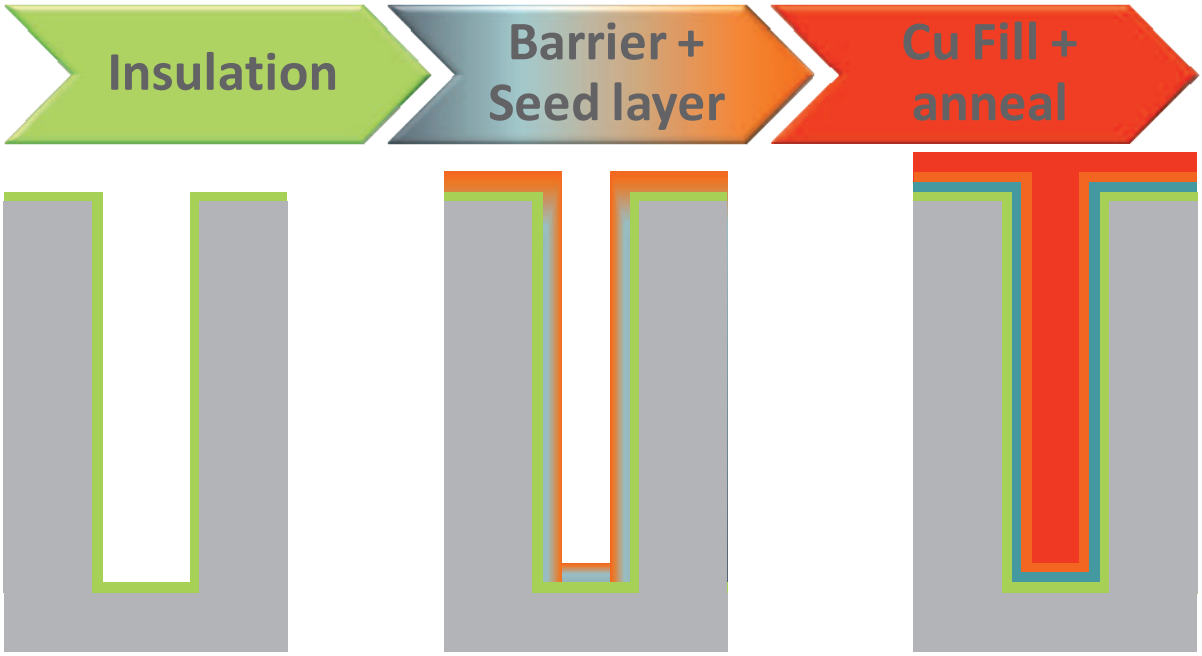

Fig. 6| Scheme of TSVs fabrication using self-formed barrier.

The request properties of the co-metal (M) in the Cu-M alloys are the following:

- M has to form easily an oxide, which allows the formation of an amorphous film.
- M has to form solid solution with copper and be easily separated with an annealing process
- M has to migrate faster into copper than copper itself, to avoid any reaction between copper and SiO_2.

Ding and co-workers explain the formation of self-formed barrier layer against copper diffusion with magnesium and aluminum.[7-9] Mg and Al induce the migration of silicon at the interface and subsequent migration into copper, increasing the resistivity of the resulting interconnects. Many elements (Mg, Ti, In, Sn, Al, Ag, Co, Nb, B, Ir, W) have been tested.[10] Only silver and bore present a convenient resistivity, but no information is provided concerning the interface.

Manganese (Mn) seems to be a good candidate for alloying with Cu. These alloys afford self-formation of a layer of Mn oxide at 450°C, during 30 minutes (4 nm in thickness),

with an alloy of 10 atomic percent of Mn.[6, 11-14] This barrier avoids copper diffusion without silicon diffusion. The key of this specific behavior is due to the fact that Mn diffusion in Cu is faster than the self-diffusivity of Cu. Consequently, Mn atoms migrate to the interface and form a stable oxide before noticeable reaction occurs between Cu and Si. By X-Ray absorption fine spectroscopy, the different phases formed were analyzed as the formation of $MnSiO_3$ and MnO (manganese in +II valence state).[15] However, 70 % of the Mn put into the alloy is kept in the Cu, and a Mn film is also created at the other interface.

Currently, these self-forming barrier deposits have been realized by the mean of high vacuum techniques (PVD or CVD).[14] So, there is a large field of investigation to improve the self-forming barrier process

II.4. Obtaining uniform layer for TSVs: annealing of nanoparticles

II.4.i. Direct application of 2-D technologies

Currently, as described above, TSVs synthesis is derived from the conventional 2-D process, Figure 4. The first step consists in a leaching of silicon through UV-photo irradiation of silica in HF solution.[4] The formation of oxide on the surface is only performed for Through Silicon Vias and is not necessary for conventional interconnection, since they are already performed on silica substrate.[1] Then by Physical vapor deposition (PVD) the Ta / TaN-barrier and Cu-seed layers are deposited. Next, electroplating is performed with the use of several additives in order to obtain superconformal deposit, that is filling of interconnects by the bottom.[5]

However, PVD is not a uniform technique. Table 1 presents the thickness of barrier Ta / TaN obtained after PVD process.

Table 1| PVD Ta/TaN barrier layer deposited on TSV of 5x50 µm.[16]

Place	Above	Sidewall	Bottom Side wall	Bottom
Thickness obtained in nm	134	6.6	3.0	2.1

Due to several technical problems (non-uniformity), other techniques (more conformal) are studied. For copper seed layer, the chemical vapor deposition (CVD) or for barrier layer atomic layer deposition (ALD) which allows deposition of very thin uniform layer by depositing successive mono-atomic layers.[2, 3] All of these processes using high vacuum are too expensive.[5]

Electroless deposition and electroplating are also studied for synthesizing these layers.[17, 18] There are some drawbacks as for electroless deposition the low speed of deposition and for electrodeposition the need of an electrode to be performed.

For this purpose, new innovative pathways have to be developed to improve TSVs production.

II.4.ii. Film synthesis from nanoparticles

Quite recently, the formation of uniform film from metallic nanoparticles (MNPs) has been reported. The CuNPs obtained from mesitylcopper (I) (Mes-Cu) by H_2 reduction in the presence of octylamine as stabilizer, form a film when annealed. However, the resulting resistivity is higher than the pure Cu, ($10x10^{-6}$ Ω cm vs. $1.72x10^{-6}$ Ωcm for bulk Cu). This could result from the presence of holes and / or presence of carbon inclusions into the films: due to the use of organic materials. Moreover, many defects are present (Figure 7a and 7b). Even if improving of the films is obtained by direct decomposition of Mes-Cu by H_2 onto the substrate, Figure 7c, carbon incorporation in the deposit leads to a dramatical increase of the resistivity ($52x10^{-6}$ Ωcm). Finally, a better uniformity film and a relatively good conductivity

($3x10^{-6}$ Ωcm) are obtained by using as reductant $^{i}Pr_2NBH_2$ instead of H_2, Figure 7d and 7e.[19]

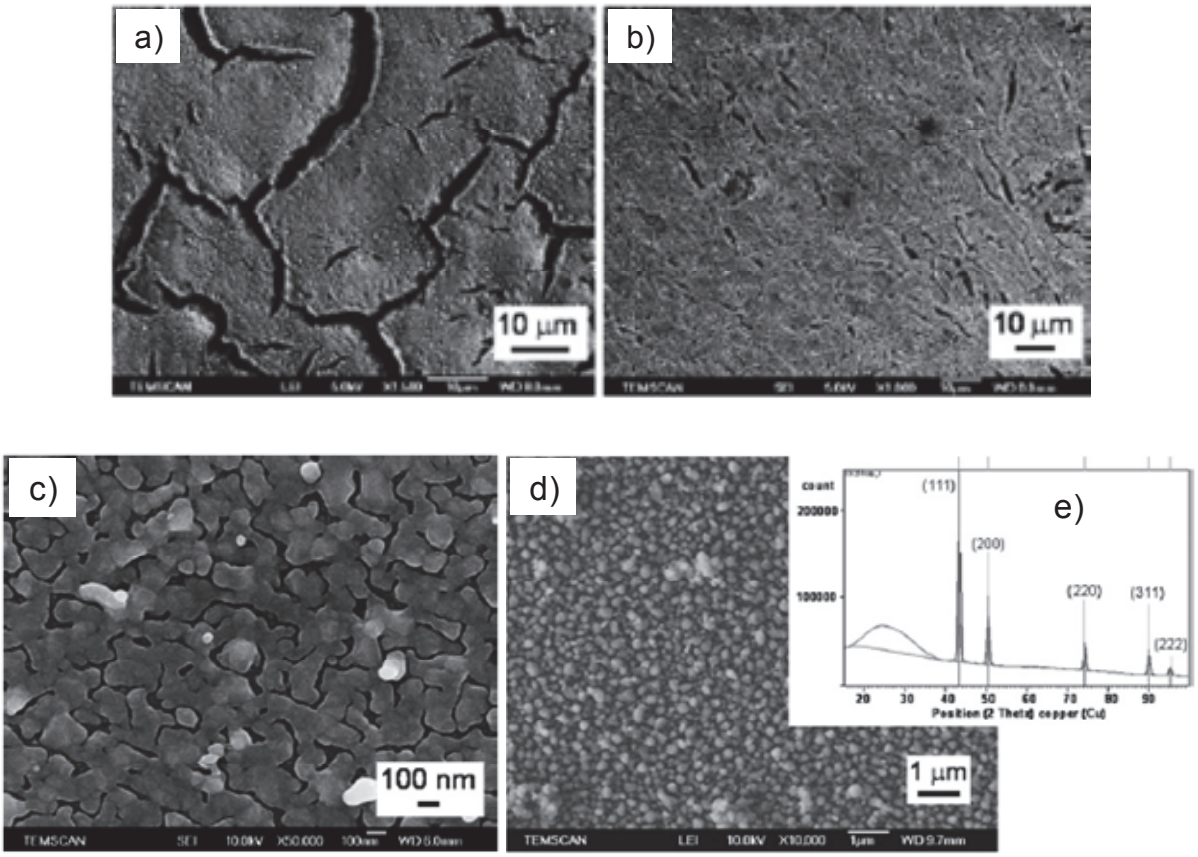

Fig. 7| SEM picture of: a) film obtained from drop deposition of dodecylamine stabilized CuNPs; b) film obtained from drop deposition of octylamine stabilized CuNPs; c) film formed by direct decomposition of Mes-Cu by H_2; d) film formed by reduction of Mes-Cu by $^{i}Pr_2NBH_2$. X-Ray diffraction pattern of copper layer obtained in d). Adapted from [19].

Another well used technique is dip-coating. This method deposits thin suspension layer on the substrate from NPs suspension. Then, controlled solvent evaporation from the liquid forms a thin layer of NPs.[20, 21] One other way to remove the excess solvent is to use a cylinder which rotate near the surface.[22] This method called roll cast allows formation of different shape structures by annealing in the same time. These physical methods are however difficult to apply in very narrow structures, as for instance in TSVs. Using dip coating, films of AgNPs and CoNPs have been obtained.[23, 24] A suspension of AgNPs with a mean size of 150 nm (81 %wt in solution with 1 %wt of dispersing agent) annealed at 180 °C for

10 min, induces NPs sintering. A film with a thickness of 1.44 µm and a resistivity of 7.3 mΩ/sq is obtained on 10 µm via hole, Figure 8.[23]. This resistance is certainly due to the mixing of organic contaminant, silver oxidation and non-uniform film obtained. However, for Ag as for CoNPs, the negative effect of the non-controlled NP size distribution has been highlighted.[23, 24]

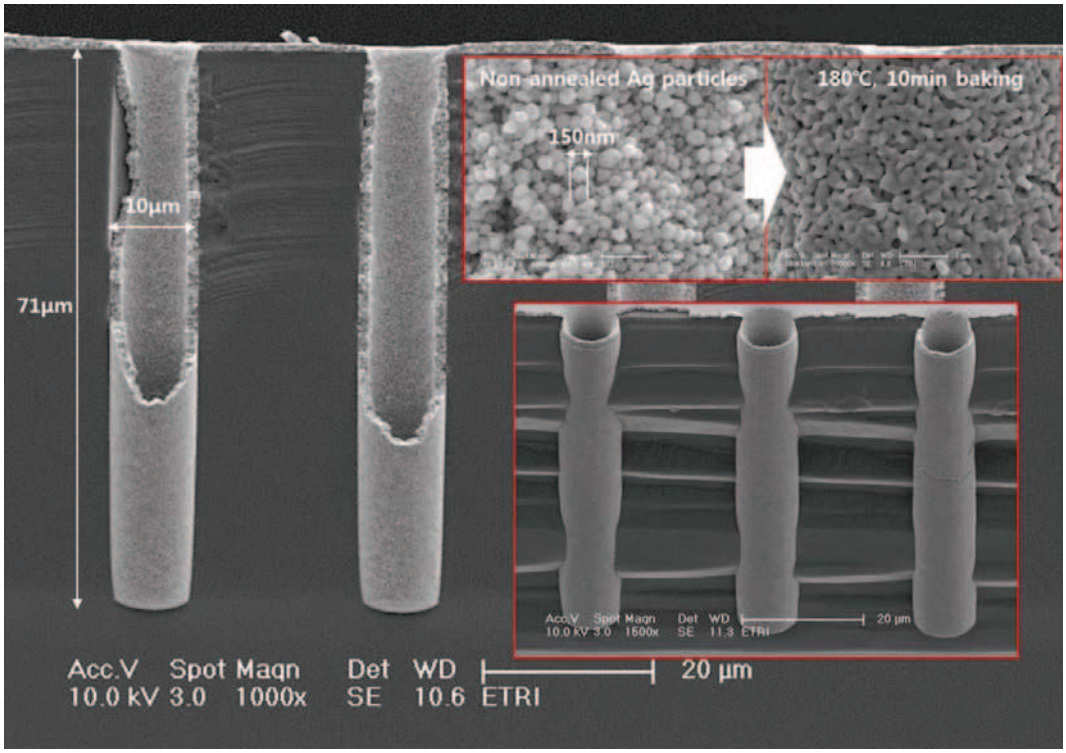

Fig. 8| Cross-sectional SEM image of Ag metal liner.[23]

These methods could be easily used in ink-jet printing, but for microelectronic, the major property for Cu or Ag layers, is the possibility to use them as seed layers, with allowing electrical contact and electroplating on this surface. Here it seems that stabilizers integration in layer decreases the conductivity. Moreover, the plating have been performed onto silica, no barrier layer coats the substrate.[19, 23]

Developing the surface functionalization allows enhancing surface adhesion with NPs. This has been performed for example with silane.[25] Alkyls amines stabilized NPs are used

in order to obtain conductive pattern on a substrate.[26] NPs sintering could be enhanced by addition of sintering agent as chloride.[27] However, this will leads to chloride incorporation in the layers and thus create high decrease of conductivity, important for seed-layer. The sintering of NPs on polymer surface has been also achieved.[28]

AgNPs have been used in order to synthesize conductive film. Nanoparticles are concentrated through decantation and the paste obtained is spread on the substrate. The annealing is performed in aqueous solution.[29] This method seems to be limited to silver since no example is given with other interesting noble metals, as gold and copper.

II.5. Conclusion

In conclusion, Koike and co-workers have demonstrated that the synthesis of Mn-Cu alloy will allow a great improvement of conventional 2-D process, with synthesis in one step of barrier and seed layers. However, the syntheses using high vacuum techniques are too expensive for TSVs synthesis.

Barriere and co-workers have formed films from CuNPs. Nevertheless the presence of stabilizers used during the synthesis of NPs in organic solvents produce a carbon deposit during the annealing. This carbon incorporation decreases sharply the conductivity of layers.

Conjoining these two breakthroughs, using bimetallic M_1M_2NPs to form self-formed barrier would allow realizing a versatile new low cost TSVs process.

In our laboratory, the synthesis of controlled size monometallic MNPs in ionic liquids (ILs) without stabilizing agents, and their deposit onto technical surface have been reported. In this Ph.D work, the following question is addressed: is this approach extendible to the synthesis of bimetallic nanoparticles, M_1M_2NPs?

III. Synthesis of bimetallic nanoparticles

III.1. Synthesis of nanoparticles

In recent years, the synthesis of MNPs has become a major challenge, as they are used in a variety of applications such as preparative catalysis, the fabrication of sensors or other nano-structures.[30-34] These MNPs could be of interest for the fabrication of advanced interconnecting structures. They could be deposited onto substrates to form conducting layers or initiate the growth of more complex objects such as layers, nanowires or nanotubes.[19, 33, 35, 36] In both instances, an accurate control of the size of these MNPs is mandatory. In particular, a narrow size distribution is key: it will ensure optimal coverage after deposition, or guarantee a uniform size of the nanowires or nanotubes grown from these metallic clusters.

The controlled synthesis of nanoparticles in the range of 1 to 10 nm is still an ongoing challenge as the understanding of their stabilization and agglomeration.[30, 37] Indeed, transition-metal nanoparticles remain only kinetically stable, the thermodynamic minimum being bulk metal. Consequently, substantial effort has been centered on stabilizing transition-metal nanoparticles. Furthermore, their formation and stabilization (inhibition of coalescence) are closely related issues.[38]

Several processes could be used for formation of NPs, as top-down methodology, from bulk to NPs, generally performed under high vacuum and bottom-up methodology from atoms. High vacuum techniques are too expensive for a large variety of application. In both strategies, the difficulty comes from stabilizing MNPs. The use of polymers, ligands and organic or inorganic templates allows formation of NPs in organic solvent or water.[30, 37] Unlike traditional solvents, ionic liquids (ILs) can be used to generate MNPs by several physical and chemical routes and stabilize them in the absence of further additives, inhibiting metal agglomeration to the bulk.[39]

Bimetallic NPs could be performed by majority of experimental methods used for monometallic NPs synthesis with minor change. An interesting method is to use galvanic replacement of a metal by a nobler one. Ramos and co-workers have developed the synthesis of Ag-core Au-shell NPs by placing Ag metallic NPs in a solution of Au ions.[40] Munoz-Flores and co-workers have recently made a review on the possibility to form bimetallic NPs or metallic nanoalloys.[41] Several processes are described, as for instance syntheses assisted by microwaves, ion-beam technique, chemical vapor deposition, electrochemistry, thermal decomposition and chemical reduction. They also describe the main applications for which nanoalloys are studied, that are catalysis. Ferrando and al. summarized studies performed on nanoalloys. They reported experimental techniques for characterization of nanoalloys as well as their theoretical structural, optical and magnetic properties.[42] They described the catalytic properties and melting characteristics of such objects.

Nanostructures consisting of an alloy or composite of different elements, such as core/shell nanoparticles, are of great interest for fundamental studies. In this context, the control of homogeneity, dispersion, and alloying extent is key, as these characteristics have profound influence on the surface properties of the M_1-M_2NPs, which in turn affect their stability.[42, 43] However, their synthesis is non-trivial.[44] To address this challenge, chemical methods offer a promising pathway.

III.2. Ionic liquids for nanoparticles synthesis

Ionic liquids have been successfully used in numerous applications.[45] They are developed at the origins for battery due to their large electrochemical window. Ionic liquids are salts generally liquid at room temperature. They are composed of a bulky organic cation and an

inorganic or organic anion. ILs are interesting media since they are liquid on a large temperature window (-20 to 300 °C, for 1-butyl-3-methylimidazolium bis(trifluoromethanesulphonyl)imide), depending on cation and anion used. Their large thermal, but also chemical (and electrochemical) stability allow the possibility of use them in a large panel of application, as organic synthesis, recycling, catalysis, lubricant … Moreover, the possibility to tune IL through change of cation or anion should entail rapid optimization of process. In comparison to other common solvent used in industry, ILs show negligible vapor pressure. This leads to improvement of working conditions with less risk and possibility to use ILs in high vacuum (analysis in ultra-high vacuum at 10^{-9} Pa X-Ray photoelectron spectroscopy chamber possible).[46]

Due to their interesting properties, there is a large panel of methods for synthesizing NPs in ILs. Nano-objects could be obtained for example by pulsed electrodeposition, high vacuum techniques, and other chemical ways. NPs on the 1-10 nm are only kinetically stable. Stabilizers are needed for avoiding agglomeration and aggregation. This tunable class of solvent allows synthesizing NPs without the use of further additives or stabilizing agent in the solution. Small narrow size distribution NPs with sometimes different shapes could be prepared by decomposition or reduction of organometallic precursors generally in presence of dihydrogen. In imidazolium based ILs, the synthesis and stabilization occurs through the use of their typical highly hydrogen bonded organized supramolecular structure, leading to the formation of polar and non-polar domains. ILs form a protection coating for NPs generated, against agglomeration but also oxidation.[47]

A large variety of NPs have been already obtained in ILs as Group VIII metal (Fe, Co, Ru, Rh, Pd, Os, Ir, Pt), and noble metal (Cu, Ag, Au).[39] These NPs have been obtained through in a large part chemical reduction of salts by chiefly sodium borohydride or

hydrazine, but also through less conventional techniques, as microwave irradiation and sonochemical decomposition. Janiak and coworkers have also studied the synthesis of NPs in IL with several group VIII metals achieved and refractory metals (Cr, Mo, W).[48] They use (CO) based precursors and thermal decomposed them at relatively high temperature, generally superior to 100 °C. Re and Mn metallic NPs have been also obtained through this way.

Numerous techniques have been used for synthesis NPs in ILs, as reported in Dupont review.[39] From these, CuNPs have been performed from electrochemical reduction, PVD and organometallic precursor decomposition / reduction, which are very interesting.[49, 50] Indeed, these techniques present the advantage to form surface without partial oxidation which is of great interest for catalysis or microelectronic applications. Bretthole et al. use plasma electrodeposition to obtain rapidly NPs without the use of pulsed electrochemistry.[49] Plasma is used as an electrode and only a small degradation of ILs is observed. Richter and coworkers use a high vacuum technique, PVD in order to form controlled size NPs without any possible contaminants at the surface.[51] The size of NPs seems to be controlled by the length of alkyl chain. Gutel use imidazolium based ILs for RuNPs synthesis.[52] The 3-D structure of these ILs is mainly due to segregation of imidazolium ring alkyl chain. This creates non-polar domains in an ionic network composed of cations and anions. The segregation of polar and non-polar domains changes their solvation properties. Indeed, neutral substrates, as organometallic precursors are mainly dissolved in non-polar domains, and ionic one in polar domains. Size and shape of resulting NPs could be tuned by varying the volume (in quantity and quality) of these areas. Our group have recently demonstrated the synthesis of RuNPs from (η^4-1,5-cyclooctadiene)(η^6-1,3,5-cyclo-octatriene)ruthenium(0), Ru(COD)(COT). Interestingly enough, the size of resulting zero-valent NPs varies in function of temperature, with smaller size at smaller temperature. Thus,

1 nm mean size is obtained at 0 °C and 2-3 nm at 25 °C, contrary of what obtained in organic solvents. This seems due to a better control of the 3-D structure of the ILs at low temperature, with less thermal stirring, and then a better isolation of organometallic precursors in apolar domains.[52, 53]

RuNPs prepared at 0 °C under stirring agglomerate to form larger superstructure of 2-3 nm in size. NPs present in this structure are however well defined.[52] Without stirring, no NPs agglomeration is observed. These results show a better stabilization of ILs at lower temperature. This effect is directly related to the organization of ILs. A better organization of ILs is observed without stirring and at lower temperature, leading to smaller size NPs without agglomeration. Presence of stirring (even thermal) perturbs this 3-D structure entailing worse mono-dispersed small size NPs.

Influence of ILs supramolecular structure on the size of RuNPs has been studied.[53] A linear relationship between RuNPs and alkyl chain length sizes is observed. Moreover, the size of RuNPs corresponds quite well to the size of non-polar domains modeled and measured.[54, 55] Consequently, the NPs size could also be controlled by the local quantity of precursors in non-polar areas, which is directly in relationship with the length of alkyl chains. This technique will be used in order to obtain control size NPs usable in microelectronic, as copper, tantalum and manganese.

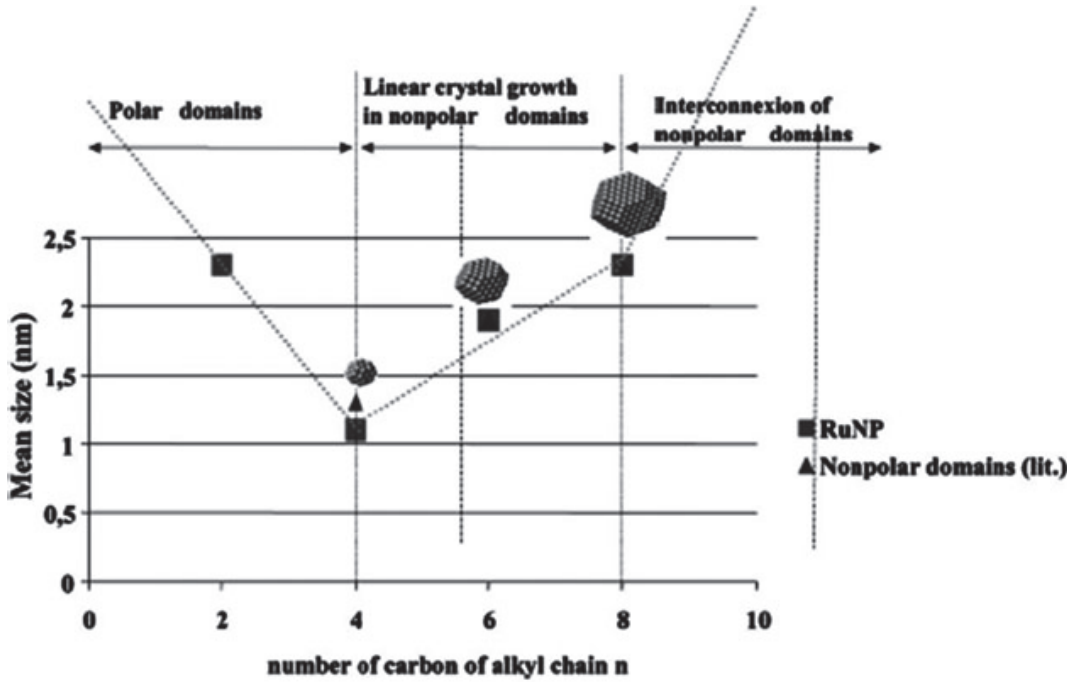

Fig. 9| Scheme showing correlation between RuNPs size and number of carbons in the ILs alkyl chain. Adapted from [53].

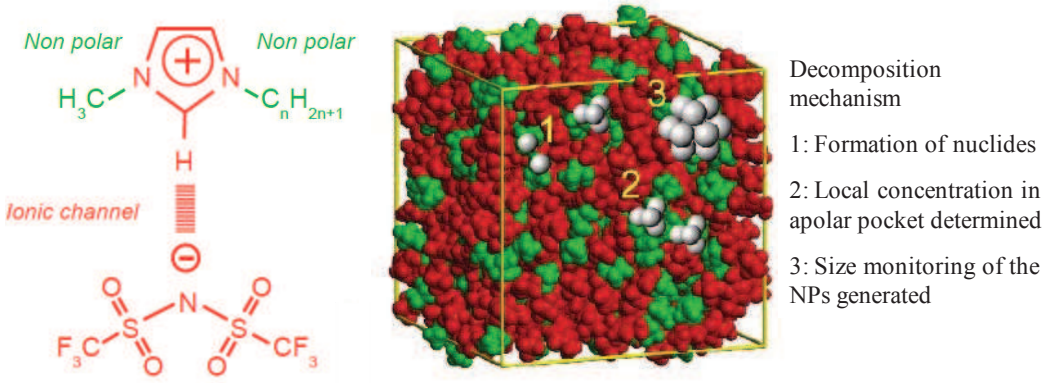

Fig. 10| Imidazolium ILs used, 3-D structures modeled and decomposition of OM in IL. Adapted from [53].

At our knowledge, this technique has not been developed for synthesis of bimetallic NPs. Numerous methods corresponding to bottom-up or top-down strategies are successfully developed for synthesis NPs. A large part of these methods could be used for synthesis of bimetallic NPs, for example with the use of an alloy for top down strategy and the use of two precursors in same time for bottom up strategy. Nevertheless, few examples are reported concerning the synthesis of bimetallic NPs in ILs. Okazaki and al. have successfully

synthesized Au-AgNPs with physical vapor deposition of Au and Ag in same time and formation of NPs in ILs.[56] They have applied this technique for obtaining non-conventional alloy of Au-Pt with mean size between 1-3 nm.[57] Electrochemistry could be used for synthesis of supported NPs. Moreover, ILs are also considered as a very good electrolyte. Tsai and al. have achieved the synthesis of Au-AgNPs in ILs by this method.[58] Pd-Ni have also been co-deposited on the form of a layer in IL.[59] Xi and coworker use the IL $C_1C_4ImBF_4$ as solvent and reductant for synthesis of Au-Pd bimetallic NPs.[60] Several other authors use solid ILs to modified surface electrode. With electrodeposition assisted by ultrason in aqueous solution, they achieve to obtain Au-Pt, and Pt-M (M: Ru, Pd, Au) on the form of nanoparticles without the use of pulsed electrodeposition.[61, 62]

Some people use ILs only as stabilizer during the synthesis or for storage of their NPs. Dash and coworkers have synthesized bimetallic Au-PdNPs in methanol and transferred in a second time into ILs.[63, 64] These NPs have been performed by chemical reduction of $HAuCl_4$ by $NaBF_4$. Some Au-PdNPs have been directly performed in $C_1C_4ImPF_6$ [65]. By galvanic replacement of Pd(0) by Au^{3+} in water, bimetallic Au-PdNPs are obtained on microsphere based on vinyl polymerized ILs.[66] Galvanic replacement has been also used in IL-water micro-emulsions system to obtained Au-PdNPs.[67] In other article, a two steps chemical reduction of first Au salts followed by Pt allows formation of Au-PtNPs of 2-10 nm. Phosphonium chloride ILs are only used as stabilizer during synthesis in dioxane, leading to small particles, and after evaporation as protection against agglomeration and oxidation.[68]

Sol-gel process has been used for synthesis of bimetallic Ru-CuNPs by impregnation on bentonite and use of ILs as stabilizer.[69]

By simultaneous thermal decomposition of two carbonyl precursors in ILs, Andanson and co-workers achieved the synthesis of bimetallic Fe-RuNPs with small size. They remark that mixing the two precursors allows obtaining smaller NPs, 1.7 nm (Fe:Ru = 1:9), compared

to the pure metal, 11 nm for Fe and 3 nm for Ru. This broadening of Janiak way for obtaining NPs, should be performed at high temperature of 250 °C, but could be a good way for synthesis bimetallic NPs in ILs.[48]

Two techniques could be investigated, simultaneous decomposition or step by step decomposition of the two organometallic precursors in order to obtain bimetallic NPs, as obtained in organic solvent.[70, 71] By this chemical route, controlled structure core-shell NPs could be foreseen following the reduction / decomposition rate of the two precursors.

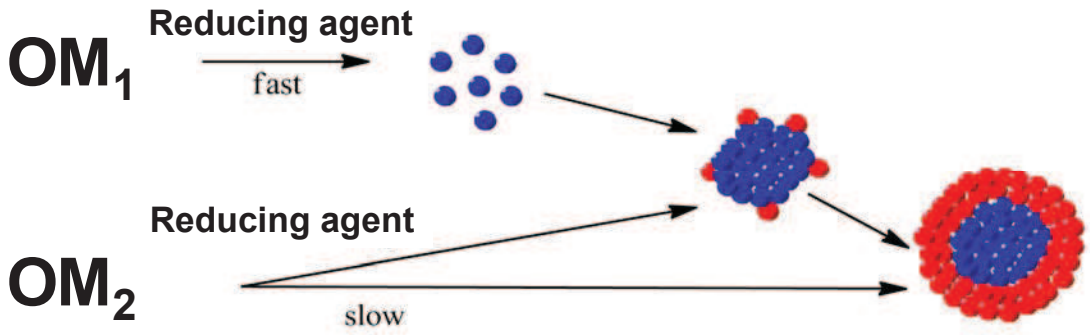

Reducing Agent = H_2, OM_1 = $Rh(\eta^3\text{-}C_3H_5)_3$, OM_2 = $Fe[N(SiMe_3)_2]_2$
Reducing Agent = $iPr_2NH.BH_3$, OM_1 = $Fe[N(SiMe_3)_2]_2$, OM_2 = $Rh(\eta 3\text{-}C_3H_5)_3$

Fig. 11| Scheme of formation of bimetallic core-shell NPs from OM with different decomposition kinetics, in organic solvent.

III.3. Conclusion

Indeed, nanostructures consisting of an alloy or composite of different elements, such as core/shell nanoparticles, are of great interest for fundamental studies. In this context, the control of homogeneity, dispersion, and alloying extent is key, as these characteristics have profound influence on the surface properties of the M_1-M_2NPs, which in turn affect their stability. However, their synthesis is non-trivial. To address this challenge, chemical methods offer a promising pathway to the synthesis of bimetallic, M_1-M_2NPs using reduction/decomposition of OM precursors in ILs under dihydrogen.

IV. Conclusion

In this chapter, we describe two major breakthroughs in the TSVs formation. Firstly, the development of self-formed layer Cu:M by Koike, which reduces to one step the layers formation for TSVs.[6] Secondly, the formation of film from annealing of NPs, obtained through a chemical route which allows reducing process cost.[19]

The LCOMS expertise in the synthesis of size controlled NPs in IL, and the results obtain in the use of these NPs suspension in microelectronic applications, leading us to choose this route to form copper bimetallic NPs in ILs. In this goal, we report in the second chapter the synthesis of monometallic NPs of Cu and Mn, then bimetallic one in Chapter III and finally in chapter IV, our attempts to form a film from bimetallic Cu-based NPs, in ILs.

References

[1] M.G. Farooq, ECS Trans., 35 (2011) 83-94.
[2] P. Doppelt, Coord. Chem. Rev., 178-180 (1998) 1785-1809.
[3] S.-H. Kim, S.S. Oh, K.-B. Kim, D.-H. Kang, W.-M. Li, S. Haukka, M. Tuominen, Appl. Phys. Lett., 82 (2003) 4486-4488.
[4] G. O'Sullivan, D. Kilbane, R. D'Arcy, J. Modern Optics, 59 (2012) 855-872.
[5] A. Roule, T. Morel, P.H. Haumesser, O. Pollet, M. Cordeau, S. Maitrejean, J. Klocke, T. Ritzdorf, G. Passemard, Adv. Met. Conf. 2004, Proceedings of the Conference, San Diego, CA, United States, Oct. 19-21, and Tokyo, Japan, Sept. 28-29, 2004, (2005) 341-346.
[6] J. Koike, M. Wada, Appl. Phys. Lett., 87 (2005).
[7] P.J. Ding, W.A. Lanford, S. Hymes, S.P. Murarka, Appl. Phys. Lett., 64 (1994) 2897-2899.
[8] P.J. Ding, W.A. Lanford, S. Hymes, S.P. Murarka, Appl. Phys. Lett., 65 (1994) 1778-1780.
[9] W.A. Lanford, P.J. Ding, W. Wang, S. Hymes, S.P. Muraka, Thin Solid Films, 262 (1995) 234-241.
[10] K. Barmak, A. Gungor, C. Cabral, Jr., J.M.E. Harper, J. Appl. Phys., 94 (2003) 1605-1616.
[11] M. Haneda, J. Iijima, J. Koike, Appl. Phys. Lett., 90 (2007) 252107/252101-252103.
[12] J. Koike, M. Haneda, J. Iijima, Y. Otsuka, H. Sako, K. Neishi, J. Appl. Phys., 102 (2007) 043527-043521-043527.
[13] J. Koike, M. Wada, T. Usui, H. Nasu, S. Takahashi, N. Shimizu, M. Yoshimaru, H. Shibata, AIP Conference Proceedings, (2006) 43-51.
[14] K. Neishi, S. Aki, K. Matsumoto, H. Sato, H. Itoh, S. Hosaka, J. Koike, Appl. Phys. Lett., 93 (2008) 032106-032101-032103.
[15] J.M. Ablett, J.C. Woicik, Z. Tokei, S. List, E. Dimasi, Appl. Phys. Lett., 94 (2009) 042112 (042113).
[16] J. Guillan, K. Haxaire, D. Galpin, S. Chhun, J.C. Giraudin, D. Ney, L. Arnaud, D. Guiheux, R. Pantel, in: Materials for advanced metallisation, Grenoble, 2012.
[17] A.E.B. Marques, S.G. Santos Filho, S. Martini, Phys. Stat. Solidi C 4(2007) 256-258.
[18] S. Schaltin, A. Shkurankov, K. Binnemans, J. Fransaer, ECS Trans., 25 (2010) 119-128.
[19] C. Barriere, G. Alcaraz, O. Margeat, P. Fau, J.B. Quoirin, C. Anceau, B. Chaudret, J. Mater. Chem., 18 (2008) 3084-3086.
[20] B.Y. Jung, S.-H. Min, C.-W. Kwon, S.-H. Park, K.-B. Kim, T.-S. Yoonc, J. Electrochem. Soc., 156 (2009) K86-K90.
[21] M. Acet, C. Mayer, O. Muth, A. Terheiden, G. Dyker, J. Crystal Growth, 285 (2005) 365-371.
[22] L. Chen, M. Coelle, M.J. Goulding, in, (Merck Patent GmbH, Germany). Application: WO, 2011, 2011072787.
[23] Y.-H. Ham, D.-P. Kim, K.-H. Baek, K.-S. Park, M. Kim, K.-H. Kwon, K. Lee, L.-M. Doa, Electrochem.Solid-State Lett., 15 (2012) H145-H147.
[24] L. Peña, M. Varón, Z. Konstantinovic, L. Balcells, B. Martínez, V. Puntes, J. Mater. Chem., 21 (2011) 16973-16977.
[25] H. Kuroda, T. Tauchi, in, (Ube Nitto Kasei Co., Ltd., Japan). Application: JP 2008, 2008133535.

[26] H. Saito, M. Ueda, N. Terada, Y. Matsuba, in, (Harima Chemicals, Inc., Japan). Application: JP, 2009, 2009070727.
[27] S. Magdassi, M. Grouchko, A. Kamyshny, in, (Yissum Research Development Company of the Hebrew University of Jerusalem, Ltd., Israel). Application: WO, 2010, 2010109465.
[28] K. Ochi, in, (Mitsuboshi Belting Ltd., Japan). Application: JP, 2009, 2009001883.
[29] M.A. Mastropietro, G.A. Jablonski, in, (PChem Associates, Inc., USA). Application: US, 2011, 7931941.
[30] D. Astruc, in, Wiley-VCH, Weinheim, 2008.
[31] A.T. Bell, Science, 299 (2003) 1688-1691.
[32] H. Bönnemann, K.S. Nagabhushana, Metal Nanoclusters: Synthesis and Strategies for their Size Control, in: B. Corain, G. Schmid, N. Toshima (Eds.) Metal Nanoclusters in Catalysis and Materials Science, Elsevier, Amsterdam, 2008, pp. 21-48.
[33] G. Schmid, Nanoparticles: From Theory to Application, Wiley-VCH, Weinheim, 2004.
[34] M. Valden, X. Lai, D.W. Goodman, Science, 281 (1998) 1647.
[35] S. Deleonibus, J.-M. Basset, P. Campbell, T. Gutel, P.-H. Haumesser, G. Marchand, C. Santini, CEA, EP, 2010, 2234115A1.
[36] P.H. Haumesser, J.M. Basset, P. Campbell, S. Deleonibus, T. Gutel, G. Marchand, C. Santini, FR, 2010, 2943850A1.
[37] H. Bönnemann, K.S. Nagabhushana, R.M. Richards, Colloidal Nanoparticles Stabilozed by Surfactants or Organo-Aluminium Derivatives: Perparation and Use as Catalyst Precursors, in: D. Astruc (Ed.) Nanoparticles and Catalysis, Wiley-VCH, Weinheim, 2008, pp. 49-92.
[38] L.S. Ott, R.G. Finke, Coord. Chem. Rev., 251 (2007) 1075-1100.
[39] J. Dupont, J.D. Scholten, Chem. Soc. Rev., 39 (2010) 1780-1804.
[40] M. Ramos, D.A. Ferrer, R.R. Chianelli, V. Correa, J. Serrano-Matos, S. Flores, J. Nanomater., (2011) 374096, 374095 pp.
[41] B.M. Munoz-Flores, B.I. Kharisov, V.M. Jimenez-Perez, P. Elizondo Martinez, S.T. Lopez, Ind. Eng. Chem. Res., 50 (2011) 7705-7721.
[42] R. Ferrando, J. Jellinek, R.L. Johnston, Chem. Rev., 108 (2008) 845-910.
[43] L.-L. Wang, D.D. Johnson, J. Am. Chem. Soc., 131 (2009) 14023-14029.
[44] C.J. Serpell, J. Cookson, D. Ozkaya, P.D. Beer, Nat. Chem., 3 (2011) 478-483.
[45] P. Wasserscheid, T. Welton, in, Wiley-VCH, Weinheim, 2008.
[46] P.S. Campbell, C.C. Santini, F. Bayard, Y. Chauvin, V. Colliere, A. Podgorsek, M.F. Costa Gomes, J. Sa, J. Catal., 275 (2010) 99-107.
[47] K. Richter, A. Birkner, A.V. Mudring, Phys. Chem. Chem. Phys., 13 (2011) 7105-7110.
[48] C. Vollmer, C. Janiak, Coord. Chem. Rev., 255 (2011) 2039-2057.
[49] M. Brettholle, O. Hoefft, L. Klarhoefer, S. Mathes, W. Maus-Friedrichs, S. Zein El Abedin, S. Krischok, J. Janek, F. Endres, Phys. Chem. Chem. Phys., 12 (2010) 1750-1755.
[50] K. Richter, T. Baecker, A.-V. Mudring, Chem. Comm., (2009) 301-303.
[51] K. Richter, A. Birkner, A.-V. Mudring, Angew. Chem., Int. Ed., 49 (2010) 2431-2435, S2431/2431-S2431/2439.
[52] T. Gutel, J. Garcia-Anton, K. Pelzer, K. Philippot, C.C. Santini, Y. Chauvin, B. Chaudret, J.-M. Basset, J. Mater. Chem., 17 (2007) 3290-3292.
[53] T. Gutel, C.C. Santini, K. Philippot, A. Padua, K. Pelzer, B. Chaudret, Y. Chauvin, J.-M. Basset, Journal of Materials Chemistry, 19 (2009) 3624-3631.

[54] A.A.H. Padua, M.F. Costa Gomes, J.N.A. Canongia Lopes, Acc. Chem. Res., 40 (2007) 1087-1096.
[55] A. Triolo, O. Russina, H.-J. Bleif, E. Di Cola, J. Phys. Chem. B, 111 (2007) 4641-4644.
[56] K.-i. Okazaki, T. Kiyama, K. Hirahara, N. Tanaka, S. Kuwabata, T. Torimoto, Chem Commun (2008) 691-693.
[57] S. Suzuki, T. Suzuki, Y. Tomita, M. Hirano, K.-i. Okazaki, S. Kuwabata, T. Torimoto, CrystEngComm, 14 (2012) 4922-4926.
[58] T.-H. Tsai, S. Thiagarajan, S.-M. Chen, J. Appl. Electrochem., 40 (2010) 493-497.
[59] H.-Y. Huang, P.-Y. Chen, Electrochim. Acta, 56 (2011) 2336-2343.
[60] J. Xi, W.-s. Dong, Shaanxi Shifan Daxue Xuebao, Ziran Kexueban, 38 (2010) 62-64.
[61] F. Xiao, F. Zhao, D. Mei, Z. Mo, B. Zeng, Biosens. Bioelectron., 24 (2009) 3481-3486.
[62] Y. Yu, X. Liu, D. Jiang, Q. Sun, T. Zhou, M. Zhu, L. Jin, G. Shi, Biosens. Bioelectron., 26 (2011) 3227-3232.
[63] P. Dash, N.A. Dehm, R.W.J. Scott, J. Mol. Catal. A: Chem., 286 (2008) 114-119.
[64] P. Dash, S.M. Miller, R.W.J. Scott, J. Mol. Catal. A: Chem., 329 (2010) 86-95.
[65] P. Dash, R.W.J. Scott, Chem. Commun. (Cambridge, U. K.), (2009) 812-814.
[66] B. Hu, T. Wu, K. Ding, X. Zhou, T. Jiang, B. Han, J. Phys. Chem. C, 114 (2010) 3396-3400.
[67] G. Zhang, H. Zhou, C. An, D. Liu, Z. Huang, Y. Kuang, Colloid Polym. Sci., (in press) Ahead of Print.
[68] A. Maclennan, A. Banerjee, R.W.J. Scott, Catal. Today, (in press) Ahead of Print.
[69] T. Jiang, Y. Zhou, S. Liang, H. Liu, B. Han, Green Chem., 11 (2009) 1000-1006.
[70] N. Atamena, D. Ciuculescu, G. Alcaraz, A. Smekhova, F. Wilhelm, A. Rogalev, B. Chaudret, P. Lecante, R.E. Benfield, C. Amiens, Chem. Commun. (Cambridge, U. K.), 46 (2010) 2453-2455.
[71] D. Ciuculescu, C. Amiens, M. Respaud, A. Falqui, P. Lecante, R.E. Benfield, L. Jiang, K. Fauth, B. Chaudret, Chem. Mater., 19 (2007) 4624-4626.

Chapter II

Monometallic Copper and Manganese Nanoparticles Synthesis and *in situ* Characterization in Ionic Liquids

Chapter II

Monometallic Copper and Manganese Nanoparticles Synthesis and *in situ* Characterization in Ionic Liquids

I. Introduction

In recent years, the synthesis of metallic nanoparticles (MNPs) has become a major challenge, as they are used in a variety of applications such as preparative catalysis, the fabrication of sensors or other nano-structure.[1-5]. These MNPs are also of huge interest for the fabrication of advanced interconnect structures. They can be deposited onto substrates to form conducting layers or to initiate the growth of more complex objects such as nanowires or nanotubes.[4, 6] In both instances, an accurate control of the size of these MNPs is mandatory. In particular, a narrow size distribution is key: it will ensure optimal coverage after deposition, or guarantee a uniform size of the nanowires or nanotubes grown from these metallic clusters.

However, the controlled synthesis of nanoparticles in the range of 1 to 10 nm is still an ongoing challenge as the understanding of their stabilization and agglomeration.[1, 7] Indeed, transition-metal nanoparticles remain only kinetically stable, the thermodynamic minimum being bulk metal. Consequently, substantial effort has been centered on stabilizing transition-metal nanoparticles. Furthermore, their formation and stabilization (inhibition of coalescence) are closely related issues.[8] As we reported in Chapter I, in bottom-up methodologies, the use of polymers, ligands and organic or inorganic templates allows formation of NPs in organic solvent or water.[1, 7] Unlike traditional solvents, ionic liquids (ILs) can be used to generate a large variety of NPs mainly from Group VIII metals (Fe, Co, Ru, Rh, Pd, Os, Ir, Pt), and from noble metals (Cu, Ag, Au) by several physical and chemical routes and stabilize them in the absence of further additives.[9] In order to avoid possible surface contamination, the synthesis of NPs from organometallic precursors (OM) are largely reported. Indeed, after decomposition under H_2 atmosphere, they form volatile by-products that can be easily removed from the solution.[9, 10] Moreover, ILs are liquid at room temperature, show a high thermal stability and a negligible vapor pressure which facilitates the work up (synthesis, and in situ ultra-high vacuum analysis in the same medium).[9, 11]

Based on the previous results obtained at LCOMS and other data available in the literature, the syntheses of CuNPs and MnNPs were realized by chemical reduction of organometallic precursors (OM) under dihydrogen in imidazolium derived ionic liquids. This chapter first reviews the literature on the syntheses of CuNPs and MnNPs. Then, all experimental parameters tested in order to obtain small NPs (inferior to 5 nm) with narrow size distribution are described. Finally, their characterization by transmission electron microscopy (TEM) and X-Ray photoelectron spectroscopy (XPS) is reported.

II. State of the art: synthesis of nanoparticles in ionic liquids

II.1. Synthesis of copper nanoparticles IL

Copper has been adopted as the advanced interconnect material in microelectronic devices. Its use is now extended to the fabrication of Through Silicon Vias (TSVs) in 3D chip stacking approaches. In this metallization scheme, the deposition of a copper seed layer to initiate electroplating becomes more and more challenging. Currently, Cu seed layers are deposited by physical vapor deposition (PVD), which suffers from lack of conformity. Therefore, alternative techniques are investigated such as CVD (chemical vapor deposition) or ALD (atomic layer deposition).[12, 13] However, these high vacuum techniques are not economically adapted for 3D technologies. A new and efficient metallization process of silica surfaces involving a suspension of copper nanoparticles (CuNPs) generated from an organic solution of mesitylcopper would be a real breakthrough in the access of thin conductive copper films on silicon substrates.[6]

Several strategies are developed for synthesis of CuNPs in ILs. CuNPs can be formed by using plasma electrochemical deposition,[14] sol-gel process, [15] chemical or electrochemical reduction from copper salts (Cl^-, NO_3^-, SO_4^{2-}) [16-19] involving several washing steps and a possible oxidation of the surface of the NPs.

More recently, thermolysis of coordination complexes and decomposition by a reductant of organometallic complexes in the presence of a surfactant (ligand) to avoid the aggregation of CuNPs have been described.[6, 20, 21] The synthesis of CuNPs was obtained by PVD from metallic copper in ILs, leading to spherical particles with a mean diameter of 3 nm. Interestingly, these CuNPs are stabilized by an electrostatic protective layer of ionic liquid (IL).[22]

Applications of CuNPs are diverse due to their optical and catalytical properties.[15, 23-25] There are also used in solar cells and in the separation of propane and propylene.[26, 27]

II.2. Synthesis of manganese nanoparticles IL

Manganese is among the most complex magnetic elements. The most stable form of Mn metal, α-Mn, adopts an elaborate body centered cubic structure that contains 58 atoms per unit cell. MnNPs have been limited because of difficulties in their synthesis and stabilization. The large negative reduction potentials of soluble Mn salts (e.g., $E°_{Mn2+/Mn}$=-1.185 V/$_{SHE}$) make it difficult to generate zerovalent Mn in solutions using conventional reducing agents usually employed in colloidal syntheses. The oxophilicity of Mn also renders MnNPs highly reactive in air.

Hence, most of the literature concerns nanoparticles of Mn oxides, which are used as electrodes in lithium-ion batteries [28], as additives of Zn particles exhibiting luminescent properties [29], as supercapacitors due to their special pseudocapacitive property [30], in catalysis [31] and in other applications related to their magnetic properties [32, 33].

Some studies on the synthesis of MnNPs through physical vapor deposition, laser ablation and inert gas condensation technique [34] or through chemical reduction of a Mn salt [35-37] are reported (Table 1). However, all authors highlighted the difficulty to preserve the metallic structure from oxidation.

Table 1| Reported techniques for the synthesis of MnNPs.

Ref	Method	Size of NPs	Oxidation state
[38]	Laser ablation	25 to 100 nm	Metallic
[34]	Inert gas condensation technique	5 to 200nm diameter	<20 nm: full oxide/ >20 nm: β Mn core oxide shell
[35]	Chemical reduction of $MnCl_2$ by BuLi	13.1 ± 3.3 nm	α Mn metallic
[36]	Chemical reduction of $MnCl_2$ by lithium sand	2.5 ± 1.5 nm	Metallic
[37]	Sol gel process	10.5 ± 2.5 nm/21 ± 5 nm	Metallic not stable
[39]	Arc plasma under H_2/He	60 nm	Mn_3O_4 core, metallic shell, not stable

Recently, the synthesis of MnNPs (4.3 ± 1.0 nm) has been reported by microwave induced decomposition of the metal carbonyl $Mn_2(CO)_{10}$ in the functionalized IL 1-methyl-3-(3-carboxyethyl)-imidazolium tetrafluoroborate $C_1C_2CO_2HImBF_4$. The presence of the functional group leads to smaller MnNPs with narrower size distribution as compared to those obtained in $C_1C_4ImBF_4$ (under the same conditions the particle diameter is 29 ± 12 nm). Yet, under prolonged storage of the NPs suspension, the size of the NPs decreases to 2.4 ± 0.5 nm, due to a slow redox reaction between reactive surface metal atoms and carboxylic acid which yields some molecular metalcarboxylate complexes and H_2. Consequently, this rather strong interaction of the IL with the NP surface casts some doubt on the oxidation state of MnNPs. However, no further analyses are reported.[40] The reduction of $MnCl_2$, at 200 °C, by *n*-BuLi in the presence of oleic acid as a stabilizer yields air stable α-MnNPs with a mean size of 13.1 ± 0.3 nm. However, powder X-ray diffraction (XRD) as well as X-ray photoelectron spectroscopy (XPS) data for the Mn 2p core level region confirms that the surface of the NPs consists of an oxidized shell, although it is difficult to unambiguously distinguish among the MnO, Mn_2O_3, and Mn_3O_4 oxides. Nonetheless, the XPS spectrum shows a broad Mn $2p^{3/2}$ peak at 641.2 eV, a Mn $2p^{1/2}$ peak at 652.9 eV with peak shapes (including the satellites at

644.1 and 656.5 eV) similar to spectra previously reported for MnO. However, the HRTEM images confirm the presence a crystalline Mn core based on observation of the characteristic (033) and (220) lattice planes.[35] To our knowledge, no decomposition under H_2 of Mn organometallic precursors has been reported in the literature for the synthesis of metallic NPs in IL as a solvent.

III. *In-situ* generated CuNPs in imidazolium based ILs

Barriere and al. have reported the formation of CuNPs at 100 °C from Mesitylcopper (I) (Mes-Cu) under H_2 in organic solvent in the presence of amine as ligand.[6] We repeat this chemical approach in order to generate CuNPs in ILs without any stabilizer.

III.1. Influence of experimental parameters on the size of NPs

Several experimental parameters can influence the size of NPs: stirring, temperature of reaction, and nature of the IL.[41] Some others, such as pressure or precursor concentration could also alter the kinetics of reaction and influence the mechanism of formation of nuclides.[42] For instance, in the synthesis of RuNPs from the organometallic complex (η^4-1,5-cyclooctadiene)(η^6-1,3,5-cyclooctatriene)ruthenium(0), Ru(COD)(COT) in various imidazolium bis(trifluoromethanesulphonyl)imide based ILs: $C_1RImNTf_2$ ($R=C_nH_{2n+1}$ with n=2 ; 4 ; 6 ; 8 ; 10), it has been observed that, in all ILs, i) the size of RuNPs was smaller at 0°C than at 25°C, ii) the stirring induced agglomeration, and iii) the dihydrogen pressure has an influence on the reaction rate. In all conditions, $C_1C_4ImNTf_2$ afforded to the narrowest size distribution of homogenously dispersed RuNPs.[10, 41] Moreover, in $C_1C_4ImNTf_2$, no decantation of the RuNPs suspension was observed after several months under argon atmosphere.[43] Consequently, the first reaction of Mes-Cu under H_2 has been performed under the optimal conditions found for the synthesis of RuNPs. Note that in all experiments, the only side product analyzed by GC-Mass was the mesitylene (Mes-H) distilled from the media under vacuum, Scheme 1.

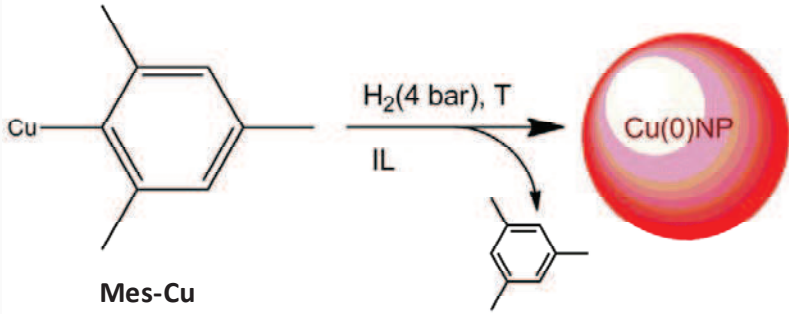

Scheme 1| Reduction of Mes-Cu under H_2.

Influence of the nature of the IL

Two ILs were selected: $C_1C_nImNTf_2$, n = 4 and 6. The synthesis of CuNPs, with a concentration in Mes-Cu of $6x10^{-3}$ M, was carried out at 30°C, under 0.5 MPa of H_2 under stirring. Relatively uniform NPs of 7.5 [3.9; 14.8] nm were obtained in $C_1C_4ImNTf_2$, whereas larger particles with less uniformity were formed in $C_1C_6ImNTf_2$ (14 [7; 30] nm). This is clearly attributed to the influence of the length of the alkyl chain.[10, 41]

Influence of stirring

The same experiment was performed in $C_1C_4ImNTf_2$ without stirring. NPs with narrower size distribution, 7.7 [4.6; 12.9] nm were obtained (Figure 1). Therefore, $C_1C_4ImNTf_2$ in the absence of stirring was selected for further experiments.

Influence of initial concentration of organometallic precursor

When a more concentrated solution of Mes-Cu ($5x10^{-2}$ M instead of $6x10^{-3}$ M) was used in the same conditions, similar NPs were obtained, CuNPs of 7.6 [4.0; 14.1] nm, but some agglomerates were observed. Consequently, the following experimental attempts have been performed with a Mes-Cu concentration equal to $6x10^{-3}$ M.

Influence of dihydrogen pressure

The role of H_2 pressure on the formation of NPs is scarcely reported, although intuitively it is expected that higher H_2 pressure must facilitate the decomposition reaction. Indeed, when the reaction was conducted under a H_2 pressure of 0.9 MPa instead of 0.5 MPa, smaller CuNPs of 6.4 [3.7; 10.9] nm were formed (Figure 1).

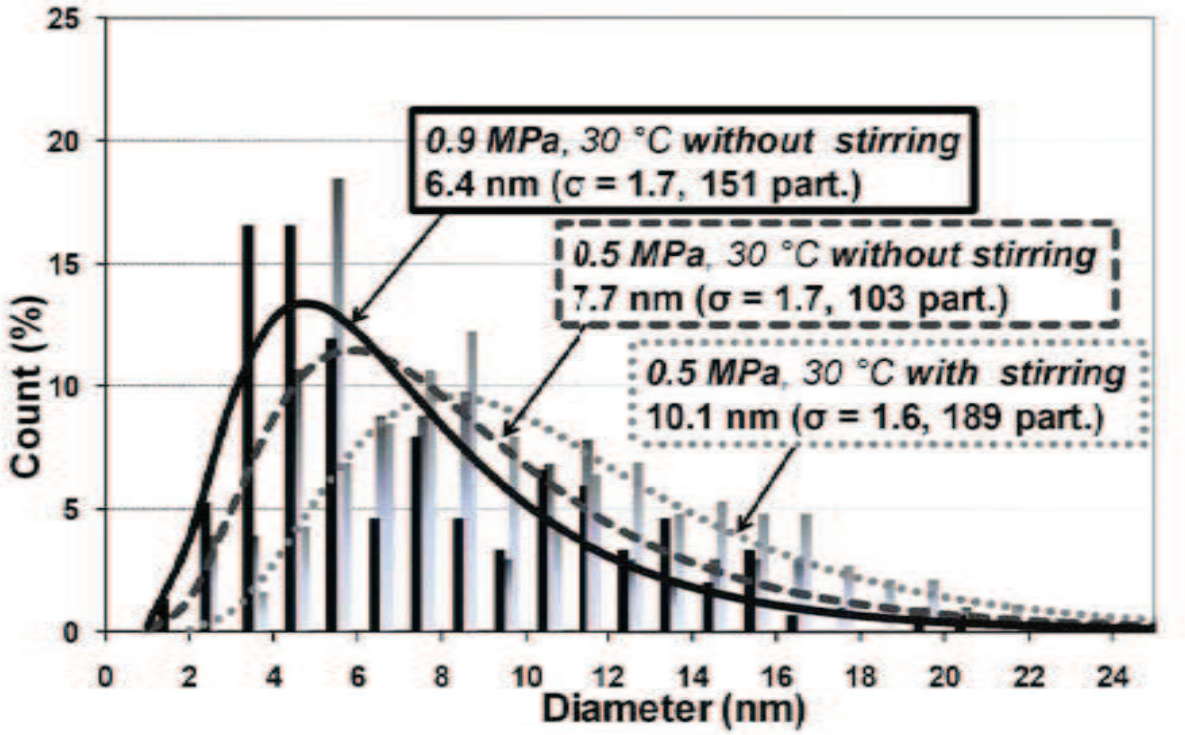

Fig. 1| Size distributions histograms and log-normal fits of CuNPs obtained in $C_1C_4ImNTf_2$ at 30°C under 0.5 MPa of H_2, with and without stirring, and at 30 °C without stirring under 0.9 MPa of H_2.

Influence of temperature

However, all the above results were obtained after one week reaction duration. In order to accelerate the process, the effect of temperature has been studied. Solutions of Mes-Cu ($6x10^{-3}$ M) in $C_1C_4ImNTf_2$, have been heated at 30, 50 and 100 °C under 0.5 MPa of H_2 without stirring. CuNPs were formed in one week at 30 °C, 24 hours at 50 °C and 2 hours at 100 °C. Yet, the evolution of the mean size was not correlated to the temperature, since for the experiment runs at 30 °C, NPs present a mean size of 7.7 [4.6; 12.9] nm versus 14 [16; 25] nm for NPs synthesized at 50 °C. The effect of temperature on the size of CuNPs

already reported is the inverse in ILs to that observed in a THF/MeOH mixture in which low temperatures favor large particle size whereas high temperatures favor small particle size. [41, 44]

Surprisingly, at 100 °C, small CuNPs with a narrow size distribution of 8.5 [5.1; 14.0] nm were observed, with shortest reaction time.

Most of collected information through these different experiments highlights the impact of the reduction rate of Mes-Cu on the size of NPs. High pressure of H_2, high temperature, low concentration seem favor smaller NPs, so these conditions were retained for further experiments.

III.2. Understanding the synthesis of CuNPs in IL

Optimization of the synthesis of CuNPs

From the above results, the reaction has been reproduced with a Mes-Cu concentration of $6x10^{-3}$ M in $C_1C_4ImNTf_2$, at 100°C, under **0.9 MPa of H_2** without stirring. After 2 h, CuNPs with a mean size of ~ 4.5 nm were repeatedly obtained (4.5 [3.1; 6.5] nm). Remarkably, the decrease of reaction time from two to one hour afforded larger CuNPs (7.4 [5.6; 9.9] nm) (Figure 2).

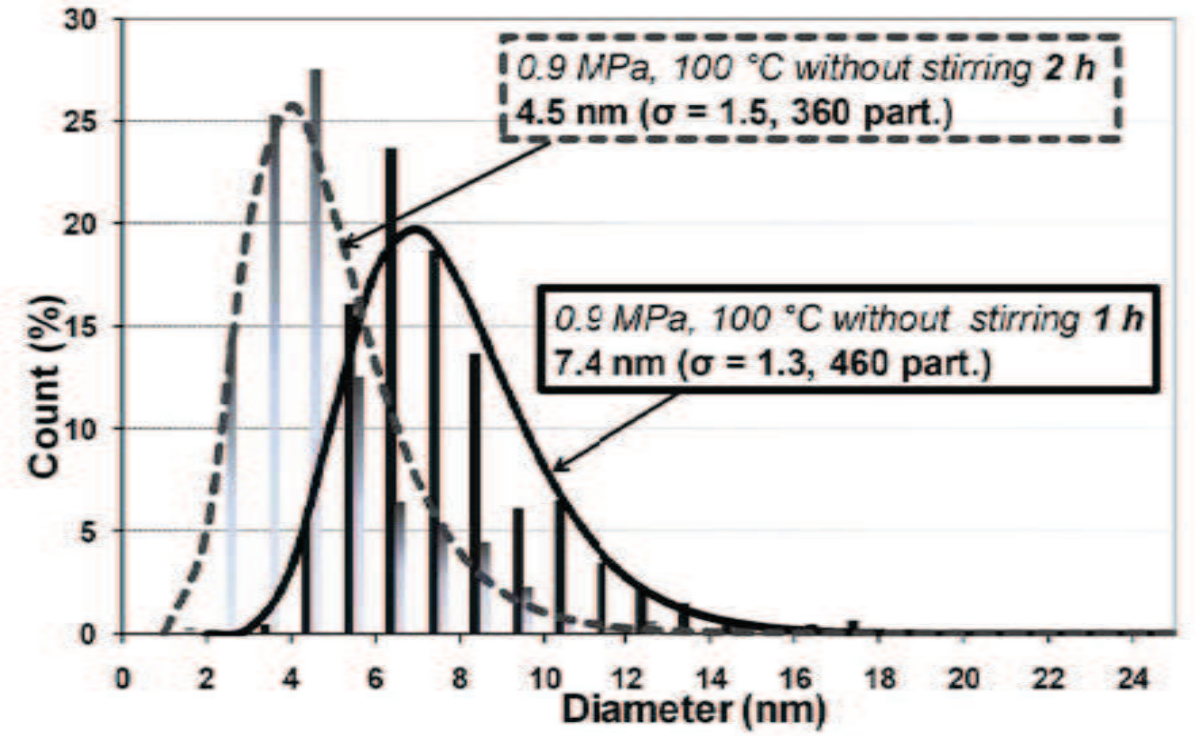

Fig. 2| Size distributions histograms and log-normal fits of CuNPs obtained in $C_1C_4ImNTf_2$ under 0.9 MPa of H_2 without stirring at 100 °C, with reaction durations of one and two hours.

Stability of CuNPs suspensions

In a glove box under argon atmosphere, the CuNPs flocculate within a few days. It is nevertheless possible to re-disperse them in the IL without significant change of their size. There is consequently no irreversible agglomeration or coalescence of these NPs. This could be due to a small ionic layer that stabilizes the CuNPs as observed by Richter and co-workers.[45]

When an amount of water is added to a stable suspension of CuNPs in IL, TEM images show the agglomeration of the NPs, supporting the fact that the CuNPs (as RuNPs) are originally isolated from the 3D network of ionic channels.[46] (Chapter I) It is clear that before coalescing the NPs must agglomerate, so preventing agglomeration has an indirect influence on the stability.[43]

Mechanism of formation

From the investigation of the effect of different reaction conditions (reaction temperature, concentration of the precursors, H_2 pressure) on the size distribution of NPs, we observe that the size control achieved in this system is of purely kinetic nature. This observation could be related to the mechanisms of formation of NPs from nuclides.[42] It has been demonstrated that NPs formed from organometallic precursors in different experimental conditions (reaction temperature, concentration of stabilizing agents, ratio between precursors, etc.) nucleate and grow to their final size at an early stage of the synthesis with no Ostwald ripening observed upon further heating. In this case, the nanocrystals size can be controlled only via proper balance between the rate of nucleation and the rate of growth from the molecular precursors.[42] Generally, a faster nucleation leads to more particles of smaller size, while a slower nucleation gives fewer particles of larger size.[42, 47, 48] In the case of Ru(COD)(COT), the decomposition is fast allowing rapid formation of nuclides by decomposition of OM and nucleation of these nuclides. This allows the synthesis of small NPs with controlled size (2.4 [2.1; 2.8] nm at 30°C under 0.5 MPa of H_2).[41] With Mes-Cu, there is a slow reduction of the precursor allowing a possible reaction of Mes-Cu on nuclides or NPs already formed. In this case, larger NPs are obtained with a very poor control of the size (7.6 [4.0; 14.1] nm at 30°C under 0.5 MPa of H_2).

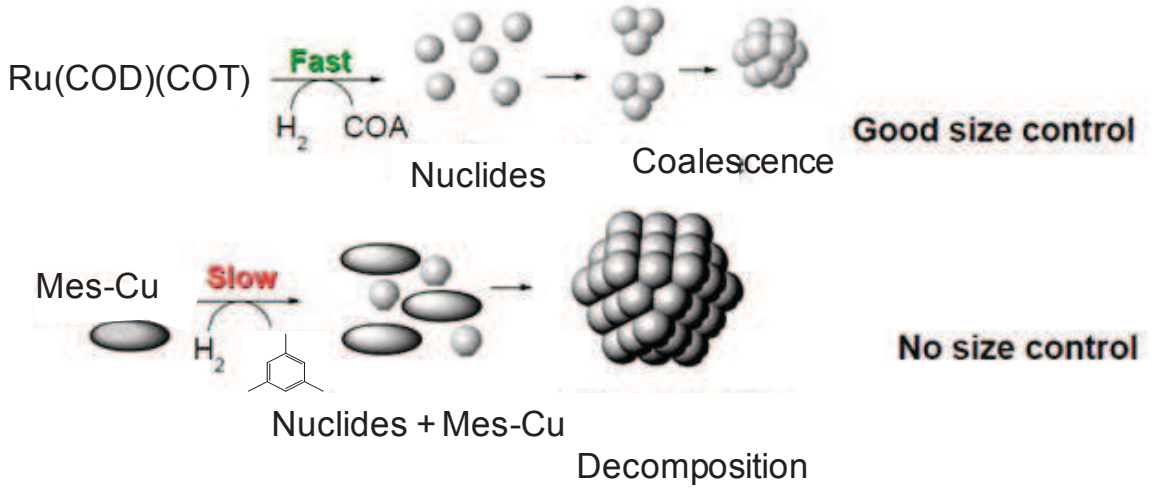

Fig. 3| Mechanism of synthesis of NPs. If the reaction is fast, formation of size controlled NPs; if the decomposition is slow, poor size control of NPs. (Adapted from reference [42])

In our case, after one hour at 100 °C, the reduction of Mes-Cu was not complete. Consequently, at the end of the experiment, when H_2 atmosphere was replace by argon, the medium contained a mixture of unreacted Mes-Cu and CuNPs. Under storage of the suspension, the residual Mes-Cu could be slowly reduced on the surface of CuNPs leading to larger NPs. This hypothesis is supported by the fact that when nanocrystals grow by consuming molecular precursors from surrounding solution, the size of smaller particles increases faster than that of the larger ones. In this case, the increase of the mean particle size is accompanied by a narrowing of the initial particle size distribution. Figure 2 shows that the particle size distribution decreases from $\sigma = 1.5$ to 1.3 when the CuNPs size increases. After a two hour reaction, there is less OM available at the end of the experiment, and the CuNPs remain small. Hence, even if critical size and free energy barriers continue to be central concepts describing the formation of NPs (Figure 4), potential mechanisms for controlling the process appear to be greater in number and diversity. And the kinetics of attachment and detachment become of equal importance in determining growth rates and crystal shapes. Consequently, the kinetic coefficient shows a clear scaling with molecular size.[49]

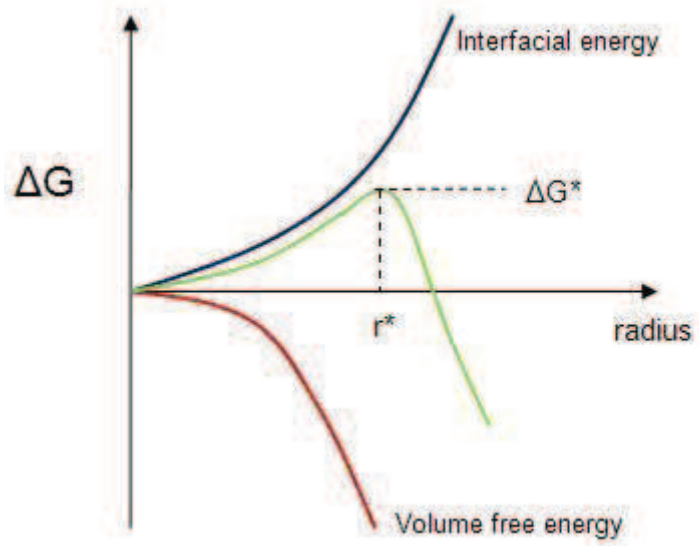

Fig. 4| Competition between nucleation and growth of crystals. r* corresponds to the critical radius with dissolution of grain formed behind it.[49]

III.3. Characterization of CuNPs

Cu NPs ~ 5 nm should provide a surface Plasmon resonance between 500 and 600 nm.[15, 45, 50] Several UV-vis analyses has been performed but no surface plasmon resonance has been observed due to high absorption at high wavelength, which could be due to agglomeration of CuNPs in presence of water, or to their oxidation during analysis.[43]

X-Ray photoelectron spectroscopy (XPS) analysis

In order to determine the oxidation state of the CuNPs, X-Ray photoelectron spectroscopy (XPS) and X-Ray Auger electron spectroscopy (XAES) have been performed. Due to the weak concentration of the solution and the limited escape depth of the photoelectrons in the solution, no peaks corresponding to Cu binding energies were observed when the analyses were carried out directly on the CuNPs/IL suspension. Samples were therefore prepared by filtering the CuNPs onto filter paper under inert atmosphere and eliminating as much IL as possible, by washing under dry acetonitrile. One has to mention that IL was still present on

the support after filtration because F, S and N atoms were detected.[11] However, this residual IL was not in sufficient quantity to totally hide the signal from the support.

The Cu $2p_{3/2}$ peak is located at 932.4 eV for Cu_2O instead of 932.5 eV for metallic Cu, Figure 5a. In Figure 5b obtained from Moulder and co-workers, the Cu $2p_{3/2}$ peak comprises two contributions with binding energies at 932.3 and 933.3 eV.[51] The additional peak around 943 eV (orange line) in the Cu $2p_{3/2}$ is an indication of CuO, this shake up is due to the open 3d shell of Cu^{2+}.[52, 53] The energetic peak position for the Cu $2p_{3/2}$ around 933.3 eV is in very good agreement with the value given in the literature for CuO.[53] The structure at 932.3 eV could be either assigned to clean copper or to copper in Cu_2O. In vacuum CuO can be easily reduced to Cu_2O.[53]

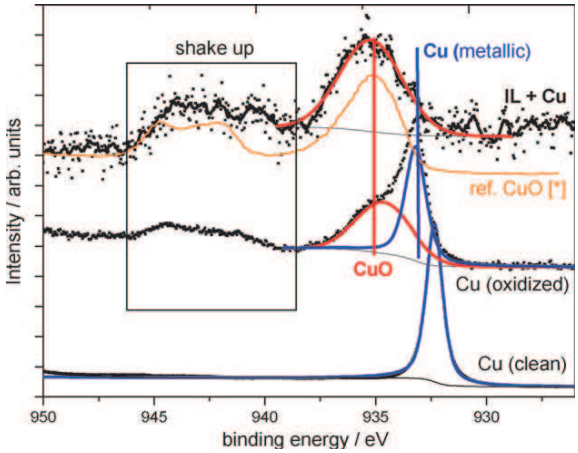

Fig. 5| XPS spectra of Cu $2p_{3/2}$ region of Cu.[51]

It has been shown that a combined study of XPS (Binding energy) and X-Ray Auger electrons spectroscopy (XAES) (Kinetic energy) lines is suitable to determine the chemical state of copper species and distinguish between Cu metal, Cu_2O and CuO.[54] In the Cu LMM Auger spectra, kinetic energies of $2p_{3/2}$ from CuO and Cu are significantly different.

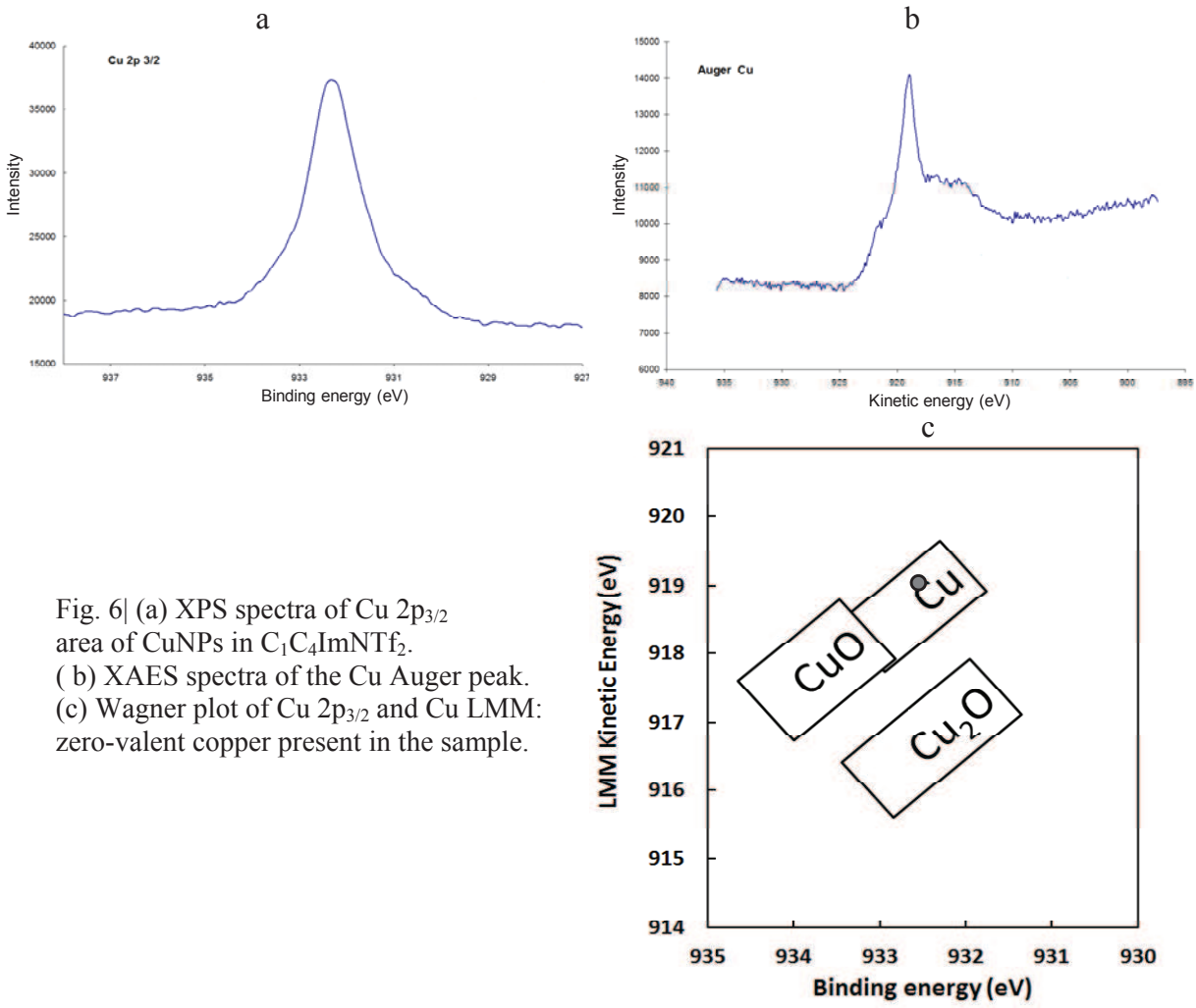

Fig. 6| (a) XPS spectra of Cu $2p_{3/2}$ area of CuNPs in $C_1C_4ImNTf_2$. (b) XAES spectra of the Cu Auger peak. (c) Wagner plot of Cu $2p_{3/2}$ and Cu LMM: zero-valent copper present in the sample.

The resulting Wagner plot reporting the kinetic energy of the measured Cu LMM Auger peak (918.9 eV) as a function of the binding energy of the $2p_{3/2}$ (932.3 eV) line is depicted in Figure 6c. The position of the copper chemical state in the Wagner plot clearly indicates a metallic state for copper.[55, 56] Moreover, the shape of the Cu LMM XAES line is nearly identical to those already observed for copper metal.[57] In our case, clearly different spectra are observed, as compared to those obtained by Moulder et al., confirming the fact that metallic Cu is formed.[51]

High Resolution Transmission Electron Microscopy (HRTEM)

The last analysis is the high resolution TEM (HRTEM). The picture clearly shows the presence of crystalline CuNPs. Metallic copper is detected in several NPs indicated by the interplanary distance of 0.21 nm, which corresponds to the 111 direction in the face-centered cubic metallic copper.[58] By comparison with Cu_2O, no distance of 0.21 nm could be obtained.[58] Nevertheless, two distances and one angle are necessary to unambiguously describe the crystalline structure of the NPs.

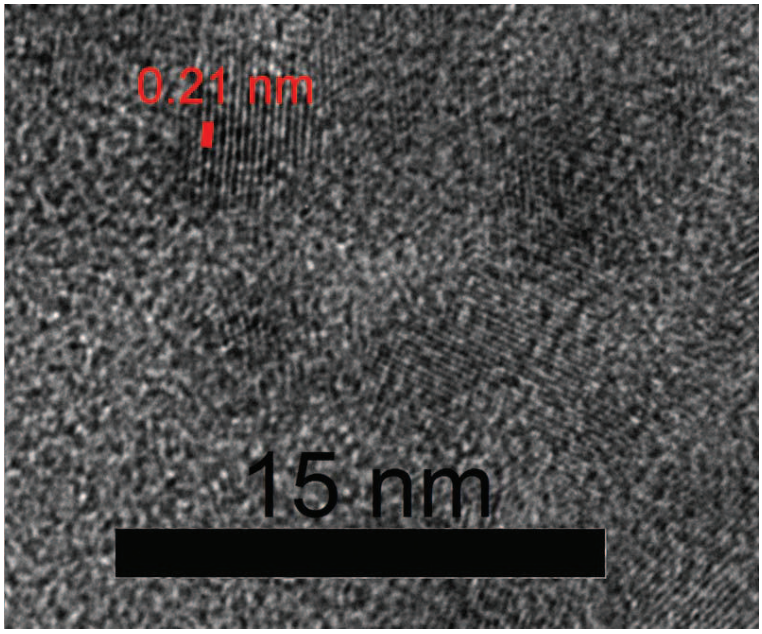

Fig. 7| HRTEM picture of CuNPs obtained after two hours.

III.4. Conclusion

In this study, we have investigated a new route for the synthesis of copper NPs, with controlled size, without contaminating ligands, by a liquid process under mild conditions. CuNPs were successfully synthesized from Mes-Cu in solution of $C_1C_nImNTf_2$ with n = 4 and 6. Several parameters were examined: the nature of IL, stirring, H_2 pressure and temperature. Under optimal conditions, well dispersed CuNPs of 4.5 nm with narrow size distribution were

obtained. The results of both HRTEM and XPS analyses indicate that crystalline metallic zero-valent CuNPs are obtained.

The resulting stable suspensions of Cu(0)NPs are promising starting materials to form conformal copper seed layers in high aspect ratio interconnect structures.

IV. *In-situ* generated MnNPs in imidazolium based ILs

Two routes have been developed to form MnNPs in ILs: i) from commercial Mn CVD precursors known to decompose at temperature up to 200 °C, ii) from the decomposition under H_2 of Mn organometallic precursors such as bis(neopentyl) manganese(II) ($MnNp_2$), which has never been reported in the literature to our knowledge.

IV.1. Synthesis of manganese nanoparticles from CVD precursors

Several manganese CVD precursors are commercially available, Table 2.

Table 2| CVD precursors commercially available from Sigma Aldrich.

Formula	CAS number	State	TSC
$C_{10}H_7MnO_4$	12116-28-8	Solid	41-46
$Mn(C_5H_4C_2H_5)_2$	101923-26-6	Liquid	80
$Mn(C_5(CH_3)_5)_2$	67506-86-9	Solid	230 (dec)
$C_{18}H_{26}Mn$	101932-75-6	Solid	98-112
$BrMn(CO)_5$	14516-54-2	Solid	
$C_5H_5Mn(CO)_3$	12079-65-1	Solid	72-76
$C_2H_5C_5H_4Mn(CO)_3$	12116-56-2	Liquid	245
$Mn_2(CO)_{10}$	10170-69-1	Solid	154

TSC: Temperature of state change

A yellow solution of manganese carbonyl $Mn_2(CO)_{10}$ ($5x10^{-2}$ M) in $C_1C_4ImNTf_2$ was treated under 0.5 MPa of H_2 at 100 °C in a procedure based on the one develop to synthesize CuNPs. No change in the color was observed as MnNPs should produce. This solution was then heated up to 120 °C, decomposition temperature of $Mn_2(CO)_{10}$ under vacuum. After 3 days of reaction, the solution becomes black.[59, 60] TEM pictures show large aggregates of NPs with a mean diameter of 21 nm, Figure 8.

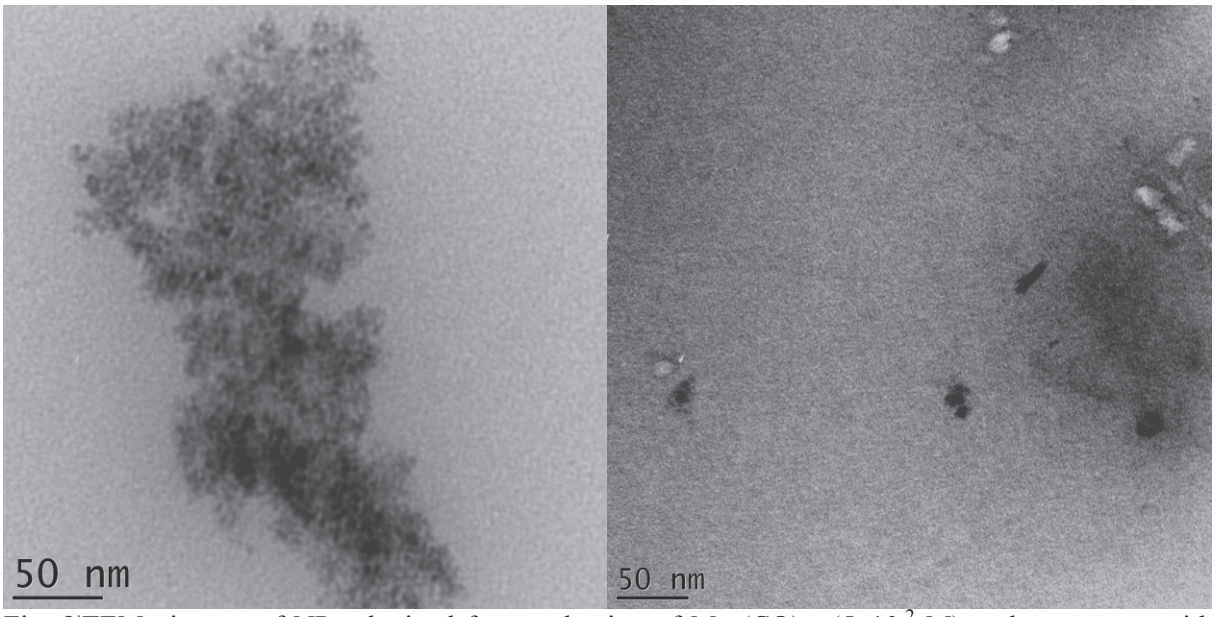

Fig. 8|TEM pictures of NPs obtained from reduction of $Mn_2(CO)_{10}$ ($5x10^{-2}$ M) under vacuum, with stirring at 120 °C in $C_1C_4Im\ NTf_2$ during three days.

With methylcyclopentadienyl manganese tricarbonyl (η^5-$MeCpMn(CO)_3$) in $C_1C_4ImNTf_2$, whatever the experimental conditions (temperature between 30 and 120 °C, 0.5 and 0.9 MPa of H_2), **no** NPs could be obtained. This OM compound is too stable, probably due to the presence of the CO ligands. Some examples of the thermal decomposition of carbonyl derivatives affording metallic NPs, are reported, generally there is **no** NP size control. Moreover, the CO ligand stays on the NPs surface or forms a carbon deposit.[61] For these reasons, as confirmed by our experiments with $Mn_2(CO)_{10}$ and η^5-$MeCpMn(CO)_3$, carbonyl-based OM precursors were not further considered in this study. Indeed, based on results with Cu, the synthesis of bimetallic Mn-CuNPs will require a higher temperature (100 °C).

Instead, bis(ethylcyclopentadienyl) manganese (II) ($(EtCp)_2Mn(II)$) (red liquid) was dissolved in 2 mL of $C_1C_4ImNTf_2$ affording an orange solution at a concentration of $1.1x10^{-2}$ M. Without stirring, this solution has been treated during 3 days in different conditions of temperature and H_2 pressure, Table 3. NPs have been formed in all conditions. The NPs suspensions have been analyzed with TEM imagery. Clearly the NPs size increases

with pressure and temperature. Moreover, the NPs size mainly remains under 5 nm. Given these properties, ($(EtCp)_2Mn(II)$) is a good candidate for synthesis of MnNPs. However, the kinetics of decomposition have not been further tested.

At this temperature, $(EtCp)_2Mn$ is in gaseous form and thus it should be difficult to form bimetallic NPs while precursors could be separated during decomposition. No further attempts have been performed in this way.

Table 3| Attempts to synthesize MnNPs from decomposition of $(EtCp)_2Mn$ in $C_1C_4ImNTf_2$.

Experiment	Pressure	Temperature	Color after reaction	Mean Size
MnCVD-LP-LT-1	0.4 MPa	30 °C	Brown	3.3 [2.5; 4.4] nm
MnCVD-LP-LT-2	0.4 MPa	30 °C	Brown	4.1 [3.0; 5.6] nm
MnCVD-HP-LT	0.9 MPa	30 °C	Brown	3.6 [2.4; 5.2] nm
MnCVD-HP-HT	0.9 MPa	70 °C	Brown	5.3 [3.7; 7.7] nm

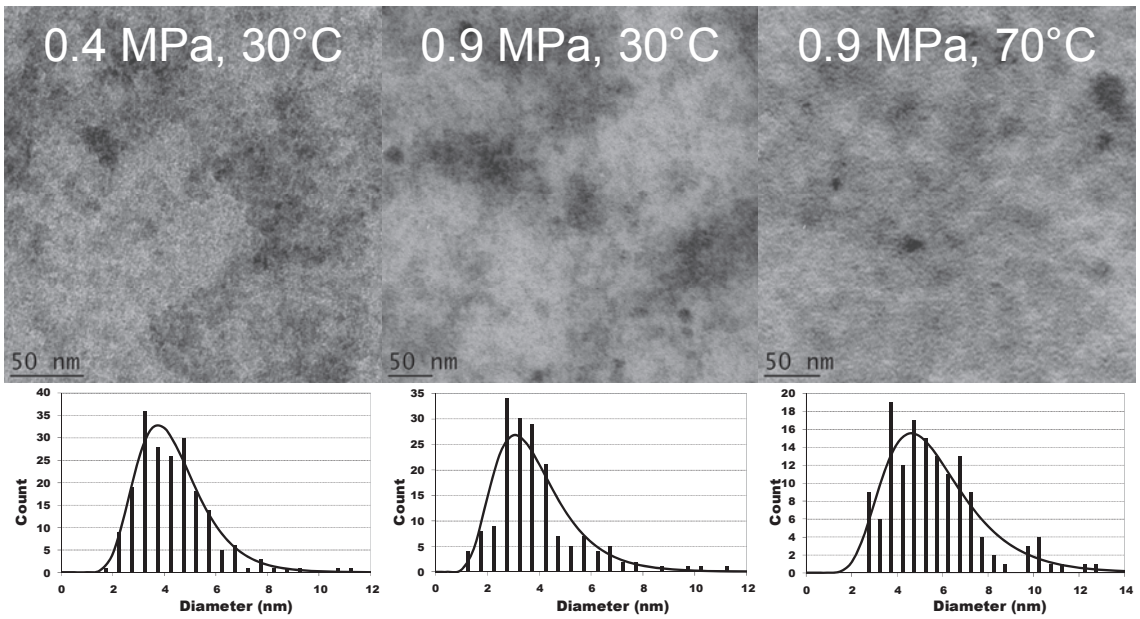

Fig. 9|TEM pictures and size distribution histogram of NPs obtained from reduction of $(EtCp)_2Mn(II)$ ($1.1x10^{-2}$ M) during three days.

IV.2. Synthesis and stability of alkyl manganese

Alkyl manganese precursors were synthesized from the reaction of a Grignard reagent on manganese salt as chloride, Table 4.[62]

Table 4| Synthesis of Mn organometallic precursors as described by Tamura[62]

Reaction	Solvent	Molar Ratio	Temp (°C)	Isolated
Alkylmanganese species from Grignard reagents and manganous chloride				
$CH_3MgBr + MnCl_2 \rightarrow CH_3MnCl + MgBrCl$	THF	1/1	25	No
$CH_3MnCl + CH_3MgBr \rightarrow (CH_3)_2Mn + MgBrCl$	THF	1/2	25	Yes
Mechanism of decomposition of alkylmanganese species				
$(CH_3CH_2CH_2)_2Mn \rightarrow CH_3CH=CH_2 + HMnCH_2CH_2CH_3$				
$HMnCH_2CH_2CH_3 \rightarrow CH_3CH=CH_2 + Mn\ H_2$				
$MnH_2 \rightarrow Mn° + H_2$				

Nevertheless, only a few of the compounds depicted in this work could be isolated in large amount. The other known alkyl- or arylmanganese compounds are stabilized by ligands such as CO [63] or chloride *e.g.* [2,6-bis[2,6-(i-Pr)$_2$PhNd=C(Me)]$_2$(C_5H_3N)]$MnCl_2$ which in presence of 4 equivalent of MeLi affords metallic manganese.[63, 64] There is nevertheless high probability that chloride atoms remain on the surface of NPs.[64]

The (η^5-C_5H_5)Mn(C_2H_5)$_3$ decomposes at 60 °C under H_2.[65] However, its synthesis needs the use of a toxic cadmium intermediate. Pure diphenylmanganese and dimesitylmanganese are also reported. However, the dimesitylmanganese is trimeric MesMn(μ-Mes)$_2$Mn(μ-Mes)$_2$MnMes and the diphenylmanganese has a polymeric structure $(MnPh_2)_\infty$. Finally, we retained two precursors: bis(bis(trimethylsilyl)amido)manganese(II) and bis(neopentyl) manganese(II).[66-68]

IV.3. Synthesis of bis(bis(trimethylsilyl)amido)manganese(II)

Bis(bis(trimethylsilyl)amido)manganese(II), cannot be considered as an OM precursor. We selected it, because its iron analogue bis(bis(trimethylsilyl)amido)iron(II) has been widely used to generate FeNPs under H_2 atmosphere.[69] Moreover, the hydrogenolysis of

bis(bis(trimethylsilyl)amido)manganese(II) yields amine ligands, which are known to stabilize the resulting NPs in both organic solvents and ionic liquids.[44, 70]

The bis(bis(trimethylsilyl)amido)manganese(II) was synthesized from anhydrous manganese dichloride. The latter was obtained by the reaction of commercial manganese chloride with the chlorotrimethylsilane, Scheme 2.[71] Then, the reaction of lithium bis(trimethylsilyl)amide on anhydrous manganese dichloride under inert conditions afforded a black mud from which the expected compound which was distilled at 112-120 °C, Scheme 3.[66, 72]

$$MnCl_2.xH_2O + 2x\ (CH_3)_3SiCl \rightarrow MnCl_2 + [(CH_3)_3Si]_2O + 2x\ HCl$$

Scheme 2| Synthesis of anhydrous manganese dichloride.

$$MnCl_2 + 2\ LiN(SiMe_3)_2 \rightarrow Mn[N(SiMe_3)_2]_2 + 2\ LiCl$$

Scheme 3| Synthesis of Bis(bis(trimethylsilyl)amido)manganese(II).

IV.4. NPs from Bis(bis(trimethylsilyl)amido)manganese(II) under dihydrogen

A solution of $5x10^{-2}$ M of ($C_{12}H_{36}Si_4N_2Mn$) in $C_1C_4ImNTf_2$ was treated in autoclave under 0.9 MPa of H_2 at 100 °C during three days. No color change was observed, although, TEM analysis indicate that NPs with wide distribution and a mean size of 5.3 [3.9; 7.1] nm have been obtained. Moreover, large aggregates were observed on TEM grids. Unanticipated, the presence of amine had no effect on the stabilization and the size control of the MnNPs. This precursor was consequently not considered for further experiments.

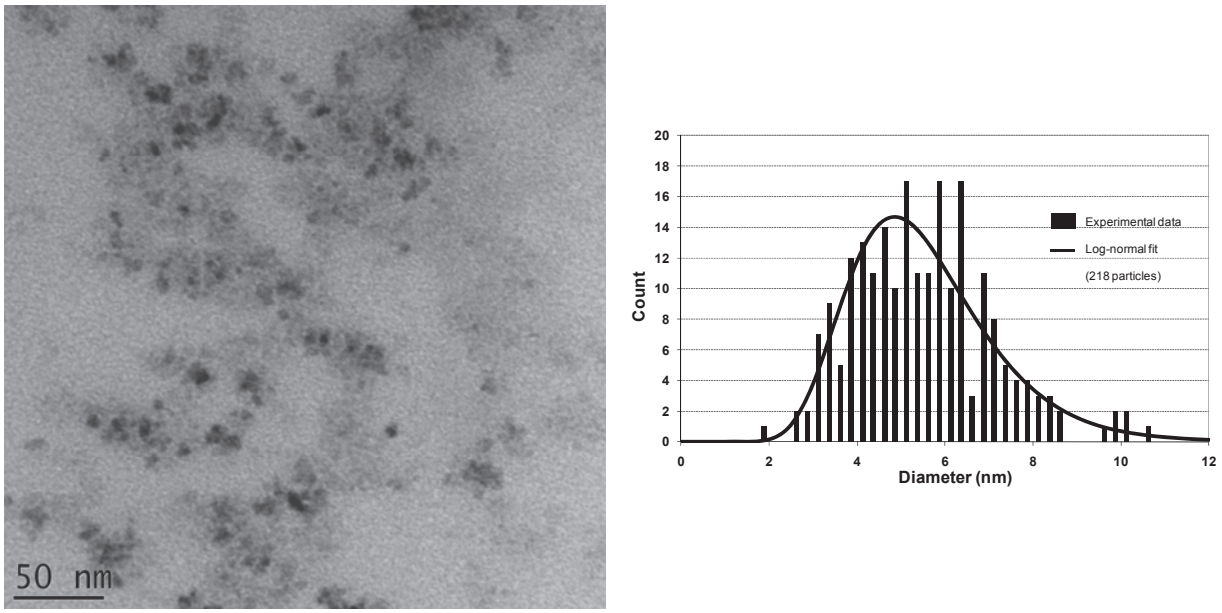

Fig. 10| TEM picture and size distribution histogram of MnNPs obtained from reduction of $C_{12}H_{36}Si_4N_2Mn$, $5.0x10^{-2}$ M under 0.9 MPa of H_2 at 100 °C in $C_1C_4Im\ NTf_2$ during three days.

IV.5. Synthesis of bis(neopentyl) manganese(II)

The bis(neopentyl) manganese(II) $Mn(^tBuCH_2)_2$, referred as to $MnNp_2$, is synthesized by the reaction of bis neopentyl magnesium on anhydrous manganese dichloride.[67] The solution of neopentylmagnesiumchloride in tetrahydrofuran (THF) was prepared by the reaction of neopentyl chloride with metallic magnesium. The titration of [Mg(Np)Cl] in diethyl ether was determined by addition of a solution of benzyl alcohol (1 M) in THF in the presence of 2,2 bisquinoleine. Then, the stoichiometric amount of dioxane was added yielding bis(neopentyl)magnesium in solution in THF and precipitation of chloride magnesium salt, Scheme 4.

$$Mg + NpCl \rightarrow Mg(Np)Cl$$

$$2\ Mg(Np)Cl + dioxane \rightarrow Mg(Np)_2 + MgCl_{2(dioxane)}$$

$$Mg(Np)_2 + MnCl_2 \rightarrow Mn(Np)_2 + MgCl_2$$

Scheme 4| Synthesis of bis(neopentyl)magnesium

After filtration of $MgCl_2$, the required volume of this solution was added to a solution of anhydrous $MnCl_2$ in degassed toluene. The obtained grey solution was kept under stirring two days at room temperature, until the solution became grey-brown. The solvents were removed under vacuum, and $MnNp_2$ was extracted from residual solid with pentane. The evaporation of pentane yielded a brown powder which was dried under high vacuum then kept in freezer of a glove box, Scheme 5.

$$MnCl_2 + MgNp_{2(dioxane)} \rightarrow MnNp_2 + MgCl_{2(dioxane)}$$

Scheme 5| Synthesis of bis(neopentyl) manganese.

IV.6. Hydrogenolysis of $MnNp_2$ in continuous flow reactor

In a 100 mL autoclave connected to a continuous flow reactor, a solution (4 mL) of $MnNp_2$ ($5x10^{-2}$ M) in $C_1C_4ImNTf_2$ was treated under H_2 (0.4 MPa) at 100 °C, Figure 11.

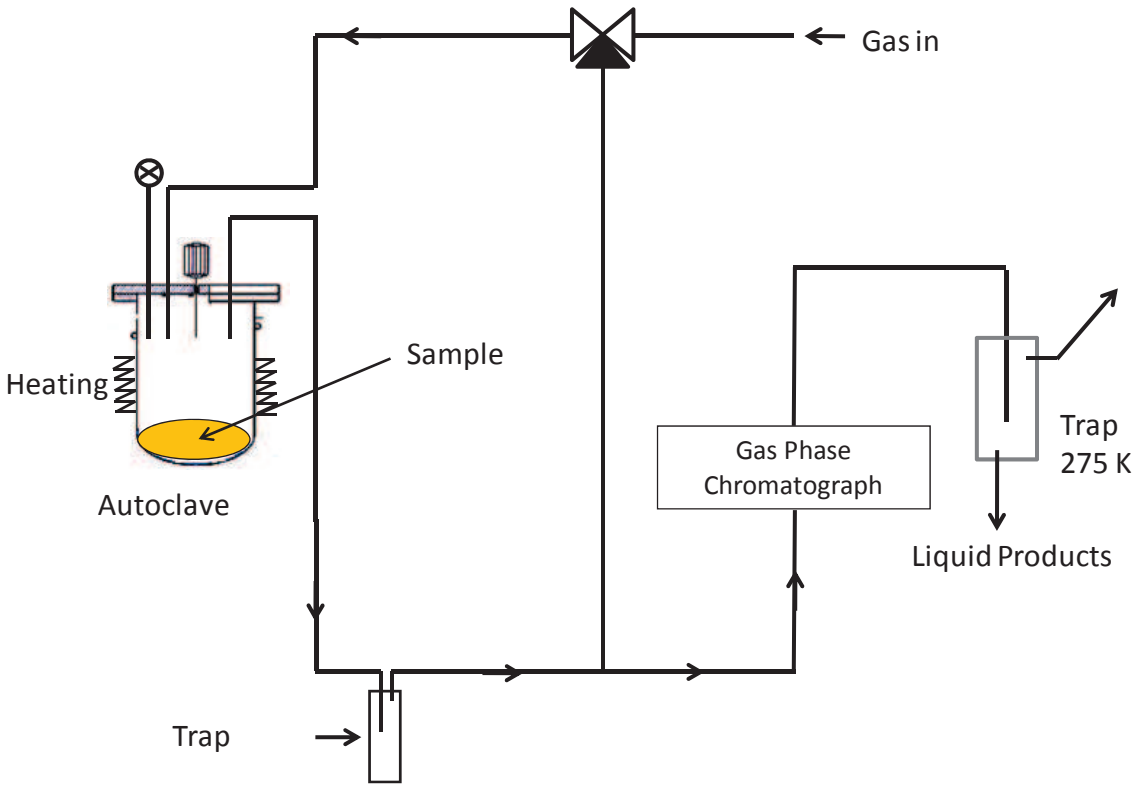

Fig. 11| Scheme of the circuit and autoclave used.

First, the reactor was heated up to 100 °C. Evolved gases were continuously analyzed by gas chromatography. Below 100 °C, only neopentane was detected. This could be due either to a partial hydrolysis due to residual humidity in the reactor and / or to a slight decomposition of $MnNp_2$ with temperature. At 100 °C, GC analysis of the formed volatiles was performed every 6 min. Figure 12 indicates the instantaneous concentration of products as compared to the concentration of metal.

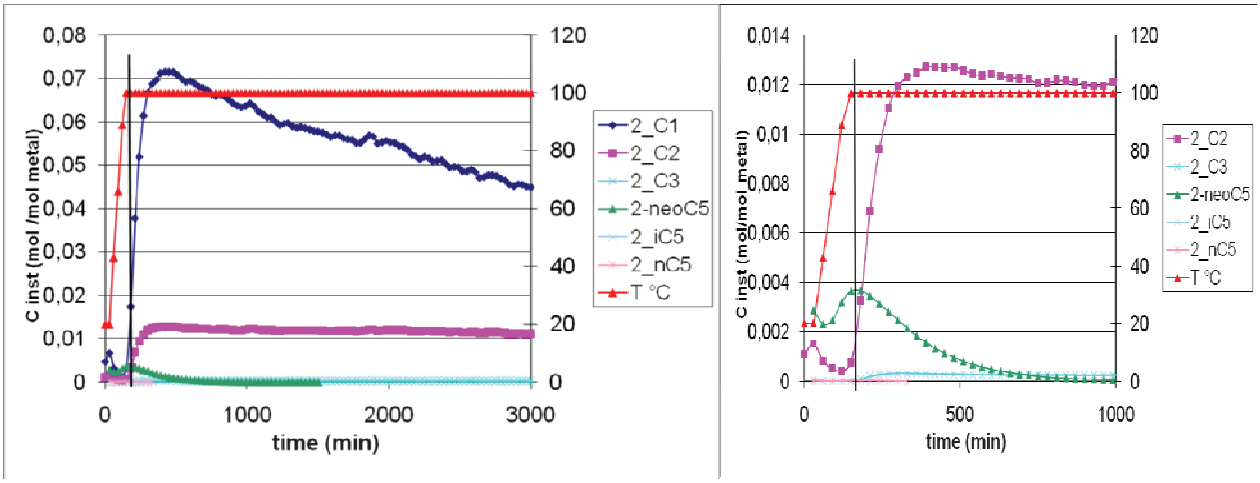

Fig. 12| Instantaneous concentration of products detected by GC as compared to initial concentration of metal.(left, total spectra) (right a focus of the first 1000 min).

After 3000 minutes, the equivalent of 8.5 C / Mn (*i.e.* 1.7 Np ligand over 2) is evolved as alkanes (mainly: methane C_1, ethane C_2, neopentane $neoC_5$ and propane C_3). $MnNp_2$ reacts with dihydrogen to form manganese hydride bond(s) which activate(s) the C-H bonds of neopentane via a σ-bond metathesis reaction. The formation of C_1, C_2 and C_3 is due to successive C-H activation alkane and C-C activation of the alkyl groups via β-methyl migration steps, Scheme 6. This kind of result has been largely reported in hydrogenolysis of alkyl metal.[73]

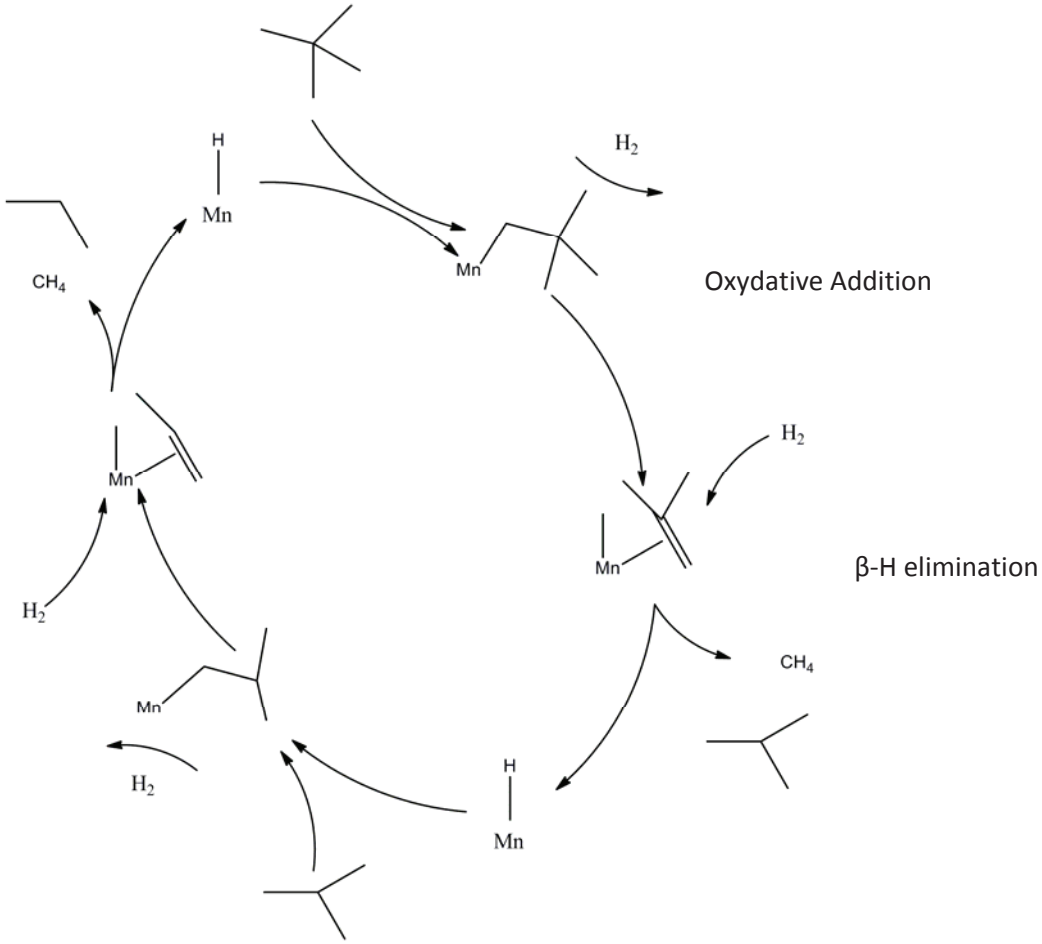

Scheme 6| Alkane Hydrogenolysis of neopentane on Mn hydride.

It is worth to note that after 24 hours at 100 °C, $MnNp_2$ is only partially hydrogenolized since unreacted precursor (~ 15 %) is still present. This could be due to a weak dissolution of H_2 in the IL, which is governed by the diffusivity.

IV.7. Synthesis of MnNPs from $MnNp_2$

Based on the results described above, a yellow solution of $MnNp_2$ ($5x10^{-2}$ M) in $C_1C_4ImNTf_2$ has been treated during 48 h under different experimental conditions; LT: 30 °C; MT: 50 °C; HT: 100 °C and LP: 0.4 MPa of H_2; HP: 0.9 MPa of H_2. TEM analysis of the very dark suspensions formed shows that NPs are obtained in all cases. Table 5 summarizes these results.

Table 5 | Summary of attempts to synthesize MnNPs from MnNp2.

Attempt	Repetition 1	Δ	Repetition 2	Δ	Color
Mn-LT-LP	2.7 [1.9; 3.7] nm	10	1.8 [1.4; 2.3] nm	3	Black
Mn-MT-LP	4.1 [2.9; 5.8] nm	10	1.6 [1.1; 2.3] nm	3	Black
Mn-HT-LP	***1.4 [0.8; 2.5] nm***	***3***	***1.6 [1.1; 2.3] nm***	***3***	***Black***
Mn-LT-HP	1.1 [0.8; 1.7] nm	10	1.9 [1.3; 2.7] nm	3	Brown
Mn-MT-HP	1.4 [0.8; 2.4] nm	10	2.2 [1.7; 2.8] nm	3	Brown
Mn-HT-HP	Rods ~ 50nm	15	Rods ~ 50nm	3	Brown

Δ: Time interval in days between the synthesis and the analysis of MnNPs
LT: 30 °C; MT: 50 °C; HT: 100 °C.
LP: 0.4 MPa of H_2, HP: 0.9 MPa of H_2.

In the LP experiments, NPs show a mean size ~ 2 nm. Nevertheless, besides the run Mn-HT-LP (at 100 °C, 0.4 MPa), the results are no repeatable. Moreover, we observe that the time interval (Δ) between the end of the synthesis and the TEM analyses alters the MnNPs mean size, increasing of (Δ) induces increasing of MnNPs mean size. Consequently, the only reproducible experiments Mn-HT-LP also have the same Δ.

In extreme case (Mn-HT-HP), large rods (≈ 50 nm length) are even formed. Therefore, it appears that a high H_2 pressure compromises size control of MnNPs.

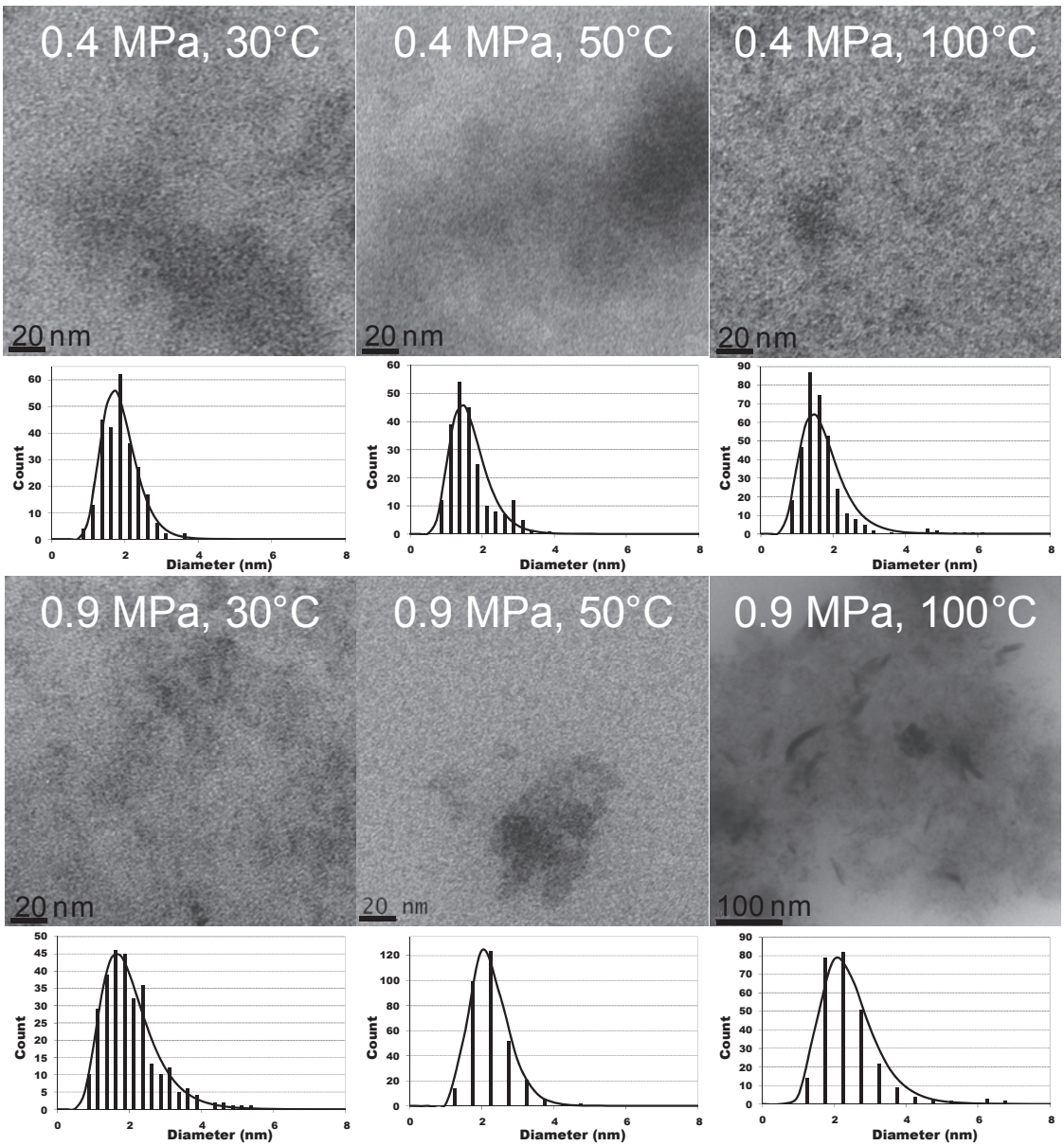

Fig. 13| TEM pictures and size distribution histograms of MnNPs obtained in different condition from $MnNp_2$.

IV.7.i. Optimization of the synthesis procedure: effect of reaction time

In a second series of experiments, $MnNp_2$ solutions ($5x10^{-2}$ M) in $C_1C_4ImNTf_2$ have been treated at 100 °C under 0.4 MPa of H_2 for 1, 2, 6, 24 and 48 h. At the end of the reaction, the medium has been analyzed after similar time interval (Δ). All runs afford NPs with mean size decreasing as the reaction time increases, Figure 14.

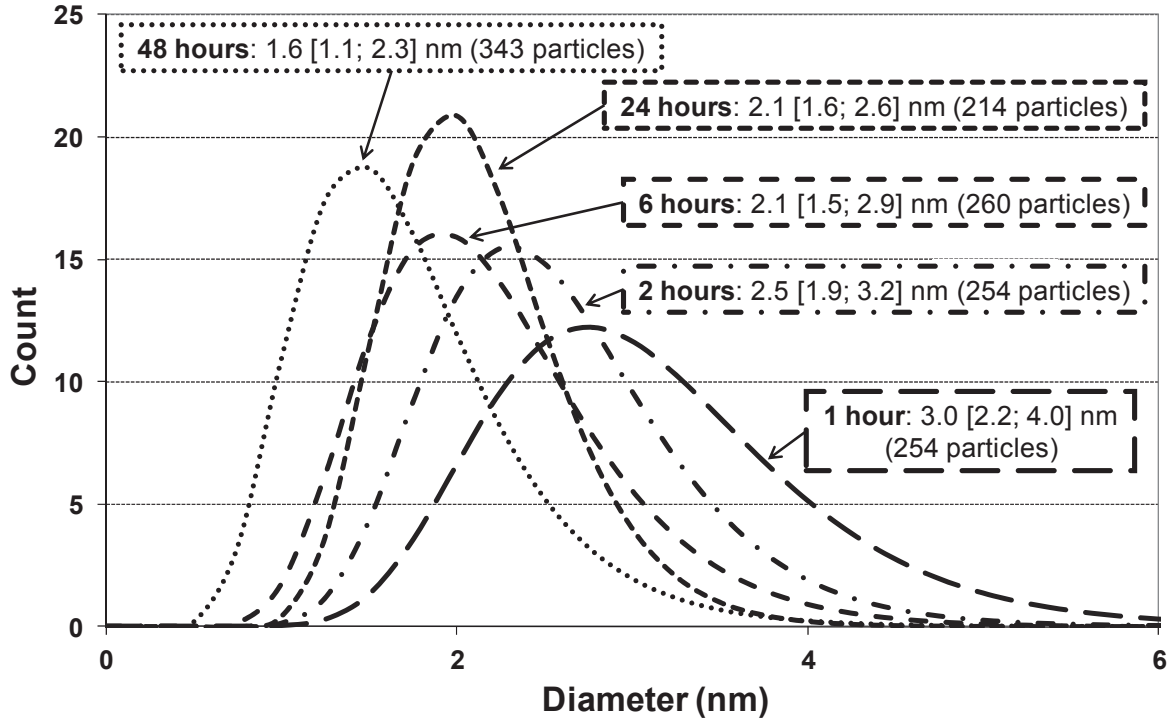

Fig. 14| Evolution with reaction duration of size distribution of MnNPs obtained at 100 °C under 0.4 MPa of H_2 without stirring.

Note that when a suspension of ~3 nm NPs obtained after one hour (Kin-1h-HT-LP) is next kept 23 h at 100°C under 0.4 MPa of H_2, a large increase of the size of NPs 4.1 [3.1; 5.4] nm is observed. This could suggest that i) in the experiments run with longer reaction time, the small NPs are not form from large ones, ii) the agglomeration of MnNPs under H_2 is favored contrarily to RuNPs stabilized due to the presence of surface Ru-H bonds.[43]

IV.7.ii. Optimization of the synthesis procedure: influence of the quantity of H_2

Most of the above observations could be related to NPs formation kinetics. The available quantity of H_2 in ILs could also be a main factor. To confirm this, a set of experiments has been realized on the same volume (2 mL of $MnNp_2$ solutions ($5x10^{-2}$ M) in $C_1C_4ImNTf_2$), during 1 h at 100 °c without stirring.

The quantity of H_2 available for the reaction was varied:

- By increasing H_2 pressure (0.4 and 0.9 MPa)
- By decreasing the height of liquid in the reactor (using a larger autoclave, liquid height was reduced from 10 to 5 mm).

With increasing the quantity of available H_2 in the ionic liquid, by increasing the contact surface or by increasing the pressure of H_2, the NPs size decreases, Table 7.

Table 6| Comparison between attempts, influence of H_2 diffusivity.

Attempt		Duration (hour)	Mean size (nm)
Kin-1h-HT-LP	Smaller Autoclave	1	3.0 [2.2; 4.0]
Mech-1h-HT-LP	Larger Autoclave	1	2.7 [2.0; 3.5]
Mech-1h-HT-HP	High Pressure	1	2.3 [1.7; 3.2]

The quantity of H_2 thus influences the size of NPs. Clearly, this effect is related to the rate of decomposition reaction of $MnNp_2$. The higher this kinetic (with increasing H_2 diffusivity), the smaller the NPs. This has been evidenced by Shevchenko and also observed in the case of CuNPs synthesis, *vide supra*.[42, 74]

IV.7.iii. Discussion

From the experimental results described above, the following conclusions can be drawn concerning the synthesis of MnNPs from $MnNp_2$.

- The reaction of $MnNp_2$ with H_2 at 100 °C is slow. Experiments in flow reactor show that after 24 h, only 85 % of starting compound is hydrogenolysed.
- The results in Figure 14 suggest that an incomplete decomposition of $MnNp_2$ leads to larger MnNPs with broader size distribution.

- This is further demonstrated by the influence of the quantity of H_2 available for reaction (either by increased H_2 pressure or exchange surface area with the liquid). The larger this quantity, the more advanced this reaction, the smaller the NPs.

These observations are consistent with the theory of nucleation of NPs from nuclides.[42] Ideally, the decomposition of the OM precursor should lead to the formation of isolated atoms, or nuclides, which then coalesce to form nuclei (Figure 15a). In this case, the size of the NPs is well controlled and depends on the spatial organization of the IL. In the case of slowly reacting OM, NP nucleation may occur while unreacted OM precursor is still present. Both species may react, providing an additional pathway to the growth of NPs, which competes with the nucleation / growth from nuclides, and allows the formation of large NPs (Figure 15b). Hence, any variation of experimental conditions that reduces decomposition rate of the OM precursor is expected to compromise size control of metallic NPs.

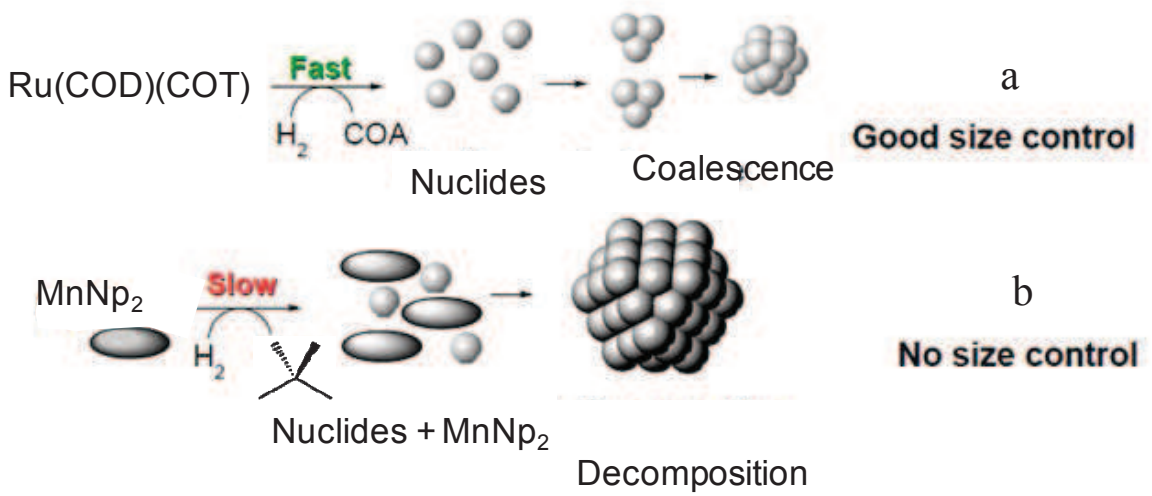

Fig. 15| Mechanism of synthesis of NPs. If the reaction is fast, formation of size controlled NPs; if the decomposition is slow, poor size control of NPs.

IV.8. Characterization of MnNPs

Two TEM grids are prepared with the solution of Mn-LT-LP-1 and Mn-MT-HP-1, the EDX spectra obtained from these areas confirm the presence of manganese. TEM pictures of both samples, give experimental data very close to cubic metallic β-manganese, with angle calculated and length measured thanks FID, Figure 16. A comparison with existing Mn oxide with cubic crystalline structure has been performed. However, no manganese oxide has been found to agree with experimental results. Attempt of XPS analyses performed on the NPs deposited on filter paper, demonstrate that the Mn surface is oxidized, Figure 17. It is however very difficult to give clearly the oxidation state of Mn in this attempt due to the weak energy difference of these peaks (1 eV) and their large full width at half maximum (3.5 eV).[75] This surface oxidation should be due to unwished reaction during the preparation of the XPS sample and should be analyzed more deeply.

However, metallic manganese nanoparticles seem to be got through this synthesis process (HRTEM).

Table 7| Comparison between experimental and Mn Cubic (JCPDS n°89-4857) crystalline structure for the two HRTEM pictures.

Spot 1	hkl	d(exp.)(nm)	d(theo.)(nm)	Angle(exp.)	Angle(theo.)
1	220	0.2170	0.2232	0	0
2	2-20	0.2164	0.2232	89.98	90
Spot 2	hkl	d(exp.)(nm)	d(theo.)(nm)	Angle(exp.)	Angle(theo.)
1	210	0.2784	0.2824	0	0
2	312	0.1669	0.1688	34.06	33.21
3	102	0.2752	0.2824	67.66	66.42
4	-1-12	0.2483	0.2578	123.13	123.21

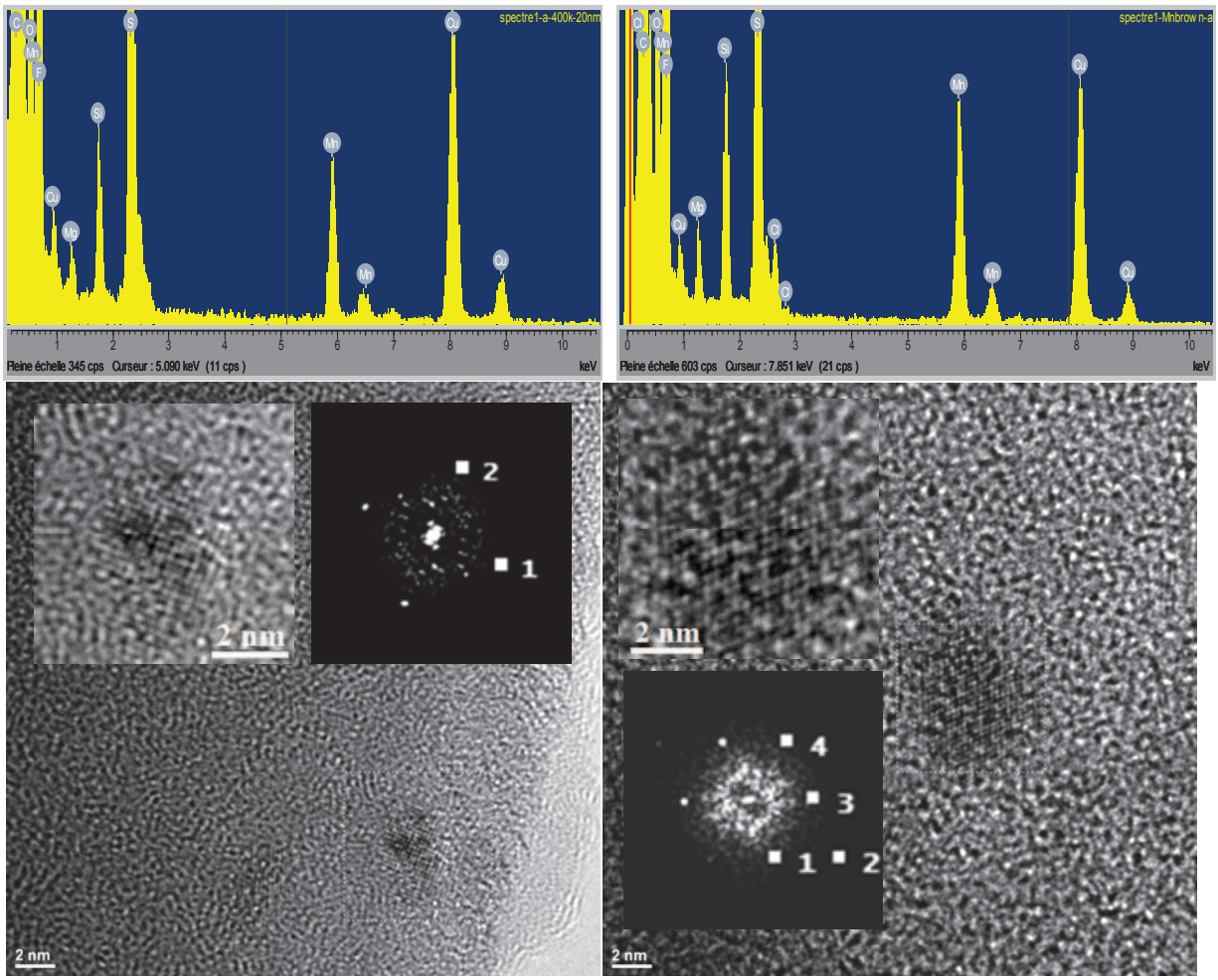

Fig. 16| EDX spectra and HRTEM pictures of MnNPs obtained from reduction of $MnNp_2$ (concentration, $5.0x10^{-2}$ M); left: Mn-LT-LP-1, right: Mn-MT-HP-1, under left 0.4 MPa of H_2, without stirring at 30 °C in $C_1C_4ImNTf_2$ and right under 0.9 MPa of H_2, without stirring at 50 °C in $C_1C_4ImNTf_2$, during 48 hours.

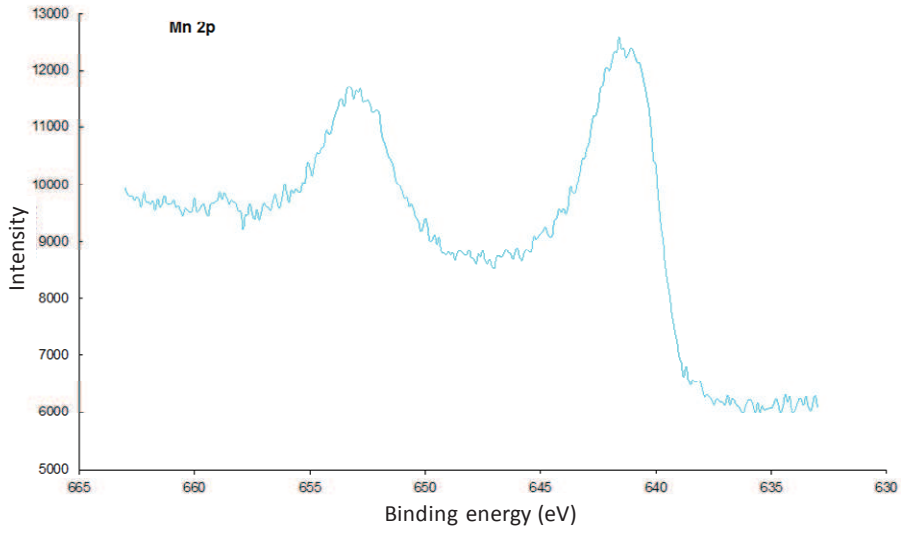

Fig. 17| XPS spectra of MnNPs obtained from reduction of $MnNp_2$ (concentration, $5.0x10^{-2}$ M); under left 0.4 MPa of H_2, without stirring at 30 °C in $C_1C_4ImNTf_2$ during 48 hours.

IV.9. Conclusion

Alkyl Mn precursors $MnNp_2$ have been used for the first time to form MnNPs. A step by step kinetic study confirms that the formation of smaller NPs is favored when the rate of decomposition of $MnNp_2$ increases. The presence of unreacted $MnNp_2$ induces uncontrolled growth of NPs. Contrarily to RuNPs, the formed MnNPs continuously grow under the effect of temperature and H_2. XPS has confirmed for RuNPs and CuNPs the zero-valent state of the metal surface, not with MnNPs. These differences could be attributed to a different less stabilized interface IL /NP surface, in the case of Mn. This needs further investigation.

However, in optimized conditions MnNPs (2.3 nm) are isolated and sufficiently stable to be analyzed by HRTEM and EDX proving that they are crystalline, metallic and composed of cubic Mn.

V. Conclusion

Our objective to synthesize in a repetitive way metallic Mn and CuNPs with controlled size. These NPs may be good precursors to form barrier and seed layers in advanced interconnects.

Ionic liquids (ILs) are used as solvents to generate a large variety of NPs by several physical and chemical routes and to stabilize them in the absence of further additives. Moreover, in order to avoid possible surface contamination, the synthesis of NPs from organometallic precursors (OM) under H_2 atmosphere affords volatile by-products easily removed from the solution.

By this route, CuNPs of 4 nm and MnNPs of 2 nm, homogeneously dispersed in the solution and with narrow size distribution, have been successfully formed from Mes-Cu and $MnNp_2$, respectively.

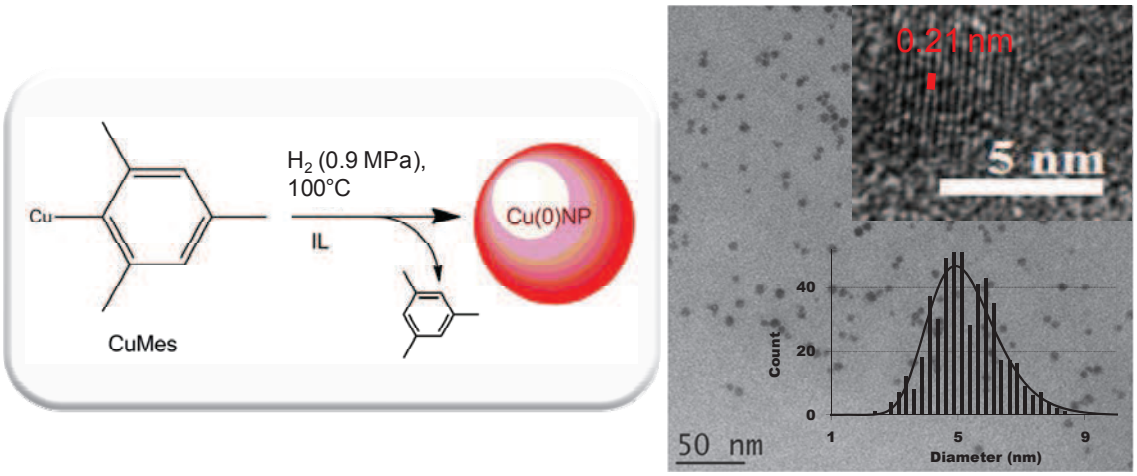

Fig. 18| Reaction scheme for the synthesis of CuNPs, TEM picture, HRTEM picture and size distribution histogram of the resulting CuNPs.

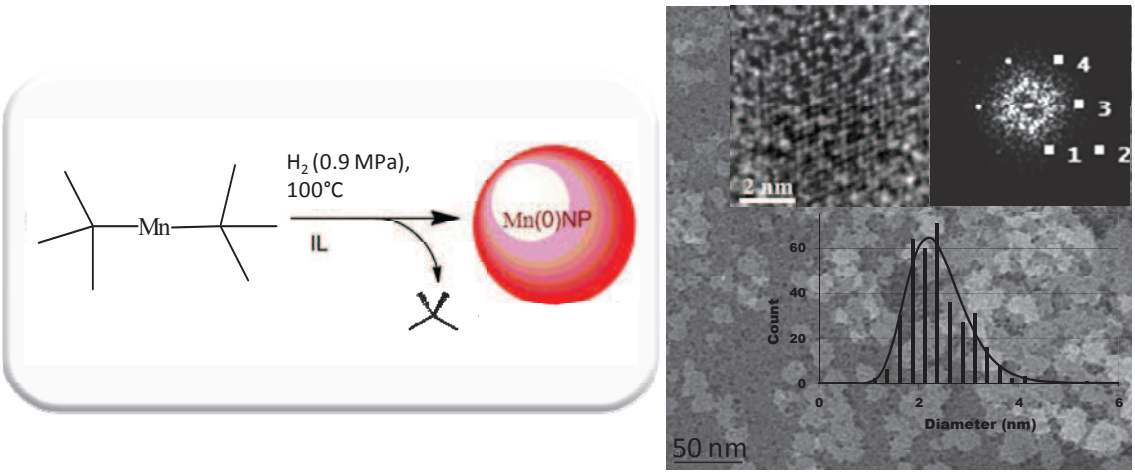

Fig. 19| Reaction scheme for the synthesis of MnNPs, TEM picture, HRTEM picture, diffraction pattern and size distribution histogram of the resulting MnNPs.

These NPs have been characterized by several methods. HRTEM and XPS (Auger) are in favor of the synthesis of crystalline and zero-valent NPs. Several experiments with both OM have been performed to decrease size and narrow the distribution. The information from the different procedures provides a possible guide for understanding the mechanism of NPs growth.

In all case, the rate of the decomposition / reduction of organometallic precursor (K_1) controls the growth of NPs. The higher this rate of decomposition, the smaller the resulting NPs. This has been correlated to a further surface reaction of unreacted OM. This side reaction (K_4) is favored when (K_1) is lowered (low temperature, low H_2 pressure, low concentration, low reaction time) and affords the poor size controlled large NPs, Figure 20. However, the rate of nucleation (K_2) and growth (K_3) steps depend of the nature of organometallic precursor and metal.

If growth (K_3) step has not been evidenced since, already formed RuNPs (~2 nm) are stable at 100 °C under pressure of H_2, CuNPs and MnNPs show a high tendency to form large aggregates or rods under these experimental conditions. A higher control on the formation and

growth of NP in IL will be improved only through the knowledge of the stabilizing effect of IL, *i.e.* the understanding of the nature of the interface of IL/metal surface.

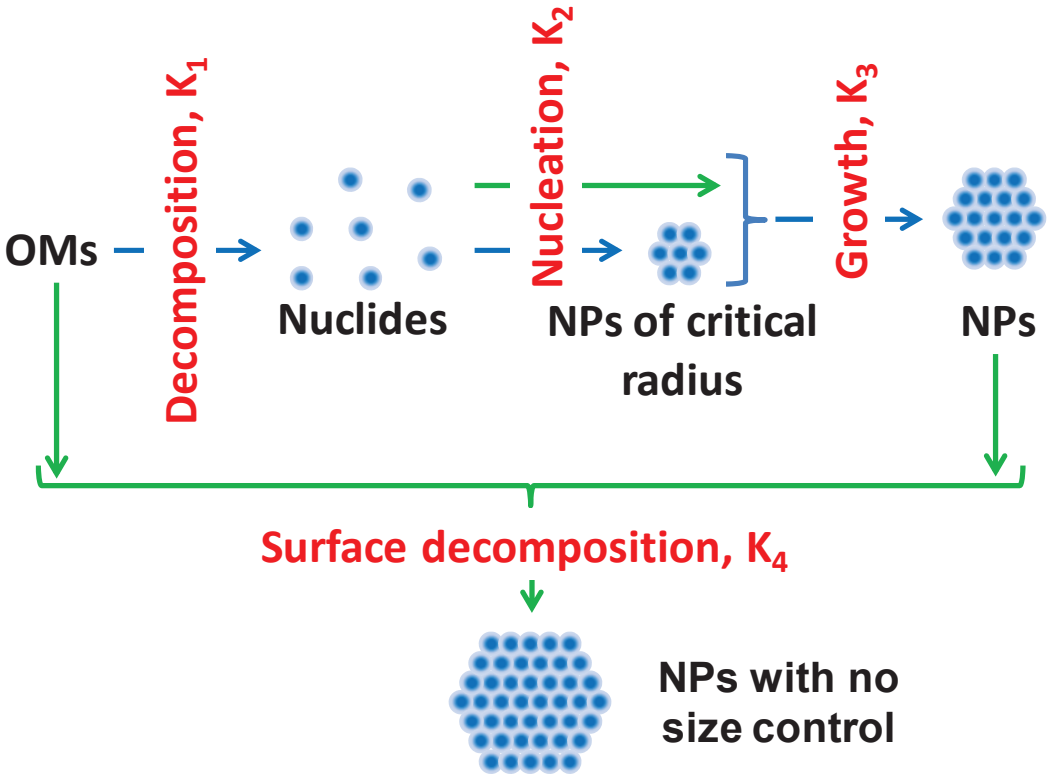

Fig. 20 Reaction scheme for the synthesis of Cu and MnNPs.

The following question to answer is: is it possible to apply this methodology to synthesize bimetallic NPs? In other words, is it possible to mix two organometallic precursors in order to form bimetallic NPs by this way?

A simultaneous decomposition of two organometallic precursors has been performed in organic solvent in presence of ligands.[76, 77] To our knowledge, this route has not yet been adapted with ILs. These attempts to form bimetallic NPs are presented in Chapter III.

References

[1] D. Astruc, in, Wiley-VCH, Weinheim, 2008.
[2] A.T. Bell, Science, 299 (2003) 1688-1691.
[3] H. Bönnemann, K.S. Nagabhushana, Metal Nanoclusters: Synthesis and Strategies for their Size Control, in: B. Corain, G. Schmid, N. Toshima (Eds.) Metal Nanoclusters in Catalysis and Materials Science, Elsevier, Amsterdam, 2008, pp. 21-48.
[4] G. Schmid, Nanoparticles: From Theory to Application, Wiley-VCH, Weinheim, 2004.
[5] M. Valden, X. Lai, D.W. Goodman, Science, 281 (1998) 1647.
[6] C. Barriere, G. Alcaraz, O. Margeat, P. Fau, J.B. Quoirin, C. Anceau, B. Chaudret, J. Mater. Chem., 18 (2008) 3084-3086.
[7] H. Bönnemann, K.S. Nagabhushana, R.M. Richards, Colloidal Nanoparticles Stabilized by Surfactants or Organo-Aluminium Derivatives: Perparation and Use as Catalyst Precursors, in: D. Astruc (Ed.) Nanoparticles and Catalysis, Wiley-VCH, Weinheim, 2008, pp. 49-92.
[8] L.S. Ott, R.G. Finke, Coord. Chem. Rev., 251 (2007) 1075-1100.
[9] J. Dupont, J.D. Scholten, Chem. Soc. Rev., 39 (2010) 1780-1804.
[10] T. Gutel, C.C. Santini, K. Philippot, A. Padua, K. Pelzer, B. Chaudret, Y. Chauvin, J.-M. Basset, J. Mater. Chem., 19 (2009) 3624-3631.
[11] P.S. Campbell, C.C. Santini, F. Bayard, Y. Chauvin, V. Colliere, A. Podgorsek, M.F. Costa Gomes, J. Sa, J. Catal., 275 (2010) 99-107.
[12] Z. Li, A. Rahtu, R.G. Gordon, J. Electrochem. Soc., 153 (2006) C787-C794.
[13] P. Doppelt, Coord. Chem. Rev., 178-180 (1998) 1785-1809.
[14] M. Brettholle, O. Hoefft, L. Klarhoefer, S. Mathes, W. Maus-Friedrichs, S. Zein El Abedin, S. Krischok, J. Janek, F. Endres, Phys. Chem. Chem. Phys., 12 (2010) 1750-1755.
[15] O.A. Yeshchenko, I.M. Dmitruk, A.M. Dmytruk, A.A. Alexeenko, Mater. Sci. Eng., B, 137 (2007) 247-254.
[16] P. Christian, M. Bromfield, J. Mater. Chem., 20 (2010) 1135-1139.
[17] V. Engels, F. Benaskar, D.A. Jefferson, B.F.G. Johnson, A.E.H. Wheatley, Dalton Trans., 39 (2010) 6496-6502.
[18] R. Prucek, L. Kvitek, A. Panacek, L. Vancurova, J. Soukupova, D. Jancik, R. Zboril, J. Mater. Chem., 19 (2009) 8463-8469.
[19] L. Yu, H. Sun, J. He, D. Wang, X. Jin, M. Hu, G.Z. Chen, Electrochem. Comm., 9 (2007) 1374-1381.
[20] J. Hambrock, R. Becker, A. Birkner, J. Weiss, A. Fischer Roland, Chem. Comm. (Cambridge, Eng.), (2002) 68-69.
[21] Y.H. Kim, D.K. Lee, B.G. Jo, J.H. Jeong, Y.S. Kang, Colloids Surf. A, 284+285 (2006) 364-368.
[22] K. Richter, A. Birkner, A.-V. Mudring, Angew. Chem., Int. Ed., 49 (2010) 2431-2435, S2431/2431-S2431/2439.
[23] P. Singh, A. Katyal, R. Kalra, R. Chandra, Catal. Comm., 9 (2008) 1618-1623.
[24] P. Singh, A. Katyal, R. Kalra, R. Chandra, Tetrahedron Lett., 49 (2008) 727-730.
[25] P. Singh, K. Kumari, A. Katyal, R. Kalra, R. Chandra, Catal. Lett., 127 (2009) 119-125.
[26] F.-L. Chen, I.W. Sun, H.P. Wang, C.H. Huang, J. Nanomater., (2009).
[27] K.I. Han, S.W. Kang, J. Kim, Y.S. Kang, J. Membr. Sci., 374 (2011) 43-48.
[28] M. Egashira, A. Kanetomo, N. Yoshimoto, M. Morita, Electrochemistry (Tokyo, Jpn.), 78 (2010) 370-374.
[29] G. Murugadoss, B. Rajamannan, V. Ramasamy, J. Lumin., 130 (2010) 2032-2039.

[30] J.-K. Chang, C.-H. Huang, W.-T. Tsai, M.-J. Deng, I.W. Sun, J. Power Sources, 179 (2008) 435-440.
[31] Z. Liu, C. Tao, J. Du, X. Fan, D. Li, X. Zhou, D. Sun, R. Liu, Z. Zuo, M. Li, J. Sha, S. Sun, S. Xi, in, (Chongqing University, Peop. Rep. China). Application: CN, 2010, 101824335.
[32] P.Z. Si, Z.D. Zhang, Int. J. Mod. Phys. B, 23 (2009) 3895-3901.
[33] N. Wang, X. Cao, L. He, W. Zhang, L. Guo, C. Chen, R. Wang, S. Yang, J. Phys. Chem. C, 112 (2008) 365-369.
[34] M.B. Ward, R. Brydson, A.P. Brown, R.F. Cochrane, J. Phys.: Conf. Ser., 126 (2008) No pp given.
[35] J.F. Bondi, K.D. Oyler, X. Ke, P. Schiffer, R.E. Schaak, J. Am. Chem. Soc., 131 (2009) 9144-9145.
[36] F. Nador, Y. Moglie, C. Vitale, M. Yus, F. Alonso, G. Radivoy, Tetrahedron, 66 (2010) 4318-4325.
[37] O.A. Yeshchenko, I.M. Dmitruk, A.A. Alexeenko, A.M. Dmytruk, Appl. Surf. Sci., 254 (2008) 2736-2742.
[38] R.A. Ganeev, A.S. Zakirov, G.S. Boltaev, R.I. Tugushev, T. Usmanov, P.K. Khabibullaev, T.W. Kang, A.A. Saidov, Opt. Mater. (Amsterdam, Neth.), 33 (2011) 419-423.
[39] S. Pang, L. Wang, G. Li, Z. Zhang, Surf. Coat. Technol., 201 (2007) 5451-5453.
[40] D. Marquardt, Z. Xie, A. Taubert, R. Thomann, C. Janiak, Dalton Trans., 40 (2011) 8290-8293.
[41] T. Gutel, J. Garcia-Anton, K. Pelzer, K. Philippot, C.C. Santini, Y. Chauvin, B. Chaudret, J.-M. Basset, J. Mater. Chem., 17 (2007) 3290-3292.
[42] E.V. Shevchenko, D.V. Talapin, H. Schnablegger, A. Kornowski, O. Festin, P. Svedlindh, M. Haase, H. Weller, J. Am. Chem. Soc., 125 (2003) 9090-9101.
[43] P.S. Campbell, C.C. Santini, D. Bouchu, B. Fenet, K. Philippot, B. Chaudret, A.A.H. Padua, Y. Chauvin, Phys. Chem. Chem. Phys., 12 (2010) 4217-4223.
[44] K. Philippot, B. Chaudret, C. R. Chim., 6 (2003) 1019-1034.
[45] K. Richter, A. Birkner, A.V. Mudring, Phys. Chem. Chem. Phys., 13 (2011) 7105-7110.
[46] A.A.H. Padua, M.F. Costa Gomes, J.N.A. Canongia Lopes, Acc. Chem. Res., 40 (2007) 1087-1096.
[47] T. Teranishi, M. Hosoe, T. Tanaka, M. Miyake, J.X. Xu, C. Lin, Phys. Chem. B, 103 (1999) 3818-3827.
[48] Y. Wang, X. Xu, Z. Tian, Y. Zong, H. Cheng, C. Lin, Chem. Eur. J., 12 (2006) 2542-2549.
[49] J.J. De Yoreo, P.G. Vekilov, in Principles of Crystal Nucleation and Growth, Chap 3.
[50] E. Cottancin, G. Celep, J. Lerme, M. Pellarin, J.R. Huntzinger, J.L. Vialle, M. Broyer, Theor. Chem. Acc., 116 (2006) 514-523.
[51] J.F. Moulder, W.F. Stickle, P.E. Sobol, K.D. Bomben, in: J. Chastainand, R.C.J. King (Eds.), Physical Electronics, Inc., USA, 1995.
[52] P.E. Larson, J. Electron Spectrosc. Relat. Phenom., 4 (1974) 213.
[53] G. Schön, Surf. Sci., 35 (1973) 93.
[54] C.D. Wagner, A. Joshi, J. Electron. Spectrosv. Relat. Phenom., 47 (1988) 283-313.
[55] G. Moretti, in: H.K. G. Ertl, J. Weitkamp (Ed.) Handbook of Heterogeneous Catalysis, Wiley-VCH: Weinheim, 1997, pp. 632.
[56] G. Moretti, G. Ferraris, G. Fierro, M.L. Jacono, Surf. Interface Anal., 38 (2006) 224-228.

[57] S. Poulston, P.M. Parlett, P. Stone, M. Bowker, Surf. Interface Anal., 24 (1996) 811-820.
[58] K.W. Andrews, D.J. Dyson, S.R. Keown, Interpretation of Electron Diffraction Patterns. 2nd ed, 1971.
[59] C. Vollmer, E. Redel, K. Abu-Shandi, R. Thomann, H. Manyar, C. Hardacre, C. Janiak, Chem. Eur. J., 16 (2010) 3849-3858.
[60] E.O. Brimm, M.A. Lynch, Jr., J.W. Sesny, J. Am. Chem. Soc., 76 (1954) 3831-3835.
[61] C. Vollmer, C. Janiak, Coord. Chem. Rev., 255 (2011) 2039-2057.
[62] M. Tamura, J. Kochi, J. Organometal. Chem., 29 (1971) 111-129.
[63] X. Yin, J.-A.M. Andersen, A. Cotton, J.R. Moss, J. Organomet. Chem., 564 (1998) 267-276.
[64] D. Reardon, G. Aharonian, S. Gambarotta, G.P.A. Yap, Organomet., 21 (2002) 786-788.
[65] J.L. Latten, R.S. Dickson, G.B. Deacon, B.O. West, E.R.T. Tiekink, J. Organomet. Chem., 435 (1992) 101-108.
[66] R.A. Andersen, D.J. Berg, L. Fernholt, K. Faegri, Jr., J.C. Green, A. Haaland, M.F. Lappert, W.P. Leung, K. Rypdal, Acta Chem. Scand., Ser. A, A42 (1988) 554-562.
[67] R.A. Anderson, E. Carmona-Guzman, J.F. Gibson, G. Wilkinson, J. Chem. Soc., Dalton Trans.: Inorg. Chem. (1972-1999), (1976) 2204-2211.
[68] V. Riollet, E.A. Quadrelli, C. Coperet, J.-M. Basset, R.A. Andersen, K. Kohler, R.-M. Bottcher, E. Herdtweck, Chem. Eur. J., 11 (2005) 7358-7365.
[69] O. Margeat, F. Dumestre, C. Amiens, B. Chaudret, P. Lecante, M. Respaud, Prog. Solid State Chem., 33 (2006) 71-79.
[70] G. Salas, A. Podgorsek, P.S. Campbell, C.C. Santini, A.A.H. Padua, G.M.F. Costa, K. Philippot, B. Chaudret, M. Turmine, Phys. Chem. Chem. Phys., 13 (2011) 13527-13536.
[71] J.H. So, P. Boudjouk, Inorg. Chem., 29 (1990) 1592-1593.
[72] R.A. Andersen, K. Faegri, Jr., J.C. Green, A. Haaland, M.F. Lappert, W.P. Leung, K. Rypdal, Inorg. Chem., 27 (1988) 1782-1786.
[73] J.M. Basset, Surface organometallic chemistry: molecular approaches to surface catalysis, North Atlantic Treaty Organization. Scientific Affairs Division, Kluwer Academic Publishers, 1988.
[74] P.P. Arquillière, P.-H. Haumesser, C.C. Santini, Microelectron. Eng., 92 (2012) 149-151.
[75] M. Okua, K. Wagatsuma, T. Konishi, J. Electron Spectrosc. Relat. Phenom., 98-99 (1999) 277-285.
[76] N. Atamena, D. Ciuculescu, G. Alcaraz, A. Smekhova, F. Wilhelm, A. Rogalev, B. Chaudret, P. Lecante, R.E. Benfield, C. Amiens, Chem. Commun. (Cambridge, U. K.), 46 (2010) 2453-2455.
[77] D. Ciuculescu, C. Amiens, M. Respaud, A. Falqui, P. Lecante, R.E. Benfield, B. Chaudret, Chem. Mater., 19 (2007) 4624

Chapter III

Synthesis of Bimetallic Nanoparticles in Ionic Liquids, Unexpected Size and Structure Control of Resulting Nano-objects

Chapter III

Synthesis of Bimetallic Nanoparticles in Ionic Liquids, Unexpected Size and Structure Control of Resulting Nano-objects

I. Introduction

To meet the constant challenges of miniaturization in the microelectronics industry, traditional methodologies must be replaced by new innovative pathways to produce nano-objects. Defined as particles, whose dimensions are on the nanoscale, they coincide with a transition between bulk and molecular states and exhibit unique characteristics related to the discontinuities and quantum effects of such a transition, e.g. enhanced magnetic and catalytic properties, etc. The controlled synthesis of nanoparticles (NPs) in the range of 1 to 10 nm is still an ongoing challenge as the understanding of their stabilization and agglomeration.[1-4] Indeed, transition-metal NPs remain only kinetically stable, the thermodynamic minimum being bulk metal. Consequently, substantial effort has been centered on stabilizing transition-metal NPs. Furthermore, their formation and stabilization (inhibition of coalescence) are closely related issues.[3]

Several strategies are known to stabilize metallic NPs (MNPs), such as the use of polymers, ligands and organic or inorganic templates.[1, 5] Unlike traditional solvents, ionic liquids (ILs) can be used to generate MNPs by several physical and chemical routes and stabilize them in the absence of further additives, inhibiting metal agglomeration to the bulk.[6] As it was demonstrated in the last chapter, this class of molten salts allows generating size-controlled Cu and Mn monometallic NPs by decomposition under dihydrogen (H_2) of organometallic precursors.[7, 8] In this chapter, the following question is addressed: is this approach extendible to the synthesis of bimetallic nanoparticles, M_1-M_2NPs?

Bimetallic NPs corresponding to alloyed or segregated structures could play a key role in numerous applications. The synthesis of bimetallic Mn-CuNPs should enable the formation in a further annealing step of self-formed barrier and copper seed layers needed in microelectronic devices. In this context, the control of homogeneity, dispersion, and alloying

extent is key, as these characteristics have profound influence on the surface properties of the M_1-M_2NPs, which in turn affect their stability.[9, 10] Two strategies could be used for synthesis of such NPs; the bottom-up one, with synthesis of NPs by agglomeration of nuclides; and the top down strategy, with fragmentation of bulk in order to obtain NPs. Many of these methods could be used for synthesis of bimetallic NPs, for example with the use of an alloy for top down strategy and the use of two precursors in same time for bottom up strategy. Nevertheless, few examples are reported concerning the synthesis of bimetallic NPs in IL. Okazaki and al have successfully synthesized Au-AgNPs in IL with simultaneous physical vapor deposition of Au and Ag.[11] Electrochemistry could be used for the synthesis of supported NPs. Indeed, ILs usually are very good electrolytes. Tsai et al have achieved the synthesis of Au-AgNPs in IL by this method. [12] Xi and coworker used $C_1C_4ImBF_4$ IL as a solvent and a reductant for the synthesis of Au-Pd bimetallic NPs.[13] Dash and coworkers have synthesized bimetallic Au-PdNPs in methanol, then transferred them into IL.[14, 15] These NPs were formed by chemical reduction of $HAuCl_4$ with $NaBF_4$. Some Au-PdNPs have been directly formed in C_1C_4Im PF_6 [16]. A sol-gel process has been used for the synthesis of bimetallic Ru-CuNPs by impregnation on bentonite and use of IL as a stabilizer.[17] Our methodology is to use organometallic precursors for the synthesis of NPs in ILs. Indeed, Chaudret and coworkers have demonstrated the synthesis of bimetallic NPs in organic solvent by simultaneous decomposition of two organometallic precursors (OMs) in the presence of a ligand.[19] Previously at LCOMS and as shown in Chapter II, we have shown that ILs allow tuning the experimental conditions in order to control the size of resulting NPs from decomposition / reduction of organometallic precursors (OM) under H_2.[7, 8, 20]

In this chapter, a new and versatile route to obtain bimetallic, size-controlled M_1-M_2NPs has been investigated using various OM precursors in ILs. In order to accurately control the size of these nano-objects, diverse experimental conditions have been examined.

II. Study of the formation of bimetallic NPs: Ru-Cu case

II.1. Decomposition of Ru and Cu precursors in separate IL media

As Ru and CuNPs have been well studied and characterized, Ru-Cu bimetallic system was first considered. Recently, we have depicted the synthesis of ruthenium nanoparticles (RuNPs) in ILs from the decomposition of organometallic (OM) precursors under H_2. Monometallic RuNPs (1.1 [0.9; 1.3] nm) with controlled size were formed at 0°C under 0.4 MPa H_2 during 3 days by the decomposition of (η^4-1,5-cyclooctadiene)(η^6-1,3,5-cyclooctatriene)ruthenium(0), Ru(COD)(COT), in 1-butyl-3-methylimidazolium bis(trifluoromethylsulphonyl)imide, $C_1C_4ImNTf_2$.[7] As shown in Chapter II, this synthetic route has recently been successfully extended to Cu using mesitylcopper(I), Mes-Cu, as a precursor, enabling the generation of well dispersed 5.1 [4.2; 6.3] nm CuNPs at 100°C under 0.9 MPa H_2 for 4 h.[21] Under these conditions, the Ru(COD)(COT) decomposed to form RuNPs of 4.0 [2.8; 5.7] nm, Figure 1. Therefore, these conditions were retained for the synthesis of bimetallic Ru-CuNPs.

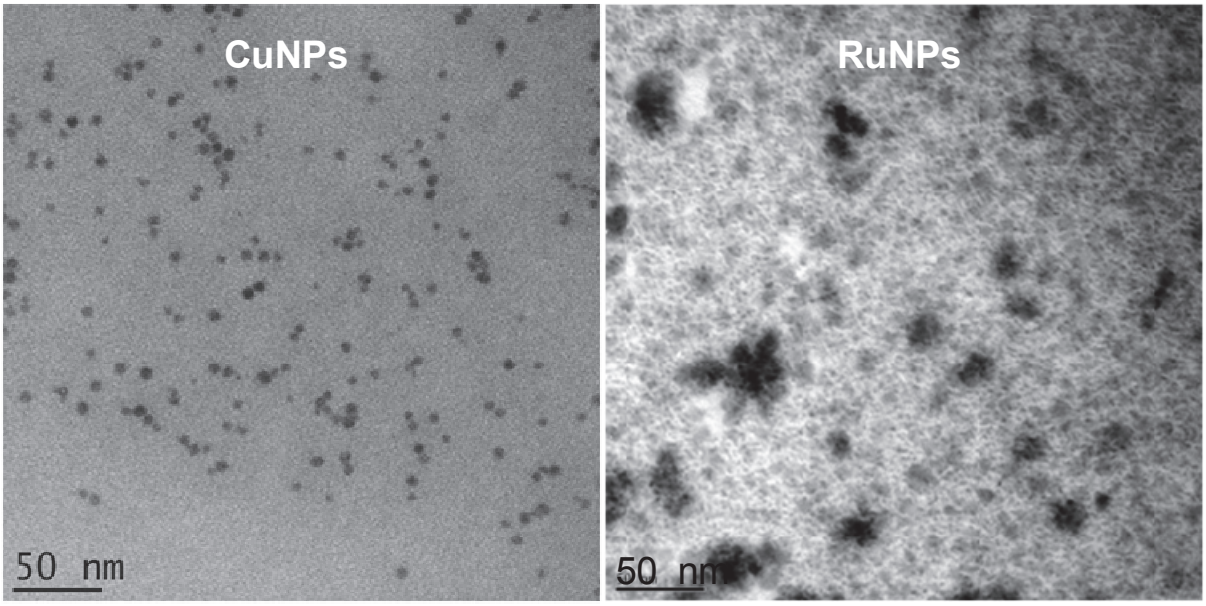

Fig. 1| TEM pictures of left CuNPs and right RuNPs obtained after 4 h under 0.9 MPa of H_2, without stirring, in $C_1C_4ImNTf_2$ at 100 °C.

II.2. Simultaneous decomposition of Ru and Cu precursors in the same IL

In a first approach, Ru-Cu bimetallic NPs were tentatively synthesized from a solution containing both OM precursors, according to Equation (1).

$$\alpha\ Ru(COD)(COT) + \beta\ Mes\text{-}Cu + x\ H_2 \rightarrow Ru_\alpha Cu_\beta + 2\alpha\ COA + \beta\ Mes\text{-}H \quad (1)$$

Two solutions of $5x10^{-2}$ M of Ru(COD)(COT) and of $5x10^{-2}$ M of Mes-Cu in $C_1C_4ImNTf_2$ were prepared and mixed with various molar fraction of Cu ($\chi_{Cu} = \beta/(\alpha+\beta)$ ranging from 0.005 to 0.995). The total metal concentration was kept at $5x10^{-2}$ M and α and β values were controlled by gas chromatography (GC).

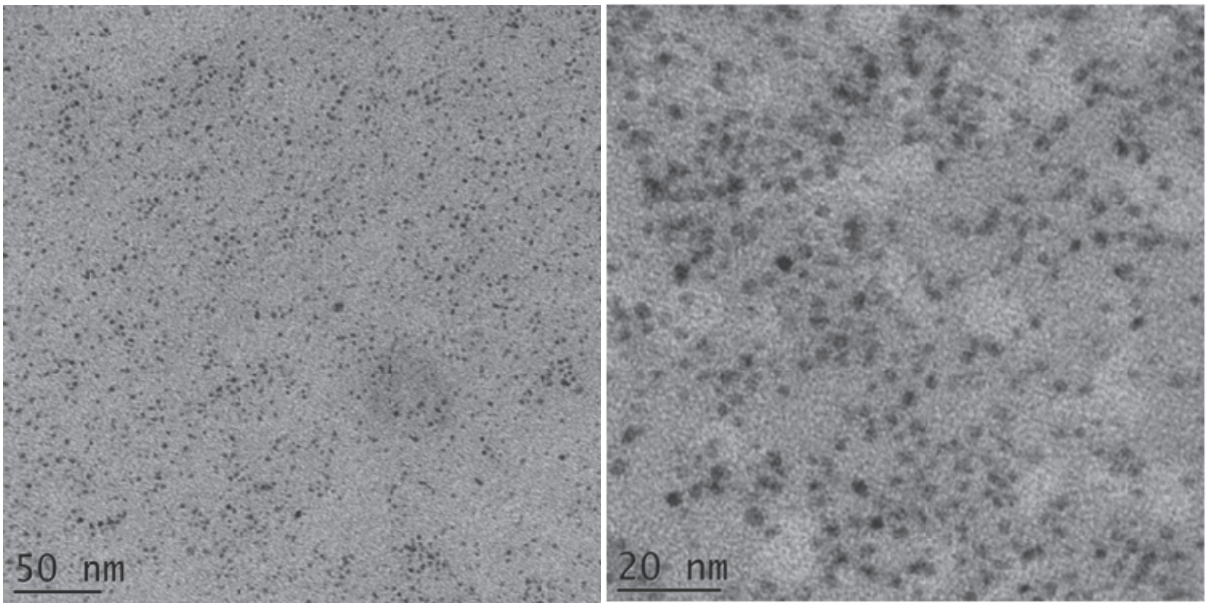

Fig. 2| TEM pictures of NPs obtained by mixing Ru(COD)(COT) and Mes-Cu ($\chi_{Cu} = 0.5$) decomposed for 4 h under 0.9 MPa of H_2, without stirring, in $C_1C_4ImNTf_2$ at 100 °C.

A shown in Figure 2, the resulting NPs are smaller with narrower size distribution than the monometallic NPs obtained in the same conditions. By comparison with the different size distribution histograms presented in Figure 3, it is further observed that the NPs obtained by mixing the two precursors do not present two separate distributions. Clearly, an effect due to mixing the two precursors is observed. This is a good argument in favor of the synthesis of bimetallic Ru-CuNPs.

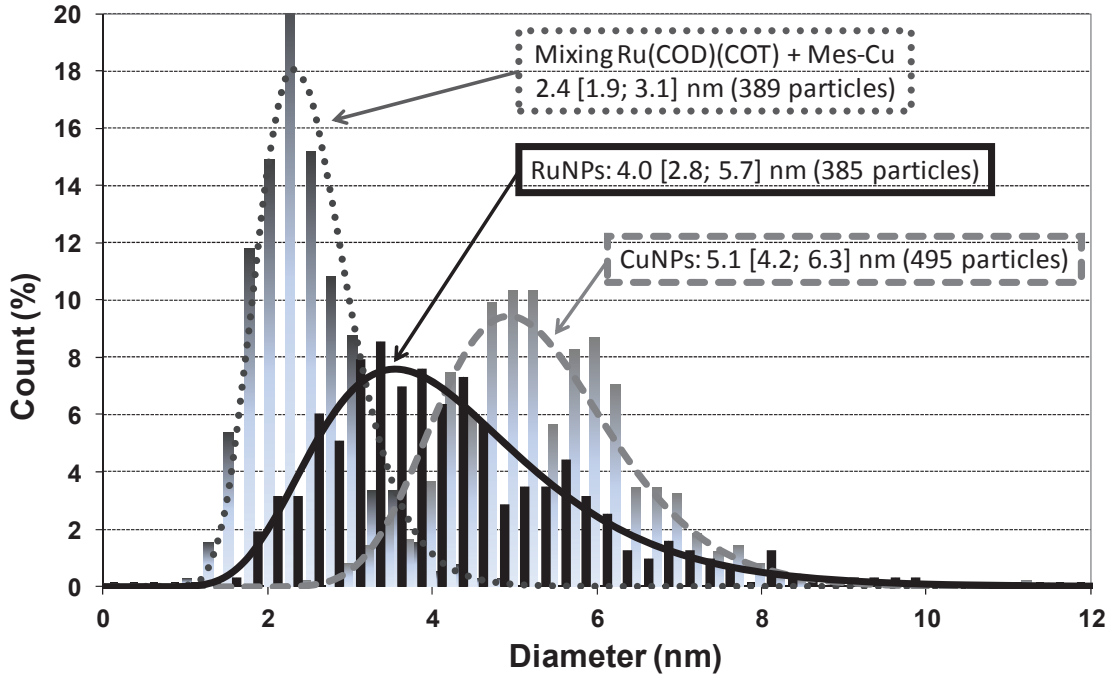

Fig. 3| Comparative size distribution histogram fitted by log-normal law of NPs obtained by decomposition / reduction during 4 h under 0.9 MPa of H_2, at 100 °C of Ru(COD)(COT), of Mes-Cu and of a mixture Ru(COD)(COT) / Mes-Cu ($\chi_{Cu} = 0.5$).

Interestingly enough, the size control holds true for a very large composition range with χ_{Cu} varying from 0.005 to 0.91, Figure 4. For instance, the mixture of only 1 % of Mes-Cu with Ru(COD)(COT) (99 %) solution yields Ru-CuNPs of 2.0 [1.6; 2.4] nm, Figure 5. In this domain, around 2 nm NPs are formed. Their sizes increase progressively from 1.8 [1.4; 2.3] nm ($\chi_{Cu} = 0.005$) to 3.4 [2.6; 4.3] nm ($\chi_{Cu} = 0.91$). For higher χ_{Cu}, NPs are significantly larger and size is less controlled; 4.1 [3.0; 5.4] nm for $\chi_{Cu} = 0.99$, and 11 [6; 20] nm for $\chi_{Cu} = 0.995$.

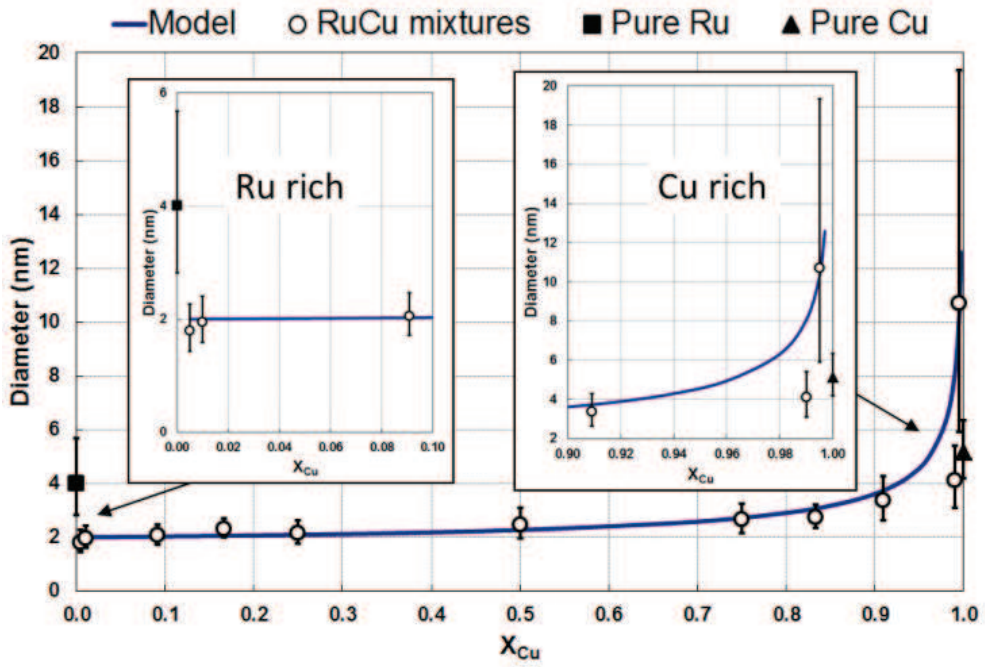

Fig. 4| Size evolution of Ru-Cu bimetallic NPs with initial composition of the solution. The size of Ru-Cu NPs (white circles) is plotted as a function of the molar fraction of Cu (χ_{Cu}) in solution, and compared with pure Ru and pure Cu. Error bars correspond to ±2 standard deviations in the log-normal distribution. The solid line represents the size evolution expected from the formation of core-shell NPs with a 2 nm core of Ru and a shell of close-packed Cu.

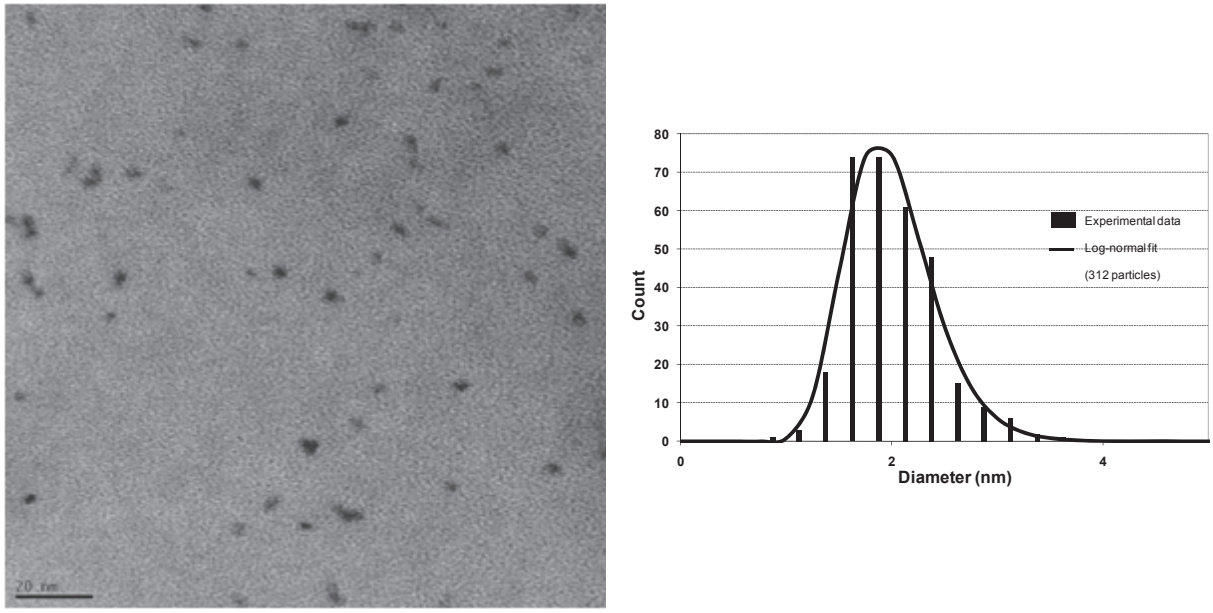

Fig. 5| TEM picture and size distribution histogram of Ru-CuNPs obtained with a solution Ru(COD)(COT)/ Mes-Cu (χ_{Cu} = 0.01) decomposed during 4 h at 100 °C under 0.9 MPa of H_2 without stirring.

II.3. Characterization of the NPs

Several analytical techniques were used in order to obtain more information on the NPs obtained when mixing the two precursors. It has been demonstrated that CuNPs and RuNPs obtained in this conditions are metallic.[8, 20] First, EDX analysis was performed on TEM grids coated with the suspension of NPs in IL.

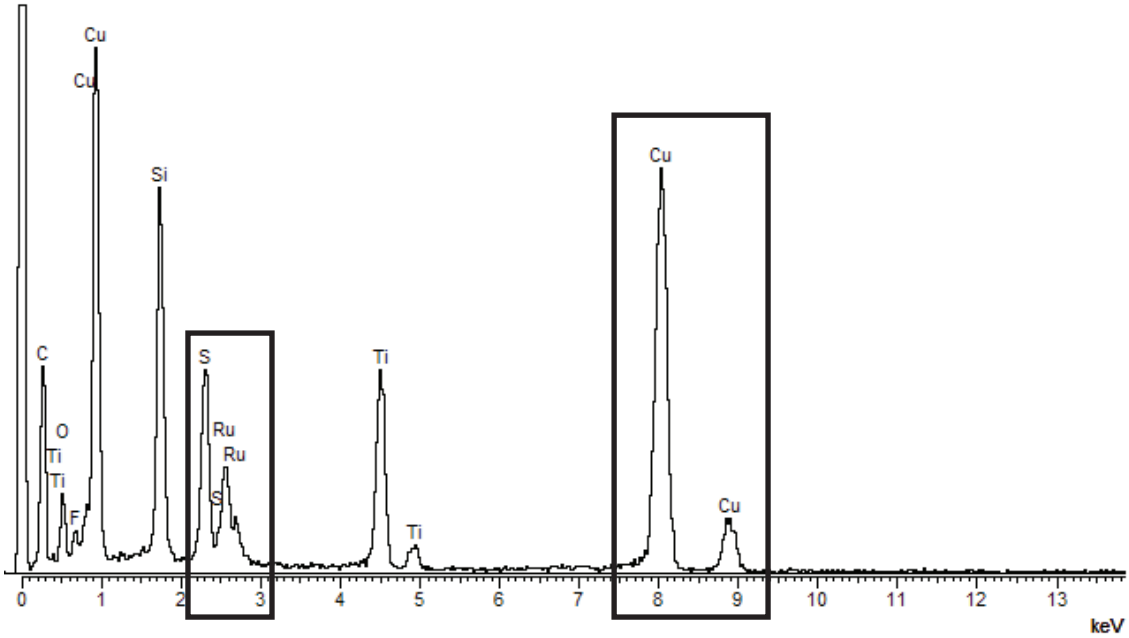

Fig. 6| EDX analysis of an area where NPs obtained from a Ru(COD)(COT) Mes-Cu mixed solution and decomposed at 100 °C under 0.9 MPa of H_2 during 4 hours are present.

In this analysis, oxygen, fluorine, sulfur are due to the IL used. Carbon could be either due to the carbon films present on the TEM grid or to IL presents in the solution. Titanium comes from the TEM grid. Ruthenium and copper originate from the NPs. EDX analyses on single particles have not been achieved to prove their bimetallic nature. However, the combined presence of Ru and Cu in solution and the smaller size observed show that the synthesis of NPs was performed with interaction between Cu and Ru precursors, with a great chance to lead to bimetallic NPs.

HRTEM analysis was also performed on this suspension of NPs. Figure 7 gives the HRTEM picture, showing the crystalline structure of the NPs. The Fourier transform picture allows determining the crystal structure more precisely.

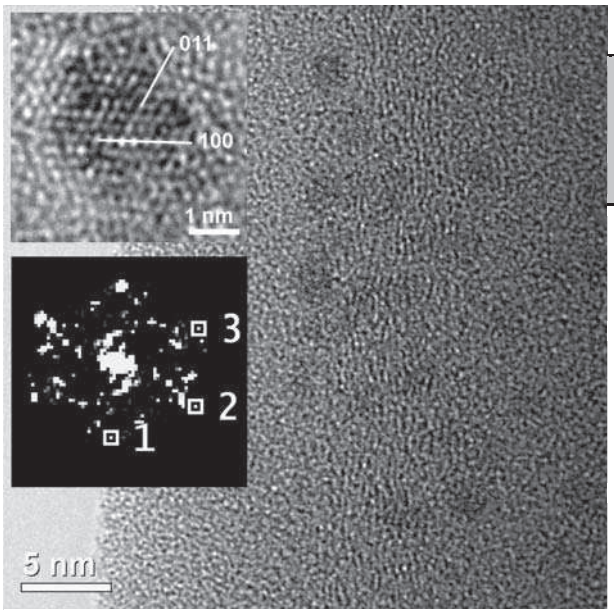

	hkl	d (exp.) Å	d (theo.) Å	Angle (exp.) °	Angle (theo.) °
1	100	2.43	2.38	0	0
2	011	2.11	2.08	64.66	64.09
3	-111	2.08	2.08	115.93	115.91

Fig. 7| HRTEM picture of NPs obtained from the mixed solution, corresponding Fourier transform picture and comparative table between Ru hcp structure and crystalline structure observed in our NPs.

The NPs exhibit a hexagonal closed packed structure which is characteristic of metallic Ru (JCPDS file n°88-1734). No CuNPs were detected, Cu could be still dissolved in the IL. To verify this hypothesis, XPS analysis coupled with X-Ray Auger electron spectroscopy were performed.

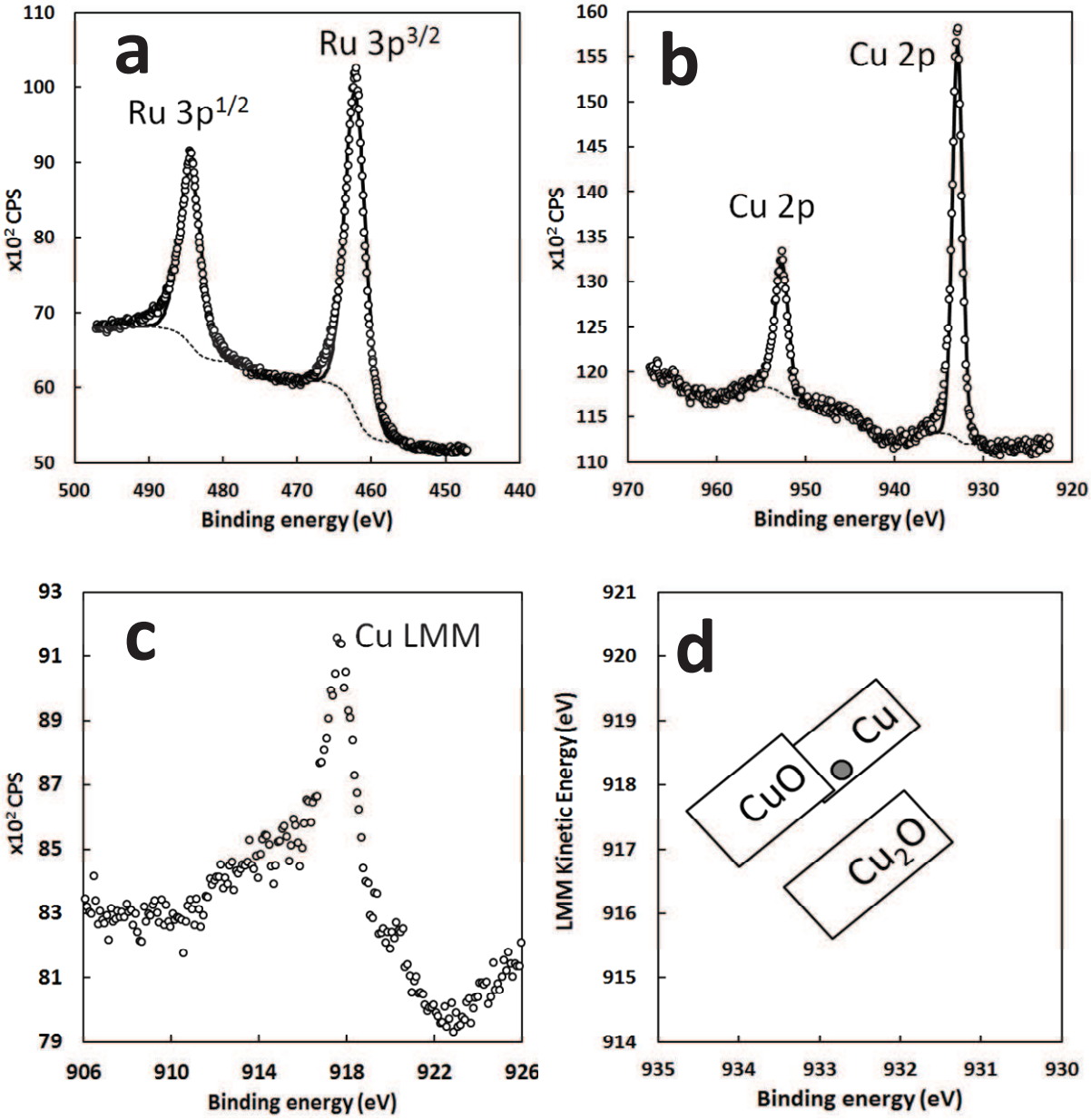

Fig. 8| XPS and XAES analysis of suspensions of Ru-CuNPs, points: experimental data, line approximation. (a) Ru $3p_{1/2}$ and Ru $3p_{3/2}$ peaks. (b) Cu $2p_{1/2}$ and $Cu2p_{3/2}$ peaks. (c) Cu LMM Auger peaks. d) Wagner plot of Cu $2p_{3/2}$ and Cu LMM: zero-valent copper present in the sample.

X-Ray photoelectron spectroscopy (XPS) spectrum in the Ru 3p region confirms the metallic nature of Ru in the NPs (Figure 8a). Indeed the peak of Ru in this area corresponds to metallic Ru (Ru $3p_{3/2}$ = 461.5 eV) and the full width at half maximum (FWHM) is equal to 2.8 eV, characteristic of a single Ru species. For the same sample, the presence of Cu is also attested by XPS measurements with presence of Cu peaks such as: Cu $2p_{3/2}$ = 932.2 eV

(Figure 8b). The latter results were combined with X-Ray Auger electron spectroscopy (XAES) (Cu LMM = 918.2 eV, Figure 8c). The resulting Wagner plot (binding energy of Cu $2p_{3/2}$ XPS vs. kinetic energy of Cu LMM Auger lines, Figure 8d) unambiguously demonstrates the metallic nature of Cu.[22, 23] Hence, metallic Cu is present in the sample, while no crystalline or pure CuNPs are distinguished by HRTEM analysis. By considering that all NPs are bimetallic and formed of a 2.45 nm Ru core, 168 Cu atoms would be necessary to totally cover the RuNP surface with a mono layer of Cu atoms, Figure 9. Consequently, with $\chi_{Cu} = 0.5$, there are not enough Cu atoms to form a full mono-layer on the RuNPs surface. This could explain why Cu is not detected with HRTEM. Moreover, several Cu layers are needed to form a crystalline lattice.

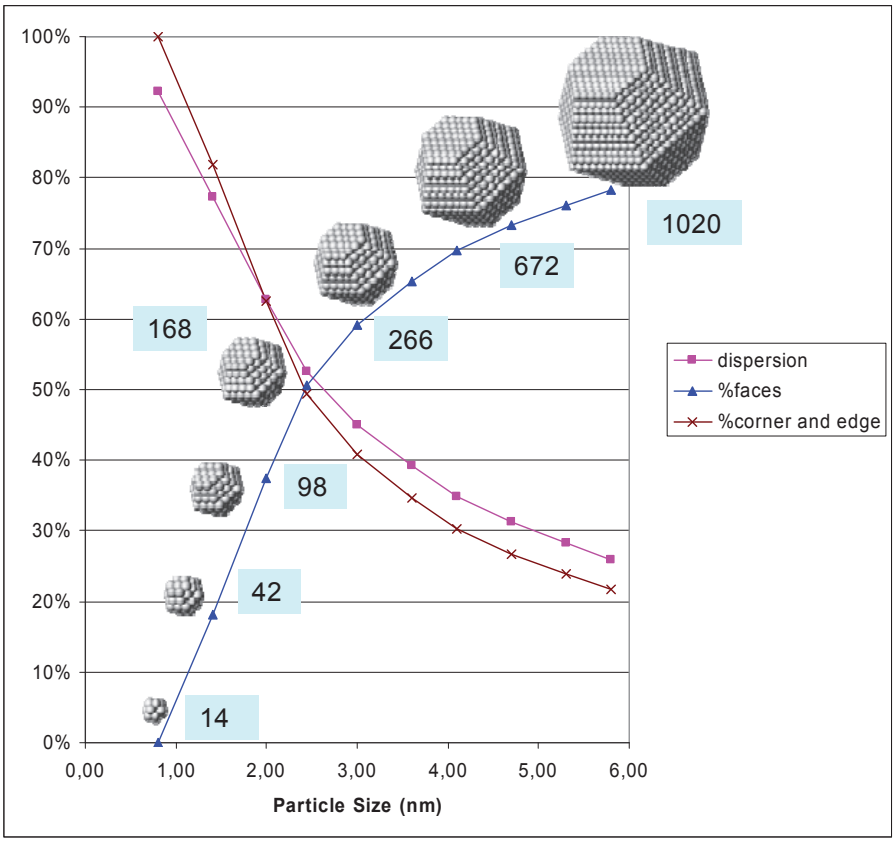

Fig. 9| Simulation results for RuNPs with ideal hcp structure for all metal dispersion with, in blue, the maximal number of Cu atoms needed to cover the RuNP surface with a mono layer of Cu atoms.

Atamena and co-workers have demonstrated the possibility to control the structure of bimetallic NPs formed in organic solvent with the use of two OMs with different

decomposition kinetics.[24, 25] By varying the decomposition kinetics of the two precursors they were able to tune the structure of resulting NPs. Under H_2, Rh OM decomposes fastly and form Rh core, on which Fe OMs decompose. By choosing a less reactive reductant, only Fe OM could be reduced and Rh is reduced on Fe core. Variation of kinetics consequently allows monitoring the shape of the structure, allowing formation of core-shell structure.

In our experiments, Ru(COD)(COT) and Mes-Cu have different decomposition kinetics. We have reported that at 30 °C the complete decomposition of Ru(COD)(COT) requires 24 h, whereas one week is necessary for Mes-Cu.[8, 20] Ru(COD)(COT) is thus decomposed much faster than Mes-Cu. According to Atamena's work, Ru core Cu shell NPs should be formed.

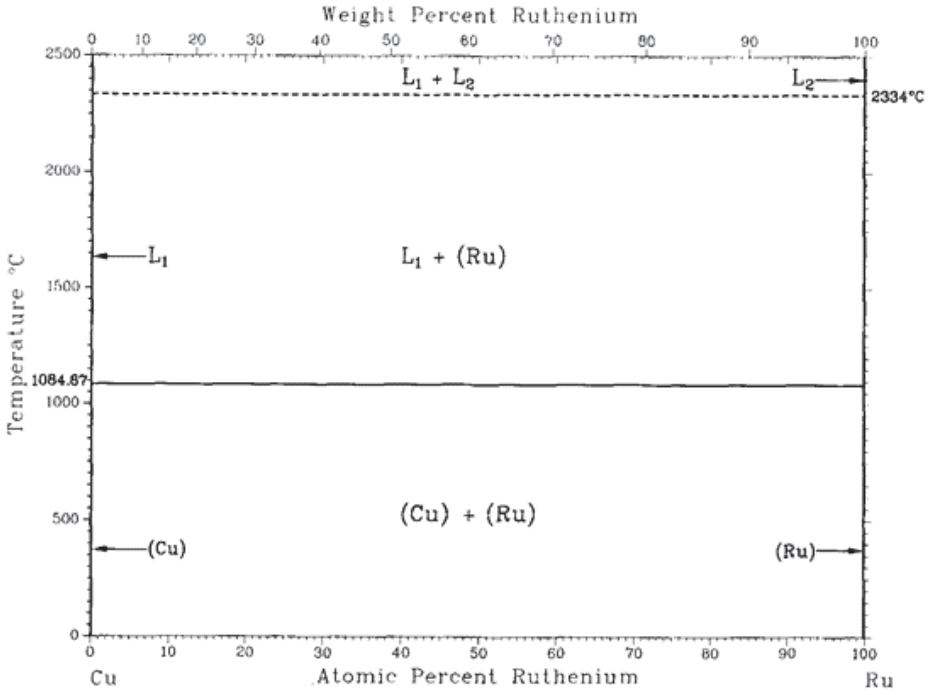

Fig. 10| Binary alloy phase diagram of Ru and Cu.[26]

Furthermore, no alloy or solid solution is present in the binary alloy phase diagram of Ru-Cu. The deposition of single layer of Cu on a Ru single crystal is possible without mixing.[26, 27]. Moreover, the values of the surface energies of Ru and Cu, (2850 dynes.cm^{-1} versus 1600 dynes.cm^{-1}, respectively) are also in favor of the presence of Cu at the surface of

RuNPs.[28] Hence, it is suggested that the reduction of Mes-Cu occurs at the RuNPs rapidly formed surface affording a Ru core and a Cu shell.

II.4. Synthesis of bimetallic Ru-CuNPs in two steps

In order to obtain more information about the formation and the structure of Ru-CuNPs, a synthesis in two steps has been performed. For this purpose, a suspension of RuNPs of 1.8 [1.4; 2.2] nm, was first previously prepared from Ru(COD)(COT) at 30 °C under 0.4 MPa of H_2. Note that, the original RuNPs size of 1.8 [1.4; 2.2] nm, treated 4 h at 100 °C under 0.9 MPa of H_2, became 1.9 [1.5; 2.4] nm. No significant size change is thus observed upon treatment due to the stabilization of RuNPs by surface hydrides, as demonstrated by Campbell et al.[29]

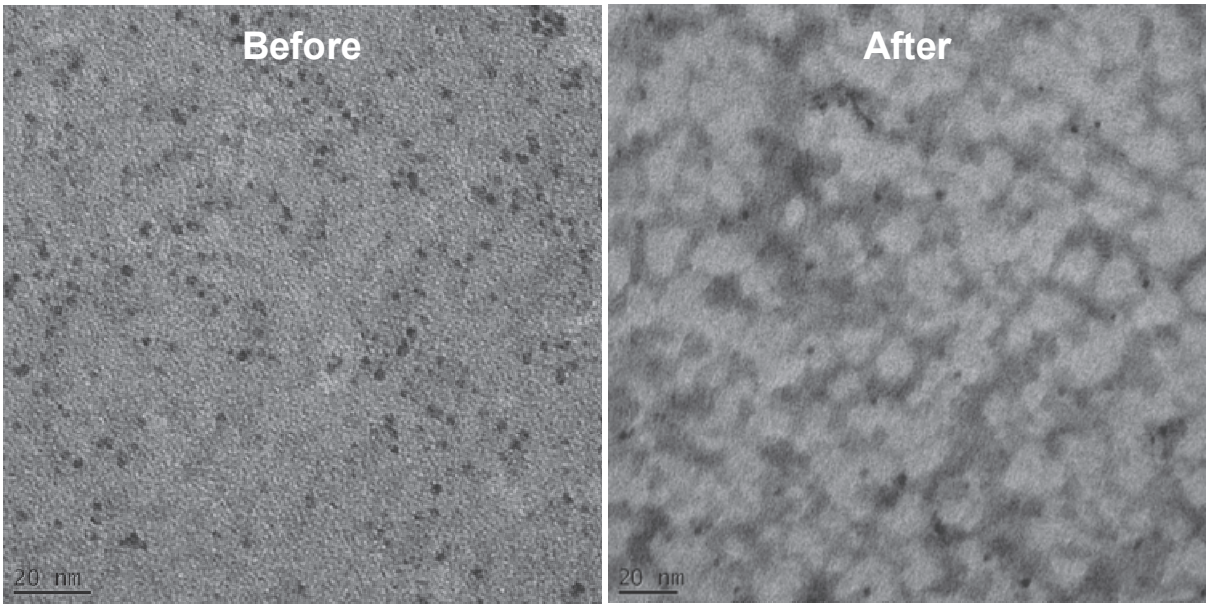

Fig. 11| TEM pictures of RuNPs in $C_1C_4ImNTf_2$ left before and right after treatment under 0.9 MPa of H_2, without stirring, at 100 °C.

A solution of Mes-Cu ($\chi_{Cu} = 0.5$) was then added to this suspension in order to form a solution of $5x10^{-2}$ M total concentration of metals. When the mixture was heated at 100 °C during 4 hours under 0.9 MPa of H_2 without stirring, larger NPs 2.7 [2.1; 3.4] nm were

observed, Figure 12, 13. This clear size increase is associated to the reaction of Mes-Cu onto RuNP surface.

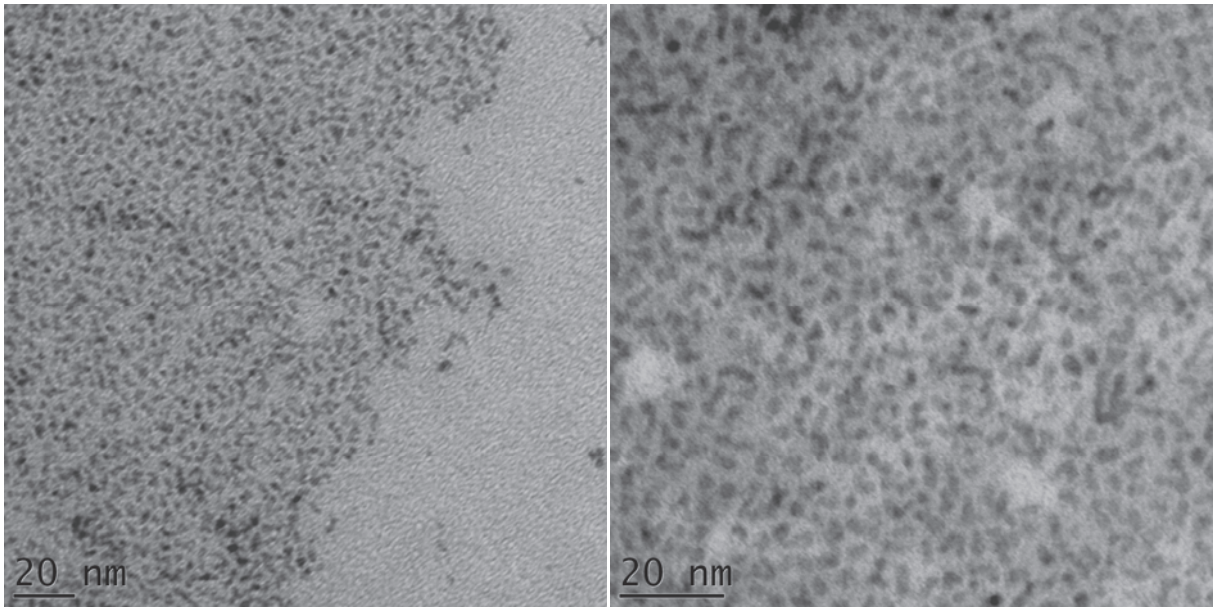

Fig. 12| TEM pictures of NPs obtained by reaction of Mes-Cu on RuNPs already formed under 0.9 MPa of H_2, without stirring, in $C_1C_4ImNTf_2$ at 100 °C.

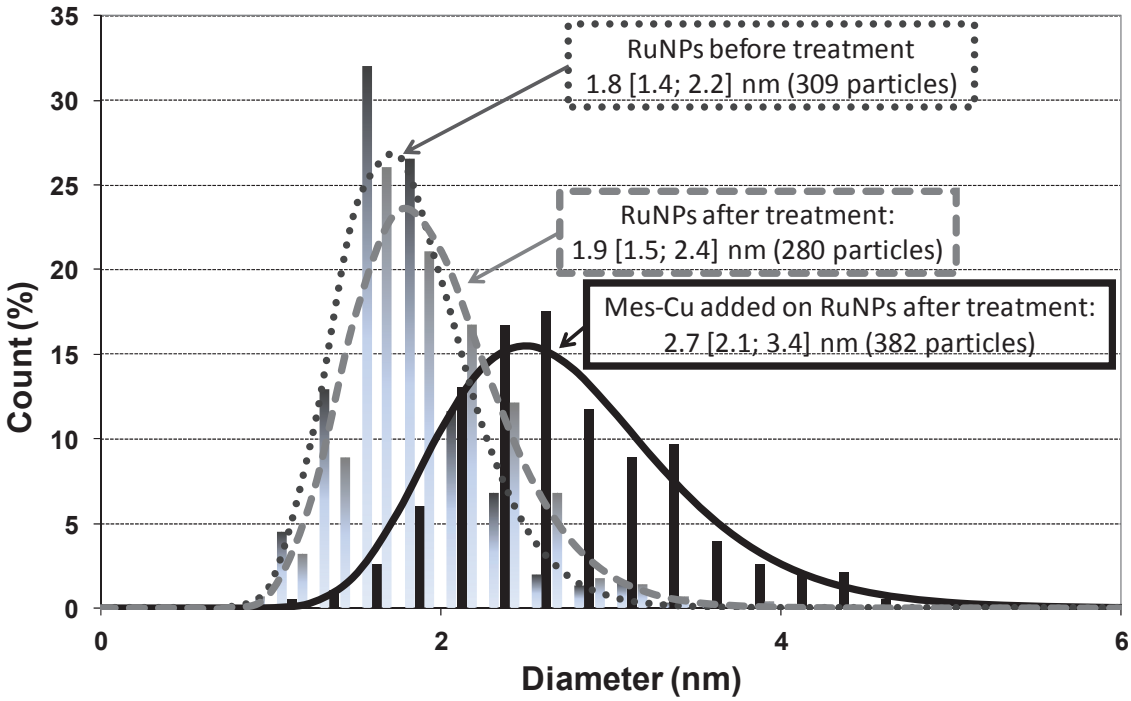

Fig. 13| Comparative size distribution histograms fitted by log-normal law of RuNPs obtained at 0 °C under 0.4 MPa of H_2 without stirring, RuNPs after treatment at 100 °C under 0.9 MPa of H_2, without stirring, in $C_1C_4ImNTf_2$ with or without mixing with a solution of Mes-Cu.

EDX analysis was performed on this sample and presents the same peaks as observed in the synthesis of bimetallic Ru-CuNPs in one step, with presence of both Ru and Cu in the suspension, Figure 14. EDX on a single particle could not be performed due to the high concentration of NPs on grid.

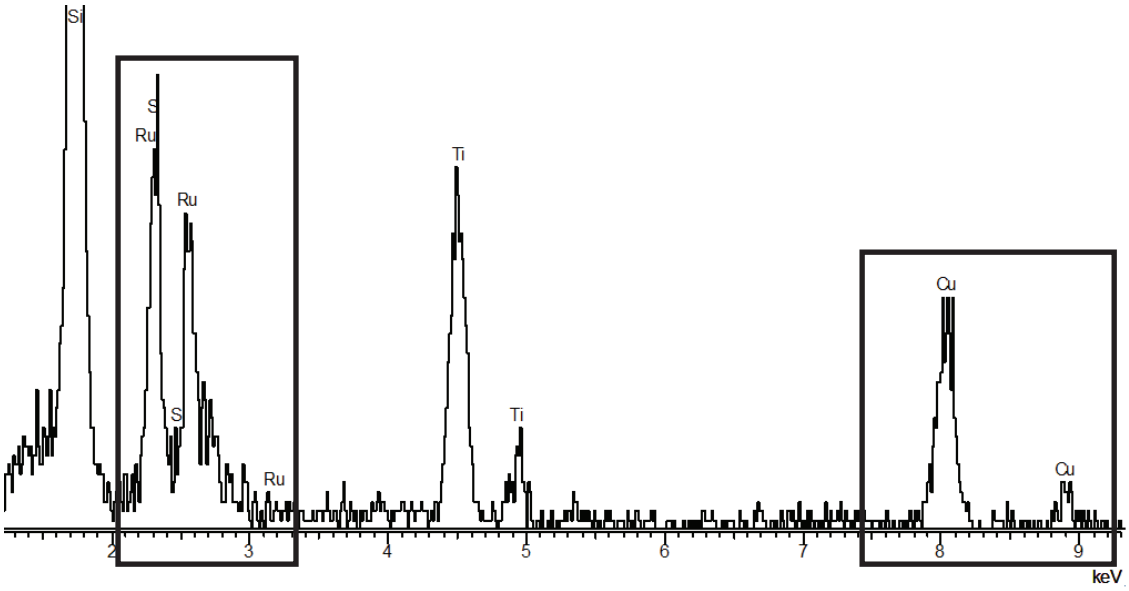

Fig. 14| EDX analysis of NPs obtained from Mes-Cu decomposed on RuNPs already formed; decomposition at 100 °C under 0.9 MPa of H_2 during 4 hours.

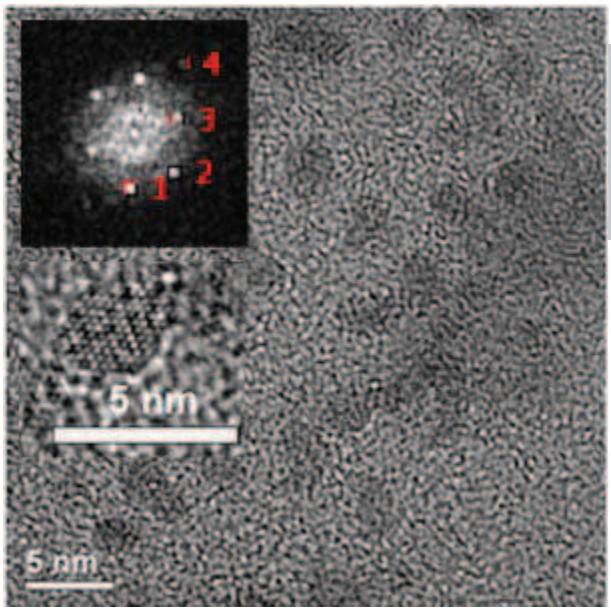

	hkl	d (exp.)	d (theo.)	Angle (exp.)	Angle (theo.)
		Å	Å	°	°
1	101	2.048	2.082	0	0
2	011	2.059	2.082	49.68	51.82
3	-110	2.408	2.382	116.18	115.91
4	-21-1	1.288	1.31	150.79	150.37

Fig. 15| HRTEM picture of NPs obtained from the mixed solution of RuNPs and Mes-Cu, corresponding Fourier transform, and comparative table between Ru hcp structure and crystalline structure observed in our NPs.

HRTEM analysis shows that the NPs formed in two steps are also crystalline. Moreover, as it was the case for Ru-CuNPs formed in one step, only Ru metallic hcp structure is found. No separate CuNPs are observed on this sample, Figure 15. Electron energy loss spectroscopy (EELS) at Cu edge was performed in dark field in order to determine the localization of Cu. Before Cu edge, Cu atoms are not visible in the picture and appear black, as the matrix. After Cu edge, Cu atoms appear in white. In Figure 16, after Cu edge, the NPs appear larger, which suggest that Cu is present around the RuNPs. Bimetallic Ru core Cu shell NPs are consequently obtained by decomposition of Mes-Cu on already formed RuNPs.

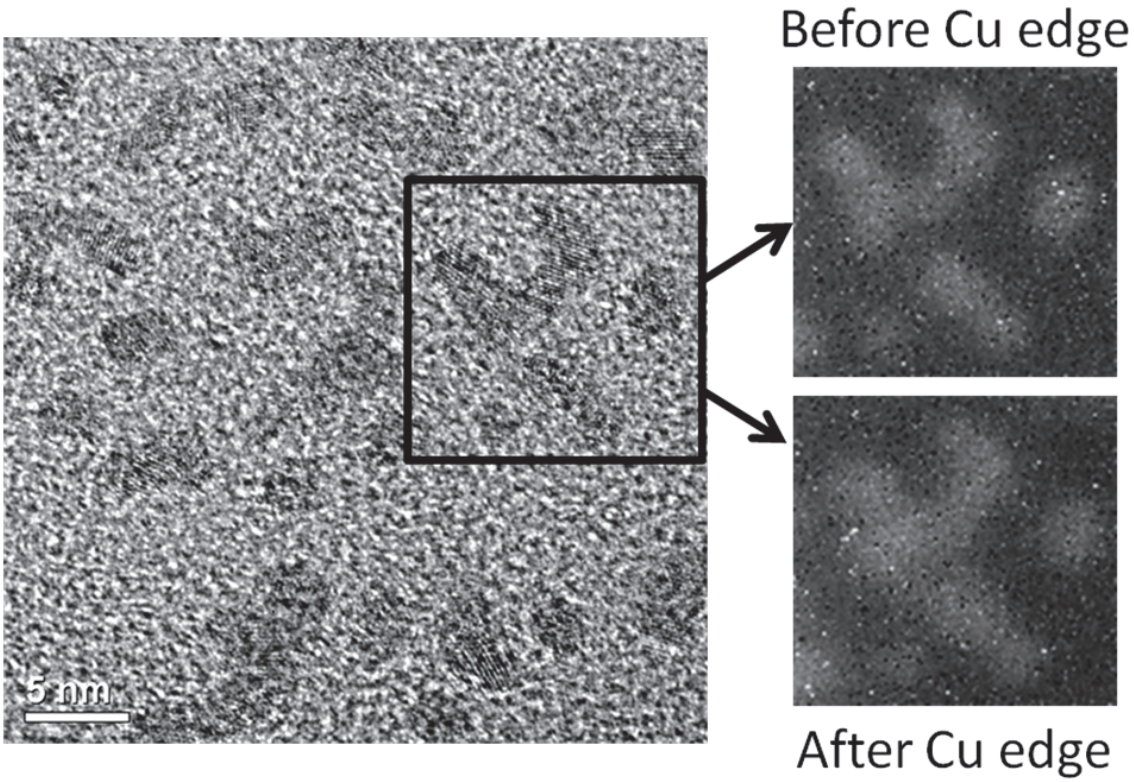

Fig. 16| HRTEM picture and EELS analysis before and after Cu edge.

II.5. Hydrogenation with Ru-CuNPs

In heterogeneous catalysis, Ruthenium-copper alloys have been reported as catalysts in hydrogenation.[30] Generally, a decrease of the activity is reported with increasing copper content.[31-34]

The hydrogenation of benzene into cyclohexane with Ru@Cu NPs in $C_1C_4ImNTf_2$ was studied as a function of copper content maintaining constant all the others conditions of temperature, time, pressure of H_2 and mass transfer. Activity of bimetallic NPs is reported in Figure 17, as a function of χ_{Cu}. A reduction of the activity is clearly observed as copper content increases. A strong decrease of conversion can be seen when the copper content exceeds $\chi_{Cu} = 0.5$. The highest activity is found with nanoparticles with lower Cu content ($\chi_{Cu} = 0.17$). This clearly shows that copper is at the surface of the RuNPs.

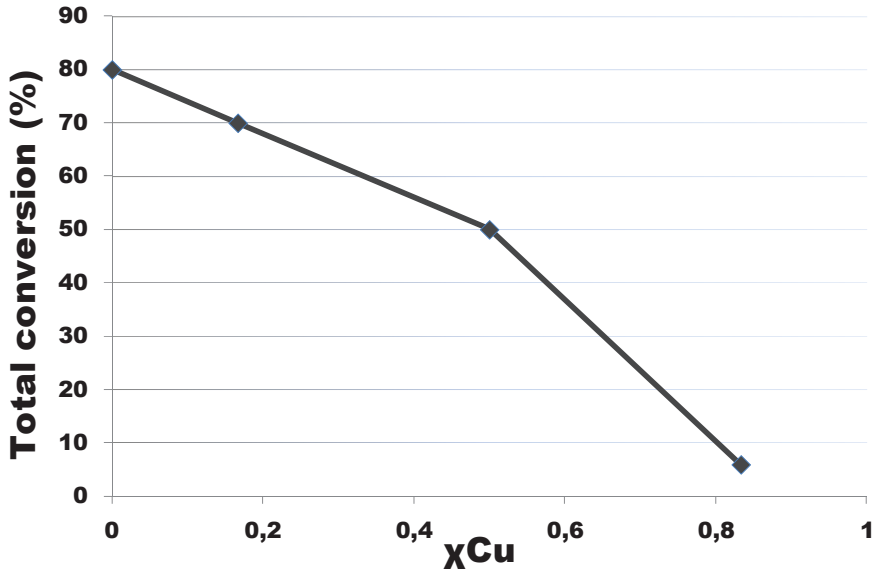

Fig. 17| Conversion in function of molar fraction of Cu in bimetallic Ru-CuNPs.

II.6. Conclusion

Bimetallic Ru-CuNPs are obtained through two processes, decomposition of a solution containing the two precursors or decomposition of Mes-Cu in a suspension of RuNPs. These NPs show smaller size and narrower distribution than the NPs of pure metal obtained in the same conditions. This is certainly due to the mechanism of formation of these NPs, which is in the two cases the same, that is first the decomposition of Ru OM to form RuNPs then reaction of Mes-Cu at the surface. In absence of Mes-Cu, the formation of RuNPs is not controlled (Figure 1).

However, all above results and analytical data suggested that in the reaction of

$$\alpha\ Ru(COD)(COT) + \beta\ Mes\text{-}Cu + x\ H_2 \rightarrow Ru_\alpha Cu_\beta + 2\alpha\ COA + \beta\ Mes\text{-}H$$

RuNPs are firstly formed, then the reduction of Mes-Cu occurs onto the RuNP surface (Figure 18), affording controlled size metallic Ru(0) at the core and metallic Cu(0) at the surface, Ru@Cu, for molar fractions of Mes-Cu ($\chi_{Cu} = \beta/(\alpha+\beta)$) ranging from 0.005 to 0.995, Figure 4. A more comprehensive study of the precise mechanism of the observed phenomena is currently under progress in the laboratory.

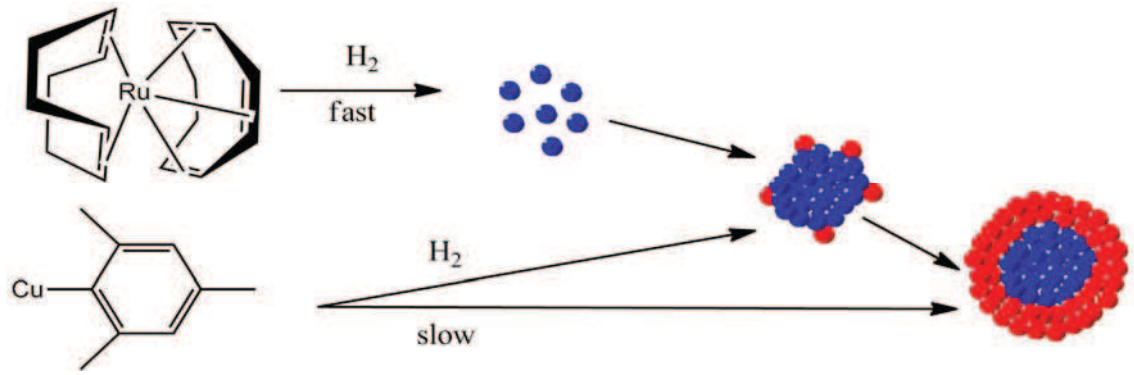

Fig. 18| Hypothetic scheme of formation of bimetallic Ru-CuNPs.

III. Generalization to formation of other bimetallic nanoparticles

Following the previous results with bimetallic Ru-CuNPs and Chaudret's group, if two organometallic precursors (OM_1 and OM_2) exhibit a different rate of decomposition, this chemical route should afford to size and structure controlled bimetallic M_1M_2NPs.[21, 24, 25]

To prove this hypothesis, this chemical approach was applied to other bimetallic systems. As Ru(COD)(COT) is easily decomposed, it was mixed with different organometallic precursors of Ni, Ta , Pt, whose decomposition kinetics are slower. Further experiments were also realized with Cu as slowest decomposition OM: Ni-Cu and Mn-Cu systems were investigated.

III.1. Ruthenium-core based nanoparticles

III.1.i. Ruthenium-nickel

Bis(1,5-cyclooctadiene) nickel, $Ni(COD)_2$ was used as a Ni precursor and 1-hexyl-3-methylimidazolium bis(trifluoromethylsulphonyl)imide, $C_1C_6ImNTf_2$, as a solvent, due to the low solubility of $Ni(COD)_2$ in $C_1C_4ImNTf_2$.

Figure 19 shows the size of the obtained NPs as a function of the molar fraction of Ni: $\chi_{Ni} = \beta/(\alpha+\beta)$ varying from 0.09 to 0.91 where α and β corresponds to OM initial concentration for Ru and Ni respectively.

$$\alpha\ Ru(COD)(COT) + \beta\ Ni(COD)_2 + x\ H_2 \rightarrow Ru_\alpha Ni_\beta + 2\alpha+2\beta\ COA \quad (2)$$

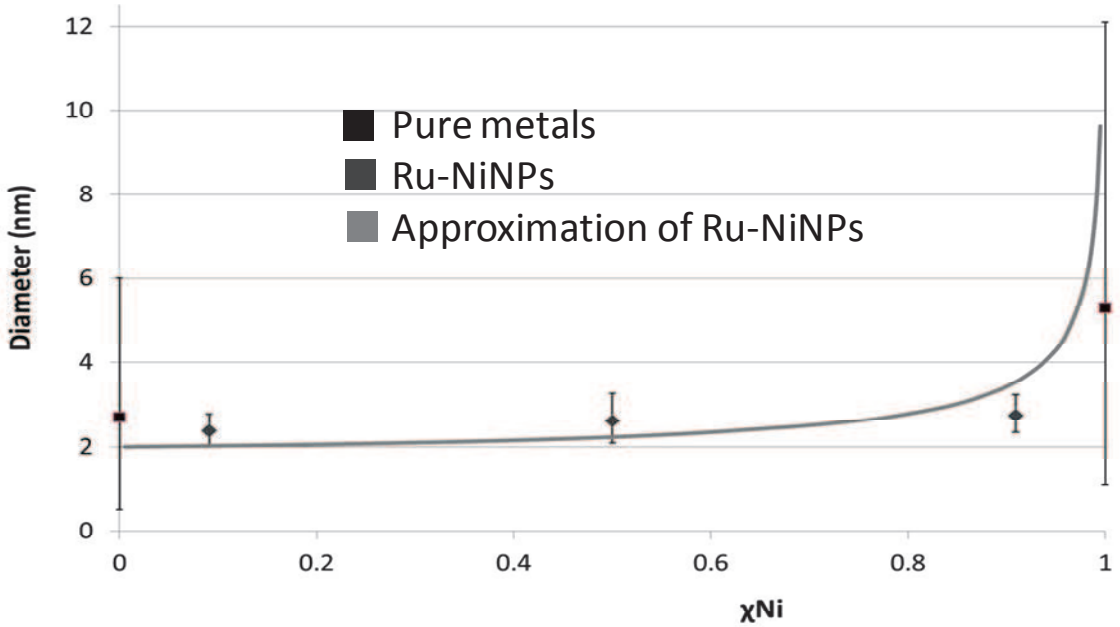

Fig. 19| Graph presenting the size and the distribution of Ru-NiNPs as a function of the molar fraction of Ni OM, $\chi_{Ni} = \beta/(\alpha+\beta)$, obtained at 100 °C under 0.9 MPa of H_2 without stirring during 4 h in $C_1C_6ImNTf_2$.

Note that in these attempts, the total metal concentration was reduced to $1.8x10^{-4}$ M. This low concentration associated to the use of IL $C_1C_6ImNTf_2$ instead of $C_1C_4ImNTf_2$ induces a reduction of the size of RuNPs from 4 to 2.7 nm.

III.1.ii. Ruthenium-tantalum and ruthenium-platinum

Some attempts have been performed with tris(neopentyl)neopentylidenetantalum(V) ($Np_3Ta=CHCMe_3$) and (1,5-cyclooctadiene) dimethylplatinum(II) ($(COD)PtMe_2$) in $C_1C_4ImNTf_2$. Separate decomposition of these two OMs at 100°C under 0.9 MPa H_2 for 4 h affords bulk metal. Surprisingly, a 1:1 molar mixture of Ru(COD)(COT) and $(COD)PtMe_2$, or Ru(COD)(COT) and $Np_3Ta=CHCMe_3$ treated in $C_1C_4ImNTf_2$ at 100°C under 0.9 MPa H_2 for 4 h, yielded NPs with a mean size of 2.6 [2.0; 3.2] nm and 2.4 [1.6; 3.2] nm respectively; compared to RuNPs of 4.0 [2.8; 5.7] nm.

Then, Ru-PtNPs have been also synthesized in two steps. The size obtained of 3.0 [2.3; 3.9] nm is nearly the same than Ru-PtNPs formed in one step. As for Ru-CuNPs, this proves that the decomposition of $(COD)PtMe_2$ occurs onto RuNPs surface.

III.1.iii. Conclusion

Remarkably, a general trend already emerges from these results. A synergetic effect seems to occur when two organometallic precursors (Ru-M_2) are mixed. Smaller NPs than for the pure metals are formed in a large range of molar fractions, except for M_2 rich compositions. This synergetic effect could result from the formation of bimetallic Ru-M_2NPs. The mechanism of formation of Ru-CuNPs seems valid for all Ru-M_2NPs yielding Ru-core bimetallic Ru-M_2NPs, Figure 20.

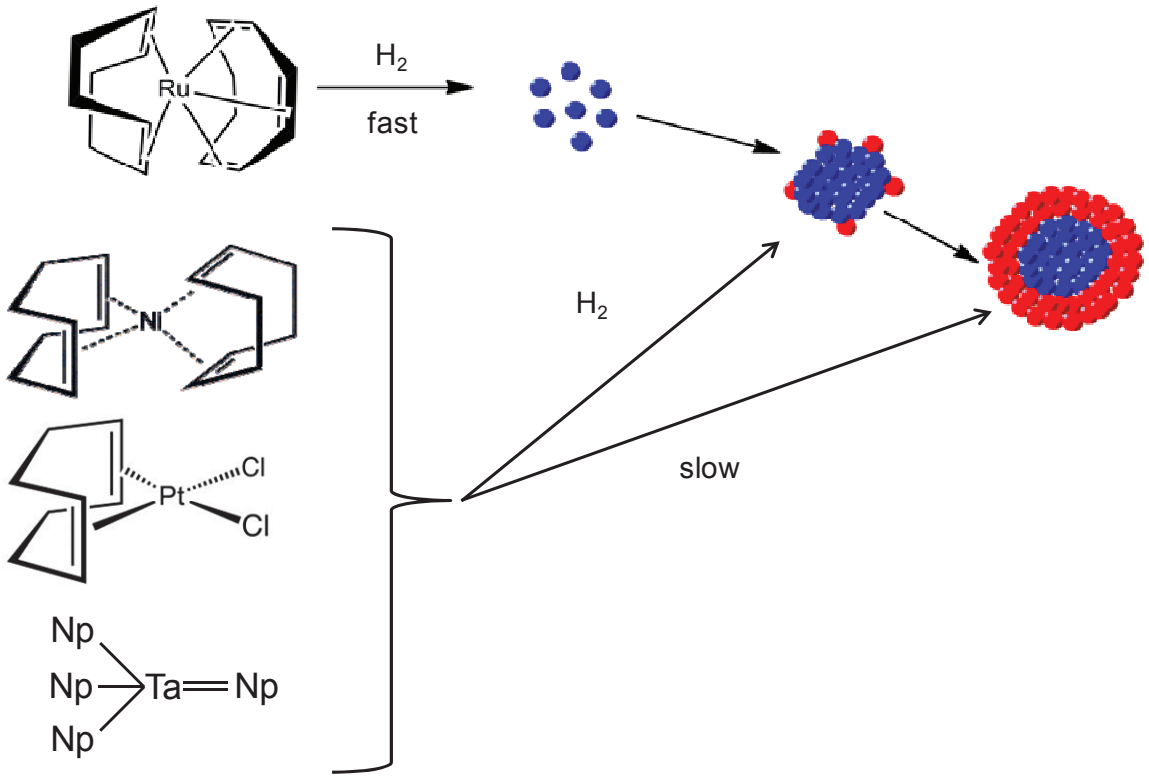

Fig. 20| Hypothetic scheme of formation of bimetallic NPs with Ru-core.

III.2. Synthesis of bimetallic Cu based nanoparticles: Ni-CuNPs

The mechanism of formation of all Ru-M_2NPs yielding Ru-core and M_2 shell is mainly due to the behavior of Ru(COD)(COT). Does this synergetic effect still occur when two other organometallic precursors (OM_1-OM_2) are mixed? In this section, we investigate the decomposition of Mes-Cu in the presence of $Ni(COD)_2$ at 100°C under 0.9 MPa H_2 for 4 h in $C_1C_6ImNTf_2$.

The molar fraction of Cu: $\chi_{Cu} = \beta/(\alpha+\beta)$ was varied from 0.09 to 0.91 where α and β corresponds to OM initial concentration for Ni and Cu, respectively.

$$\alpha\ Ni(COD)_2 + \beta\ Mes\text{-}Cu + x\ H_2 \rightarrow Ni\alpha Cu\beta + 2\alpha COA + \beta\ Mes\text{-}H \quad (3)$$

Comparatively to NiNPs of 5.3 [4.2; 6.8] nm and CuNPs of 4.6 [3.6; 5.9] nm, the Ni-Cu mixture affords slightly smaller NPs (< 4 nm), for $\chi_{Cu} = \beta/(\alpha+\beta)$ ranging between 0.09 and 0.83, Figure 21, Table 2. This effect is less pronounced since decomposition rates of two precursors are closer.

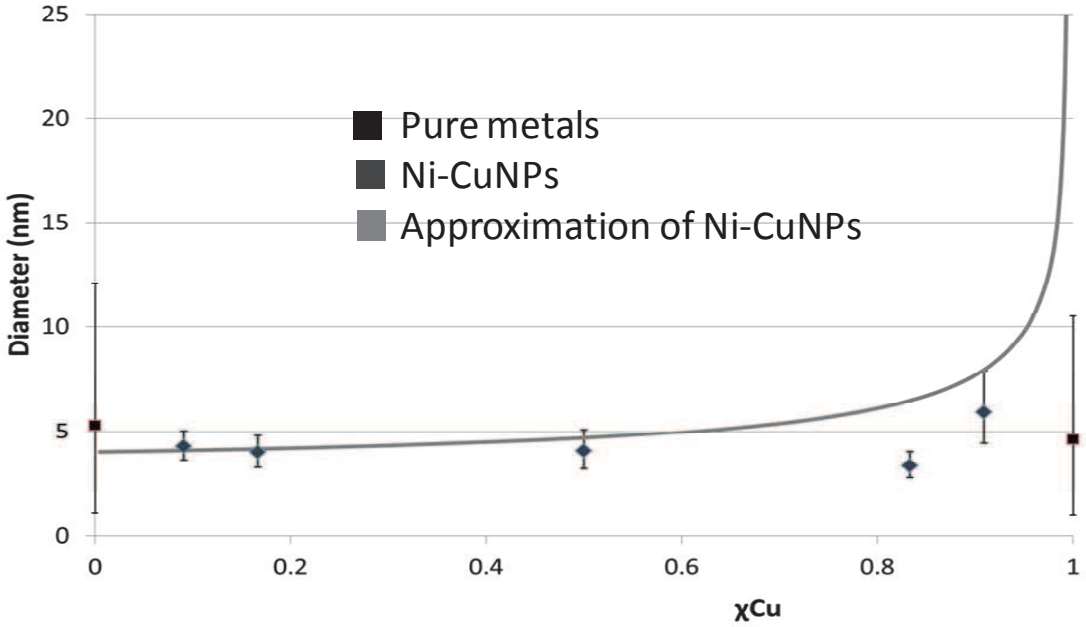

Fig. 21| Size and distribution of Ni-CuNPs as a function of the molar fraction of Cu OM, obtained at 100 °C under 0.9 MPa of H_2 without stirring during 4 h.

The binary phase diagram of Ni-Cu shows that alloy formation is possible whatever the Cu concentration. However, as the Ni surface energy value (1700- 1900 dynes.cm^{-1}) is higher than the Cu one (1100 at 1300 dynes.cm^{-1}), it could be expected that the Cu preferentially remains on Ni surface. In order to support this hypothesis, the catalytic activity of these bimetallic NPs has been studied in the isomerisation reaction of cyclic diene.

Ni catalysts are active in the 1,5-cyclooctadiene (1,5-COD) isomerisation following the catalytic cycle depicted in Figure 22.[35] Contrarily, Cu is known to be inactive. This catalytic reaction was thus conducted in the presence of Ni-CuNPs as a catalyst, in order to study the effect of χ_{Cu} on the catalytic activity.

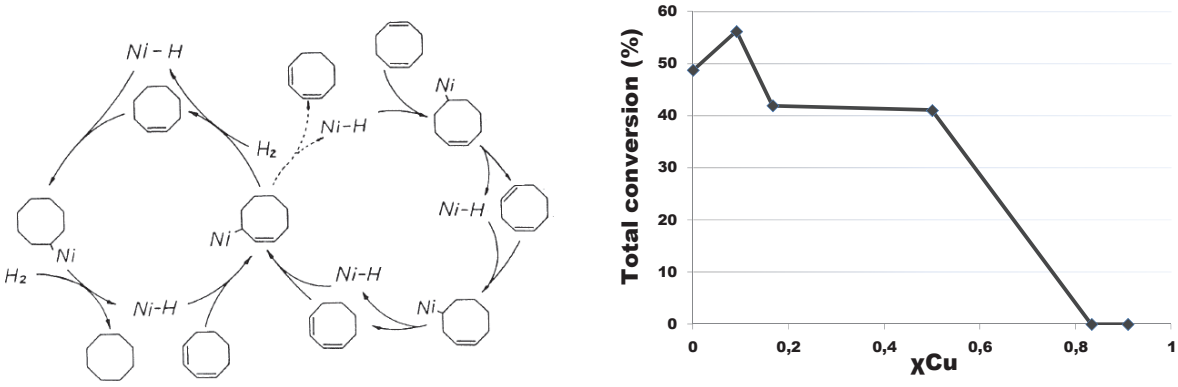

Fig. 22| Catalytic cycle of isomerisation and hydrogenation of 1,5-COD.[35]
Conversion and selectivity in function of molar fraction of Cu in bimetallic Ni-CuNPs.

Besides the molar ratio χ_{Cu}, all others parameters were identical (0.2 MPa of H_2, stirring speed: 1000 rpm, reaction temperature 60 °C, reaction time 2 h, ratio in volume 1,5 COD / IL equal to 0.1, and ratio 1,5 COD / Ms ratio equal to 1000). Increasing χ_{Cu} induces a reduction of 1,5-COD conversion, Figure 22. For χ_{Cu} = 83 %, no more conversion is observed. This result provides evidence that Ni is less accessible when χ_{Cu} increases, probably due to a Cu rich surface in Ni-CuNPs.

III.3. Synthesis of Mn-CuNPs

The synthesis of bimetallic NPs with various metals has been studied in precedent paragraphs. The kinetic control of size and structure of the resulting NPs has been achieved in most of cases in a variety of ratio of metals. Ru-Cu and the others bimetallic M-Cu (M = Ta, Ni,...) reported in Chapter III and Appendix 1 have no major interest in microelectronics. Contrarily, bimetallic Mn-CuNPs could enable the synthesis in a further annealing step of self-formed barrier layer and copper seed layer needed in microelectronic devices.[36] In this part, we report thus our attempts to form Mn-CuNPs from a mixture of organometallic precursors (Mes-Cu and $MnNp_2$) under H_2 (Chapter II). Here also, the reduction occurs at 100 °C under 0.9 MPa of H_2 without stirring in $C_1C_4ImNTf_2$ for 4 h.

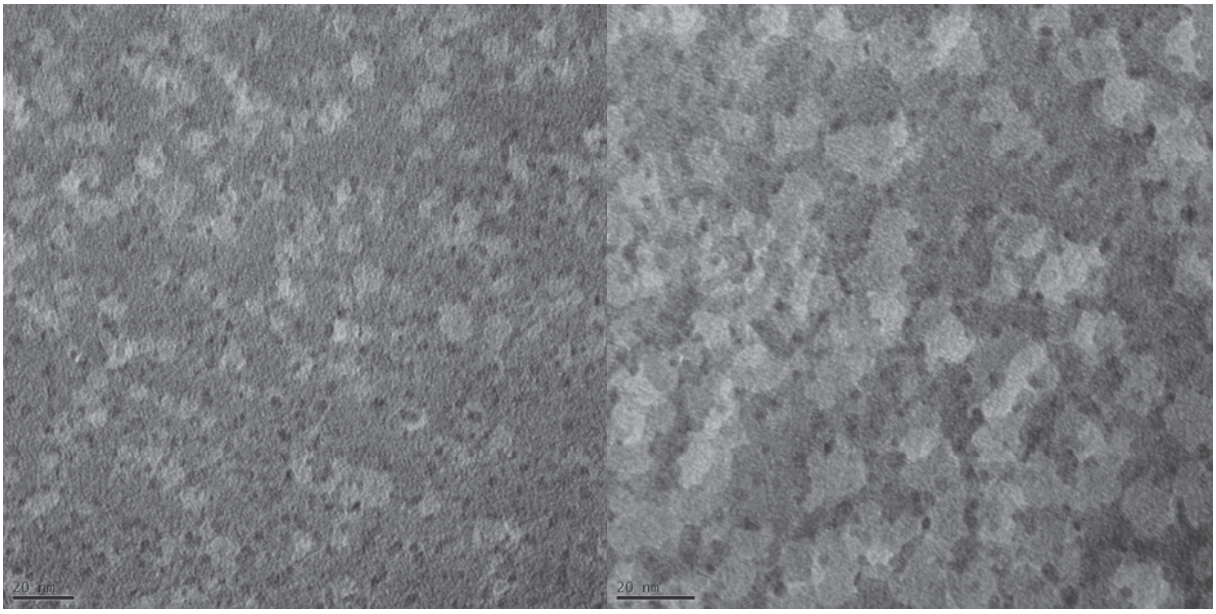

Fig. 23| TEM picture of Mn-CuNPs with 1:1 ratio of $MnNp_2$ and Mes-Cu.

Note that in these conditions, pure OMs yield CuNPs of 5.1 [4.2; 6.3] nm and MnNPs of 2.3 [1.8; 3.0] nm. As in the case of Ru-CuNPs, when χ_{Cu} varies between 0.09 and 0.91, the resulting NPs have a similar mean sizes (2.6 [2.1; 3.3] nm $\chi_{Cu} = 0.09$; 2.9 [2.3; 3.7] nm $\chi_{Cu} = 0.5$; 2.7 [2.1; 3.3] nm $\chi_{Cu} = 0.91$), Figure 24.

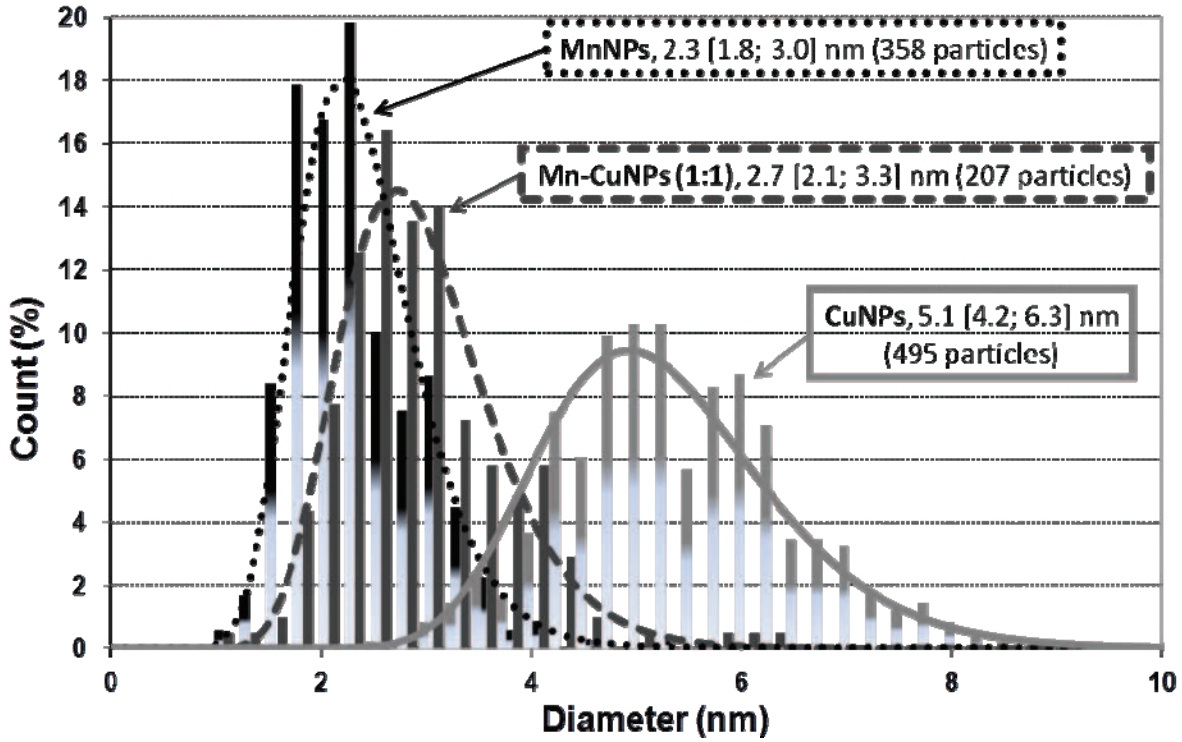

Fig. 24| Comparative size distribution histograms fitted by log-normal law of MnNPs, Mn-CuNPs ($\chi_{Cu} = 0.5$) and CuNPs obtained at 100 °C with $5x10^{-2}$ M total concentration of precursors under 0.9 MPa of H_2 without stirring during 4 hour in $C_1C_4ImNTf_2$.

In EDX analysis, these NPs are composed of Mn and Cu, Figure 25. (Ti comes from TEM grid used and Si from vacuum grease dissolved in IL).

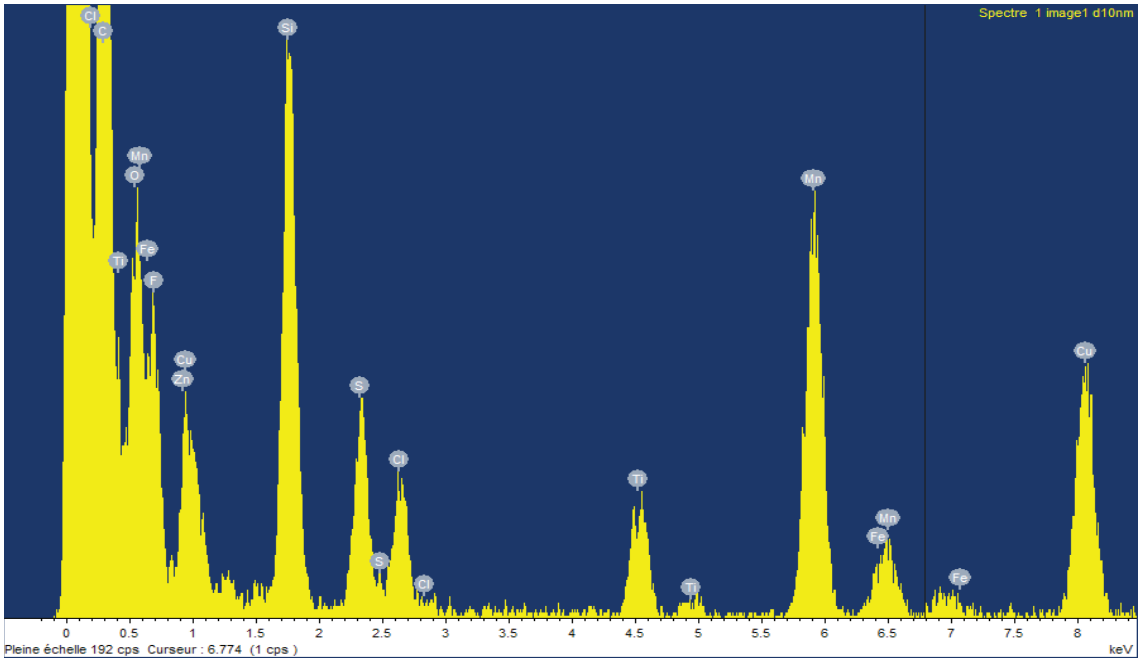

Fig. 25| EDX analysis of area where NPs are present.

HRTEM analysis has been performed on Mn-CuNPs with difficulty, since a large increase of NPs size is observed during the analysis, Figure 26. This clearly demonstrates a sintering of NPs under beam. However, it could be determined that crystalline cubic NPs are obtained, Figure 27.

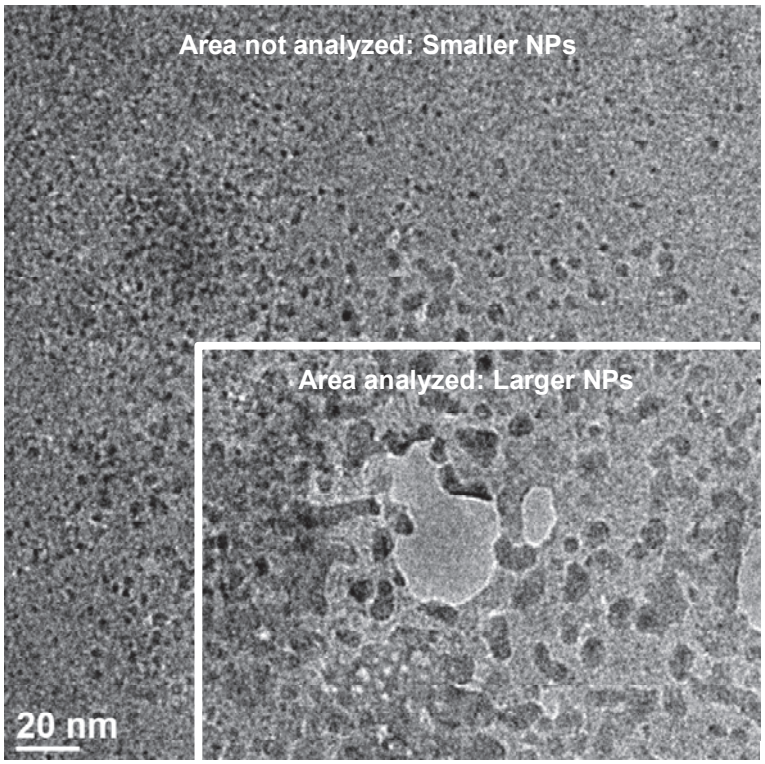

Fig. 26| TEM picture of Mn-CuNPs (ratio 1:1) showing the increase of size observed under electron beam.

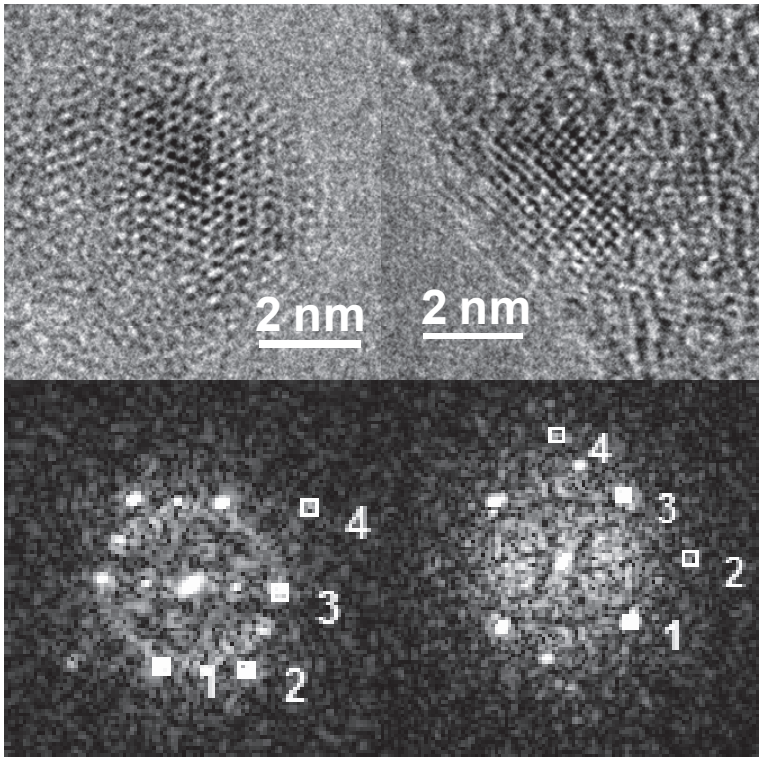

Fig. 27| HRTEM analysis of Mn-CuNPs (ratio 1:1), top: crystalline NPs obtained; bottom: diffraction patterns of NPs above.

Table 3| Comparison between experimental data and three theoretical crystalline structures: Mn Cubic (JCPDS n°89-4857), Cu_2O centered cubic (JCPDS n°01-1142) and MnO cubic (01-1206).

Picture/Spot	1/1	1/2	1/3	1/4	2/1	2/2	2/3	2/4
d(exp.)(nm)	**2.50**	**2.11**	**2.50**	**1.52**	**2.16**	**1.57**	**2.21**	**1.56**
hkl	211	022	-211	-400	220	040	-220	-400
d(Mn.)(nm)	2.58	2.23	2.58	1.58	2.23	1.58	2.23	1.58
hkl	111	200	1-1-1	0-2-2	200	220	020	-220
d(Cu_2O)(nm)	2.45	2.12	2.45	1.51	2.12	1.51	2.12	1.51
d(MnO)(nm)	2.56	2.22	2.56	1.57	2.22	1.57	2.22	1.57
Angle(exp.)	**0**	**54.22**	**107.13**	**144.30**	**0**	**44.55**	**88.56**	**135.31**
Angle(Mn)	0	54.74	109.47	144.74	0	45	90	135
Angle(Cu_2O)	0	54.74	109.47	144.74	0	45	90	135
Angle(MnO)	0	54.74	109.47	144.74	0	45	90	135

The experimental distances and angles between plans derived are reported in Table 3 from HRTEM pictures shown in Figure 27. They are compared to several metal and oxide crystal structures. From d values, it seems that centered cubic Cu_2O, cubic MnO or cubic metallic Mn or more probably a mix of these crystalline structures. XPS analysis, Figure 28, shows that no metallic Mn typical peak at 638.6 eV is observed, and that the Cu $2p_{3/2}$ (932.9 eV) and Cu LMM (914.6 eV) values correspond to Cu_2O. Mn oxide peaks are too broad and not well separated, preventing accurate determination of oxidation state (Chapter II). Hence, it is difficult to conclude from these analyses on the nature of Mn-CuNPs. However, it has been shown that metallic Cu and metallic MnNPs are obtained under the same reaction conditions (Chapter II). Oxidation could occur during the transfer or the storage of NPs. In conclusion, the control of the NP size when χ_{Cu} varies in the range between 0.09 and 0.91 and the analytical results let us suggest that there is formation of bimetallic Mn-CuNPs which have been analyzed under oxidized state. Further characterization and experiments are under progress.

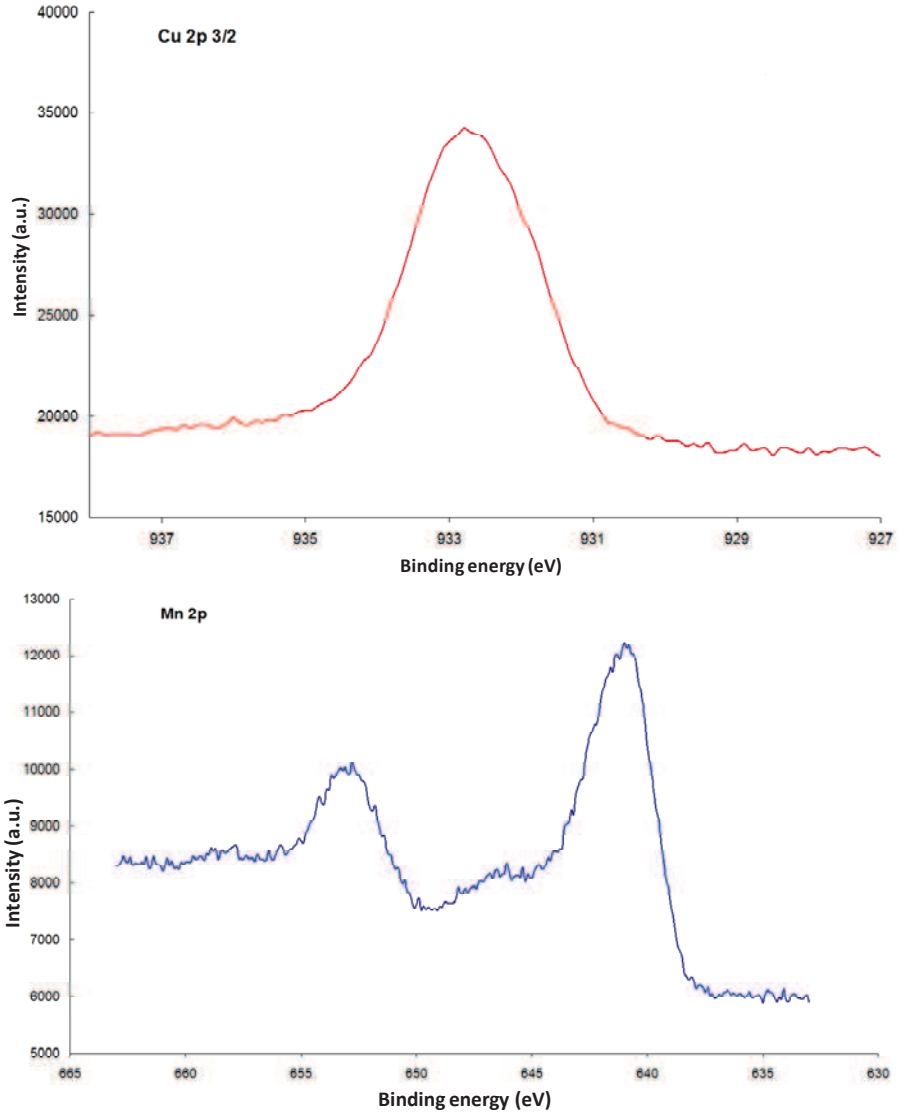

Fig. 28| XPS spectra of Mn-CuNPs (ratio 1:1), top: Cu $2p_{3/2}$ area, bottom: Mn2p area. No clear determination of LMM Cu.

III.4. Conclusion

Bimetallic NPs based on Ru core or Cu shells have been obtained by generalization of the process used mixing two OM precursors. Slighter decreases of size are observed when mixing the two precursors, due to closer kinetics of decomposition between the two precursors used.

The synthesis of bimetallic Mn-CuNPs has been achieved in a single step decomposition. The characterization of these particles is still under investigation.

IV. Conclusion

In ionic liquids, it is possible to generate size-controlled monometallic NPs by decomposition under dihydrogen of organometallic precursors.[7, 8] The aim of this chapter was to prove the possibility to synthesize bimetallic nanoparticles with controlled size by simultaneous decomposition of organometallic precursor under dihydrogen

Remarkably, a general trend emerges from our results. A synergetic effect seems to occur when two organometallic precursors OM_1-OM_2 ((1,5-cyclooctadiene)(1,3,5-cyclo-octatriene)ruthenium Ru(COD)(COT); mesitylcopper Mes-Cu; bis(1,5-cyclooctadiene) nickel $Ni(COD)_2$; tris(neopentyl)(neopentylidene) tantalum $Np_3Ta{=}CHCMe_3$; (1,5-cyclooctadiene) dimethylplatinum $Pt(COD)Me_2$; bis(neopentyl)manganese $MnNp_2$) are mixed, Figure 31. Smaller NPs than for the pure metals are formed in a large range of molar fractions, except for M_2 rich compositions. Their formation and the controlled size result from the fast decomposition of M_1 organometallic precursor (OM_1) which occurs first, followed by the reaction of OM_2 onto the M_1NP surface. This synergetic effect could lead to the formation of bimetallic M_1-M_2NPs. In the case of (M_1 = Ru, M_2 = Cu), EDX, XPS, HRTEM and EELS analyses of resulting bimetallic NPs prove that there is a metallic Ru(0) core and metallic Cu(0) at the surface, Ru@CuNPs.

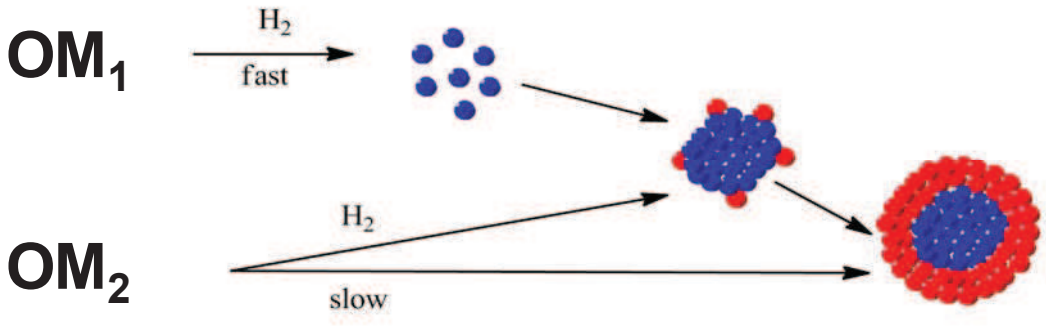

OM_1 = Ru(COD)(COT) for OM_2 = (Mes-Cu, $Ni(COD)_2$, $(COD)PtMe_2$, $Np_3Ta{=}CHCMe_3$)
OM_2 = Mes-Cu for OM_1 = (Ru(COD)(COT), $Ni(COD)_2$, $Np_3Ta{=}CHCMe_3$)
OM_1 = Mes-Cu for OM_2 = $MnNp_2$
Fig. 29| Hypothetic scheme of formation of bimetallic NPs in IL.

References

[1] H. Bönnemann, K.S. Nagabhushana, Metal Nanoclusters: Synthesis and Strategies for their Size Control, in: B. Corain, G. Schmid, N. Toshima (Eds.) Metal Nanoclusters in Catalysis and Materials Science, Elsevier, Amsterdam, 2008, pp. 21-48.
[2] G.A. Somorjai, J.Y. Park, Topics in Catalysis, 49 (2008) 126-135.
[3] D. Mott, J. Galkowski, L. Wang, J. Luo, C.-J. Zhong, Langmuir, 23 (2007) 5740-5745.
[4] G. Schmid, Nanoparticles: From Theory to Application, Wiley-VCH, Weinheim, 2004.
[5] D. Astruc, in, Wiley-VCH, Weinheim, 2008.
[6] J. Dupont, J.D. Scholten, Chem. Soc. Rev., 39 (2010) 1780-1804.
[7] T. Gutel, J. Garcia-Anton, K. Pelzer, K. Philippot, C.C. Santini, Y. Chauvin, B. Chaudret, J.-M. Basset, J. Mater. Chem., 17 (2007) 3290-3292.
[8] T. Gutel, C.C. Santini, K. Philippot, A. Padua, K. Pelzer, B. Chaudret, Y. Chauvin, J.-M. Basset, J. Mater. Chem., 19 (2009) 3624-3631.
[9] R. Ferrando, J. Jellinek, R.L. Johnston, Chem. Rev., 108 (2008) 845-910.
[10] D.S. Wang, Y.D. Li, Adv. Mater., 23 (2011) 1044-1060.
[11] K.-i. Okazaki, T. Kiyama, K. Hirahara, N. Tanaka, S. Kuwabata, T. Torimoto, Chem Commun (Camb), (2008) 691-693.
[12] T.-H. Tsai, S. Thiagarajan, S.-M. Chen, J. Appl. Electrochem., 40 (2010) 493-497.
[13] J. Xi, W.-s. Dong, Shaanxi Shifan Daxue Xuebao, Ziran Kexueban, 38 (2010) 62-64.
[14] P. Dash, N.A. Dehm, R.W.J. Scott, J. Mol. Catal. A: Chem., 286 (2008) 114-119.
[15] P. Dash, S.M. Miller, R.W.J. Scott, J. Mol. Catal. A: Chem., 329 (2010) 86-95.
[16] P. Dash, R.W.J. Scott, Chem. Commun. (Cambridge, U. K.), (2009) 812-814.
[17] T. Jiang, Y. Zhou, S. Liang, H. Liu, B. Han, Green Chem., 11 (2009) 1000-1006.
[18] B. Chaudret, C. R. Phys., 6 (2005) 117-131.
[19] C. Pan, F. Dassenoy, M.-J. Casanove, K. Philippot, C. Amiens, P. Lecante, A. Mosset, B. Chaudret, J. Phys. Chem. B, 103 (1999) 10098-10101.
[20] P.P. Arquillière, P.-H. Haumesser, C.C. Santini, Microelectron. Eng., 92 (2012) 149-151.
[21] P.P. Arquilliere, C.C. Santini, P.-H. Haumesser, M. Aouine, ECS Trans., 35 (2011) 11-16.
[22] G. Moretti, in: H.K. G. Ertl, J. Weitkamp (Ed.) Handbook of Heterogeneous Catalysis, Wiley-VCH: Weinheim, 1997, pp. 632.
[23] G. Moretti, G. Ferraris, G. Fierro, M.L. Jacono, Surf. Interface Anal., 38 (2006) 224-228.
[24] N. Atamena, D. Ciuculescu, G. Alcaraz, A. Smekhova, F. Wilhelm, A. Rogalev, B. Chaudret, P. Lecante, R.E. Benfield, C. Amiens, Chem. Commun. (Cambridge, U. K.), 46 (2010) 2453-2455.
[25] D. Ciuculescu, C. Amiens, M. Respaud, A. Falqui, P. Lecante, R.E. Benfield, B. Chaudret, Chem. Mater., 19 (2007) 4624
[26] M.J.L. Massalski T.B., Bennett L. H., Baker H., Binary Alloy Phase Diagrams. Vol. I and II. , 1986.
[27] J.A. Rodriguez, R.A. Campbell, D.W. Goodman, J. Phys. Chem., 95 (1991) 2477-2483.
[28] C.R. Hammond, CRC Handbook of Chemistry and Physics 81st edition, 2004.
[29] P.S. Campbell, C.C. Santini, D. Bouchu, B. Fenet, K. Philippot, B. Chaudret, A.A.H. Padua, Y. Chauvin, Phys. Chem. Chem. Phys., 12 (2010) 4217-4223.
[30] H. Liu, S. Liang, W. Wang, T. Jiang, B. Han, J. Mol. Catal. A: Chem., 341 (2011) 35.
[31] J.H. Sinfelt, J. Catal., 29 (1973) 308-315.

[32] J.H. Sinfelt, Int. Rev. Phys. Chem., 7 (1989) 281-315.
[33] C. Crisafulli, R. Maggiore, S. Scire, S. Galvagno, C. Milone, J. Mol. Catal., 83 (1993) 237-250.
[34] M.W. Smale, T.S. King, J. Catal., 119 (1989) 441-450.
[35] Y.L. Chow, H. Li, Can. J. Chem., 64 (1986) 2229-2231.
[36] J. Koike, M. Wada, Appl. Phys. Lett., 87 (2005).

Chapter IV

Growth of Metallic Films by Sintering of Nanoparticles through Thermal Annealing

Chapter IV

Growth of metallic films by Sintering of Nanoparticles through Thermal Annealing

I. Introduction

I.1. Use of self-formed barriers for the metallization of through silicon vias (TSVs)

The synthesis of uniform nanofilms attracts a growing interest notably in the microelectronic industry. Indeed, new pathways for the synthesis of barrier and seed layers are required to continue to use Cu in future interconnects. In particular, the development of 3-D technologies which allows the fabrication of faster and more reliable processors demands new, low-cost processes. In this way, the development of self-formed barrier layer generates a high interest, with the decreasing of steps number in metallization process. In this new process, Koike and co-workers have developed the synthesis of Mn-Cu alloy from physical or chemical vapor deposition method.[1, 2] The annealing of this alloy allows segregating of the two metals for formation in one step of barrier and seed layers. This one is also study as enhanced seed layer, with promoting barrier and binding. Indeed, Mn reacts with SiO_2 during the annealing with the formation of layer composed predominantly of amorphous $MnSiO_3$ and crystalline MnO.[3] These process use high vacuum which could be applied to common interconnection, but which are too expensive for "through silicon vias" (TSVs), a chief subject for 3-D integration. Moreover, PVD technique does not allow obtaining uniform deposition in such high aspect-ratio structures, Table 1.

Table 1| PVD Ta/TaN barrier layer deposited on TSV of 5x50 µm. [4]

Place	Above	Sidewall	Bottom Side wall	Bottom
Thickness obtained in nm	134	6.6	3.0	2.1

I.2. Formation of metallic film from nanoparticles (NPs)

Hence, for the metallization of TSVs in the 3-D integration of interconnects a technique capable of depositing thin and conformal copper, manganese and copper-manganese liners

would be of particular interest to form suitable seed, barrier and self-formed barrier layers, respectively.[2, 5] In this context, metallic nanoparticles (NPs) could be promising precursors for this application. Indeed, the synthesis of Cu layers has been demonstrated from annealing of a suspension of amine-stabilized CuNPs in an organic solvent.[6] In this case, the presence of the amine-based stabilizer leads to insufficiently conductive films, due to impurity inclusion during annealing. A film with higher conductivity was obtained with the direct decomposition of precursors in the organic solvent. More recently, a similar approach has been described for the metallization of TSVs using AgNPs in an organic solvent. By controlled evaporation of the suspension, a conformal coating composed of NPs is formed within the TSVs. After annealing, a dense film is obtained, which could be used as a seed layer for subsequent Cu electroplating.[7] Nevertheless, this process is described on SiO_2, not on barrier layers. Moreover, the presence of stabilizer in the suspension certainly induces a loss of conductivity. Yabuki and co-workers have also used such a process to sinter carbon coated CuNPs. The resistivity obtained is the same as obtained by Barriere and co-workers, 10 times higher than the resistivity of pure Cu. This is certainly due to incorporation in the structure of carbon and other defects upon annealing.[8] Therefore, in all of these attempts, the main difficulty comes from the use of stabilized NPs, leading to metal contamination and consequently loss of conductivity. Synthesis of Cu-Mn films from bimetallic NPs has not been reported at our knowledge.

In the previous chapters, we have described the synthesis of CuNPs, MnNPs as well as bimetallic Mn-CuNPs. Here, we report our attempts to form conformal layers from suspensions of CuNPs, MnNPs and Mn-CuNPs in different imidazolium ILs. Such layers are tentatively synthesized by direct application of the suspensions on oxidized silicon wafers followed by annealing. In a first section, the interaction of ILs and suspension with the sample surface will be studied using contact angle measurements. Then, diffuse reflectance infrared

Fourier transform (DRIFT) experiments will be described and the thermal stability of the suspensions will be investigated, yielding adequate conditions for annealing. Finally, the metallic coatings formed upon thermal treatment in a rapid thermal process oven (RTP-oven) will be examined by scanning electron microscopy (SEM) and profilometry techniques.

II. Wettability of imidazolium based ILs on wafer

An efficient process to form metallic films from suspensions of NPs in ILs requires a strong interaction between the liquid and the substrate. Therefore, it is necessary, in a first approach, to characterize the interaction of our ILs and suspensions towards surfaces of interest. In the final application, the Mn-Cu alloys should be deposited onto dielectric liners used to electrically insulate TSVs from the semiconducting substrates. Usually, these liners are composed of silicon oxide.[9] Therefore, the behavior of ILs and suspensions needs to be studied on such surfaces.

A simple technique to approach this question consists in measuring the contact angle of liquid drops on the surfaces of interest, as described in Chapter V. In this work, selected oxide surfaces were used to mimic insulation layers used in TSVs. Three variants of silicon oxide were considered, Ox1 (SiO_2 film deposited by silane decomposition), Ox2 (thermal oxide) and Ox3 (calcinated Ox2). On each of these surfaces, the wettability of ILs was studied, varying the nature of the IL (alkyl chain length), its water content, the nature and concentration of metallic NPS.

II.1. Influence of alkyl chain length and water content

The evolution of contact angle for $C_1C_nImNTf_2$, n = 4, 6, 8 on CVD oxide wafer (Ox1) is shown in Figure 1a. For all ILs, an initial decrease of contact angle was recorded before stabilization of drop shape. This decrease is more pronounced for shorter alkyl chains (n = 4, 6). Also, the final value is significantly lower for these ILs as compared to octyl alkyl chain ($C_1C_8ImNTf_2$). This result is consistent with previous reports, and can be attributed to the increased hydrophobicity of long alkyl substituents, leading to a decreased wetting of this hydrophilic oxide surface.[10-12] Also, after moisture uptake of $C_1C_4ImNTf_2$ under air (which is limited to 0.32 M [13]), the contact angle value is increased (Figure 1a).

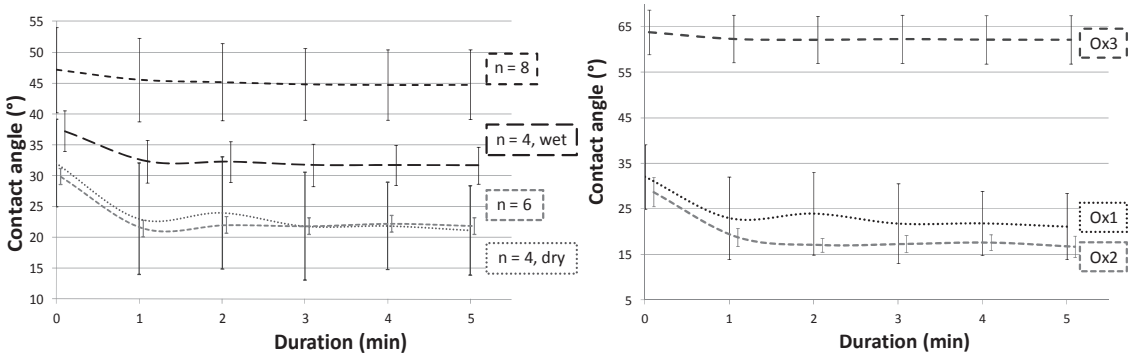

a b

Fig. 1| Evolution of contact angle over time of (a) $C_1C_nImNTf_2$ (n = 4, 6, 8) on Ox1, and (b) $C_1C_4ImNTf_2$ on different oxide surfaces: Ox1: CVD SiO_2, Ox2: thermal SiO_2, Ox3: dehydrated thermal SiO_2.

The wetting behavior of $C_1C_4ImNTf_2$ was further investigated using several flavors of silicon oxide surfaces. The contact angle results measured on CVD (Ox1) and thermal oxides (Ox2 and Ox3) are printed in Figure 1b. As expected, the nature of the surface greatly influences contact angle values. Ox1 and Ox2 exhibit similar contact angle values that are significantly lower than for Ox3.

This clearly indicates that the amount of surface silanol groups (≡Si-OH) greatly influences the wetting behavior of this IL.[14] Indeed, the various flavors of oxides have both silanol (≡Si-OH, =Si-$(OH)_2$) groups and siloxane bridges(≡Si-O-Si≡), the density and relative ratio of which are controlled by the thermal pretreatment inducing dehydration and dehydroxylation reactions (Scheme 1a and b, respectively).

a b

Scheme 1| a. Dehydration of physisorbed water on silica surface. b. Dehydroxylation reaction forming siloxane bridge by condensation.

Although the use of IL in surface-dependent processes (eg. electrodeposition, heterogeneous catalysis, dye solar cells) is common, the understanding of IL interfacial structure is still under debate. Padua and Canongia Lopes show that alkyl chains of 1-(2-hydroxyethyl)-3-methylimidazolium tetrafluoroborate are more parallel to the glass surface in first layer and perpendicular in next layers. [15] This change of structure is due to huge interaction with silica surface and thus more random distribution is observed by moving away from the interface.

Two chief opinions are distinguished for IL/silica interface. Through sum frequency generation spectroscopy and AFM experiments, Fitchett and Atkin proposed that the imidazolium cation is adsorbed first with its orientation mainly independent of cation alkyl chain length and anion structure.[12, 16] Contrarily, Wipff and coworkers, modeling the interaction of IL on hydroxylated quartz surface, found that the IL-surface interaction was mainly controlled by hydrogen bond between NTf_2^- anion and surface silanol groups.[13] They show that in all cases, the second layer of liquid is composed of imidazolium cations with the chain parallel to the surface. In the upper layers, the orientation of the cation depends on chain length, with shorter chains (n = 4, 6) mostly perpendicular to the surface, whereas longer chains (n = 8) remain coplanar to the surface. This theory could explain most of our observations.

(i) The strength of interaction between NTf_2^- and ≡Si-OH is expected to depend on silanol surface concentration. Therefore, on calcinated surface (Ox3), this interaction is weakest, which affords for the increase of contact angle.

(ii) The proximity of alkyl chains with a polar surface should lead to repulsive interactions. Hence, such effect is expected to be more prominent with the octyl chains which remain parallel to the surface even in the upper layers of liquid.

(iii) This model also predicts that water is not likely to interact directly with silica, but remains dissolved in the IL. Thus, the only effect that could account for an increase in contact angle with water absorption would be an increase of the liquid/vapor surface tension. Such an increase would be consistent with the higher surface tension of water as compared to IL.[11, 17]

Indeed, it has been demonstrated for imidazolium tetrafluoroborate salts that a large drop of liquid-gas surface tension is observed by adding a very small quantity of IL in pure distilled water. It could be reasonably suppose than an increase of liquid-gas surface tension of IL/water mixture will be observed compared to pure IL.[18]

II.2. Wetting of NPs suspension in ILs on thermal oxide surface

In the previous chapters, it was shown that $C_1C_4ImNTf_2$ is a solvent of choice for the synthesis of NPs. To maximize the response of wetting angle on the presence of metallic NPs within the surface, the experiments were conducted on Ox3 for which the interaction with IL is minimal. Contact angle evolution for two suspensions with increasing copper concentrations are compared to pure IL in Figure 3. Initially, the contact angle value is similar to that of pure IL, but drops after 1 min. The stable wetting angle becomes lower than for the pure IL, and this drop is larger with increased copper concentration. Such an effect is generally observed in all liquid media, provided that metal content is above 1 weight %.[19-21] However, the reason for this behavior is still under debate. In our case, it is reasonable to invoke the strong interaction between zero-valent copper and the oxide surface. This is an encouraging indication that suspensions of CuNPs in ILs are good candidates to metalize oxide surfaces.

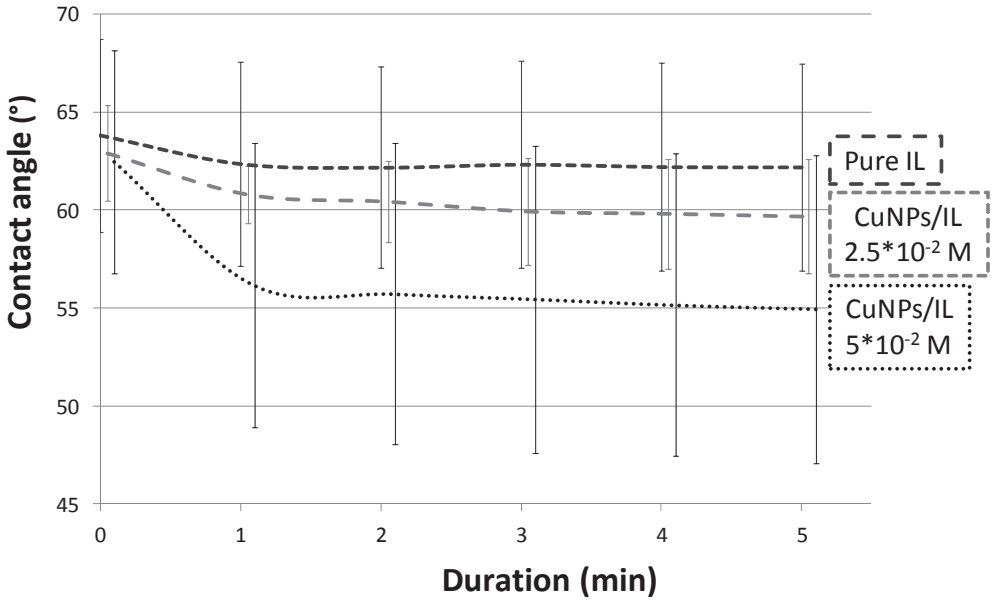

Fig. 2| Evolution of contact angle over time of pure $C_1C_4ImNTf_2$ and suspensions of CuNPs with Cu concentration of $2.5x10^{-2}$ M (CuNPs-1) and $5x10^{-2}$ M (CuNPs-2).

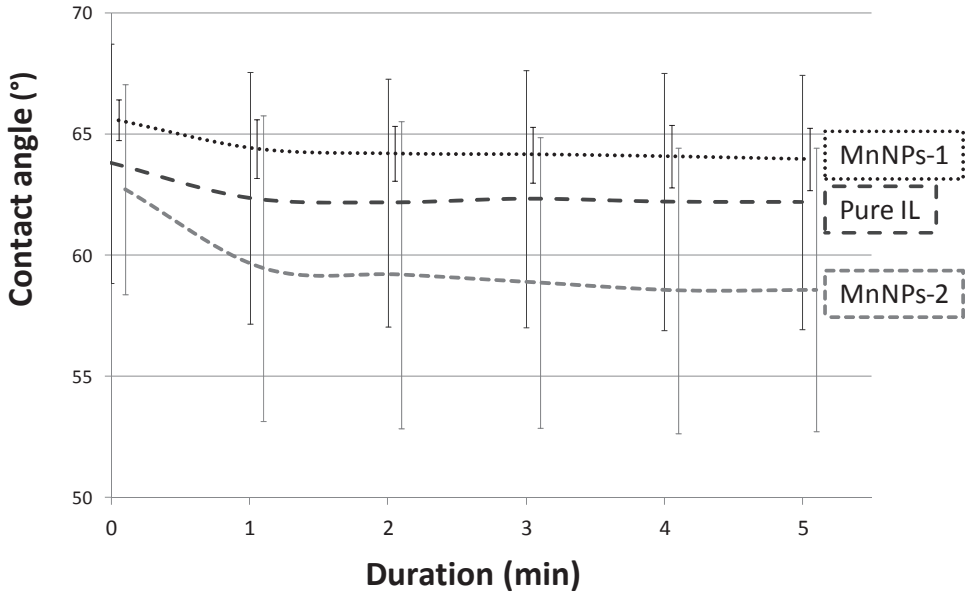

Fig. 3 Evolution of contact angle over time of pure $C_1C_4ImNTf_2$ and suspensions of MnNPs with Mn concentration of $2.5x10^{-2}$ M (MnNPs-1) and $5x10^{-2}$ M (MnNPs-2).

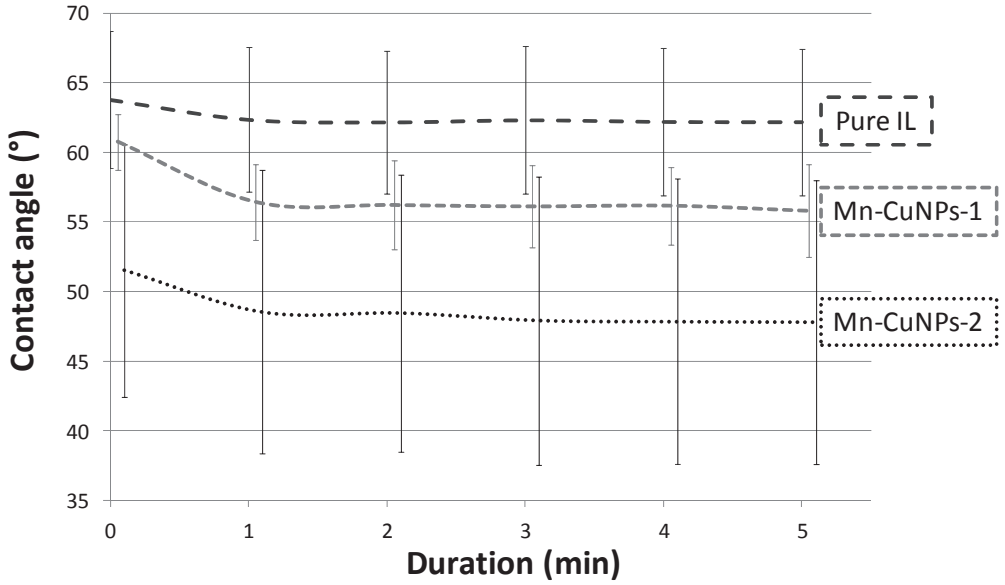

Fig. 4| Evolution of contact angle over time of pure $C_1C_4ImNTf_2$ and suspensions of Mn-CuNPs (1:1 ratio of Mn:Cu) with total metallic concentration of $2.5x10^{-2}$ M (Mn-CuNPs-1) and $5x10^{-2}$ M (Mn-CuNPs-2).

This experiment has been reproduced for Mn and Mn-CuNPs. (Figure 4 and Figure 5, respectively). As compared to CuNPs, a less important decrease is observed for MnNPs (for example, a $2.5x10^{-2}$ M suspension yields results similar to pure IL). As Mn is more oxophilic, a more pronounced decrease is expected, though. However, oxophilic NPs are also less stable under air, and more likely to be oxidized. This oxidation would decrease the interaction with the surface and consequently lead to higher contact angles.

Mn-CuNPs lead to the most pronounced decrease of contact angle. This could indicate a stronger interaction of these particles as compared to CuNPs with the surface, which is a promising result. However, this could also simply be explained by a larger number of particles in the case of Mn-Cu as compared to Cu. Indeed, the bimetallic NPs (3 nm) are significantly smaller than CuNPs (5 nm). Consequently, their numbers as well as their surfaces are increased, enhancing interaction with the substrate. Such an effect has been described by Waghmare.[19]

II.3. Conclusion

This study shows that simple contact measurements allow shedding some light into the interaction between ILs and oxide surfaces. Shorter alkyl chains lead to improved wetting, in agreement with expected interfacial arrangement at the molecular scale in the liquid and interactions with surface silanol groups. Also, the influence of water uptake can be rationalized considering a modification of the liquid/vapor surface energy. An important result is that the presence of metallic NPs generally improves wetting on the oxide, showing a favorable interaction between the NPs and the surface. However, accurate analysis of this interaction is non-trivial from our experiments. Indeed, two aspects were not fully controlled:

- The possible oxidation of the NPs (experiments conducted under air) could modify their interaction with the surface
- The number (and size) of NPs was not constant between samples, possibly modifying the extent of the interaction

From these results, it is shown that suspensions of metallic NPs in $C_1C_4ImNTf_2$ favorably interact with the oxide surfaces. Therefore, they are relevant candidates to form metallic films on such surfaces. Thus, their behavior upon thermal treatment needs now to be studied.

III. Thermal stability of IL on oxide surfaces

The thermal stability of ILs and suspensions of NPs on silica was investigated using *in-situ* diffuse reflectance infrared Fourier transform spectroscopy (DRIFT) during annealing. For this purpose, samples of Ox1 (wafer coated with 500 nm CVD oxide) were coated with a thin layer of liquid and heated up to 450°C, while recording reflectance IR spectra of the surface. After thermal treatment, the surface of the samples was examined by SEM and AFM.

Figure 5 presents IR spectra of pure IL, bare wafer and pure IL on wafer. (Figure 5a, b and c, respectively) The latter spectrum is essentially similar to that of pure IL. This suggests that the IL layer is sufficient to completely mask the wafer surface.[22] Interestingly enough, these spectra are not significantly modified upon annealing up to 320°C. (Figure 5d).[23] When temperature is increased to 450°C, the IL is largely decomposed, but organic residues are still detected on the surface (Figure 5e), whereas the IR signature of Ox1 surface remains not detected. Indeed, SEM observation shows that the Ox1 surface is still covered by a smooth organic coating (Figure 6). These experiments show that the IL can withstand annealing up to 320°C, and is partially decomposed at temperatures below 450°C.

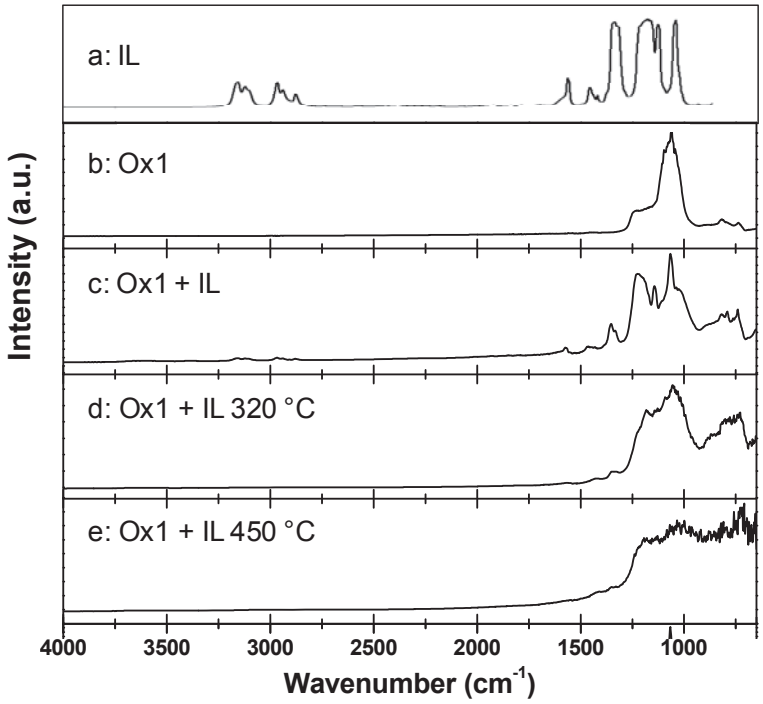

Fig. 5| FT-IR in-situ monitoring of thermal decomposition of pure $C_1C_4ImNTf_2$ on Ox1.

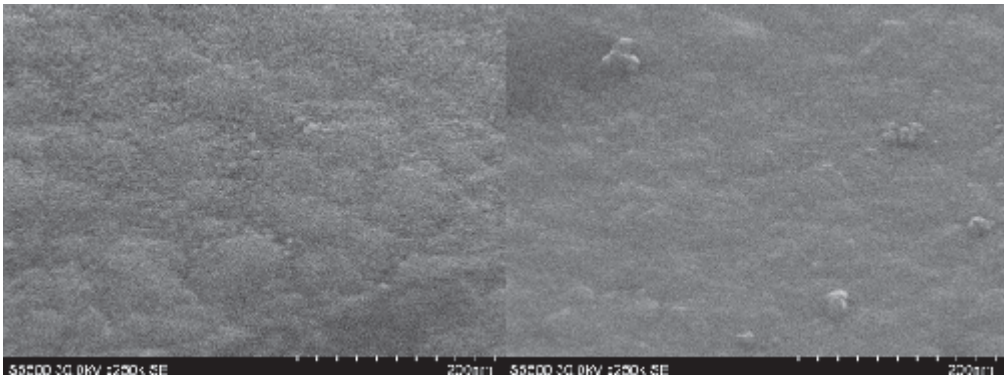

Fig. 6| SEM analysis of (left) wafer and (right) wafer with thin IL film after annealing up to 450 °C.

To confirm this result, a sample covered with pure IL was tentatively annealed in an RTP oven at 250°C under forming gas (N_2 / 3% H_2). As expected, AFM measurements show that IL is still present on the surface under the form of micrometric droplets (Figure 7).

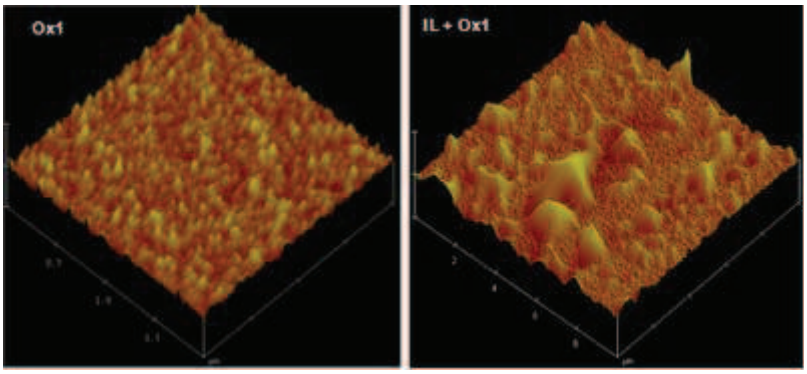

Fig. 7| AFM analysis of (left) Ox1 and (right) Ox1 coated with pure IL after anneal at 250°C.

As a conclusion, it is shown that the selected IL can endure thermal treatments at typical temperatures used in the processing of TSVs. Now, it must be verified that this holds true when metallic NPs are present in the liquid, and that this thermal treatment can efficiently transform these NPs into metallic films.

IV. Thermal treatment of monometallic NPs suspensions in IL

IV.1. Annealing of copper nanoparticles

The thermal stability of a suspension of CuNPs in IL was investigated by DRIFT analysis. The corresponding spectra are plotted in Figure 8, and show that similar results are obtained as compared to pure IL. Again, the suspension seems to be stable up to 320 °C, and is partially decomposed at higher temperatures. SEM observations confirm the presence of organic residues after anneal at 450°C, and also show that solid particles are left on the surface (Figure 9). However, their metallic nature could not be confirmed by EDX.

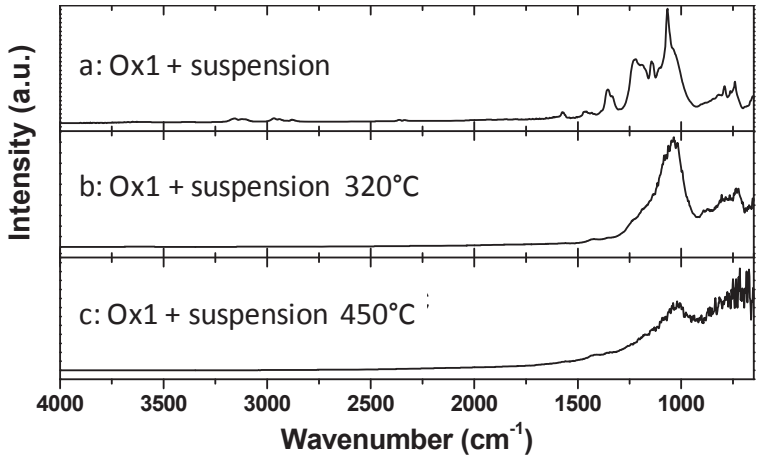

Fig. 8| FT-IR in-situ monitoring of thermal decomposition of a suspension of CuNPs in IL on Ox1.

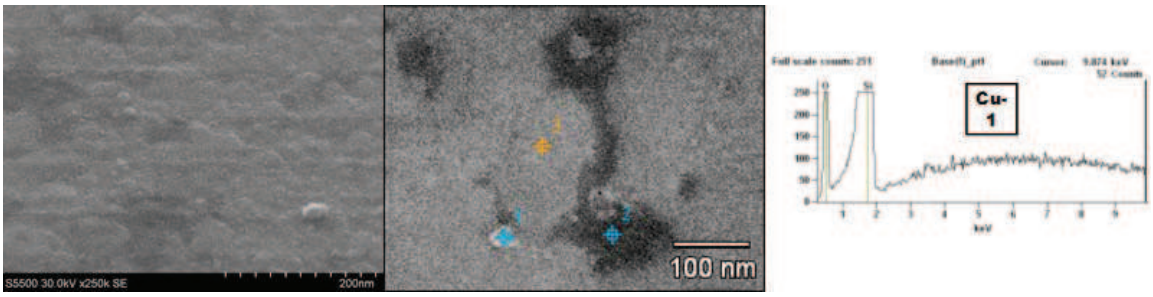

Fig. 9| SEM and EDX analysis of a sample coated with a suspension of CuNPs after anneal at 450 °C.

The same kind of sample was tentatively annealed in an RTP furnace at 250°C under forming gas, N_2 3% H_2 ($1.0x10^{-1}$ M of Cu). The sample color changed from purple to orange upon annealing, indicating the formation of bulk copper. However, this coating was not

adherent and was washed away during acetone rinse. Nevertheless, SEM inspection revealed that large solid particles (a few hundreds of nanometers) were still present on the surface. EDX analysis confirms that these are copper particles (Figure 10-1). On the same picture, a liquidlike domain similar to those observed in Figure 7 is observed, showing the coexistence of IL with the agglomerated Cu particles. Large Cu aggregates are formed during the thermal treatment with a typical white color (on SEM). As expected, Cu is detected by EDX in this domain (Figure 10-2). However, Cu is also detected in the apparently uncoated region (Figure 10-3). This could arise either from presence of a thin liquid film of Cu suspension in this region, or to the presence of an ultrathin layer of metal left after treatment.

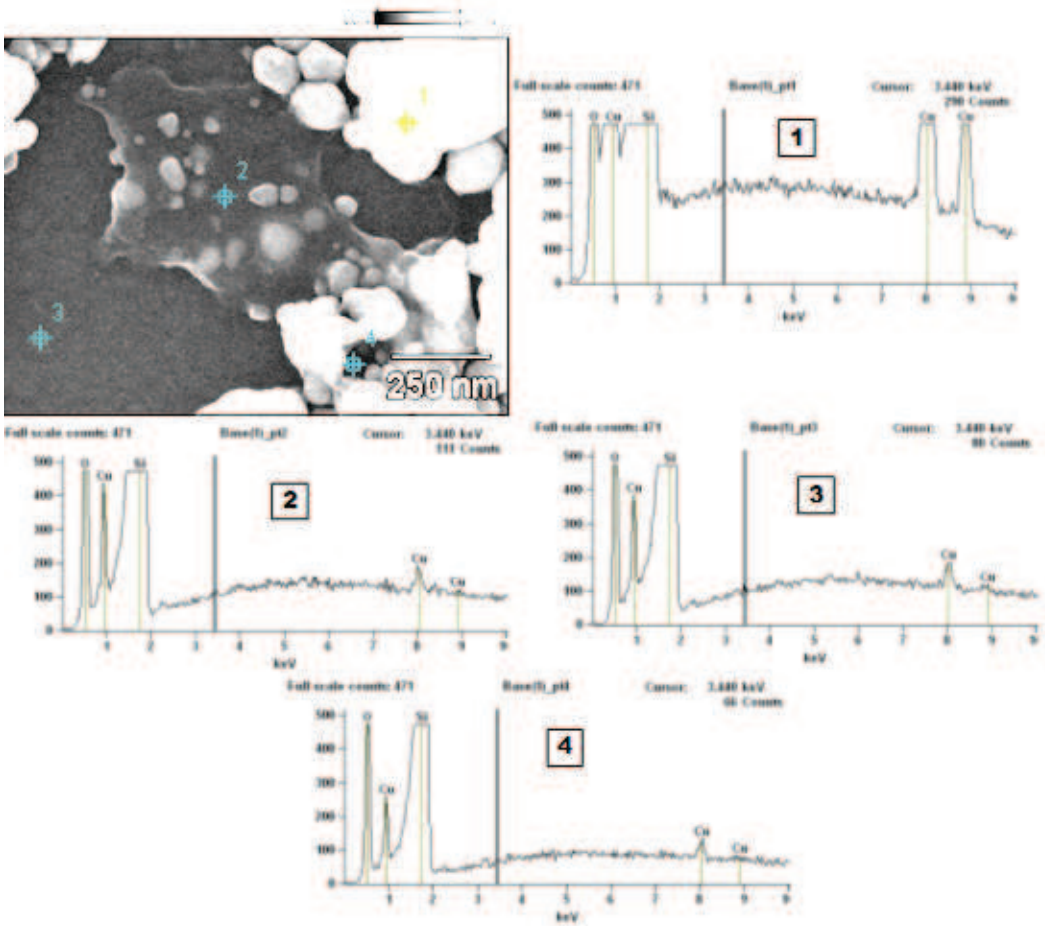

Fig. 10|. SEM and EDX analysis of Ox1 coated with a suspension of CuNPs in IL after anneal at 250°C.

IV.2. Annealing of manganese nanoparticles

The same study as for CuNPs was carried out with MnNPs. The results of the DRIFT analysis of a suspension of MnNPs are gathered in Figure 11. Again, the suspension does not seem to be modified upon annealing until reaching 320 °C. By contrast with pure IL and suspension of CuNPs, the absorption peaks corresponding to ILs are almost completely extinguished for temperatures above 320 °C. This indicates an extended decomposition of the liquid as compared to the previous cases. Nevertheless, no signal arising from the substrate was detected, suggesting the presence of a deposit masking the oxide surface.

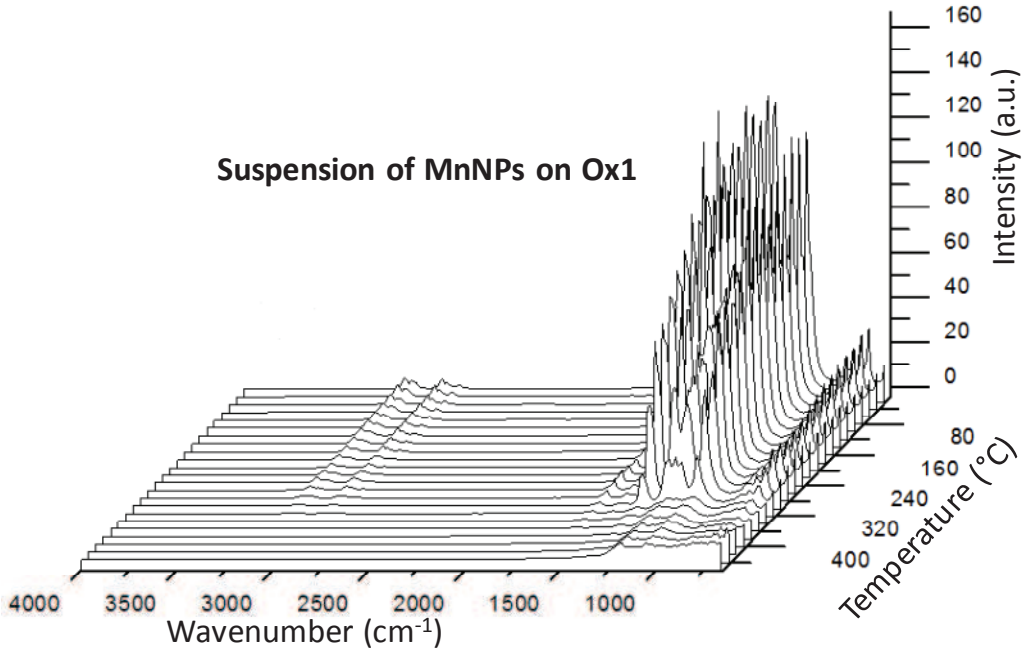

Fig. 11| FT-IR in-situ monitoring of thermal decomposition of suspension of MnNPs in IL.

Indeed, profilometry and AFM analyses show that after thermal treatment at 450 °C, there is a deposit left on the surface (Figure 12). At the mesoscopic scale (as measured by profilometry), the deposit is highly inhomogeneous, composed of agglomerated micrometric clusters. At the microscopic scale (as analyzed by AFM), the deposit is structured into particles of a few tens of nm. This structure is confirmed by SEM observation (Figure 13). EDX analysis clearly shows that Mn is present in the large agglomerates. However, no Mn

could be detected in domains covered with smaller particles, maybe due to the too high detection limit of this technique.

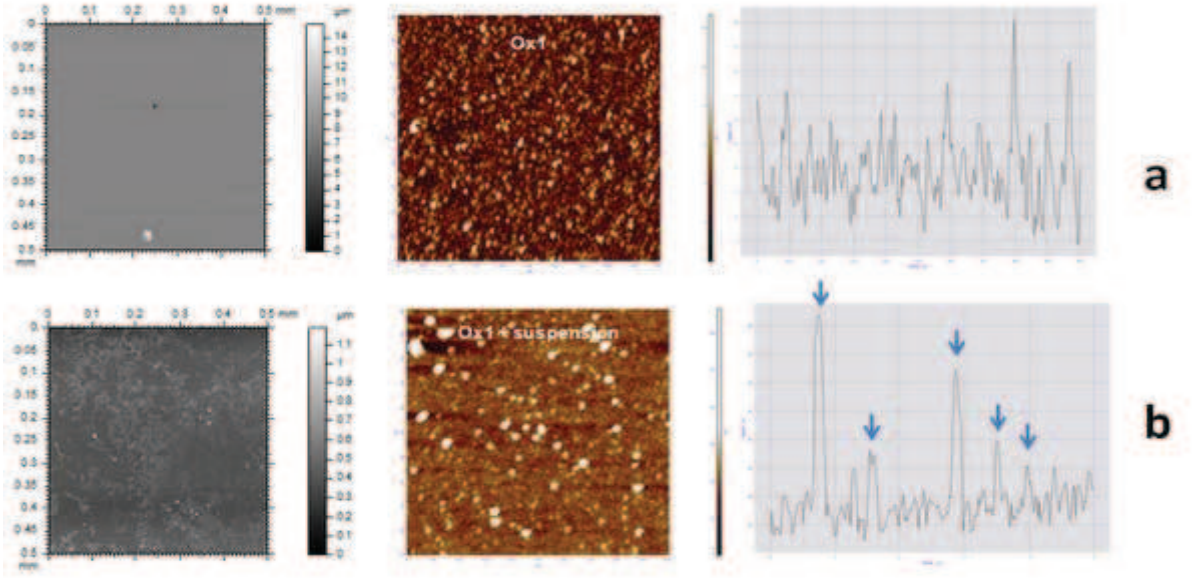

Fig. 12| Surface profile at the millimeter scale (by profilometry) 500x500 µm, AFM profile, 5x5 µm and cross section at the micrometric scale for (a) bare Ox1 surface and (b) coating of a suspension of MnNPs after anneal at 450 °C.

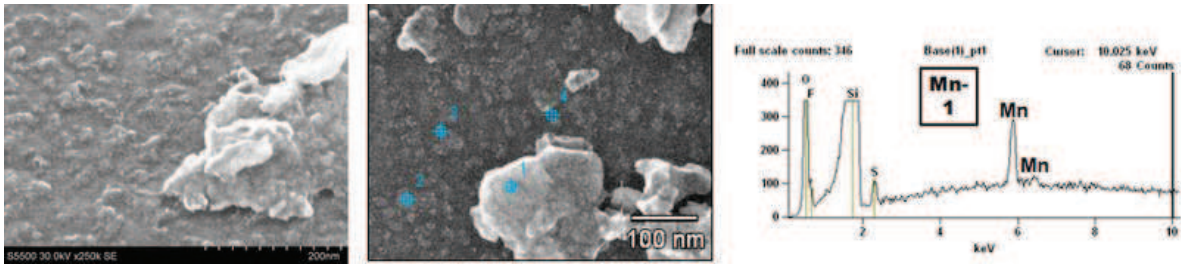

Fig. 13| SEM and EDX analysis of a deposit formed by annealing at 450 °C of a suspension of MnNPs.

To further investigate the behavior of MnNPs suspensions, an annealing was performed under inert atmosphere (Ar) rather than reducing. *In-situ* DRIFT analysis was performed during thermal treatment (Figure 13). A similar behavior is observed as under H_2: the absorption peaks of IL are visible up to ca. 300 °C, and are extinguished at higher temperature. Again, no signal arising from the substrate is visible at high temperature, suggesting that the oxide surface is masked by some deposit.

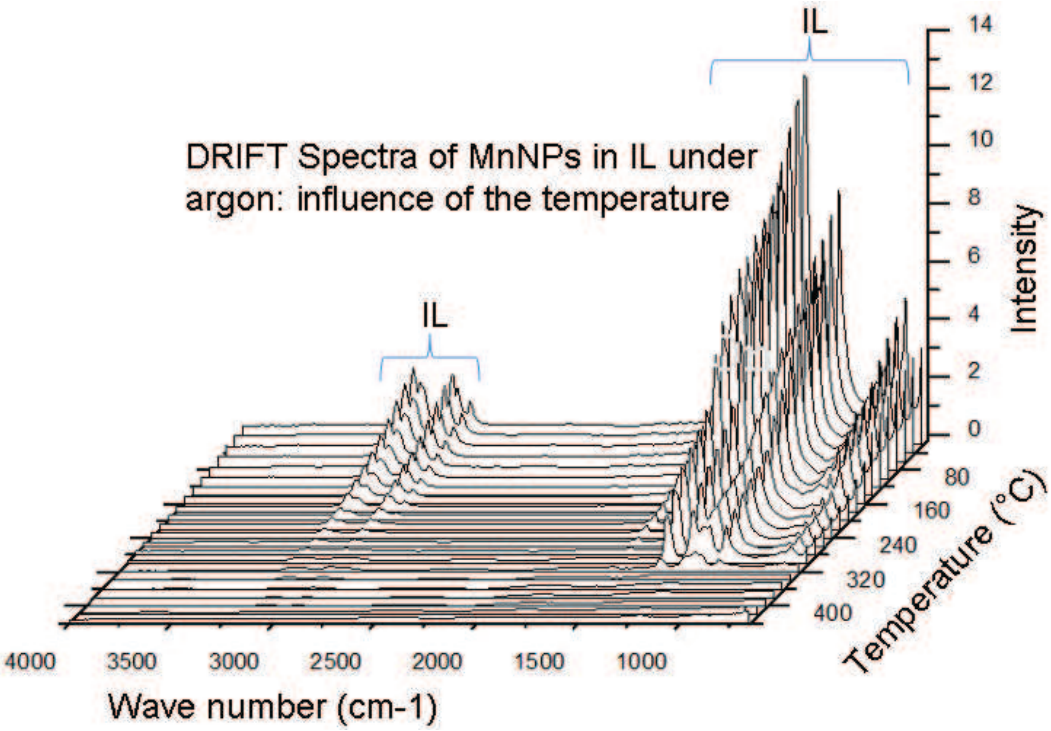

Fig. 14| FT-IR *in-situ* monitoring of thermal decomposition of MnNPs suspensions in IL.

Indeed, such a deposit is evidenced by SEM analysis (Figure 15). However, its morphology is quite different from the one formed under H_2. The most remarkable feature is the presence of a smooth, discontinuous coating that coexists with agglomerates similar to those observed under H_2. EDX analysis shows that these agglomerates contain Mn. More interestingly, some Mn seems to be detected in the smooth layer.

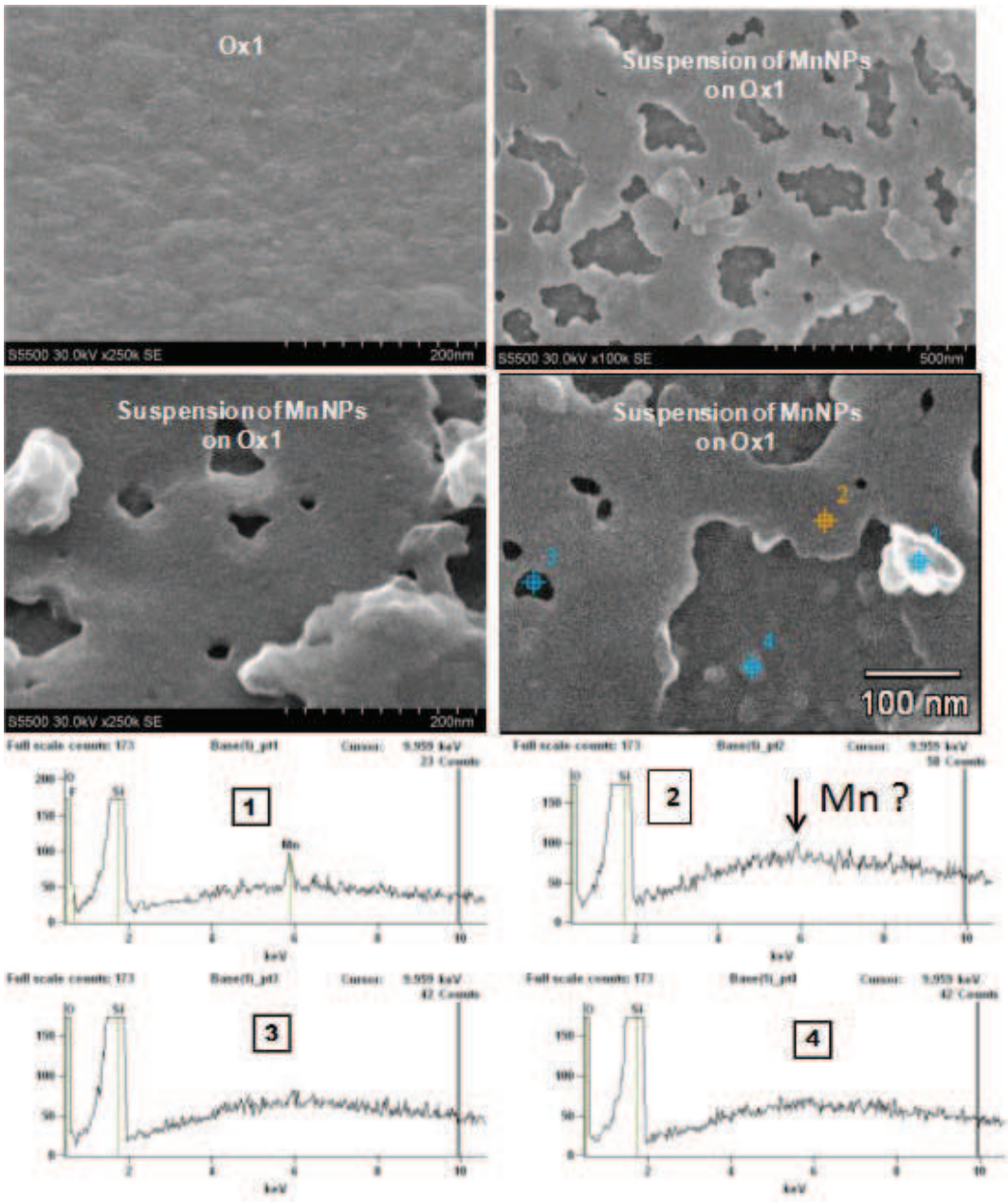

Fig. 15| SEM analysis of Ox1 covered by a suspension of MnNPs after anneal at 450 °C under Ar.

RTP annealing has been performed with concentrated MnNPs suspension ($1.0x10^{-1}$ M). A deposit is clearly observed containing Mn as detected by EDX analysis in several areas, Figure 16. No Mn is detected where no film seems present at it was observed for CuNPs. Large Mn aggregates of grey colors (on SEM) are formed during annealing of pure MnNPs suspensions.

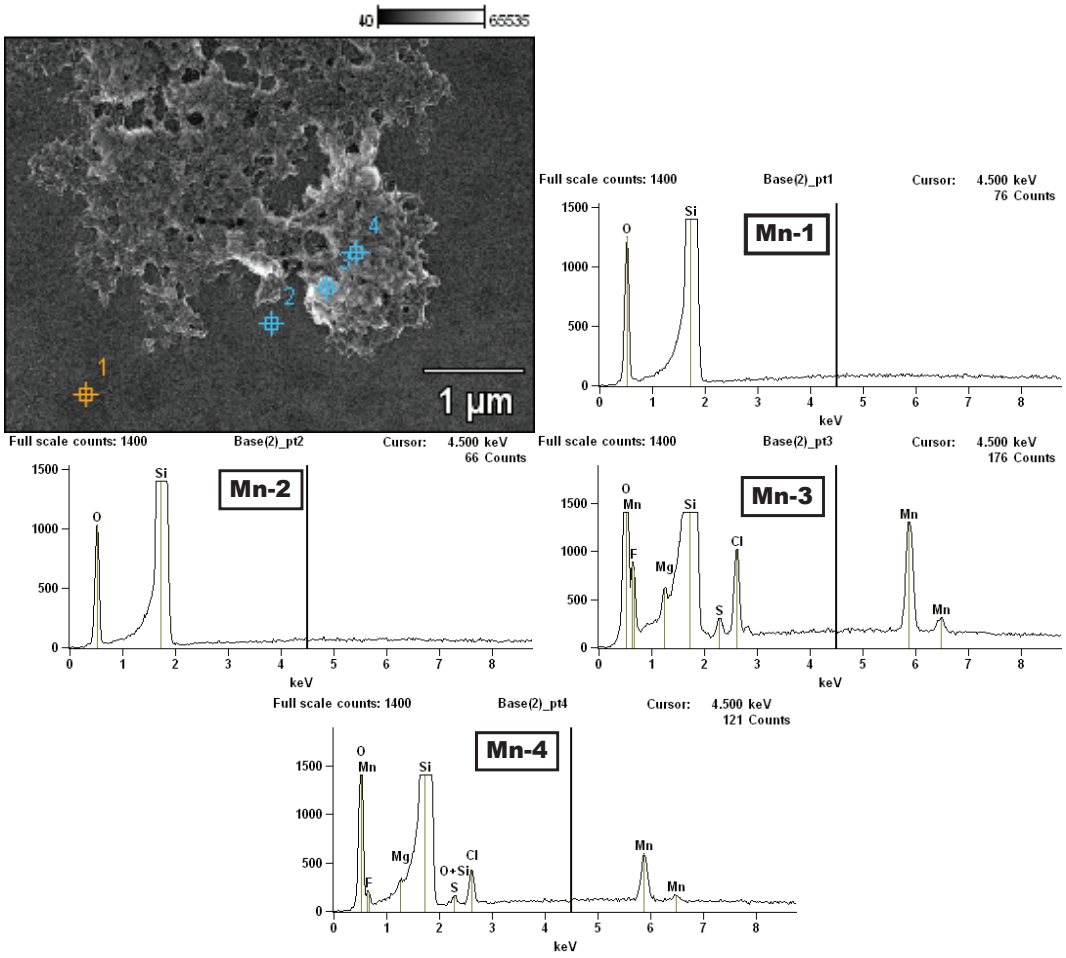

Fig. 16|. SEM and EDX analysis of Ox1 coated with a suspension of MnNPs in IL after anneal at 250°C.

V. Thermal treatment of bimetallic Mn-CuNPs suspensions in IL

V.1. Annealing followed in-situ by DRIFT analysis

The thermal decomposition under H_2 of a suspension of Mn-CuNPs in IL was monitored by DRIFT (Figure 17). Interestingly enough, this suspension seems to behave like the suspension of CuNPs, quite differently from MnNPs. Indeed, some signal related to organic residues is still present at high temperature (above 320 °C). By contrast with the suspension of MnNPs, the decomposition of the IL is only partial. The SEM observation in Figure 18 confirms the presence of organic residues on the surface along with solid clusters. However, no metal could be detected on these samples by EDX.

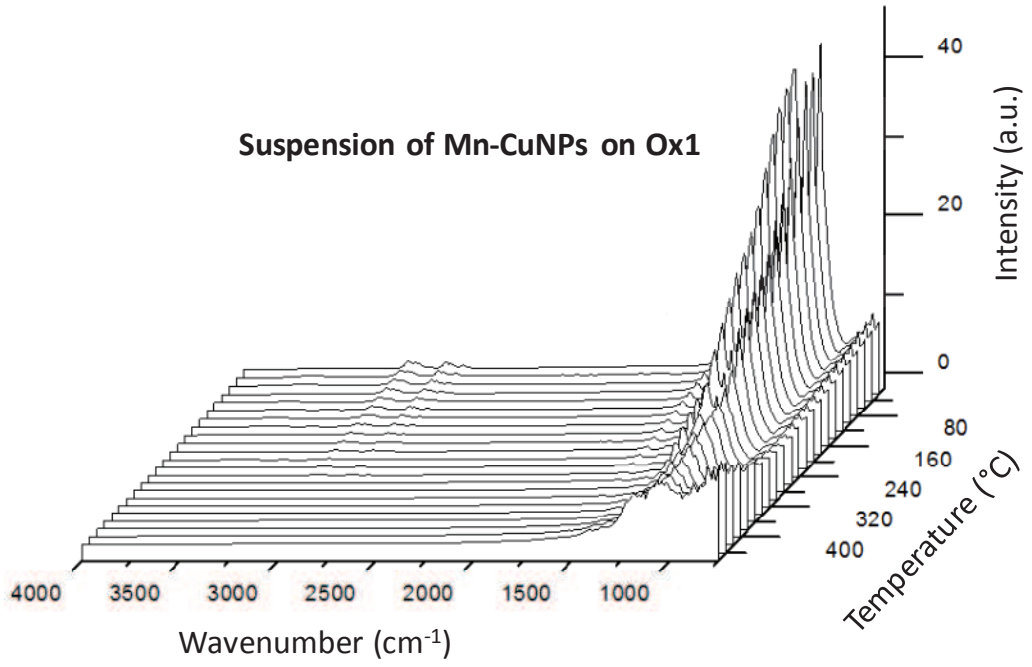

Fig. 17| FT-IR *in-situ* monitoring of thermal decomposition of a suspension of Mn-CuNPs in IL.

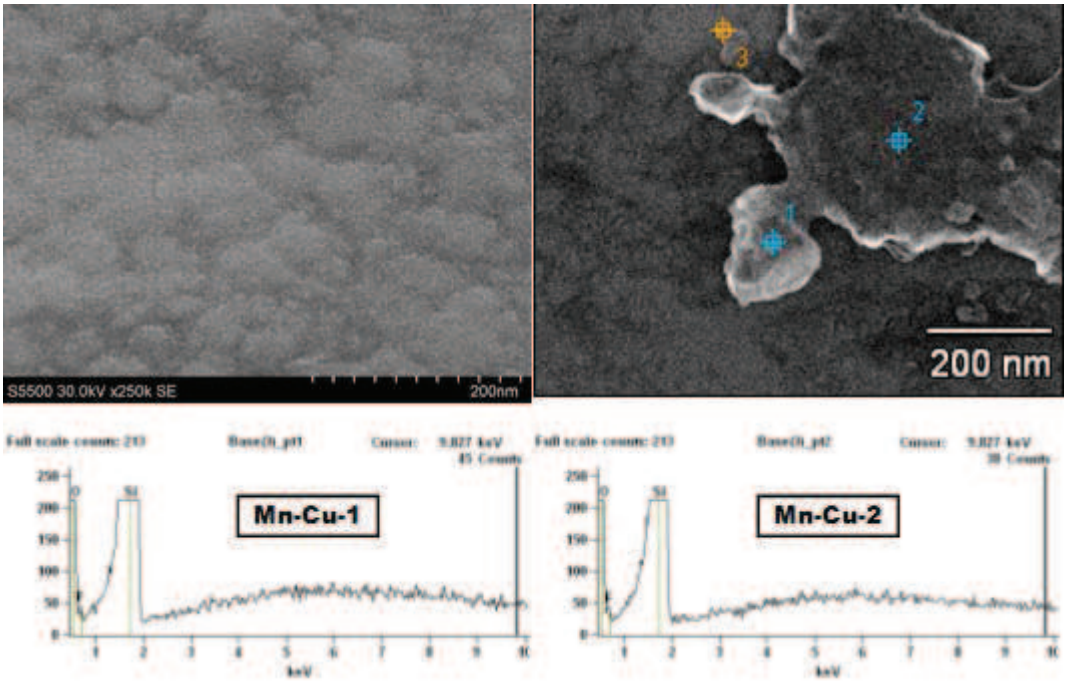

Fig. 18|. SEM and EDX analysis of Ox1 coated with a suspension of Mn-CuNPs in IL after anneal at 450°C

The thermal decomposition of these bimetallic NPs suspensions was further investigated using an RTP furnace.

V.2. Effect of concentration and composition of nanoparticles on deposit

In order to investigate the effect of concentration and composition of NPs on the deposit, samples with several compositions (Mn;Cu, 9:1, 1:1, 1:9 were annealed in an RTP furnace. The same annealing parameters were used, i.e. 100 mL.min^{-1} of N_2 3% H_2, 250 °C, during 1 hour. In order to improve the deposition, the suspensions were concentrated through centrifugation at 26000 rpm during 10 min. This treatment allows concentrating suspensions by about 2, ($1.0x10^{-1}$ M metal concentration). These attempts will be compared to a reference of Mn:Cu = 1:1 with $5x10^{-2}$ M concentration of precursors in solution.

When Cu was present in the solution, the sample color changed from purple to orange upon annealing, indicating the formation of bulk copper. However, this coating was not adherent and was washed away during acetone rinse.

As compared to pure Cu (Figure 10), the addition of even a small quantity of Mn had significantly increases the amount of deposited materials (Figure 19), without forming large aggregates. When Mn:Cu ratio increases, agglomeration occurs and the deposit morphology resembles pure Mn's.

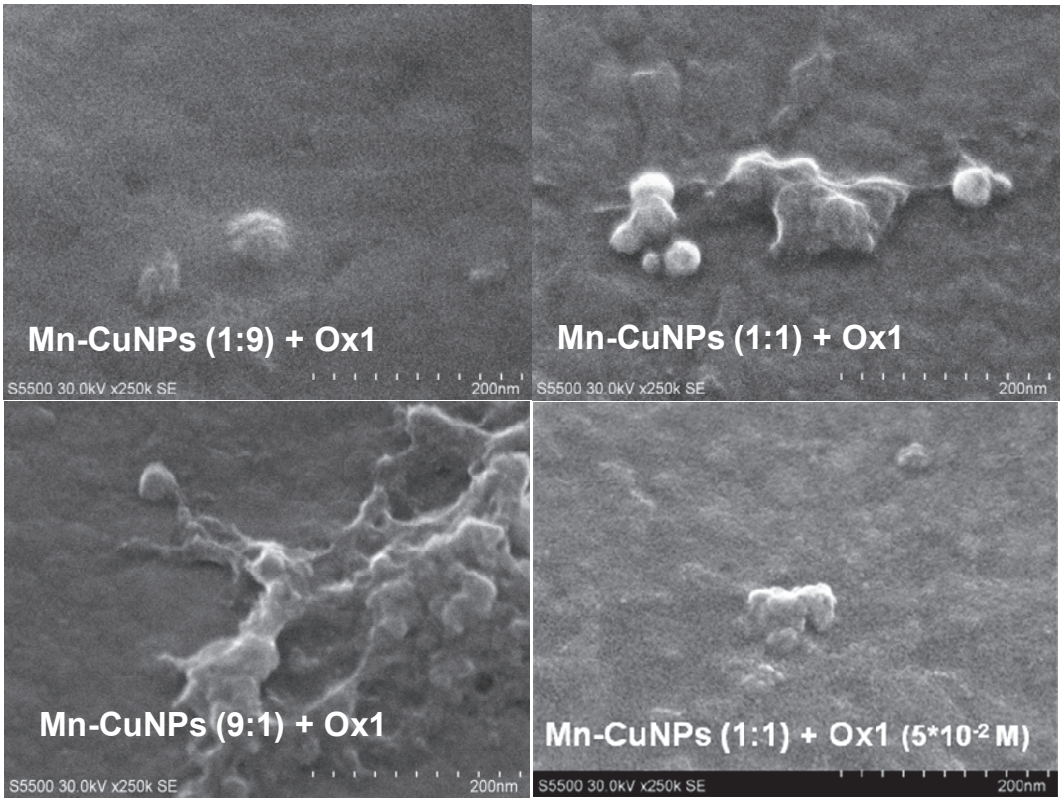

Fig. 19| SEM analysis on Ox1 of suspension of NPs after anneal at 250°C under N_2 / 3% H_2. Picture tilted at 40 °.

A thinner but more uniform deposit was observed in the case of the low metal concentration. These conditions were consequently used in further attempts.

V.3. Effect of atmosphere during annealing

For this purpose, the annealing was performed under 100 mL.min-1 of N_2 and under dynamic vacuum (10 Pa). Very uniform surfaces were observed in the case of annealing under N_2 as it was the case under N_2 / H_2 (Figure 19 and 20). Indeed, there are less deposited materials under neutral atmosphere as compared to reducing ambient. It has been shown in chapter III that Mn-CuNPs are partially oxidized. This oxidation is likely to be due extended in our annealing experiments, as suspensions were exposed to air before thermal treatment. Hence, the probable reduction into metal of the Mn-CuNPs by N_2 / H_2 is likely to be responsible of the larger amount of deposited materials.[8] However, the involved mechanism is still to be clarified.

The case under vacuum is interesting since most of the NPs present in the liquid are deposited onto the surface, Figure 20. Indeed, in our annealing conditions, distillation of IL is possible.[24] EDX analysis confirms the presence of Mn and Cu in the sample, with segregation of Cu in microparticles (less Mn) and presence of Mn and Cu in typical Mn structures. GIXRD confirms the presence of crystalline metallic Cu in this sample.

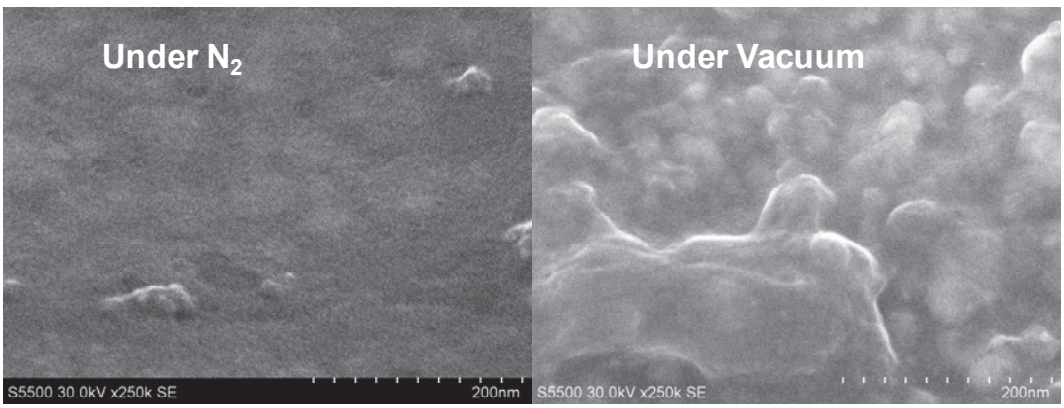

Fig. 20| SEM analysis on Ox1 of suspension of NPs after anneal at 250°C. Picture tilted at 40 °.

In conclusion, the synthesis of films under N_2 / H_2 seems to be a good alternative. Moreover, the preservation of IL clearly allows obtaining better uniformity as compared to attempts under vacuum. Hence, all experiments described below were conducted under N_2 / H_2.

V.4. Influence of temperature and duration

In this section, other experimental conditions are investigated in order to improve the uniformity of the films, and eliminate large aggregates. Experiments were performed under N_2 / H_2 and with $5x10^{-2}$ M total concentration of precursors. Temperature was varied between 150 and 250 °C and duration between 30 and 60 minutes. No higher temperature was tested since at 300 °C some decomposition of IL could occur. Figure 21 presents the morphology of the deposits.

However IL decreases the roughness of the samples, deposits are clearly visible in most cases. Increasing, duration provides smoother deposit. It is difficult to find a clear tendency of temperature on deposits. More analyses have to be performed in order to explain these results.

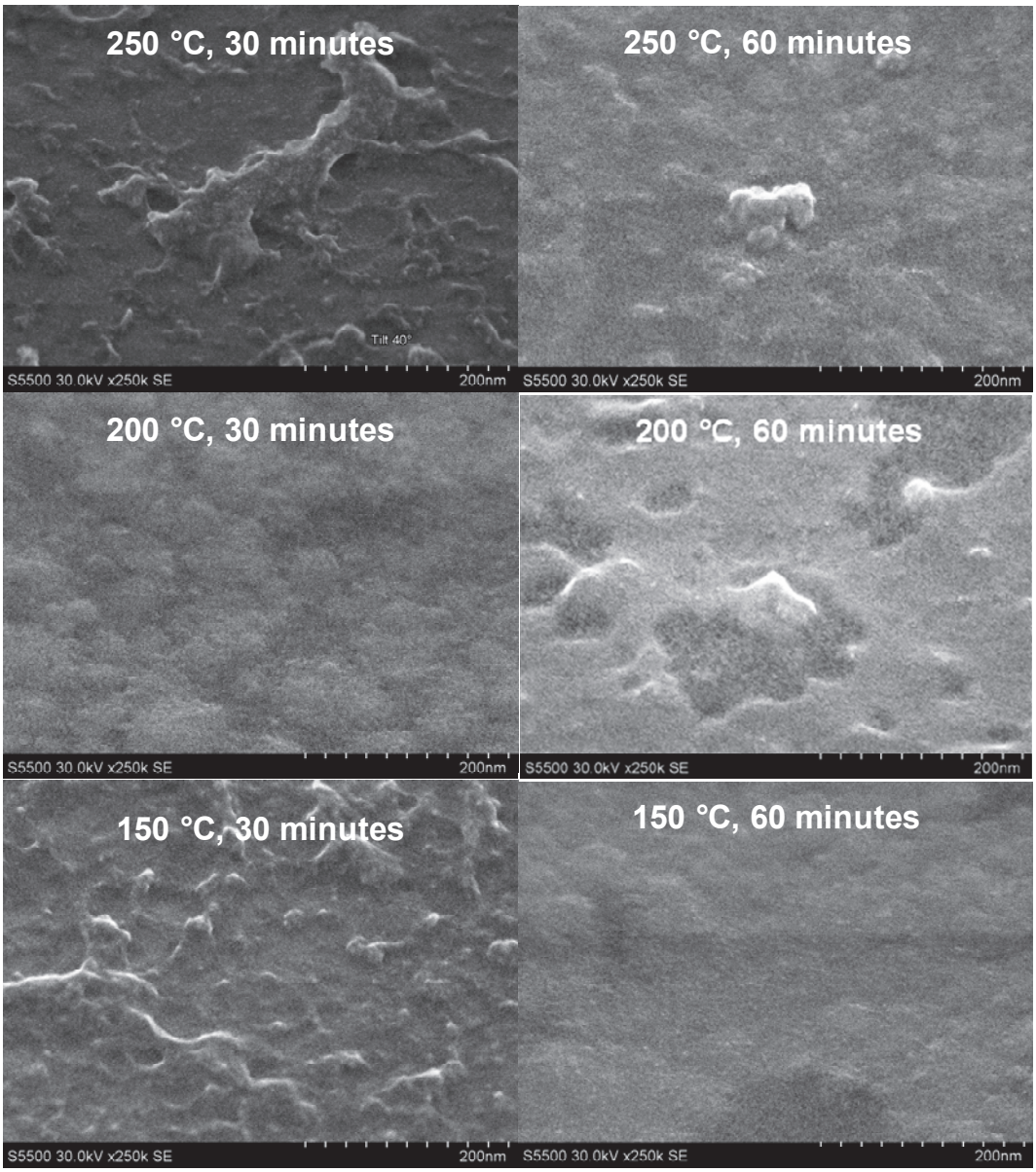

Fig. 21| SEM analysis on Ox1 of suspension of Mn-CuNPs after annealing. Picture tilted at 40 °.

V.5. Conclusion

To conclude, several attempts have been performed in order to deposit NPs on wafer and to form film through annealing. IL seems to controlling the rate of deposition and consequently uniformity of film. Here, higher viscosity IL should decrease the speed of deposition. Higher alkyl chain has to be used in this way. The mechanism of growth which has been proposed has to be demonstrated but it allows clearly an improvement of deposit obtained when the concentration of NPs is decreased. The duration and temperature are linked as demonstrated by the attempt of variation of these parameters. For 200 °C, 1 hour seems to be a good value.

VI. X-Ray photoelectron spectroscopy of deposits

X-Ray photoelectron spectroscopy was also performed on metal deposits. Three samples have been analyzed: deposits obtained from suspensions of pure CuNPs, pure MnNPs and Mn-CuNPs (Mn:Cu = 1:1). These deposits are those obtained at high metal concentration with annealing at 250 °C under N_2 / H_2 during 1 h (Figures 10, 16 and 19 respectively).

Table 2| XPS analysis of deposits obtained from suspensions of pure Cu, pure Mn and Mn:Cu (1:1), under N_2 / H_2 at 250 °C during 1 h.

Sample	Composition of sample (at%)							
	Ionic liquid					Metal		Substrate
	C1s	**O1s**	**F1s**	**N1s**	**S2p**	**Mn2p$_{3/2}$**	**Cu2p$_{3/2}$**	**Si2p**
Cu	40.10	39.65	0.78	0.46	0.73	<dl	0.49	17.79
	38.16	41.49	1.46	0.94	0.55		0.37	17.03
Mn	48.84	30.36	1.94	1.04	0.48	1.72	<dl	15.62
	50.57	28.53	1.18	0.64	0.30	1.27		17.51
Mn-Cu	34.90	41.72	1.98	0.48	0.25	1.98	1.01	17.67
	34.29	41.68	1.53	0.46	0.20	1.61	0.54	19.69

Sample	Ratio		
	Cu/Si	**Mn/Si**	**Si(III)/Si2p**
Cu	0.028	<dl	0.20
	0.022		0.18
Mn	<dl	0.110	0.49
		0.073	0.62
Mn-Cu	0.057	0.112	0.32
	0.027	0.082	0.32

<dl: below detection limit.

From Table 2, it should be noticed that no Cu are detected in the Mn attempt and vice-versa. Typically the surface composition of the sample is as follows: C (50-35 %), O (42-28 %), Si (20-15 %), Mn (2-1.2 %), F (2-0.8 %), N (1.0-0.5 %), Cu (1-0.4 %) and S (0.7-0.2 %). The presence of F, N and S suggests that a significant amount of ILs (or its decomposition products) is still present at the surface of the sample. There is no huge difference between compositions of two different areas of the same sample. All deposit seems consequently relatively uniform.

The corresponding XPS spectra are presented in Figure 22. From samples obtained by annealing suspensions of pure Cu and Mn-CuNPs, Cu is present on the Cu_2O form. Indeed, Cu $2p_{3/2}$ peaks are observed at 932.6 eV and 932.5 eV for Mn-Cu and Cu deposits, respectively. Moreover, Cu LMM is observed at 914.0 eV for Cu, 915.2 eV and 914.6 eV for Mn-Cu deposits.

Oxidation state of Mn is very difficult to determine. Indeed, this element has many states of oxidation, all of which exhibit broad emission peak, with full width at half maximum comprised between 3 and 3.5 eV. As these peaks are also very close to each other, separate by only 1 eV, it was not possible to distinguish the oxidation state of Mn. The only conclusion which could be drawn is that Mn is not in the metallic state because no peak is observed at 638.6 eV.[27]

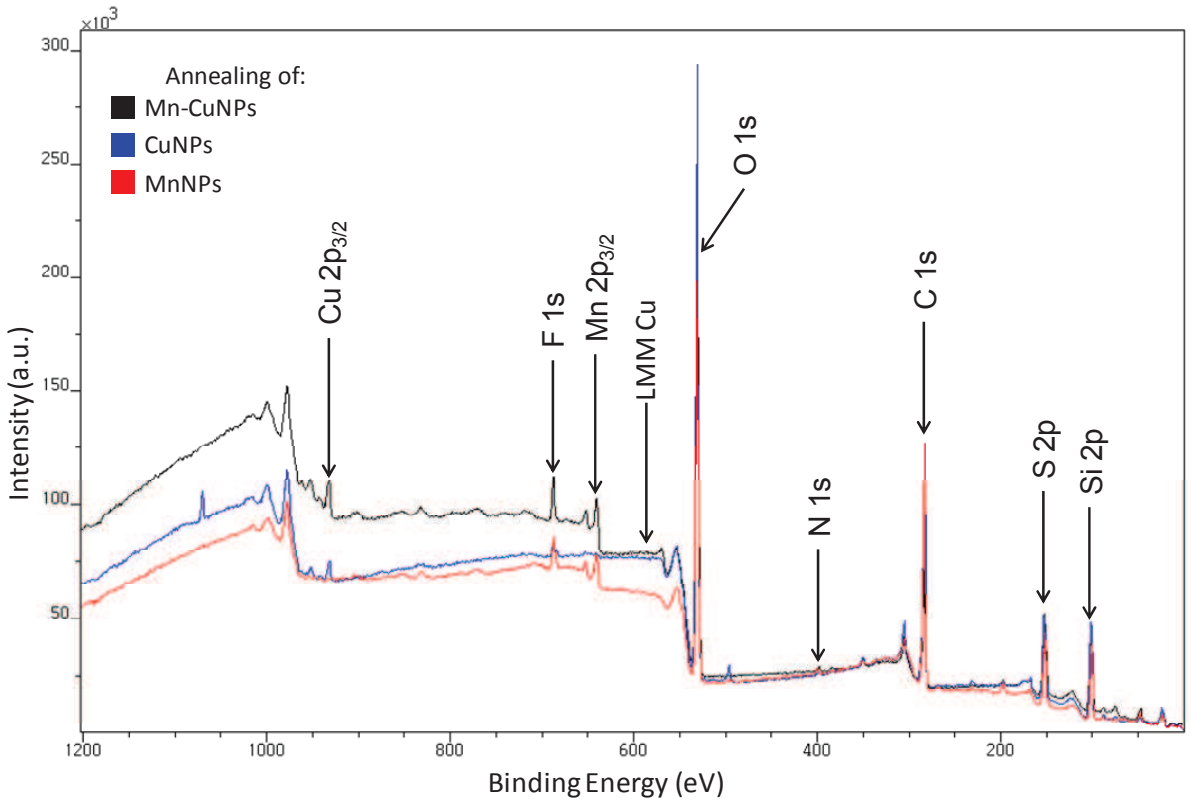

Fig. 22: XPS spectra of samples obtained by annealing suspension of nanoparticles 1°h at 250 °C under N_2 / H_2. The state of oxidation of these metals is not surprising, since these samples

have been analyzed after several weeks storage under air. However, the precise analysis of Si 2p peaks allows giving supplementary information. Indeed, two components could be determined for these peaks. On a wafer coated with SiO_2, the major peak will be the one of Si(IV) between 103.4 and 103.6 eV (traces of Si(III) are observed < 5%). However, the oxide is not perfectly stoichiometric with presence of some sub-oxides. Si oxide peaks vary from 103.6 (Si(IV)) to 99.5 eV (Si(0)). Si(III) peak is situated at 101.9 eV, Si(II) at 101.4 eV and Si(I) at 100.5 eV.[28] In our case, in addition to Si(IV), a peak attributed to Si(III) is detected between 101.9 and 102.1 eV. Interestingly enough, the ratio between these peaks is not constant in the various samples. In the case of CuNPs, the ratio corresponds to 80 % of Si(IV) and 20 % of Si(III), which could be due to partial reaction of Cu with silica surface. There is thus a high influence of CuNPs on the state of oxidation of the SiO_2 surface. The presence of Mn causes higher variation of this ratio. Indeed, in Mn-Cu deposit, the amount of Si(III) reaches 32 %. Increasing Mn concentration with the use of Mn pure deposit leads to an even higher increase of Si(III) peak, with more than 50 %, and even 62 % in one area. Clearly, the annealing of suspension of NPs in IL causes a reaction between NPs and the oxide surface, as it was supposed by contact angle measurement. Hence, the oxidation of Mn in our samples is likely not to be only caused by exposure to air, but also to a reaction with SiO_2. The latter reaction is well documented in the literature, and forms a mixed oxide of Mn and Si.[3; 26] Sun et al. have found a typical peak at 101.7 eV (for Si $2p_{3/2}$), corresponding to a silicate compound.[29] Furthermore, this reaction is the key step in the elaboration of self-formed barriers in advanced interconnects. Therefore, this result is very important, as it shows that under annealing, MnNPs, but more importantly Mn-CuNPs may react with the substrate to form the desired barrier layer. Komiyama and coworkers have obtained similar results with the formation of a Si(IV) reduced species. The quantity of Si(IV) reduced is different as

function of the metal NPs used. They hypothesize this difference by the different rate of metal diffusion into the support.[30]

The ratio between metals and silicon is also significant. Comparing pure Mn and pure Cu attempts, the atomic ratio Mn/Si is equal to 0.110 while Cu/Si is equal to 0.028. Thus Mn is attached by the silica surface in a larger extent. For Mn-Cu deposit, Mn/Si ratios are essentially the same, with 0.112 and 0.82 on the two areas analyzed. Surprisingly, a higher content of Cu is obtained with Mn-CuNPs (0.057 and 0.027) as compared to pure Cu. This could be due to a better adhesion of Cu when Mn is present. More probably, this higher Cu concentration results from the fact that the deposit is formed from truly bimetallic Mn-CuNPs. However, Mn/Si and Cu/Si ratios should theoretically be the same in this case where Mn-CuNPs with 1:1 ratio of Mn:Cu were used. The reasons of this deficit in copper need to be clarified. One possible explanation could be Cu diffusion deep into SiO_2 (at least beneath detection depth of XPS) during anneal, before the mixed oxide between Mn and SiO_2 is formed.

VII. Conclusion

The application of NPs suspensions in ILs to form metallic films on technological substrates was investigated. Wettability of IL on hydroxylated silica surfaces is rather good, with a preference to IL with short alkyl chain length. The presence of NPs further increases wettability of the liquid, indicating a favorable interaction between the NPs and the oxide surface. Diffuse reflectance infrared Fourier transform was used to determine the thermal stability of the suspensions. They seem to resist to temperatures up to 320 °C, which correspond to conventional process temperatures in the 3D integration. Preliminary attempts to form metallic films were undertaken at temperature up to 250 °C under various atmospheres. Morphological observations show the formation of metallic deposits, which is a major and encouraging result of this study. However, these deposits are often composed of large clusters which mask the possible presence of thin liners on the oxide surface. Some parameters are shown to be important to improve film quality, such as the decrease of concentration of NPs at low temperature and long duration.

XPS analysis shows clearly that a deposit have been obtained, with a high probability of reaction of NPs on the surface, leading to variation of state of oxidation of silica.

References

[1] K. Neishi, S. Aki, K. Matsumoto, H. Sato, H. Itoh, S. Hosaka, J. Koike, Appl. Phys. Lett., 93 (2008) 032106-032101-032103.
[2] J. Koike, M. Wada, Appl. Phys. Lett., 87 (2005).
[3] J.M. Ablett, J.C. Woicik, Z. Tokei, S. List, E. Dimasi, Appl. Phys. Lett., 94 (2009) 042112 (042113).
[4] J. Guillan, K. Haxaire, D. Galpin, S. Chhun, J.C. Giraudin, D. Ney, L. Arnaud, D. Guiheux, R. Pantel, in: Materials for advanced metallisation, Grenoble, 2012.
[5] A. Roule, T. Morel, P.H. Haumesser, O. Pollet, M. Cordeau, S. Maitrejean, J. Klocke, T. Ritzdorf, G. Passemard, Adv. Met. Conf. 2004, , Proceedings of the Conference, San Diego, CA, United States, Oct. 19-21, and Tokyo, Japan, Sept. 28-29, 2004, (2005) 341-346.
[6] C. Barriere, G. Alcaraz, O. Margeat, P. Fau, J.B. Quoirin, C. Anceau, B. Chaudret, J. Mater. Chem., 18 (2008) 3084-3086.
[7] Y.-H. Ham, D.-P. Kim, K.-H. Baek, K.-S. Park, M. Kim, K.-H. Kwon, K. Lee, L.-M. Doa, Electrochem.Solid-State Lett., 15 (2012) H145-H147.
[8] A. Yabuki, N. Arriffin, Thin Solid Films, 518 (2010) 7033-7037.
[9] M.G. Farooq, ECS Trans., 35 (2011) 83-94.
[10] Y. Zhao, M. Li, Q. Lu, Langmuir, 24 (2008) 3937–3943.
[11] T. Batchelor, J. Cunder, A.Y. Fadeev, J. Colloid Interface Sci., 330 (2009) 415-420.
[12] J.B. Rollins, B.D. Fitchett, J.C. Conboy, J. Phys. Chem. B, 111 (2007) 4990-4999.
[13] N. Sieffert, G. Wipff, J. Phys. Chem. C, 112 (2008) 19590-19603.
[14] L.T. Zhuravlev, Colloids Surf., A, 173 (2000) 1-38.
[15] K. Shimuzu, A. Pensado, P. Malfreyt, A.A.H. Padua, J.N. Canongia Lopes, Faraday Discuss., 154 (2012).
[16] R. Hayes, G.G. Warr, R. Atkin, Phys. Chem. Chem. Phys., 12 (2010) 1709-1723.
[17] M.G. Freire, P.J. Carvalho, A.M. Fernandes, I.M. Marrucho, A.J. Queimada, J.A.P. Coutinho, J. Colloid Interface Sci., 314 (2007) 621-630.
[18] I.B. Malham, P. Letellier, M. Turmine, J. Phys. Chem. B, 110 (2006) 14212-14214.
[19] P.R. Waghmare, S.K. Mitra, Langmuir, 26 (2010) 17082-17089.
[20] K. Seffiane, J. Skilling, J. MacGillivray, Adv. Colloid Interface Sci., 138 (2008) 101-120.
[21] S. Vafaei, T. Borca-Tasiuc, M.Z. Podowski, A. Purkayastha, G. Ramanath, P.M. Ajayan, Nanotech., 17 (2006) 2523-2537.
[22] K. Noack, P.S. Schulz, N. Paape, J. Kiefer, P. Wasserscheid, A. Leipertz, Phys. Chem. Chem. Phys., 12 (2010) 14153-14161.
[23] C.P. Fredlake, J.M. Crosthwaite, D.G. Hert, S.N.V.K. Aki, J.F. Brennecke, J. Chem. Eng. Data, 49 (2004) 954-964.
[24] M.J. Earle, J.M.S.S. Esperanca, M.A. Gilea, J.N. Canongia Lopes, L.P.N. Rebelo, J.W. Magee, K.R. Seddon, J.A. Widegren, Nat., 439 (2006) 831-834.
[25] J. Koike, M. Haneda, J. Iijima, Y. Otsuka, H. Sako, K. Neishi, J. Appl. Phys., 102 (2007) 043527-043521-043527.
[26] M. Haneda, J. Iijima, J. Koike, Appl. Phys. Lett., 90 (2007) 252107/252101-252103.
[27] M. Okua, K. Wagatsuma, T. Konishi, J. Electron Spectrosc. Relat. Phenom., 98-99 (1999) 277-285.
[28] F.J. Himpsel, F.R. McFeely, A. Taleb-Ibrahimi, J.A. Yarmoff, G. Hollinger, Phys. Rev. B: Condens. Matter, 38 (1988) 6084-6096.

[29] H. Sun, X. Qin, F. Zaera, J. Phys. Chem. Lett. 2 (2011) 2525-2530.
[30] M. Komiyama and T. Shimaguchi, Surf. Interface Anal., 32 (2001) 189-192.

Chapter V

Experimental Part,
From Nanoparticle to Film

Chapter V

Experimental Part,

From Nanoparticles to Film

I. Introduction

This chapter presents experimental part used in this Ph.D in order to achieve synthesis of film from annealing suspensions of nanoparticles (NPs) in ionic liquid (IL). Firstly, in material part, the purification and the synthesis of organometallic precursors and of ionic liquids are reported. Then, the procedures to generate the suspensions of metallic nanoparticles in ionic liquids and their deposition onto technical surfaces are depicted. Finally, the description of the analytical techniques used to characterize the NPs suspensions as well as the modified surface after annealing will be detailed.

II. Materials

II.1. Ionic Liquids (ILs)

1-Methylimidazole (> 99 %) was purchased from Sigma Aldrich and distilled prior to use. 1-Chlorobutane, 1-chlorohexane or 1-chlorooctane (> 99,5 %, Sigma Aldrich) were used without further purification. Bis(trifluoromethanesulphonyl)imide lithium salt (> 99 %, Solvionic) was used without further purification. Distilled water, fresh toluene (> 99 %, Sigma Aldrich) and fresh dichloromethane (> 99 %, Sigma Aldrich) were used for purification of IL. A solution of silver nitrate in distilled water was made in order to test visually chloride presence in the IL phase.

II.2. Organometallic precursors

Mesitylcopper(I), Mes-Cu, (NanoMePS), bis(1,5-cyclooctadiene) nickel, $Ni(COD)_2$ (STREM), (1,5-cyclooctadiene) dimethylplatinum(II), $Pt(COD)Me_2$ (STREM) tris(neopentyl)(neopentylidene) tantalum (V) (NanoMePS) were used without further purification.

Manganese carbonyl (Mn_2CO_{10}), methylcyclopentadienyl manganese tricarbonyl and bis(ethylcyclopentadienyl) manganese (II) ($(EtCp)_2Mn(II)$) (Sigma Aldrich) in chemical vapor deposition purity were used directly. $MnCl_2$ (Sigma Aldrich) was dried as reported.[1] Dry chlorotrimethylsilane, neopentyl chloride, dioxane and metallic magnesium (Sigma Aldrich) were used without further purification. Lithium bis(trimethylsilyl)amide (Sigma Aldrich) is used without further purification.

Ruthenium organometallic precursor was synthesized from $RuCl_3$-$3H_2O$, 1,5-cyclooctadiene, methanol and zinc powder (Sigma Aldrich).

III. Synthesis

III.1. Ionic liquid

The synthesis of 1-butyl-3-methylimidazolium bis(trifluoromethanesulphonyl)imide ($C_1C_4ImNTf_2$) is detailed below. All other imidazolium ionic liquids $C_1C_6ImNTf_2$, $C_1C_8ImNTf_2$, were synthesized in the same way.[2]

III.1.i. Chloride based ILs synthesis: 1 butyl-3-methylimidazolium chloride (C_1C_4ImCl)

1-chlorobutane was added to freshly distilled 1-methylimidazole (n(C_1Im)/n(BuCl) = 1.05). The mixture was stirred for 48 h at 65 °C. The hot solution was then transferred dropwise via a canula into cold toluene (maintained at temperature inferior to 0 °C by NaCl-ice water bath) under vigorous mechanical stirring. The white precipitate formed was then filtered and washed repeatedly with toluene (3 × 200 mL) and dried over night in vacuum in order to remove water giving a white powder (87 %). ^{1}H-NMR (CD_2Cl_2): δ (ppm) : 11.05 (s, 1H, C_2H) ; 7.33 (d, 1H, C_4H) ; 7.28 (d, 1H, C_5H) ; 4.31 (t, 2H, NCH_2) ; 4.07 (s, 3H, NCH_3) ; 1.90 (qt, 2H, $CH_2CH_2CH_2$) ; 1.41 (st, 2H, $CH_2CH_2CH_3$) ; 0.96 (t, 3H, CH_2CH_3) ; ^{13}C{^{1}H}-NMR (CD_2Cl_2) : δ (ppm) : 138.3 (C_2H) ; 122.3 (C_4H) ; 119.8 (C_5H) ; 50.1 (NCH_2) ; 36.8 (NCH_3) ; 32.5 ($CH_2CH_2CH_2$) ; 19.8 ($CH_2CH_2CH_3$) ; 13.6 (CH_2CH_3)

III.1.ii. Bis(trifluoromethanesulphonyl)imide based ILs synthesis: 1 butyl-3-methylimidazolium bis(trifluoromethanesulphonyl)imide $C_1C_4ImNTf_2$

A solution of lithium bis(trifluorosulphonyl)imide $LiNTf_2$ (1 g in 1 mL of water) was added to a solution of C_1C_4ImCl (n($LiNTf_2$)/n($C_1C_4ImNTf_2$) = 1). The solution was stirred overnight at room temperature. Dichloromethane was added into the mixture in order to facilitate liquid-liquid separation, and to decrease viscosity. The lower phase was collected and washed repeatedly with water until no chloride traces remained in the washing (tested with silver

nitrate solution). The mixture was filtered onto alumina column (dried overnight at 110 °C in oven), in order to obtain colorless liquid. Sometimes, activated charcoal was added on top of alumina column in order to improve this purification. The IL was next dry under 10 Pa one day and next overnight under high vacuum (10^{-3} Pa), resulting in the formation of colorless viscous liquid. ^{1}H-NMR (CD_2Cl_2): δ (ppm) : 8.73 (s, 1H, C_2H) ; 7.28 (d, 1H, C_4H) ; 7.24 (d, 1H, C_5H) ; 4.15 (t, 2H, NCH_2) ; 3.90 (s, 3H, NCH_3) ; 1.83 (qt, 2H, $CH_2CH_2CH_2$) ; 1.32 (st, 2H, $CH_2CH_2CH_3$) ; 0.94 (t, 3H, CH_2CH_3) ; $^{13}C\{^{1}H\}$-NMR (CD_2Cl_2) : δ (ppm) : 134.3 (C_2H) ; 124.3 (C_4H) ; 122.4 (C_5H) ; 118.2 (CF_3) ; 50.3 (NCH_2) ; 37.1 (NCH_3) ; 33.2 ($CH_2CH_2CH_2$) ; 19.8 ($CH_2CH_2CH_3$) ; 13.5 (CH_2CH_3)

III.2. Organometallic precursors

Organometallic precursors not commercially available have been synthesized.

III.2.i. (η^4-1,5-cyclooctadiene)(η^6-1,3,5-cyclo-octatriene)ruthenium(0): Ru(COD)(COT)

Ru(COD)(COT) was synthesized as reported.[3] Firstly, $RuCl_3.(H_2O)_3$ was kept overnight under vacuum. Degassed 1,5-cyclooctadiene (60 mL, 0.49 mol) filtered over alumina and zinc dust (10.0 g) were added to a solution of $RuC1_3.3H_2O$ (3.6 g, 13.7 mmol) in distilled degassed methanol (50 mL). The mixture was heated under reflux with magnetic stirring for 6 h and then filtered, washing the solid residue with dry degassed toluene. The resulting brown solution was evaporated under vacuum and extracted with n-pentane (2 mL) affording a red solution which was chromatographied on an alumina column (10 cm). The Ru(COD)(COT) precipitates to yields yellow crystals (1.7 g, 43 %), m.p. 92 - 94 °C. ^{1}H-NMR (C_6D_6) δ (ppm): 4.78 (dd, 2 H), 5.22 (m, 2 H), 6.21 (m, 2 H), 7.08 (m, 4 H), 7.78 (m, 8 H), 8.36 (m, 2 H), 9.10 (m, 2 H).

III.2.ii. Anhydrous $MnCl_2$ and bis(bis(trimethylsilyl)amido)manganese(II)

The bis(bis(trimethylsilyl)amido)manganese(II) is synthesized from anhydrous manganese dichloride under argon atmosphere. This latter was obtained by the reaction of commercial manganese chloride with chlorotrimethylsilane, added dropwise followed by 3 h at 60 °C, Scheme 1. Then, it was dried under reduced pressure 4 h (10^{-3} Pa).[4]

$$MnCl_2.xH_2O + 2x\ (CH_3)_3SiCl \rightarrow MnCl_2 + [(CH_3)_3Si]_2O + 2x\ HCl$$

Scheme 1| Synthesis of anhydrous manganese dichloride.

Reaction of lithium bis(trimethylsilyl)amide on anhydrous manganese dichloride has been performed under inert conditions. The lithium precursor solution in toluene was added dropwise on anhydrous manganese dichloride dissolved in freshly distilled tetrahydrofuran (THF). After 2 h at room temperature, the solvent was removed under vacuum. The residue was extracted with pentane. The pentane washing were cannulated in a schlenk tube. Under vacuum, pentane was removed yielding a black brown mud from which bis(bis(trimethylsilyl)amido)manganese could be distilled at 112-120 °C, Scheme 2.[5, 6]

$$MnCl_2 + 2\ LiN(SiMe_3)_2 \rightarrow Mn[N(SiMe_3)_2]_2 + 2\ LiCl$$

Scheme 2| Synthesis of Bis(bis(trimethylsilyl)amido)manganese(II).

III.2.iii. Bis(neopentyl) manganese(II)

The bis(neopentyl) manganese(II) ($MnNp_2$) was synthesized by the reaction of bis neopentyl magnesium on anhydrous manganese dichloride as described in the literature.[7] The solution of neopentylmagnesiumchloride in THF, was prepared by the reaction of neopentyl chloride with metallic magnesium. The titration of [$Mg(^tBuCH_2)Cl$] in diethylether was determined by addition of a solution of benzyl alcohol (1 M) in THF in the presence of 2,2 bisquinoleine.

Then, the stoichiometric quantity of dioxane was added yielding bis(neopentyl)magnesium in solution in THF and precipitation of magnesium chloride salt, Scheme 3.

$$Mg + {}^{t}BuCH_2Cl \rightarrow Mg({}^{t}BuCH_2)Cl \leftrightarrow Mg({}^{t}BuCH_2)_2 + MgCl_2 + \text{dioxane} \rightarrow Mg({}^{t}BuCH_2)_2 + MgCl_2$$

Scheme 3| Synthesis of bis(neopentyl)magnesium

After filtration, the required volume of this solution was added to a solution of anhydrous $MnCl_2$ in degassed toluene. The obtained grey solution, was kept under stirring, two days at room temperature, at this end the solution was grey-brown. The solvents were removed under vacuum, and $Mn({}^{t}BuCH_2)_2$ was extracted from residual solid with pentane. The evaporation of pentane yielded a brown powder which was dried under high vacuum then kept in freezer of a glove box, Scheme 4.

$$MnCl_2 + Mg({}^{t}BuCH_2)_{2(dioxane)} \rightarrow Mn({}^{t}BuCH_2)_2 + MgCl_{2(dioxane)}$$

Scheme 4| Synthesis of bis(neopentyl) manganese.

III.3 Nanoparticles

III.3.i. Monometallic nanoparticles synthesis

All operations were performed in the strict absence of oxygen and water under a purified argon atmosphere using glove box, or Schlenk techniques under argon. Typically, in a Schlenk tube, a solution of organometallic precursor in $C_1C_nImNTf_2$ at desired concentration (generally $5x10^{-2}$ M) was prepared by mixing, under stirring, at room temperature. 2 mL of the organometallic solution was taken in a syringe and put into the autoclave or Fischer-Porter bottle (in function of desired H_2 pressure) under argon. At this step, the argon atmosphere of autoclaves was evacuated under vacuum. Subsequently, reaction media were warmed to the desired temperature with or without stirring. The H_2 pressure was next inserted at the desired value during 10 min. Next H_2 entrance was shut and the reaction is let settle during the time

desired, generally until no more change of the color of the solution was observed. At the end of the reaction, the resulting dark suspension was evacuated under vacuum to eliminate volatile by-products formed and placed under argon in a glove box for storage.

In some case, the volatiles were condensed at -198 °C in order to determine precisely by gas chromatography the percent of OM precursors which have been converted. For Ru(COD)(COT), conversion was always 100 %.

III.3.ii. Bimetallic nanoparticles synthesis

For bimetallic NPs synthesis, the same procedure was applied. Generally, precursors are dissolved in two separate solutions. The mixing was performed in the autoclave during 5 minutes before vacuum. Next the solution is heated to desired temperature. The following step is the same. As bimetallic NPs are performed generally at high pressure (0.9 MPa), the NPs are synthesized in device represented in Figure 1.

In the case of bimetallic, calibrate curves have been established in order to be sure of the ratio between Ru and Cu organometallic precursors. Aliquots of 0.25 mL of IL solution containing nanoparticles were dissolved in 1.25 ml of acetonitrile in order to destroy interactions between IL with both cyclooctane (COA) and mesitylene (Mes-H). The composition of the mixture was determined by gas-phase chromatography. Peaks of COA and Mes-H were measured as only compounds present in the test. The heating program was as follows: 90 ºC for 10 min; ramp 40 ºC/min to 250 ºC, hold 10 min.

Fig. 1| Picture of autoclave and device use for synthesis of nanoparticles.

When COA and Mes-H were present in solution with the same concentration, ratio between COA signal and Mes-H signal is 1.25. This ratio is consequently inserted in calculations for determining actual ratio. All data are detailed in Table 1. It can be observed the obtained experimental ratios with respect to the theoretical values.

The results of the experimental samples present deviations from the theoretical values; furthermore, experimental values contain lower errors as concentration of Mes-H grows. There is an increasing difference in mesitylene ratio observed and COA when the quantity of COA in solution increases. COA has not a great solubility in IL. When the quantity of this compound increases, it will form at a certain time a single phase. More this phase will be present; more Mes-H will be dissolved in it. During the removing of H_2, it is possible that this

phase which is liquid will be carried by H_2 flow and thus explains the large difference observed between theoretical and experimental values.

Table 1| Comparison between the quantity theoretical and analyzed by GC for COA and Mes-H.

Ru:Cu ratio	Q COA theo (mol)	Q COA exp (mol)	Diff. (%)	Q Mes-H theo (mol)	Q Mes-H exp (mol)	Diff. (%)
10:1	$2.3x\ 10^{-5}$	1.0×10^{-5}	57	0.11×10^{-5}	0.02×10^{-5}	82
5:1	2.1×10^{-5}	1.2×10^{-5}	43	0.21×10^{-5}	0.03×10^{-5}	86
1:1	1.3×10^{-5}	0.18×10^{-5}	86	0.63×10^{-5}	0.8×10^{-5}	21
1:5	0.4×10^{-5}	0.22×10^{-5}	45	1.05×10^{-5}	0.9×10^{-5}	14
1:10	0.2×10^{-5}	0.19×10^{-5}	5	1.14×10^{-5}	1.0×10^{-5}	12

III.4. Film formations

III.4.i. Nature of wafers

All these experiments were conducted using mainly two types of wafers. A first series of samples were prepared from a wafer coated with 500 nm of SiO_2 deposited by silane decomposition, Ox1. A second series of Si samples received a thermal treatment to form 300 nm of thermal oxide. Ox2 refers to sample without pretreatment and Ox3 to wafer treated at 250 °C during 2 hours under air followed by high vacuum (10^{-3} Pa) at 250 °C overnight. All of these wafers contained surface silanol, in a less extent for Ox3.[8]

III.4.ii. In Diffuse Reflectance Infrared Fourier Transform (DRIFT) cell

DRIFT analyses were performed during thermal treatment on bare wafer, wafer with IL and wafer with a suspension of NPs in IL. For these experiments, 5 drops of NPs suspension were put onto the wafer. The wafer was next dried with filter paper and transferred in a Harrick high temperature cell under argon into the Thermo Scientific Nicolet 6700 FT-IR equipment. The sample was initially purged for 20 min under 20 $mL.min^{-1}$ of H_2. An IR spectrum was

recorded every minute between 25 and 450 °C (heating rate: 5 °C·min^{-1}) under 5 ml·min^{-1} flow of H_2.

III.4.iii. In rapid thermal process oven (RTP-oven)

RTP annealing has been performed in JIPELEC RTP oven as following: 0.05 mL of NPs suspension was deposited onto a 2x2 cm piece of wafer. The sample was purged for 5 min under primary vacuum, flushed 3 min at 500 mL.min^{-1} of N_2 containing 3% of H_2, then under 100 mL.min^{-1} of N_2 containing 3% of H_2, heated in 23 seconds to 250 °C and kept the desired duration at this temperature. The sample was cooled down and washed 3 times with acetone, dried and finally stored in air.

Annealings under N_2 and under vacuum have been also performed with changing the gas flux during purge by the one wished.

IV. Technique of analyses

IV.1. Molecular compounds: IL and OM precursor

IV.1.i. Nuclear magnetic resonance spectroscopy (NMR)

Solution NMR spectra were recorded on Bruker Avance 300 MHz spectrometer for 1H and 13C.

IV.1.ii. Diffuse reflectance infrared Fourier transform spectroscopy (DRIFT)

This kind of IR spectroscopy uses an infrared irradiation in order to analyze a thin layer at the surface of the material. Indeed, when incident light strikes a surface, light penetrates in a thin layer of the materials and is influenced by the quality and quantity met. It is after reflected in all direction. A diaphragm allows selecting a part of this light and analyzes it by a spectrometer. This kind of spectroscopy consequently allows an improved study of structural information of deposits, surfaces and coatings. However, the length of surface analyzed which could be of great information can be only obtained with modeling which have not be performed in our case.

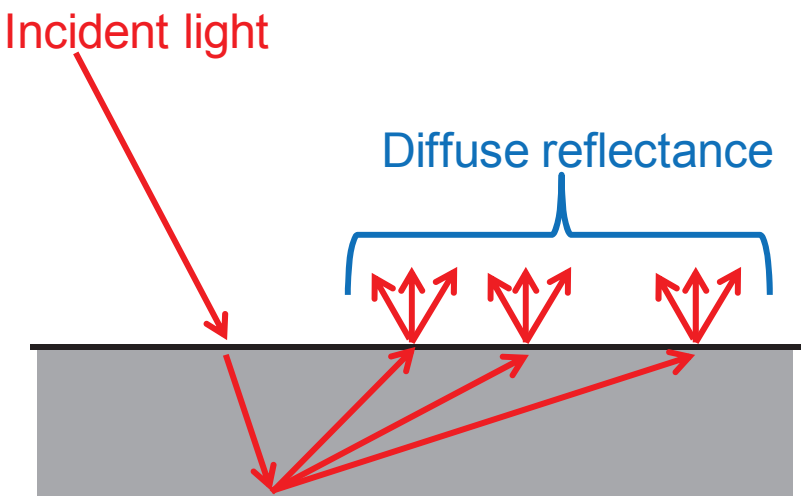

Fig. 2| Principle scheme of DRIFT spectroscopy

IV.1.iii. Gas chromatography (GC)

Two gas chromatography systems have been used for analysis the volatile by-products obtained during decomposition of organometallic precursor. For Mes-Cu, the decomposition products would be Mes-H. Moreover, due to the very small quantity produced ($6x10^{-3}$ M in solution), a very efficient system should be used. Gas chromatography coupled with a mass spectrometry (GC-MS) was performed on an Agilent Technologies 5975C, on a HP5 column ((5% Phenyl) – methylpolysiloxane). This one allows determining that Mes-H was the only product formed during reduction. Toluene and methylcyclohexane were also detected, coming from purification steps of C_1C_nImCl and hydrogenation of toluene respectively.

$MnNp_2$ decomposition products were analyzed by GC on KCl-Al_2O_3 column in a Hewlett Packard series II 5890 GC device. Neopentane and isomerisation products (isopentane, pentane) were detected with also higher carbon chain length products not further characterized (alkanes polymerization), Figure 3.

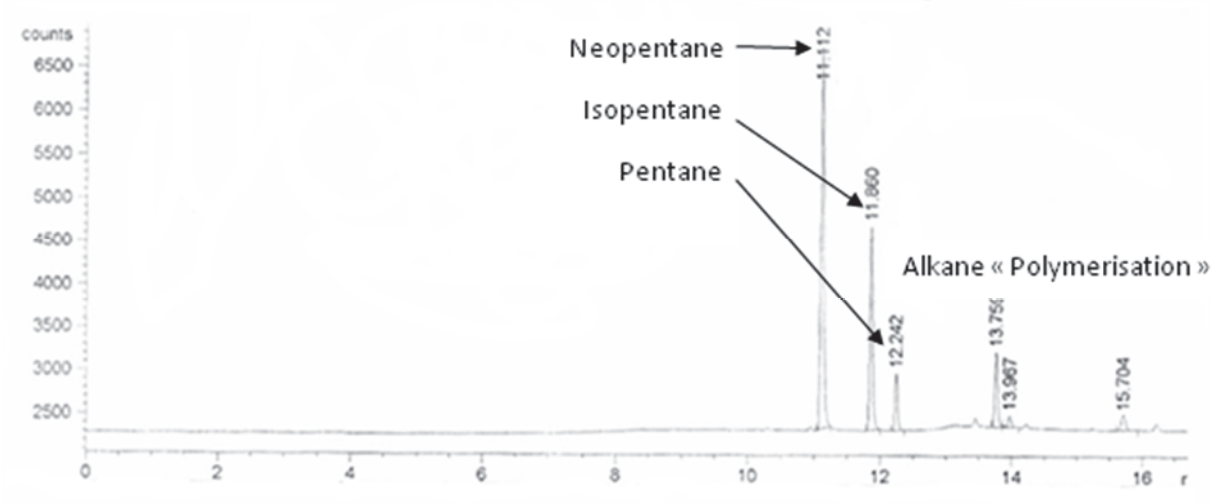

Fig. 3| GC analysis of volatile phase obtained with the decomposition of $MnNp_2$ under H_2.

IV.1.iv. Decomposition in continuous flow reactor

In a 100 mL autoclave connected to a continuous flow reactor, a solution (4 mL) of $MnNp_2$ ($5x10^{-2}$ M) in $C_1C_4ImNTf_2$ was treated under H_2 (0.4 MPa) at 100 °C, Figure 4.

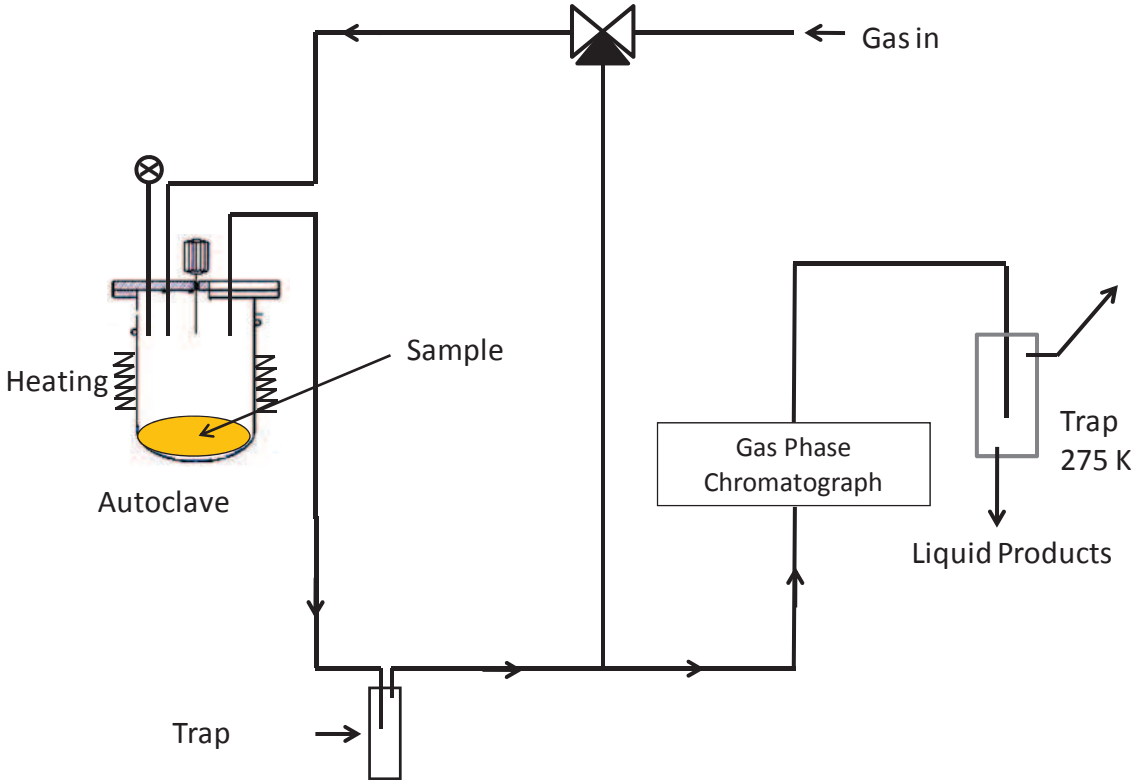

Fig. 4| Scheme of the circuit and autoclave used.

Firstly, the reactor is heated to 100 °C. Gases evolved are continuously analyzed by gas chromatography. Before H_2 insertion, only neopentane is detected. This could be due both to a partial hydrolysis from residual humidity in the reactor and / or a slight decomposition of $MnNp_2$ with the temperature. At 100 °C, GC analysis of the formed volatiles was performed every 6 min. Figure 5 indicates the instantaneous concentration of products compared to the concentration of metal.

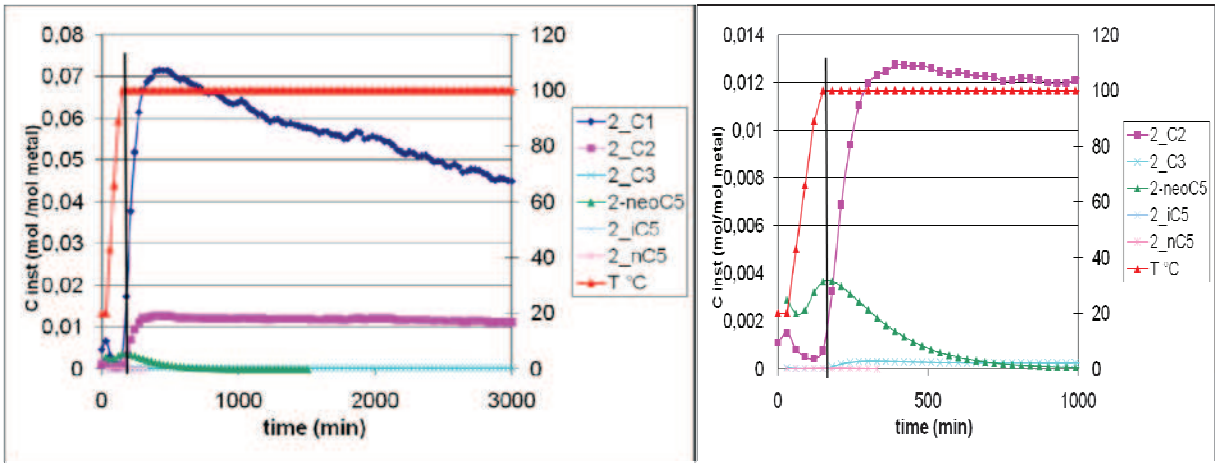

Fig. 5| Focus on concentration instantaneous of products detected by GC compared to initial concentration of metal.(left, total spectra) (right a zoom of the first 1000 min).

After 3000 minutes, the equivalent of 8.5 C / Mn (*i.e.* 1.7 Np ligand over 2) is evolved as alkanes (chiefly: methane C_1, ethane C_2, neopentane $neoC_5$ and propane C_3). $MnNp_2$ reacts with dihydrogen to form manganese hydride bond(s) which activates the C-H bonds of neopentane via a σ-bond metathesis reaction. The formation of C_1, C_2 and C_3 is due to successive C-H alkanes activation and C-C activation of the alkyl groups via β-methyl migration steps, Figure 6. This kind of result has been largely reported in hydrogenolysis of alkyl metal.[9]

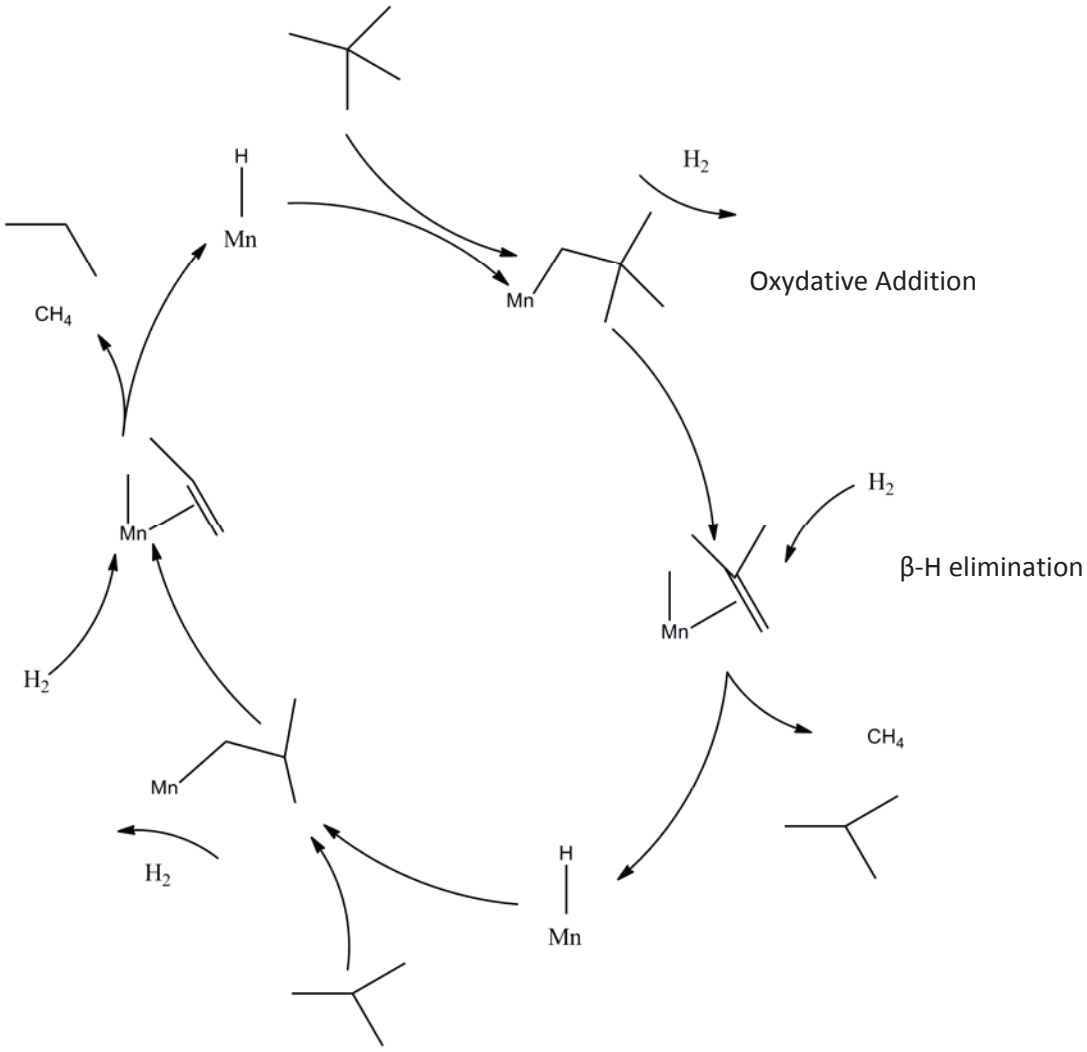

Figure 6| Alkane Hydrogenolysis of neopentane on Mn hydride.

It is worth to note that after 24 hours at 100 °C $MnNp_2$ is only partially hydrogenolized since unreacted precursor (~ 15 %) is still present. This could be due to a weak dissolution of H_2 in the IL, which is governed by the diffusivity.

IV.2. Nanoparticles

IV.2.i. Transmission electron microscopy (TEM)

Transmission electron microscopy uses as its name explained transmitted electron trough a sample to create a picture. This one should only be performed on very thin sample since electron drilling have to be possible. The resulting picture shows all the thickness of the sample and could be consequently difficult to analyze. Figure 7 shows a scheme of TEM.

Two modes could be use, a conventional one which uses irradiation of a disk of the surface (TEM) and a scanning mode which focuses in one point and scanning the surface (scanning TEM = STEM). STEM technique is aggressive and leads to high carbon contamination.

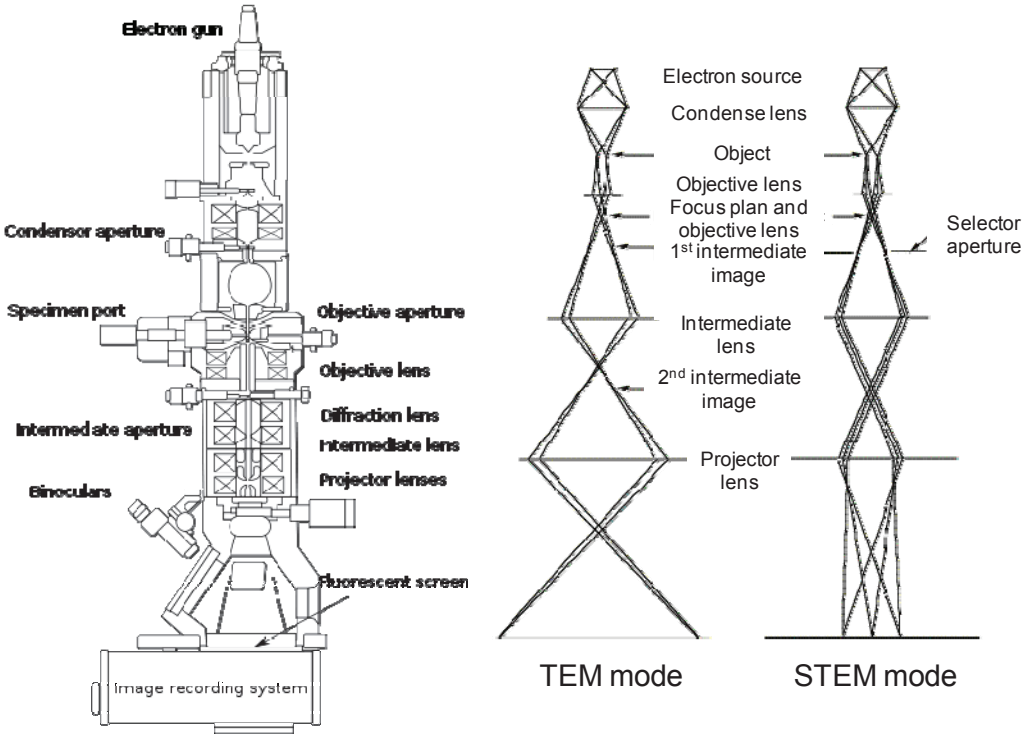

Fig. 7| Scheme of TEM and mode possible.

The NPs were observed by TEM using a Philips CM120 at 120 kV. For this purpose, the **suspensions of NPs *in situ* in IL** were deposited on a TEM grid and dried. For each sample, 200 NPs at least were measured. Their size distribution was fitted by a lognormal law, and was described with the following notation; mean size [lower limit; upper limit] nm.

For HRTEM analysis, as increasing the tension and consequently the energy of electron used, better quality image could be obtained, with for example crystalline structure observation. However, as electron are more energetic, modification (which could go up destruction) of the sample is more plausible. High Resolution Transmission Electron Microscopy (HRTEM) have been performed in Jeol JEM 2012 Lab6 and in Jeol JEM 2010 FEF (field effect gun energy filtering) working at 200 kV. As generally Cu was present in the

sample analyzed, TEM grids are chosen in other metals, as Ti or Mo in order to avoid Cu presence ***in electron dispersive X-Ray analysis***. This last technique was only used in our case to be sure that NPs analyzed were composed of metals and were not impurity or dust, and for bimetallic NPs that the two metals was present in area analyzed, Figure 8.

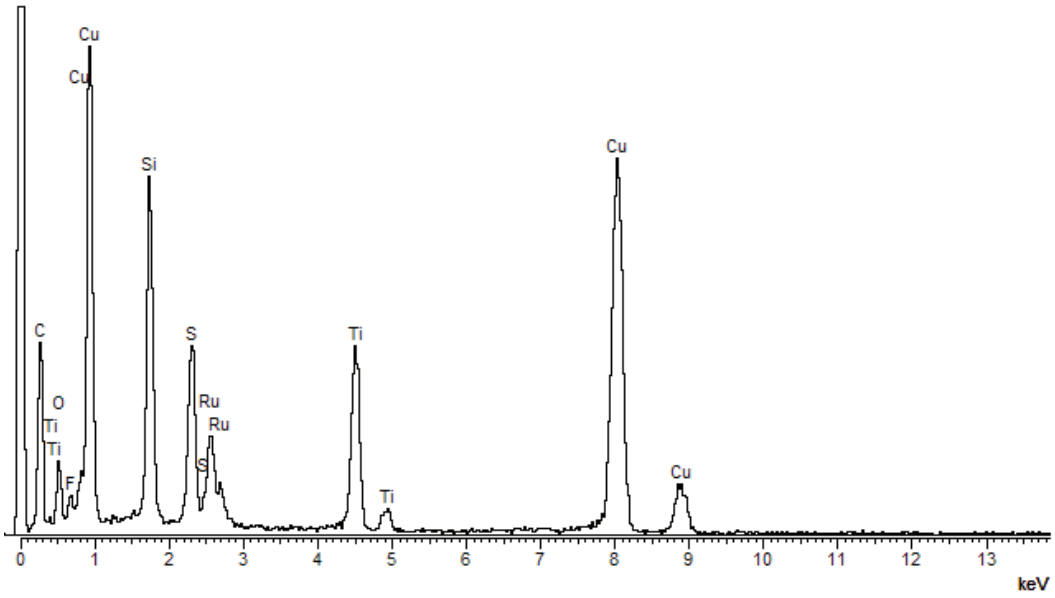

Fig. 8| EDX analysis of Ru-CuNPs area.

Bright field image is the major technique used, performed with electrons submitted to elastic contact and not diffracted. This one allows seeing crystalline structure of our NPs, Figure 9. By applying a Fourier transform of picture, a diffraction diagram is obtained, which characterizes the crystallinity of NPs. For amorphous structure, a disk is observed. For crystalline structure, well separated circle are observed corresponding to plan of same family. In the typical case of separated NPs, only points are observed corresponding to crystalline plans observed on the bright field picture. Only well oriented NPs and plan diffract, which explain the difficulty for observing crystalline lattice in our NPs. Indeed, as NPs were in IL, they could turn. Moreover, the size of NPs in these attempts should not take into account since sintering was observed under the electron beam.

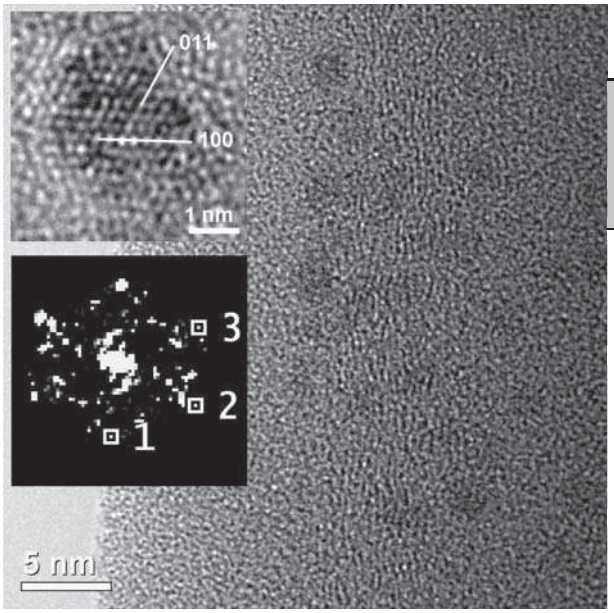

	hkl	d (exp.) Å	d (theo.) Å	Angle (exp.) °	Angle (theo.) °
1	100	2.43	2.38	0	0
2	011	2.11	2.08	64.66	64.09
3	-111	2.08	2.08	115.93	115.91

Fig. 9| HRTEM picture, Fourier transform picture of NPs obtained from the mixed solution and comparative table between Ru hcp structure and crystalline structure observed in our NPs.

² ***Electron Energy Loss Spectroscopy (EELS)*** is used in a JEM 2010 FEF in order to analyze the contribution of one metal in bimetallic NPs, Figure 10. This technique uses electrons which have been submitted to inelastic contact, leading to a loss of energy. This loss of energy is characteristic of element met and consequently elemental cartography could be performed. Less resolve pictures are generally observed since few electrons undergo energy loss. No all elements could be achieved by this way since no sufficient power is available. It was the case for Ru. Cu edge was used in order to determine where it is situated. Before Cu edge, NPs were white in a black matrix. Cu is not detected in this attempt. After Cu edge, Cu is detected. It could be observed an increase of the size of the NPs leading to the conclusion of Cu presence around Ru core.

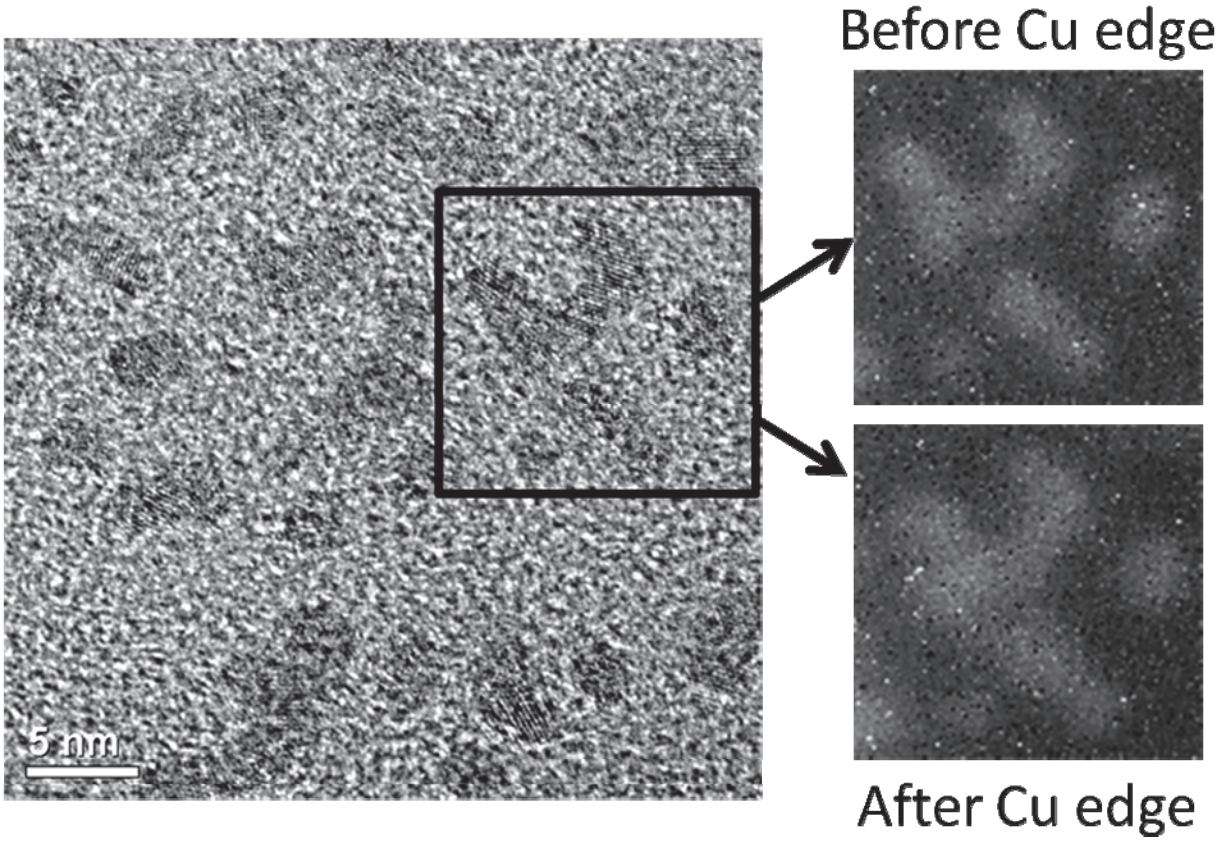

Fig. 10| HRTEM picture and EELS analysis before and after Cu edge on the part squared on the HRTEM picture.

IV.2.ii. X-Ray photoelectron spectroscopy (XPS)

XPS is surface analysis technique, using X-Ray to excite a sample surface and analyze core-electron emitted from the surface atoms. This technique is consequently element-sensitive. Moreover, this technique is performed under high vacuum (10^{-9} Pa) to avoid collision between electron analyzed and atoms. Ionic liquids, and more precisely alkyl-methylimidazolium bistriflimide based ILs could be put under this high vacuum without vaporization.[10] The sample has to be link with a source of electron since electron depletion will occur in the sample. This is not of huge importance for metals but compensation should be used when using non-conductor surface. Very surface sensitivity is obtained since X-Ray penetrate deeply in materials but only electron coming from first 10 nm of the surface could

be removed of the sample and analyzed. This leaded to high difficulty of NPs analysis in IL since IL hided NPs.[10]

One approach to isolate NPs signals from IL one was to concentrate NPs. First, centrifugation of NPs has been easily obtained with Cu-based and Mn-based NPs. Although RuNPs could not be centrifuged (with conditions tested), Ru-CuNPs decant naturally in one week. Concentration of NPs has been performed at 26000 rpm during 10 min. However, a black paste was obtained with a too high IL presence.

For further investigations, NPs were concentrated on alumina substrates by filtration. In Pasteur pipette, cotton was put following by 5 mm of dried alumina. In glove box, NPs suspension was filtered 5 times, which result of darker powder. The resulting powder containing NPs and IL traces was transferred to X-Ray photoelectron spectroscopy (XPS, KRATOS ANALYTICAL spectrometer AXIS ULTRA^{DLD}) without air break. For this purpose, alumina containing NPs was deposited on metallic indium surface. An area of 300x700 µm was analyzed using aluminum monochromatic source at 1486.6 eV. X-Ray Auger electron spectroscopy was performed on the same device. This technique allows demonstrated that our Ru-CuNPs were composed of metallic Ru due to thin peak at the good energy, and metallic Cu due to the combination of convenient binding energy and Auger peak energy, Figure 11. However, IL was always present in a great quantity; with many other analyses not usable since IL hided even completely the alumina surface. A more convenient way was sought in order to achieve analysis each time.

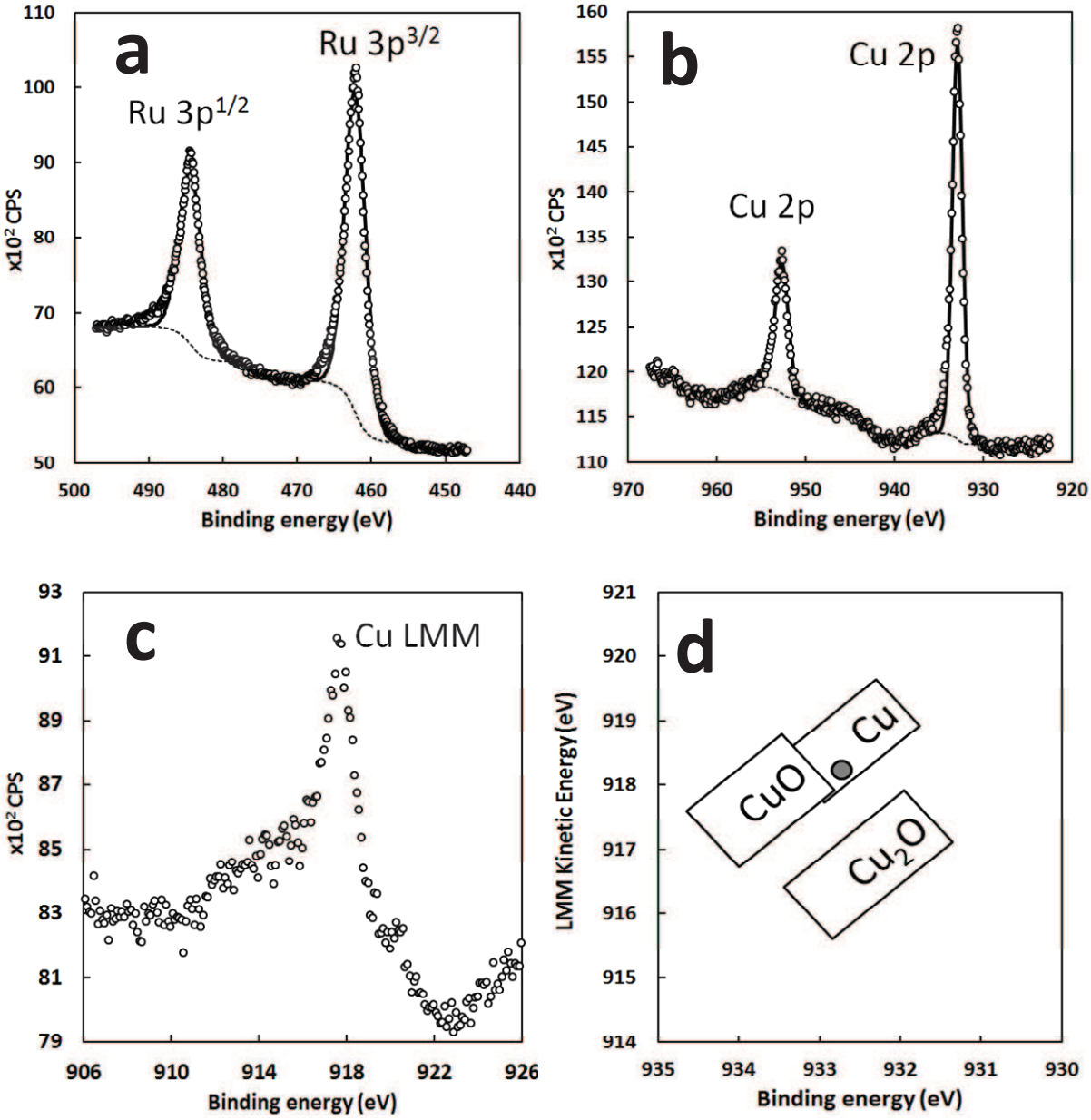

Fig. 11| XPS and XAES analysis of Ru-Cu solution of NPs, points: experimental data, line approximation. a) Ru $3p_{1/2}$ and Ru $3p_{3/2}$ peaks. b) Cu $2p_{1/2}$ and $Cu2p_{3/2}$ peaks. c) Cu LMM Auger peaks. d) Wagner plot of Cu $2p_{3/2}$ and Cu LMM: zero-valent copper present in the sample.

A third method was consequently proposed. In glove box, the NPs suspension was diluted 3 times with dried and degassed acetonitrile. The resulting suspension was passed 3 times on filter paper adapted to a syringe. Next, the filter was dry by passing 3 times argon on the filter paper. The colored filter paper was glued to sample by carbon scotch and transfer in XPS chamber under argon overpressure. This method leaded to a great improvement of NPs

concentration, with higher signal observed and consequently better precision on peaks value (notably for Cu Auger peak).

IV.2.iii. Ultraviolet-visible spectroscopy (UV-Vis)

Metal, on the form of NPs could have a surface plasmon resonance.[11] This corresponds to the formation of a dipole by concentrating electron on a part of the surface of the nanoparticles and oscillating under the action of the visible light. At a certain wavelength, there is resonance that creates an absorption peak. This peak is hidden by relaxation phenomena in most of metals. It is not the case for noble metals, which have a d-layer entire. These metals are copper, silver and gold. In this report, we will perform UV-Vis spectrometry analysis on bimetallic copper NPs obtained in ionic liquid in order to determine if plasmon is visible with these NPs.

For these analyses, a quartz cell of 1 mm optical path was filled in glove box with solution of NPs. These cells were used in order to reduce the quantity of liquid needed. One cell was filled with pure ionic liquid used for the synthesis of NPs, $C_1C_4ImNTf_2$, as reference. Other was filled with suspension of Cu-based NPs. The filling was done in glove box under argon atmosphere and closed. The cell closed was transferred to the UV-Vis home-made device and analysis was performed in this atmosphere. All suspension analyzed seemed to have a red color, but only Ta-CuNPs presented sufficient Cu for seeing clearly a plasmon resonance characterizing the metallic nature of CuNPs obtained in this experiment, Figure 12. These NPs measure 4.7 [3.1; 7.0] nm while pure Ta form bulk and pure Cu NPs of 5.1 [4.2; 6.3] nm ($C_1C_4ImNTF_2$, 0.9 MPa of H_2, 100 °C, without stirring, 4 h).

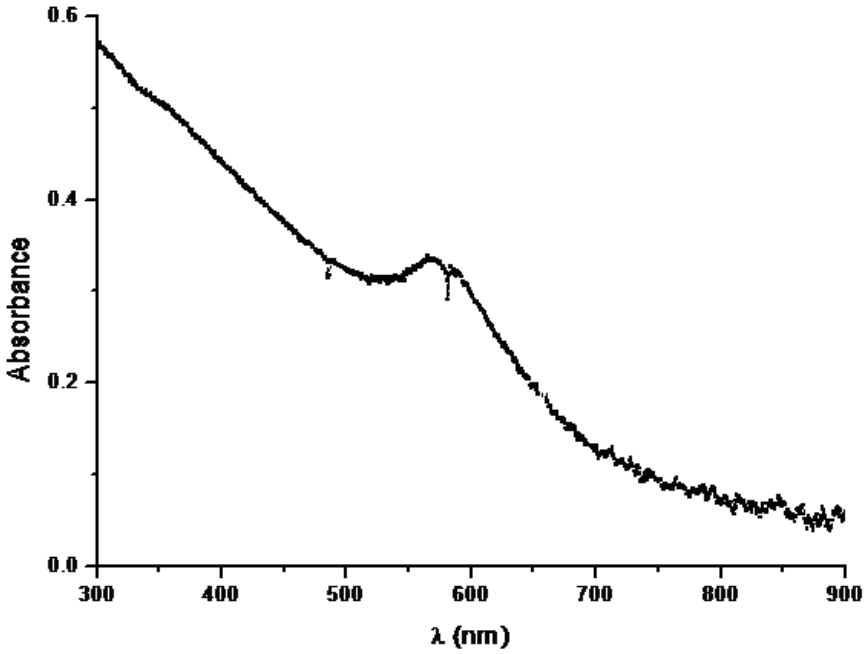

Fig. 12| UV-vis spectra obtained on Ta-CuNPs with 1:1 ratio.

IV.3. Film characterization

IV.3.i. Contact angle

Contact angle measurement is used to determine surface tension of a drop with a gas, with sessile droplet method. In our case, a drop of liquid was deposited onto surface. This method allows determining the wettability of a liquid on a solid, Figure 13.

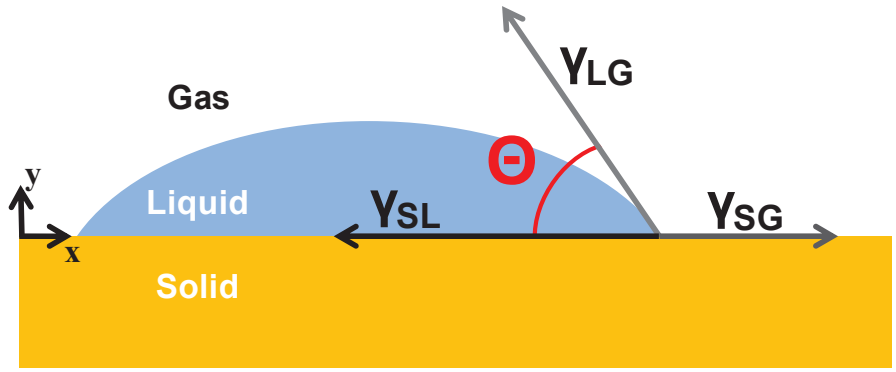

Fig. 13| Scheme representing wettability of a liquid on a surface, with formation of a drop.

If theta angle is below 90°, the liquid wet the surface. Smaller is the angle, better the wettability is. From this angle, effective surface energies γ_{SG} - γ_{SL} could be calculated with

Young equation. With the hypothesis of stability, the equation: $\gamma_{SG} - \gamma_{SL} = \gamma_{LG}\cos(\theta)$ could be deduced on the x axes. Stability hypothesis is very restrictive since neither reaction with the surface should occur, nor adsorption.

Moreover, if roughness is present at the surface, some difference could exist between measured and actual contact angle. Silica surface on wafer has very low roughness and will be neglected. This measure is very sensitive to speed and volume of drop analyzed. Due to its high viscosity, IL contact angle measures have been repeated 5 times in order to avoid these problems. Those measures were done under atmosphere in a regulated temperature area and measured at 20 °C with a Kruss DSA 100 apparatus.

IV.3.ii. Scanning electron microscopy (SEM) and electron dispersive X-Ray analysis (EDX)

SEM uses a spot of electron to scan the surface. In this device, only reflected electrons are analyzed. From these data, a picture could be formed. There is possibility to enhance chemical composition or relief with varying parameters.

SEM and EDX analyses with a Hitachi S-5500 at 30 keV and 20 µA have been performed on deposit formed. In this case, relief is favored to the detriment of composition. For this analysis, 6x4 mm sample were spitted and linked to aluminum (to wear sample) with carbon colloids glue. Resulting samples were dried at least 10 minutes under ambient atmosphere at room temperature, and then inserted in antechamber of device. Deposits were studied with two angles, 0° corresponding to horizontal wafer and 40°, in order to have more information on the roughness of the surface.

For EDX analysis, electrons emitted by SEM have collision with the atoms. This creates high energy state which will be evacuated by emission of X-Ray. This allows characterizing elements with energy of X-Ray released. However, some elements present very similar energy and consequently during interpretation care is needed. Moreover, as X-Ray is

analyzed, a large interaction pear is observed, leading to difficulty to analyzed composition of the surface in many cases. Decreasing the energy of electron beam decreases the size of interaction pear. In our case, it is not sufficient to enhance surface composition for obtaining Cu or Mn signal in our deposits. For TEM experiment, EDX should be considered as precise since very thin sample are surveyed.

IV.3.iii. Surface analysis technique: atomic force microscopy (AFM) and profilometry

Atomic force microscopy is a technique allowing observing the surface with a very thin hard tip, Figure 14 Two major modes exists, contact mode and non-contact one. Contact mode could create damage on the film and will be consequently not be used. In non-contact, tapping mode is used corresponding to create oscillation in the cantilever and measure the force during scanning the surface of the sample. Force is obtained from measure of the deflection of cantilever with a laser beam.

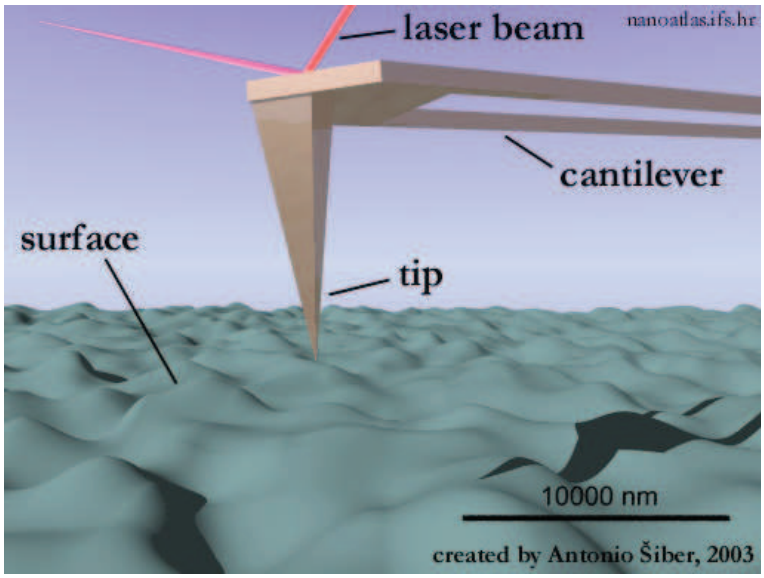

Fig. 14| Scheme of work of AFM in tapping mode.

In our case, room temperature AFM was performed, allowing analysis and direct quantification of surface relief. Several parameters could be deduced from this technique:

- Max: height of the highest summit, the lower is taken at 0.
- 10 point height: average of the 5 highest and 5 smallest values observed.
- Average: average of all height observed.
- Average roughness: gives a value of the roughness, more it is important, more roughness is present.
- RMS: gives the distribution of the roughness.
- Surface skewness: gives an idea of the symmetry of the distribution. If = 0, symmetric distribution is observed. If it is >> 1, extremely accidented surface are obtained, with for example plane surface with peaks or bearing surface with holes.
- Kurtosis coefficient: 3 for Gaussian, smaller values indicate broader distribution and vice-versa.

AFM have been performed in a DIMENSION 5000U from DI in tapping mode for RTP annealing and AFM solver Pro from NT-MDT with Nova 1.0.26 software for annealing performed in DRIFT cell.

Optical scanning profilometry analysis allows determining the same values in an easier way and generally on larger surface, with less precision. White light is focused on the sample and reflected light are analyzed by the use of a chromatic confocal sensor, analyzing the wavelength of light received, characteristic of the height of the sample in this point. This kind of profilometer has very good height sensitivity (up to nanometer) and micrometer sensitivity on horizontal plane. Nanojura NJ optimal with MoutainMap (R) Topography ST (Digital surf sarl, Besançon) software is used in this attempt.

IV.3.iv. Low-energy ion scattering (LEIS)

This analysis technique uses high vacuum and XPS apparatus. He^+ (between 500 to 20 keV) is used to bombard the surface. When ion met surface atoms, it will remove this atom and be reflected with a loss of energy, related to the weight of the element met. The first monolayer will be characterized in quality and quantity. The next layer is analyzed through the same way. This destructive method allows consequently establishing a gradient of composition in function of the depth.

IV.3.v. Grazing incidence X-Ray diffraction (GIXRD) and X-Ray reflectometry (XRR)

These two techniques use X-Ray to analyze surfaces. GIXRD is the same of XRD but in grazing incidence, allowing improving surface contribution. Diffracted X-Ray are analyzed by this technique, allowing characterizing the crystalline structure of the sample and thus generally the exact composition of this one. The major problem with this technique is to have sufficient signal and also crystalline sample. GIXRD was performed in a XPER PRO MRDXL from Panalytical.

For XRR, as its name indicates, a reflected X-Ray is analyzed which allow knowledge of the thickness on each layer where reflectivity is performed, and also composition of these layer by interaction with the component, in this case density. Roughness of the layer could be also ascertained. X-Ray reflectometry (XRR) was also performed in a XPER PRO form Panalytical.

V. Summary of catalysis attempts

Catalysis attempt have been performed on our bimetallic NPs. This method gives no high catalytic nano-objects but is a good way to further characterize them. Two types of catalytic attempts have been performed. On Ni-based NPs, tentative for isomerisation of 1,5-cyclooctadiene is performed. On Ru-CuNPs, selective partial hydrogenation is studied from cyclohexadiene and benzene.

V.1. Catalysis attempt on Ni based NPs

Isomerisation of 1,5-cyclooctadiene (1,5-COD) needs nickel hydride as bypass for isomerisation, Figure 15. Cu has no activity for this reaction and consequently the influence of Cu concentration in NPs is tested.

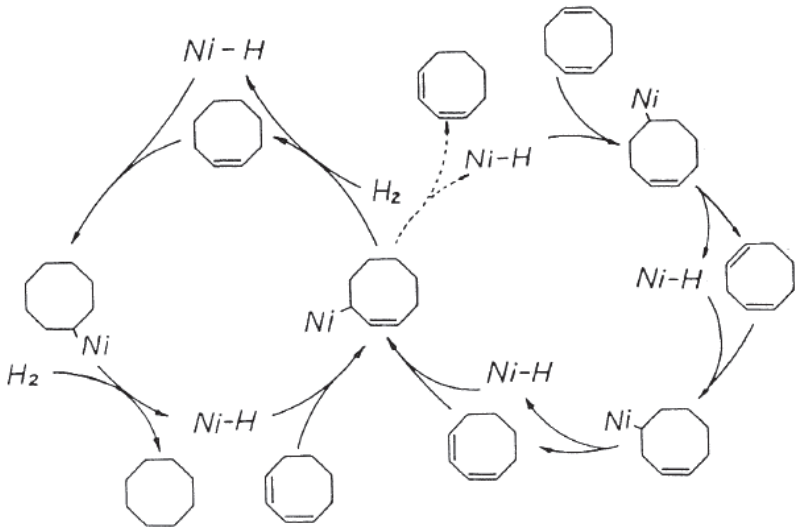

Fig. 15| Catalytic cycle of isomerisation and hydrogenation of 1,5-COD.[12]

The conditions studied for reaction is the following: under 0.2 MPa of H_2, 1000 rpm, 60 °C during 2 h. The relative ratio used during catalysis is: 0,12 mL / 1 mL for 1,5-COD / IL ratio that is 1000 for 1,5-COD / Ms ratio. Ni-CuNPs have been obtained in $C_1C_6ImNTf_2$ with different ratio, as presented above.

Increasing the concentration of Cu in NPs, with other parameters similar (NPs of similar size, same quantity of precursors …) decreases 1,5-COD conversion, Figure 16. A higher conversion is observed at low concentration of Cu which is difficult to explain. This effect needs more investigation to determine clearly its origin. The selectivity in products is similar up to 83 % of Cu and drop to zero for higher Cu concentration. The major products, cyclooctene (COE) comes from partial hydrogenation of 1,5-COD onto NPs surface, Figure 16. Very few isomerisation (1,4-COD) and complete hydrogenation (cyclooctane: COA) are obtained This is a great manner to prove that Ni is less and less accessible by increasing the Cu content in the NPs with at 83 % no more conversion due to Cu entire coverage of particles. Consequently, bimetallic Ni-core Cu-shell could be obtained.

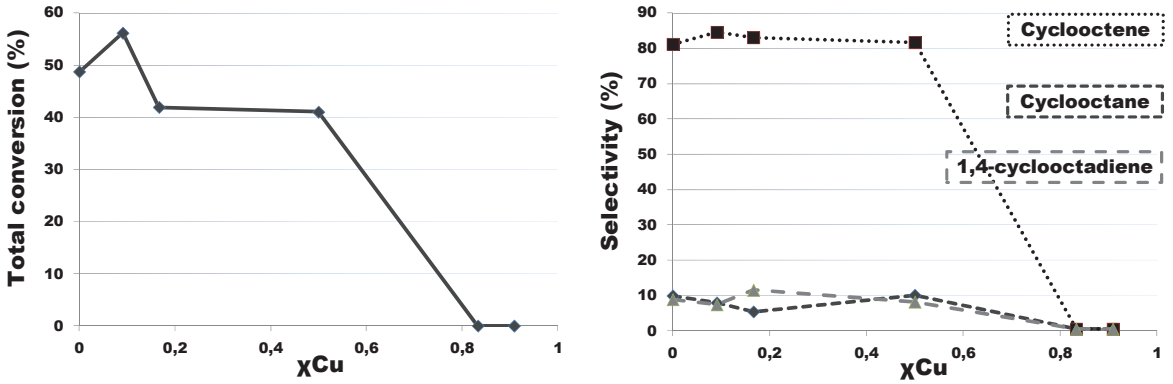

Fig. 16| Conversion and selectivity in function of molar fraction of Cu in bimetallic Ni-CuNPs.

Ru-NiNPs have been also synthesized and their catalytic activity analyzed for isomerisation of 1,5-cyclooctadiene in similar conditions, Figure 17. As they have smaller size, an improvement of activity is obtained since they have higher surface atoms content compared to Ni or Ni-CuNPs. Increasing concentration of Ni decreases the total conversion. This means that Ni is less active than Ru and that Ni cover Ru and decrease the conversion observed. Consequently, Ru-core Ni shell NPs are synthesized as it was supposed by the large difference of decomposition kinetics. There is no higher conversion observed by mixing Ru

and Ni at small concentration. Attempt at smaller concentration should be performed in order to verify this state of fact.

Pure Ru and Ru-NiNPs with high Ru content favor isomerisation in 1,3-COD. However, major product obtained during these catalyses is always COE.

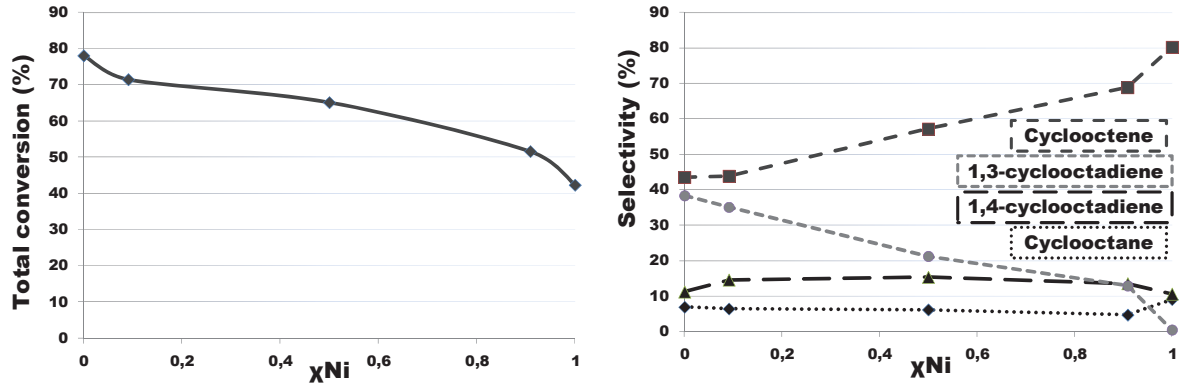

Fig. 17| Conversion and selectivity in function of molar fraction of Ni in bimetallic Ru-NiNPs.

V.2. Catalysis attempt on Ru-CuNPs

Ru-CuNPs have been also studied for catalysis, notably selective hydrogenation of 1,3-cyclohexadiene (CHD). This hydrogenation have been done in mild conditions as performed by Campbell and coworkers with pure RuNPs.[13] In this case, the influence on catalysis of Cu concentration in NPs is studied. Partial hydrogenation of CHD in cyclohexene (CHE) is observed on this catalyst. Conversely, no hydrogenation activity is observed in similar conditions in each Ru:Cu ratio, even with a very small quantity of Cu in NPs.

For having more information about this loss of activity, hydrogenation of benzene has been performed in higher conditions, which stays typical in the literature: 150 ºC during 4 hours under 0.9 MPa of H_2 under 500 rpm, Figure 18. Only cyclohexane is obtained at the end of reaction. Smaller the concentration of Cu in NPs, higher the conversion of benzene is. Thus, Cu is at the surface of the NPs and inhibits the catalytic activity of Ru by this way. Good recyclability is observed in these attempts, for example with $\chi_{Cu} = 0.09$, with a small

decrease of the activity. This is certainly due to the small increase of NPs size at the end of 5th cycle; from 2.1 [1.7; 2.5] to 3.4 [2.8; 4.1] nm mean size.

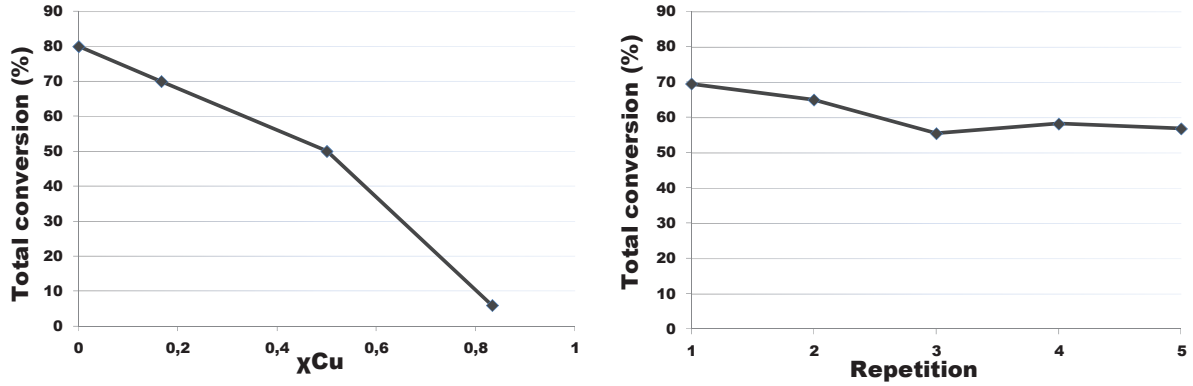

Fig. 18| Conversion in function of molar fraction of Cu in bimetallic Ru-CuNPs. Recyclability attempts with $\chi_{Cu} = 0.09$.

Monometallic Ru NPs are active and bimetallic NPs are inactive for cyclohexadiene hydrogenation. Consequently, Cu should be deposited on the surface hiding catalytic active sites of Ru. No catalysis means that cyclohexadiene has not been able to absorb on the NP surface. Using lower Cu content in Ru-CuNPs should lead to hydrogenation as observed with pure RuNPs.

In NPs catalysis, the reagent has to adsorb on the surface, for cyclic compounds like benzene, a group of adjacent atoms is necessary for adsorbing the molecule, and then hydrogenate the π-bonds. This activation makes aromatic molecules lose part of its resonance energy doing easier the hydrogenation.[14] Smale and King reported that ethane hydrogenolysis catalyzed by Ru-Cu catalyst was produced on the edge and corners of the particle.[15]

Monte Carlo simulations showed that copper cover all coins and edges with a Ru:Cu metal ratio of 9:1 (Figure 2). Therefore, hydrogenolysis of ethane occurred while the coins and edges of the NPs were free. This was in concordance with their results which showed that Ru-Cu catalytic activity did not further decrease from that ratio. In our case, we worked with nanoparticles with higher Cu content, and even then, catalysis is possible. Therefore,

adsorption and hydrogenation of benzene occurs on the planar faces of the NP. Benzene is totally hydrogenated before start breaking the aromaticity of a second molecule of benzene. Adsorption and desorption of molecules are a physic phenomena which demands energy, but much lower than the energy needed for a chemical phenomena (like hydrogenation). Working with the same nanoparticles at lower temperature could be an interesting experiment to see if cyclohexane or cyclohexadiene can be produced.

Hydrogenation of cyclohexadiene takes place on the corners and edges of the surface. This proves the suggestion of Smale and King that copper firstly adds on the low-coordinated positions, and then, on the planar faces, Figure 19.[15] It is also supported by the fact that the hydrogenation of benzene happens even when the corners and edges are blocked. In conclusion, the hydrogenation of cyclohexadiene is probably done in the corners and edges, therefore, the hydrogenation happens in only one double bond each time while for benzene is necessary firstly broke the aromaticity of the ring on a planar face.

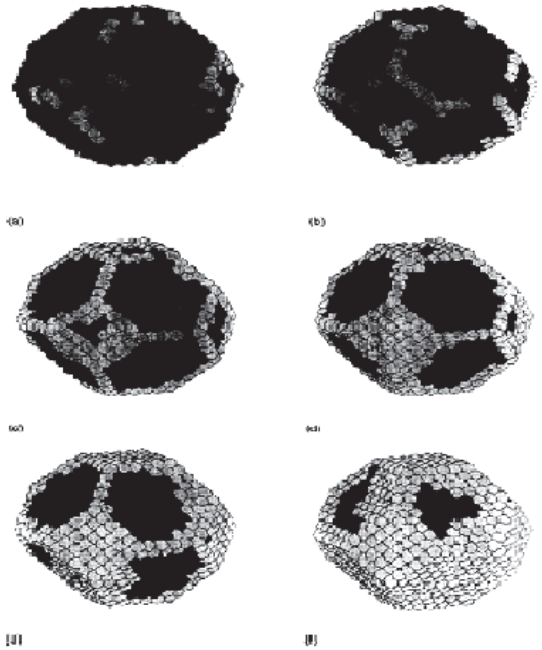

Fig. 19| Simulation for Ru-Cu. Coverage of the Ru (30% of dispersion) particle as function of Cu content; a) 2%, b)5%, c)10%, d) 15%, e) 20% and f) 30%.[15]

In conclusion, catalytic attempts with bimetallic NPs do not lead in our case to high improvement of activity or selectivity. However, it could be deduced from this attempts that Ru core Ni shell are obtained for Ru-NiNPs, Ni core Cu shell for Ni-Cu and Ru core Cu shell as it was analyzed by HRTEM for Ru-CuNPs.

VI. Work in progress

In perspective, several techniques are used in order to characterize our synthesized products. Other methods will be performed by following Ph.D students in order to better characterize our products. Small angle X-Ray scattering will be performed in conventional XRD apparatus and in synchrotron, in order to measure the size of the core and of the shell of our bimetallic nanoparticles and consequently confirm or not our hypothesis. Micro and nano hardness measures could be performed on our deposit in order to be sure that a film is obtained as well as cross section TEM analysis on sample reduced in thickness.

References

[1] E.O. Brimm, M.A. Lynch, Jr., J.W. Sesny, J. Am. Chem. Soc., 76 (1954) 3831-3835.
[2] L. Magna, Y. Chauvin, G.P. Niccolai, J.M. Basset, Organometallics, 22 (2003) 4418-4425.
[3] P. Pertici, G. Vitulli, Inorg. Synth., 22 (1983) 176-181.
[4] J.H. So, P. Boudjouk, Inorg. Chem., 29 (1990) 1592-1593.
[5] R.A. Andersen, K. Faegri, Jr., J.C. Green, A. Haaland, M.F. Lappert, W.P. Leung, K. Rypdal, Inorg. Chem., 27 (1988) 1782-1786.
[6] R.A. Andersen, D.J. Berg, L. Fernholt, K. Faegri, Jr., J.C. Green, A. Haaland, M.F. Lappert, W.P. Leung, K. Rypdal, Acta Chem. Scand., Ser. A, A42 (1988) 554-562.
[7] R.A. Anderson, E. Carmona-Guzman, J.F. Gibson, G. Wilkinson, J. Chem. Soc., Dalton Trans.: Inorg. Chem. (1972-1999), (1976) 2204-2211.
[8] L.T. Zhuravlev, Colloids Surf., A, 173 (2000) 1-38.
[9] J.M. Basset, Surface organometallic chemistry: molecular approaches to surface catalysis, North Atlantic Treaty Organization. Scientific Affairs Division, Kluwer Academic Publishers, 1988.
[10] P.S. Campbell, C.C. Santini, D. Bouchu, B. Fenet, K. Philippot, B. Chaudret, A.A.H. Padua, Y. Chauvin, Phys. Chem. Chem. Phys., 12 (2010) 4217-4223.
[11] E. Cottancin, M. Broyer, J. Lerme, M. Pellarin, Optical properties of metal clusters and nanoparticles, in: Handb. Nanophys., 2010, pp. 24/21-24/25.
[12] Y.L. Chow, H. Li, Can. J. Chem., 64 (1986) 2229-2231.
[13] P.S. Campbell, C.C. Santini, F. Bayard, Y. Chauvin, V. Colliere, A. Podgorsek, M.F. Costa Gomes, J. Sa, J. Catal. J. Catal., 275 (2010) 99-107.
[14] R.A. Van Santen, Acc. Chem. Res., 42 (2009) 57-66.
[15] M.W. Smale, T.S. King, J. Catal., 119 (1989) 441-450.

Conclusions and Outlooks

Pursuing miniaturization of integrated circuits is a constant challenge in the microelectronics industry. Nowadays, multi-core processors (3-D technologies) are used in order to improve the performances. Moreover, two recent breakthroughs indicate that nanoparticles could be used as precursors for film formation on wafers by annealing them and that the use of a bimetallic alloy could be a suitable precursor for self-formed barriers which significantly simplify the fabrication of interconnect structures.

The aim of this PhD was to replace a high vacuum technology by a low cost and versatile process using combination of these two strategies.

In Chapter I, the two major breakthroughs on which this work is based are described. First, the concept of self-formed barrier layers Cu:M is introduced. This elegant approach is also efficient, as it reduces to one step the formation of barrier and seed layers in TSVs.[1] Second, metallic films can be obtained by annealing nanoparticles (NPs) obtained through a chemical route.[2] As compared to conventional deposition processes under high vacuum, this strategy could significantly reduce process cost, while enhancing film continuity within features.

In Chapter II, the repetitive synthesis of size-controlled monometallic Mn and CuNPs in ILs from organometallic precursors (OM) under H_2 atmosphere is reported. By this route, CuNPs of 4 nm and MnNPs of 2 nm with narrow size distribution and homogeneously dispersed in the liquid have been successfully synthesized from mesitylcopper (Mes-Cu) and bis(neopentyl)manganese ($MnNp_2$), respectively.

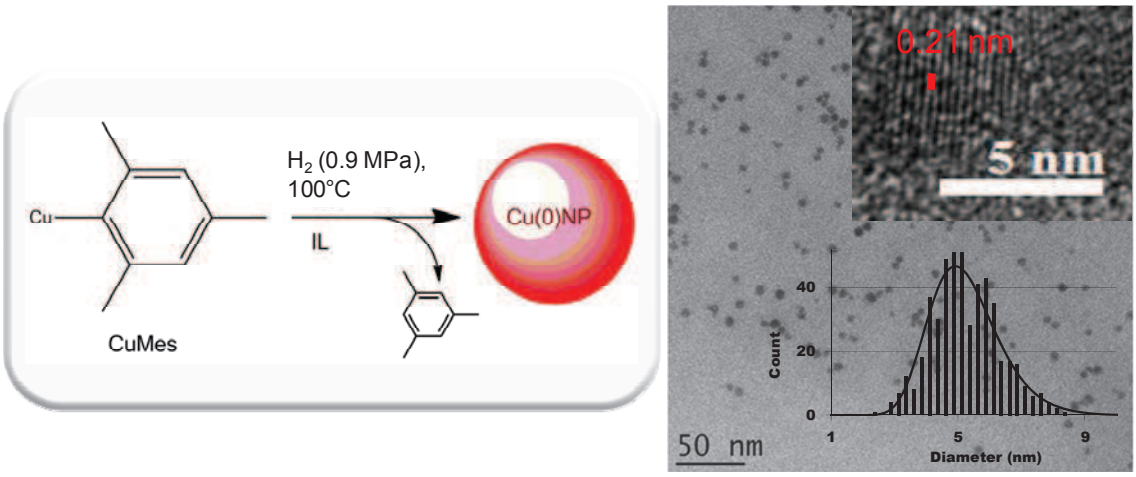

Fig. 1| Reaction scheme for the synthesis of CuNPs, TEM picture, HRTEM picture and size distribution histogram of the resulting CuNPs.

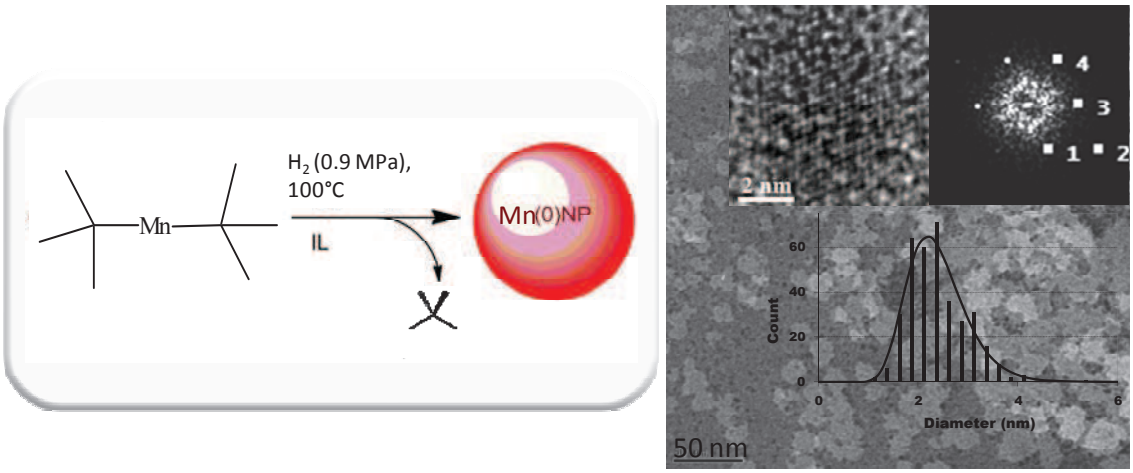

Fig. 2| Reaction scheme for the synthesis of MnNPs, TEM picture, HRTEM picture and size distribution histogram of the resulting MnNPs.

These NPs have been characterized by several methods. In particular, HRTEM and XPS (Auger) prove their crystalline and zero-valent nature.

Our experimental results shed some light upon the mechanism of NPs formation. In all cases, the rate of the decomposition / reduction of the organometallic precursor (K_1) controls the growth of NPs. The highest this rate, the smallest the resulting NPs are. This has been ascribed to a further surface reaction of unreacted OM on the freshly formed NPs (K_4). This side reaction is favored when (K_1) is lowered (low temperature, low H_2 pressure, low concentration, short reaction time) and leads to poor size control, with the formation of large NPs. However, the rates of nucleation (K_2) and growth (K_3) steps depend of the nature of

organometallic precursor and metal. CuNPs and MnNPs show a high tendency to form large aggregates or rods under these experimental conditions (K_3). A higher control on the formation and growth of NP in IL will be improve only through the knowledge of the stabilizing effect of IL, *i.e.* the understanding of the nature of the interface of IL/metal surface.

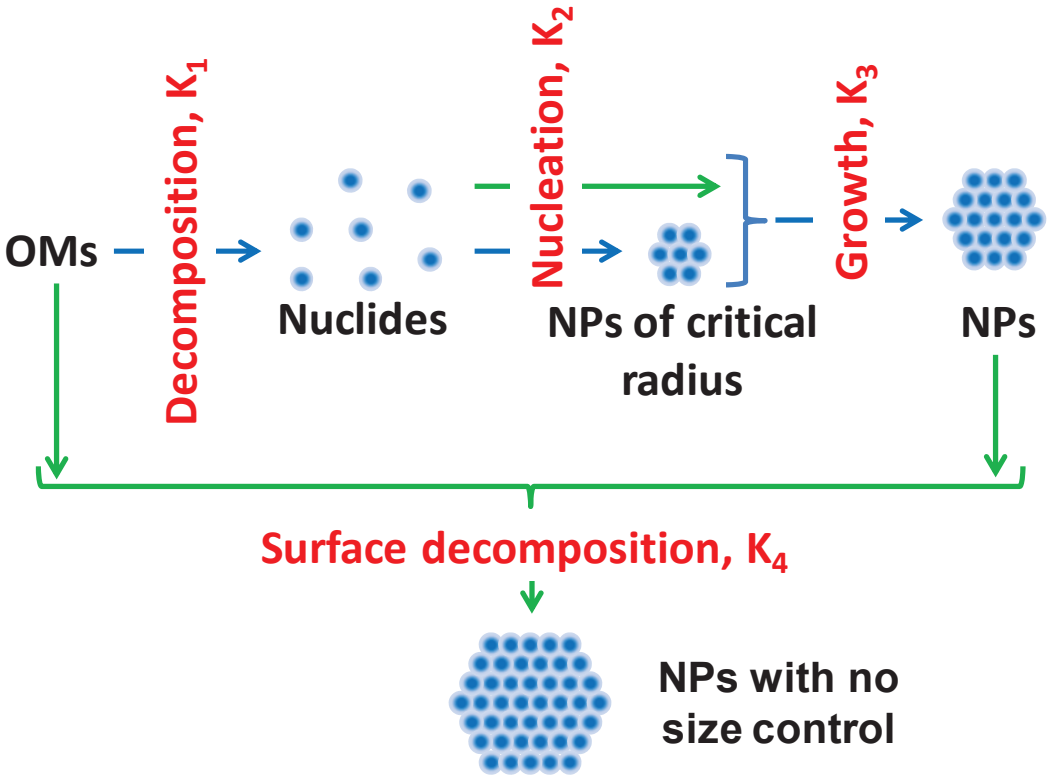

Fig. 3| Reaction scheme for the synthesis of Cu and MnNPs.

In Chapter III, the synthesis of bimetallic NPs is reported by two methods, the decomposition of a solution with mixed precursors, and the decomposition of an organometallic precursor on a suspension of already formed NPs. Remarkably, a general trend emerges from our results. A synergetic effect seems to occur when two organometallic precursors (OM_1 and OM_2) are mixed. Smaller NPs than for the pure metals are formed in a large range of molar fractions, except for M_2 rich compositions. This effect is ascribed to the fast decomposition of OM_1 followed by the reaction of OM_2 on the surface of M_1NPs. The

latter reaction would suppress further growth of M_1NPs, leading to the formation of bimetallic NPs with a M_1 core and a M_2 shell.

In the case of (M_1 = Ru, M_2 = Cu), EDX, XPS, HRTEM and EELS analyses of resulting bimetallic NPs prove that they are formed of a metallic Ru(0) core and a metallic Cu(0) shell, Ru@CuNPs.

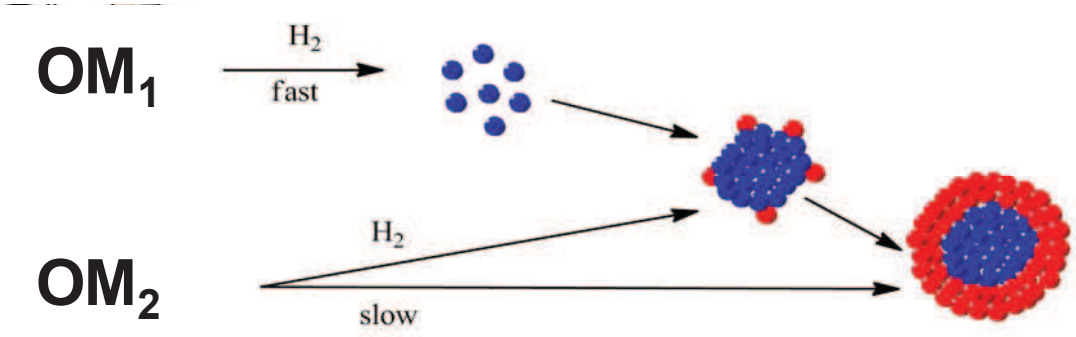

OM_1 = Ru(COD)(COT) for OM_2 = (Mes-Cu, $Ni(COD)_2$, $(COD)PtMe_2$, $Np_3Ta{=}CHCMe_3$)
OM_2 = Mes-Cu for OM_1 = (Ru(COD)(COT), $Ni(COD)_2$, $Np_3Ta{=}CHCMe_3$)
OM_1 = Mes-Cu for OM_2 = $MnNp_2$
Fig. 4| Hypothetic scheme of formation of bimetallic NPs in IL.

This mechanism, resulting from a screening of the experimental conditions to improve the size and the distribution of the resulting NPs, highlights the need of further understandings of NPs formation. This study is currently developed by Miss Inga HELGADOTTIR (CEA-PhD, 2010).

In Chapter IV, the application of these suspensions of NPs in ILs to form metallic films on technological substrates is investigated. Wettability of IL on hydroxylated silica surface is rather good, with a preference to IL with short alkyl chain length. The presence of NPs further increases wettability of the liquid, indicating a favorable interaction between the zero-valent NPs and the oxide surface. Diffuse reflectance infrared Fourier transform was used to determine the thermal stability of the suspensions. They seem to resist to temperatures up to

320 °C, which correspond to conventional process temperatures in the 3D integration. Preliminary attempts to form metallic films were undertaken at 250 °C under various atmospheres. Morphological observations show the formation of metallic deposits, which is a major and encouraging result of this study. However, these deposits are often composed of large clusters which mask the possible presence of thin liners on the oxide surface. Also, it should be noted that the attempts with Mn-CuNPs could be run with oxidized alloys, as demonstrate by easy oxidation of such objects.

For all these reasons, the latter results on film formation must be considered as preliminary attempts. Further experiments must be conducted to demonstrate the efficient fabrication of thin metallic liners by this technique. In particular, the influence of gas atmosphere should be further investigated. Also, experiments could be undertaken with more dilute suspension to limit agglomeration. Finally, other characterization techniques such as cross-section transmission electron microscopy could be used to detect a possible ultra-thin deposit on the oxide surface. This work will be carried out by Mr. Walid DARWICH (Ph.D, 2012).

In the longer term, various improvements could be performed to ensure the lowest cost to the final industrial process.

- Less expensive organometallic precursors could be used, such as, bis(ethylcyclopentadienyl)manganese, a relatively good precursors for MnNPs synthesis.

- Recycling of IL ought to be developed. In our work, an efficient separation of residual NPs from ILs, consisting in thermal agglomeration of particles at 250°C then filtration

on alumina column has been studied. ILs are then purified by standard workup (distillation) and could be reused.

References

[1] J. Koike, M. Wada, Appl. Phys. Lett., 87 (2005).
[2] C. Barriere, G. Alcaraz, O. Margeat, P. Fau, J.B. Quoirin, C. Anceau, B. Chaudret, J. Mater. Chem., 18 (2008) 3084-3086.

Appendix

Appendix 1: Size of nanoparticles

About synthesis of bimetallic Ru-CuNPs: variation of the ratio between Ru and Cu

These NPs have been synthesized under 0.9 MPa of H_2, without stirring in $C_1C_4ImNTf_2$ at 100 °C. The concentration of each precursor varies in order to have always $5x10^{-2}$ $mol.L^{-1}$ total concentrations of precursors. The following table gives the means size and distribution of NPs obtained, with χ_{Cu} corresponding to molar fraction of copper.

χ_{Cu}	Mean size (nm)	Lower limit	Upper Limit
0	4.0	2.8	5.7
0.005	1.8	1.4	2.3
0.01	2.0	1.6	2.4
0.09	2.1	1.7	2.5
0.17	2.3	2.0	2.7
0.25	2.1	1.7	2.6
0.5	2.4	1.9	3.1
0.75	2.7	2.2	3.3
0.83	2.8	2.3	3.2
0.91	3.4	2.6	4.3
0.99	4.1	3.1	5.4
0.995	11	6	19
1	5.1	4.2	6.3

In two steps decomposition, Ru-CuNPs of 2.7 [2.1; 3.4] nm are obtained with $\chi_{Cu} = 0.5$.

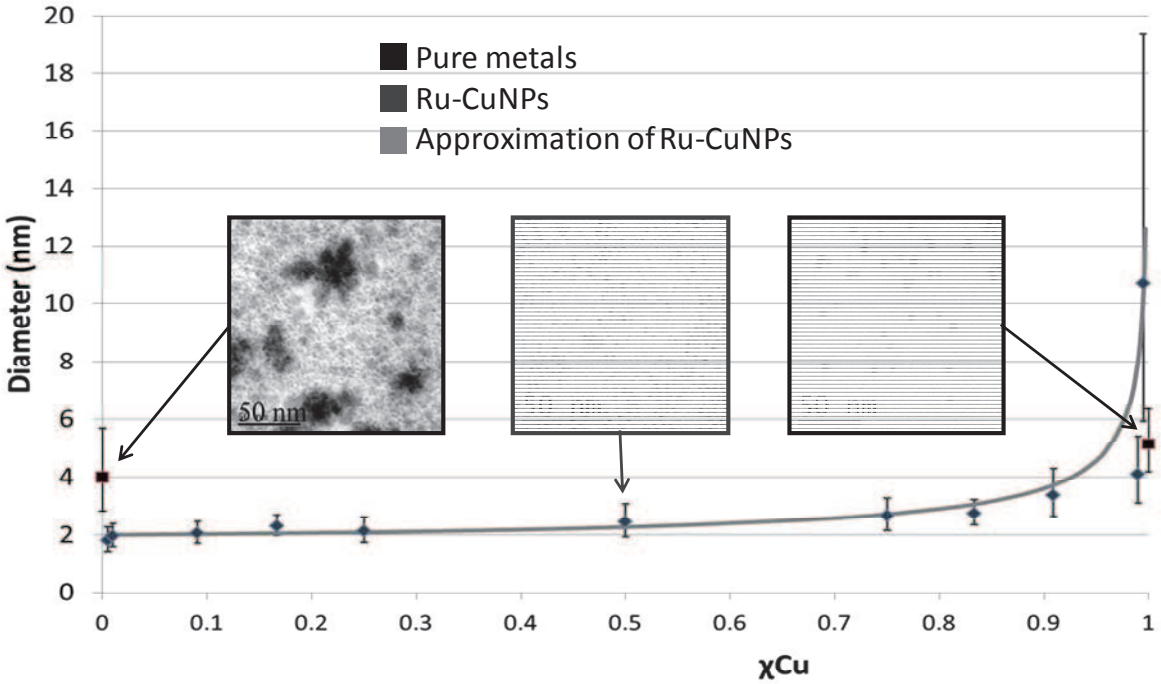

Fig. 1| Size and TEM pictures obtained for different value of χ_{Cu}, and approximation of Ru-CuNPs size obtained by a hypothetic curve: 2 nm Ru-core and Cu-shell.

About synthesis of bimetallic Ni-CuNPs: variation of the ratio between Ni and Cu

These NPs have been synthesized under 0.9 MPa of H_2, without stirring in $C_1C_6ImNTf_2$ at 100 °C. The concentration of each precursor varies in order to have always $1.8x10^{-4}$ $mol.L^{-1}$ total concentrations of precursors. The following table gives the means size and distribution of NPs obtained with χ_{Cu} corresponding to molar fraction of copper.

χ_{Cu}	Mean size (nm)	Lower limit	Upper Limit
0	5.3	4.2	6.8
0.09	4.3	3.6	5.0
0.17	4.0	3.3	4.8
0.5	4.1	3.2	5.1
0.83	3.3	2.8	4.0
0.91	5.9	4.4	7.9
1	4.6	3.6	5.9

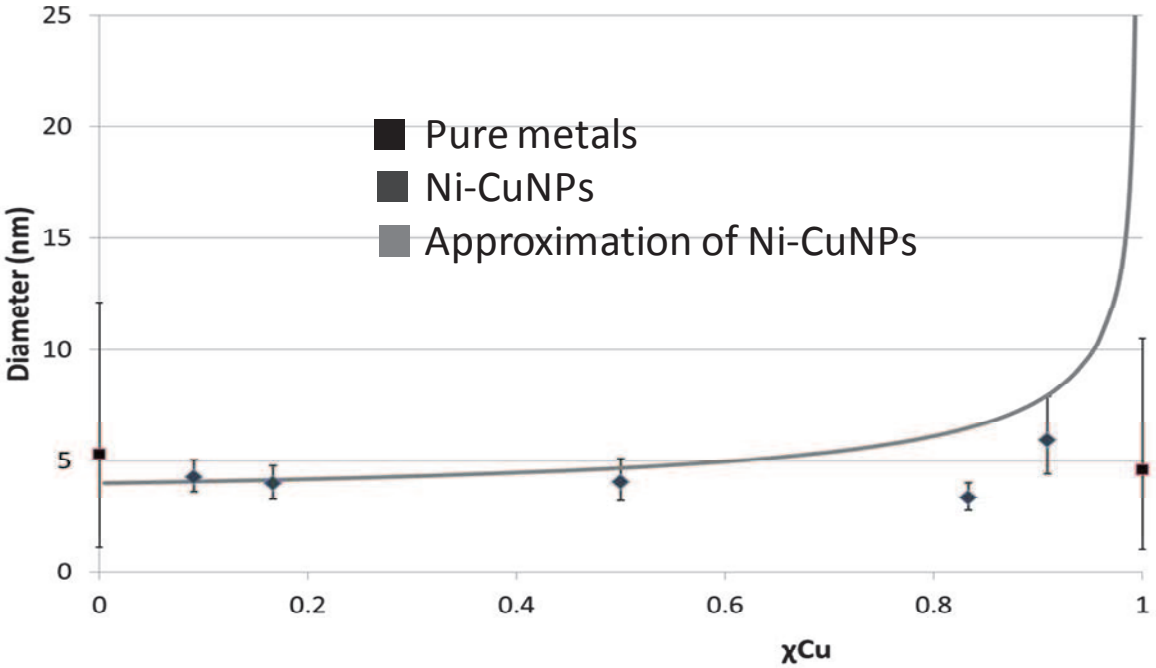

Fig. 2| Size obtained for different value of χ_{Cu}, and approximation of Ni-CuNPs size obtained by a hypothetic curve: 4 nm Ni-core and Cu-shell.

About synthesis of bimetallic Ru-NiNPs: variation of the ratio between Ru and Ni

These NPs have been synthesized under 0.9 MPa of H_2, without stirring in $C_1C_6ImNTf_2$ at 100 °C. The concentration of each precursor varies in order to have always $1.8x10^{-4}$ $mol.L^{-1}$ total concentrations of precursors. The following table gives the means size and distribution of NPs obtained with χ_{Ni} corresponding to molar fraction of nickel.

χ_{Ni}	Mean size (nm)	Lower limit	Upper Limit
0	2.7	2.2	3.3
0.09	2.4	2.0	2.8
0.5	2.6	2.1	3.3
0.91	2.7	2.3	3.2
1	5.3	4.2	6.8

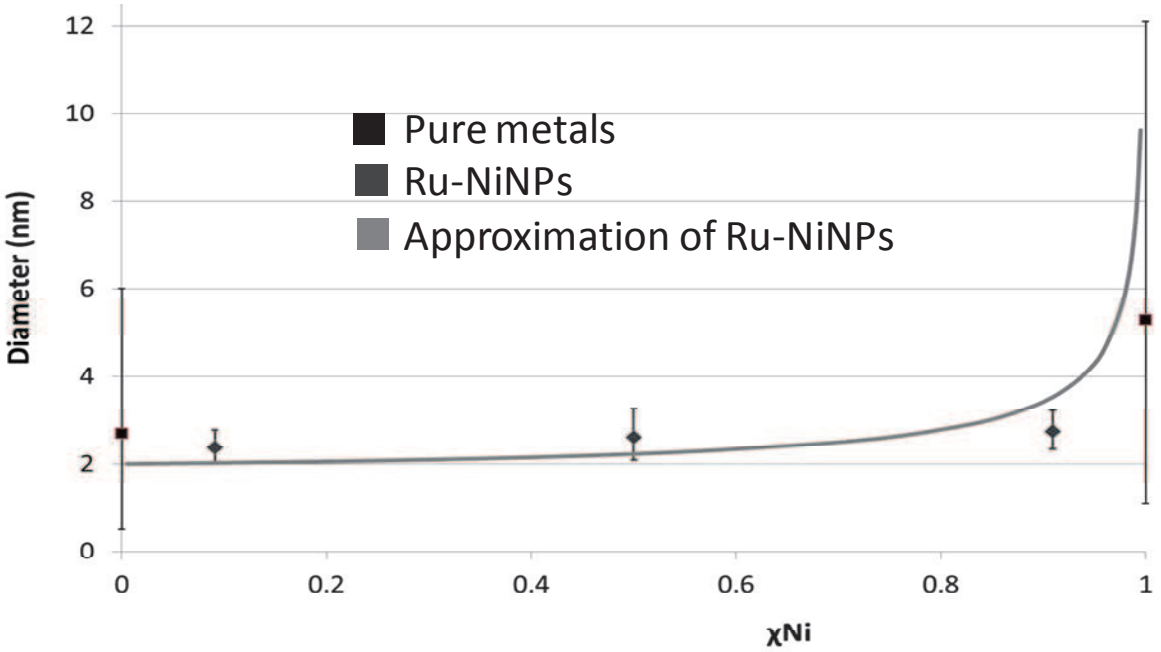

Fig. 3| Size obtained for different value of χ_{Ni}, and approximation of Ru-NiNPs size obtained by a hypothetic curve: 2 nm Ru-core and Ni-shell.

About synthesis of bimetallic Mn-CuNPs: variation of the ratio between Mn and Cu

These NPs have been synthesized under 0.9 MPa of H_2, without stirring in $C_1C_4ImNTf_2$ at 100 °C. The concentration of each precursor varies in order to have always $5x10^{-2}$ $mol.L^{-1}$ total concentrations of precursors. The following table gives the means size and distribution of NPs obtained with χ_{Cu} corresponding to molar fraction of copper.

χ_{Cu}	Mean size (nm)	Lower limit	Upper Limit
0	2.3	1.8	3.0
0.09	2.6	2.1	3.3
0.5	2.9	2.3	3.7
0.91	2.7	2.1	3.3
1	5.1	4.2	6.3

About synthesis of bimetallic Ru based NPs

Ta and Pt OMs are decomposed separately at 100 °C, under 0.9 MPa of H_2 without stirring during 4 h in $C_1C_4ImNTf_2$ ($5x10^{-2}$ mol.L^{-1}). Bulk metals are observed in the two cases. By mixing with Ru(COD)(COT) with 1:1 ratio ($5x10^{-2}$ mol.L^{-1} total OMs concentration), smaller NPs are obtained: Ru-TaNPs of 2.4 [1.6; 3.2] nm and Ru-PtNPs of 2.6 [2.0; 3.2] nm. Pt OM have been decomposed on RuNPs of 1.8 [1.4; 2.2] nm (1:1 ratio, $5x10^{-2}$ mol.L^{-1} total OMs concentration), giving Ru-PtNPs of 3.0 [2.3; 3.9] nm.

About synthesis of bimetallic Cu based NPs

Ta OM is decomposed separately at 100 °C, under 0.9 MPa of H_2 without stirring during 4 h in $C_1C_4ImNTf_2$ ($5x10^{-2}$ mol.L^{-1}). Bulk metal is observed in this case. By mixing with Mes-Cu with 1:1 ratio ($5x10^{-2}$ mol.L^{-1} total OMs concentration), smaller NPs are obtained: Ta-CuNPs of 4.7 [3.1; 7.0] nm.
Ta OM is decomposed separately at 30 °C, under 0.5 MPa of H_2 without stirring during 3 days in $C_1C_6ImNTf_2$ ($2.8x10^{-2}$ mol.L^{-1}). Ta-CuNPs of 12 [8; 20] nm are obtained. (In similar conditions: TaNPs of 3.0 [2.0; 4.1] nm and CuNPs of 14 [7; 30] nm.)

About synthesis of monometallic CuNPs

Attempts for CuNPs synthesis from decomposition of Mes-Cu

Concentration	Pressure	Temperature	IL	Stirring	Duration	Mean Size
$6x10^{-3}$ M	0.5 MPa	30 °C	**C_1C_4**	Yes	1 week	7.5 [3.9; 14.8] nm
$6x10^{-3}$ M	0.5 MPa	30 °C	**C_1C_6**	Yes	1 week	14 [7; 30] nm
$6x10^{-3}$ M	0.5 MPa	30 °C	C_1C_4	**No**	1 week	7.7 [4.6; 12.9] nm
$5x10^{-2}$ M	0.5 MPa	30 °C	C_1C_4	No	1 week	7.6 [4.0; 14.1] nm
$6x10^{-3}$ M	**0.9 MPa**	30 °C	C_1C_4	No	1 week	6.4 [3.7; 10.9] nm
$6x10^{-3}$ M	0.5 MPa	**50 °C**	C_1C_4	No	1 day	14 [16; 25] nm
$6x10^{-3}$ M	0.5 MPa	**100 °C**	C_1C_4	No	2 hours	8.5 [5.1; 14.0] nm
$6x10^{-3}$ M	0.9 MPa	100 °C	C_1C_4	No	**2 hours**	4.5 [3.1; 6.5] nm
$6x10^{-3}$ M	0.9 MPa	100 °C	C_1C_4	No	**1 hours**	7.4 [5.6; 9.9] nm
$5x10^{-2}$ M	**0.9 MPa**	**100 °C**	C_1C_4	No	**4 hours**	5.1 [4.2; 6.3] nm

About synthesis of monometallic MnNPs

All experiments have been performed in $C_1C_4ImNTf_2$ without stirring with $5x10^{-2}$ M of concentration.

Attempts for MnNPs synthesis from decomposition of $MnNp_2$ in $C_1C_4ImNTf_2$

Pressure	Temperature	Duration	Mean Size
0.4 MPa	30 °C	48 h	2.7 [1.9; 3.7] nm
0.4 MPa	30 °C	48 h	1.8 [1.4; 2.3] nm
0.4 MPa	50 °C	48 h	4.1 [2.9; 5.8] nm
0.4 MPa	50 °C	48 h	1.6 [1.1; 2.3] nm
0.4 MPa	100 °C	48 h	1.4 [0.8; 2.5] nm
0.4 MPa	100 °C	48 h	1.6 [1.1; 2.3] nm
0.9 MPa	30 °C	48 h	1.1 [0.8; 1.7] nm
0.9 MPa	30 °C	48 h	1.9 [1.3; 2.7] nm
0.9 MPa	50 °C	48 h	1.4 [0.8; 2.4] nm
0.9 MPa	50 °C	48 h	2.2 [1.7; 2.8] nm
0.9 MPa	100 °C	48 h	Rods ~ 50nm
0.9 MPa	100 °C	48 h	Rods ~ 50nm
0.4 MPa	100 °C	24 h	2.1 [1.6; 2.6] nm
0.4 MPa	100 °C	6 h	2.1 [1.5; 2.9] nm
0.4 MPa	100 °C	2 h	2.5 [1.9; 3.2] nm
0.4 MPa	100 °C	1 h	3.0 [2.2; 4.0] nm
0.4 MPa	100 °C	1 h-LA	2.7 [2.0; 3.5] nm
0.9 MPa	100 °C	1 h	2.3 [1.7; 3.2] nm
0.9 MPa	100 °C	4 h	2.3 [1.8; 3.0] nm

LA: large autoclave

Attempts for MnNPs synthesis from decomposition of $(EtCp)_2Mn$ in $C_1C_4ImNTf_2$

Experiment	Pressure	Temperature	Color after reaction	Mean Size
MnCVD-LP-LT-1	0.4 MPa	30 °C	Brown	3.3 [2.5; 4.4] nm
MnCVD-LP-LT-2	0.4 MPa	30 °C	Brown	4.1 [3.0; 5.6] nm
MnCVD-HP-LT	0.9 MPa	30 °C	Brown	3.6 [2.4; 5.2] nm
MnCVD-HP-HT	0.9 MPa	70 °C	Brown	5.3 [3.7; 7.7] nm

Other attempts for MnNPs synthesis in $C_1C_4ImNTf_2$

Precursor	Pressure	Temperature	Duration	Mean Size
$Mn_2(CO)_{10}$	0.5 MPa	100 °C	-	No NPs
$Mn_2(CO)_{10}$	vacuum	120 °C	1 days	21 nm
$C_{12}H_{36}Si_4N_2Mn$	0.9 MPa	100 °C	3 days	5.3 [3.9; 7.1] nm
η^5-$MeCpMn(CO)_3$	0.9 MPa	120 °C	-	No NPs

About synthesis of monometallic RuNPs at high temperature: influence of IL alkyl chain length

The influence of different parameters in the RuNPs synthesis has been already tested by Gutel and co-workers.[1, 2] The increase of chain length at room temperature or 0 °C allows increasing the size of resulting RuNPs. It has also been shown that increasing the temperature increases the size of NPs. It is shown in the pure metal synthesis that smaller Cu and RuNPs are obtained at 100 °C with increasing the chain length. In this part, the effect of chain length in the RuNPs synthesis will be tested at 100 °C, under 0.9 MPa of H_2, without stirring with $5x10^{-2}$ M of precursor concentration. For this purpose, three attempts are realized with increase the chain length from 4, 6 and finally 8. Surprisingly, in comparison to room temperature, at 100 °C in these conditions, the increase of alkyl chain length allows stabilizing smaller NPs. Indeed, 4.0 [2.8; 5.7] nm NPs are obtained in $C_1C_4ImNTf_2$, in comparison to 2.3 [1.7; 3.0] nm in $C_1C_6ImNTf_2$ and 1.7 [1.3; 2.1] nm in $C_1C_8ImNTf_2$.

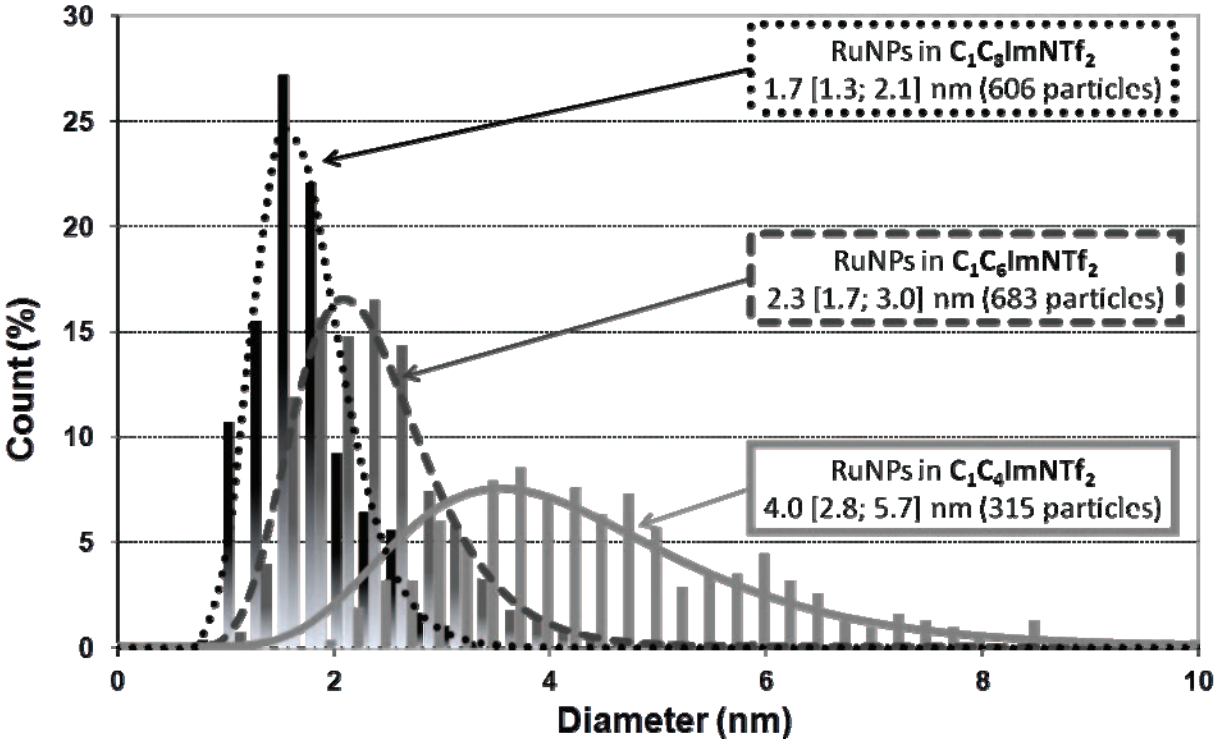

Fig. 4| Comparative size distribution histogram fitted by log-normal law of RuNPs obtained at 100 °C with $5x10^{-2}$ M of Ru(COD)(COT) under 0.9 MPa of H_2 without stirring during 4 hour in $C_1C_4ImNTf_2$, in $C_1C_6ImNTf_2$ and in $C_1C_8ImNTf_2$.

With increasing chain length, an increase of the stability of NPs in suspension at high temperature is observed. This means that it is possible to synthesize small RuNPs in relatively short duration. Indeed, 1.1 ± 0.2 nm RuNPs are obtained in 3 days at 0 °C.[2] In our case, only 4 hours (or less) are needed. Moreover, the use of longer alkyl chain allows clearly better stabilization of formed NPs. This also means that RuNPs even at 100 °C are formed next alkyl chains and stabilized by these alkyl chains. It is thus possible to obtain very small RuNPs in relatively short duration. This shows that it is not the same stabilization method which allows synthesis of small NPs at high temperature. It looks like more conventional synthesis in organic solvents.[3]

Moreover, it allows explaining that there is no huge effect of varying the concentration of OM even at this temperature. Indeed, RuNPs formed in $C_1C_6ImNTf_2$ from $1.8x10^{-4}$ M measure 2.7 [2.2; 3.3] nm compared to the 2.3 [1.7; 3.0] nm formed from $5x10^{-2}$ M. Smaller concentration seems even to increase the NPs obtained. A further investigation has to be performed with higher alkyl chains and with other organometallic precursors in order to verify the validity of these results. Moreover, a mechanism has to be deduced for NPs synthesis in these conditions.

References

[1] T. Gutel, J. Garcia-Anton, K. Pelzer, K. Philippot, C.C. Santini, Y. Chauvin, B. Chaudret, J.-M. Basset, J. Mater. Chem., 17 (2007) 3290-3292.
[2] T. Gutel, C.C. Santini, K. Philippot, A. Padua, K. Pelzer, B. Chaudret, Y. Chauvin, J.-M. Basset, J. Mater. Chem., 19 (2009) 3624-3631.
[3] K. Philippot, B. Chaudret, C. R. Chim., 6 (2003) 1019-1034.

Appendix 2: Other attempts to synthesize films

Influence of the number of deposition step

Uniform deposits are obtained in numerous attempts. Several holes are however observed as for instance after annealing at 200 °C during 1 hour, under forming gas. Without these holes, a very uniform, flat film will be obtained. In these attempts, the influence of deposition step number is tested in order to obtain this ideal flat adherent and uniform film. From all precedent attempts, the quantity of matter obtained is very low since no EDX generally detect metals. As the attempt at 200 °C seems to allow a good surface coverage of the wafer with limited inhomogeneities, this conditions was used to perform several deposition steps. The deposition is repeated 4 times at 200 °C during one hour. After annealing, the wafer is washed with acetone and a new suspension is put on the wafer and annealed.

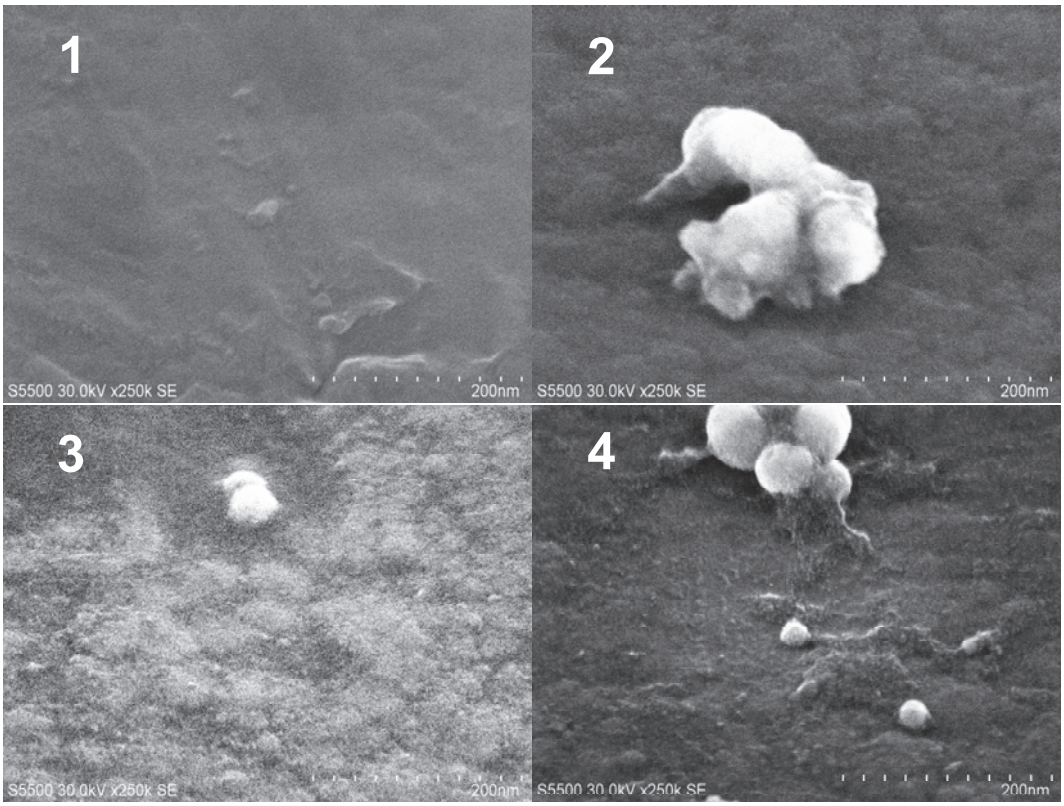

Fig.1| SEM analysis on Ox1 of suspension of Mn-CuNPs after annealing. Picture tilted at 40 °.1, 2, 3 and 4 correspond to the number of deposition steps.

From these attempts, it could be seen that the uniformity of the film decrease with increasing the number of deposition steps. In the first attempt, no Cu rich particles are observed. The number of this kind of particles seems to increase by increasing the deposition steps. Our hypothesis which suppose that a film is obtained in a first case by reaction of metal with SiO_2 substrate, followed by a decrease of the kinetic of formation leading to huge aggregates, could be valid. Indeed, increasing the deposition step leads to increase the metal deposited on the wafer. In this attempt, a very uniform film formed at 200 °C during 1 hour become less uniform with only one deposition step more. Concerning EDX analysis, the film obtained in all attempts is not sufficiently thick.

Attempts to improve the quality of the resulting films

Increasing the number of deposition steps is not a way to obtain more uniform film. It is shown that increasing duration allows in some cases increasing the uniformity of the film. Moreover, increasing concentration of NPs on the wafer leads to less uniform deposits. Consequently, this part have for aim to find best conditions allowing obtaining the most uniform film, by variation of duration and concentrations. The annealing attempt on plan wafer surface coated with 300 nm of thermal SiO_2 is performed; Ox3. The following analyses present AFM and SEM pictures of Ox3 which will be used in the following attempts. The SEM picture show that very low roughness is present on the wafer. The pictures show only small waves present at the surface. AFM analysis allows quantifying this roughness.

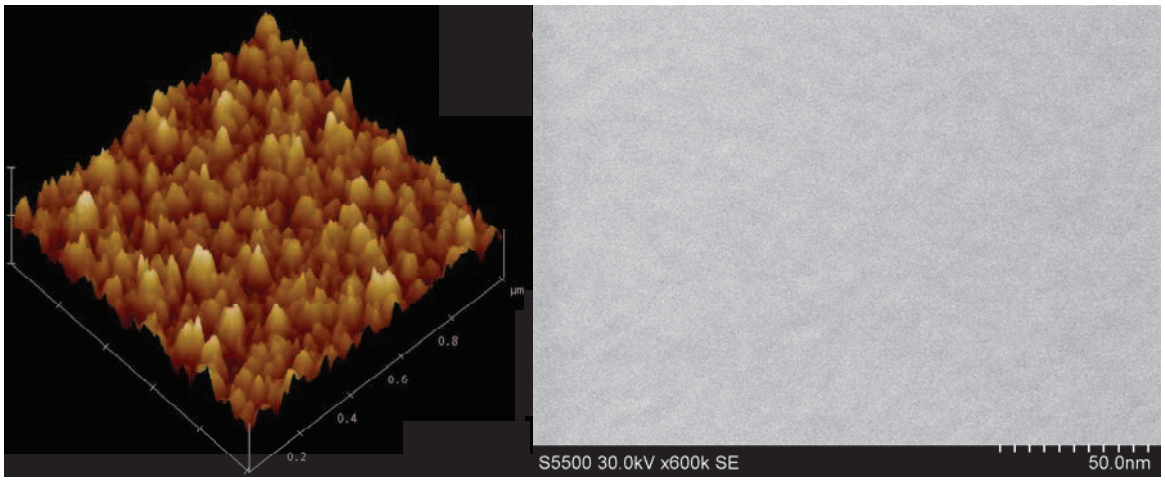

Fig. 2| AFM and SEM picture of Ox3.

As it was difficult to determine the better attempt between the annealing at 200 °C and at 150 °C, these two temperatures are tested in the following attempts. It is shown also that decreasing the concentration of NPs should allow obtaining better film, the initial concentration of deposit of $5x10^{-2}$ M was divided by two in order to prove this effect. Finally, the duration seems to increase the quality of deposition. The attempts performed in order to analyze all these parameters are presented in Table 1.

Table 1| Summary of attempts performed on plan wafer coated with 300 nm of thermal SiO_2 for obtaining better uniformity films, with solution of Mn-CuNPs in $C_1C_4ImNTf_2$.

Samples	Concentration (M)	Temperature (°C)	Duration (min)
I	$5x10^{-2}$	200	60
II	$5x10^{-2}$	**150**	60
III	**$2.5x10^{-2}$**	**200**	60
IV	**$2.5x10^{-2}$**	**150**	60
V	**$2.5x10^{-2}$**	150	**2x60**

EDX analyses are performed on all these attempts but as it was the case in precedent attempts, no sufficient metal quantity was available for seeing a peak during analysis. In all attempts, the pictures are not well defined since IL was not removed entirely, but a deposit is clearly seen. Decreasing the concentration of NPs by a factor of two allows obtaining better uniform deposit with fewer holes. The sample obtained at 150 °C with $2.5x10^{-2}$ M presents a plane deposit contrary to the hollow deposit observed with $5x10^{-2}$ M of total metal

concentration. The attempt at 200 °C with low concentration presents similar deposit than observed at 150 °C with higher concentration but with no visible holes where wafer are seen. Increasing the duration allow increasing the coverage of the wafer and also the thickness of the deposit. However, it seems that the roughness of the deposit is also increased in this case.

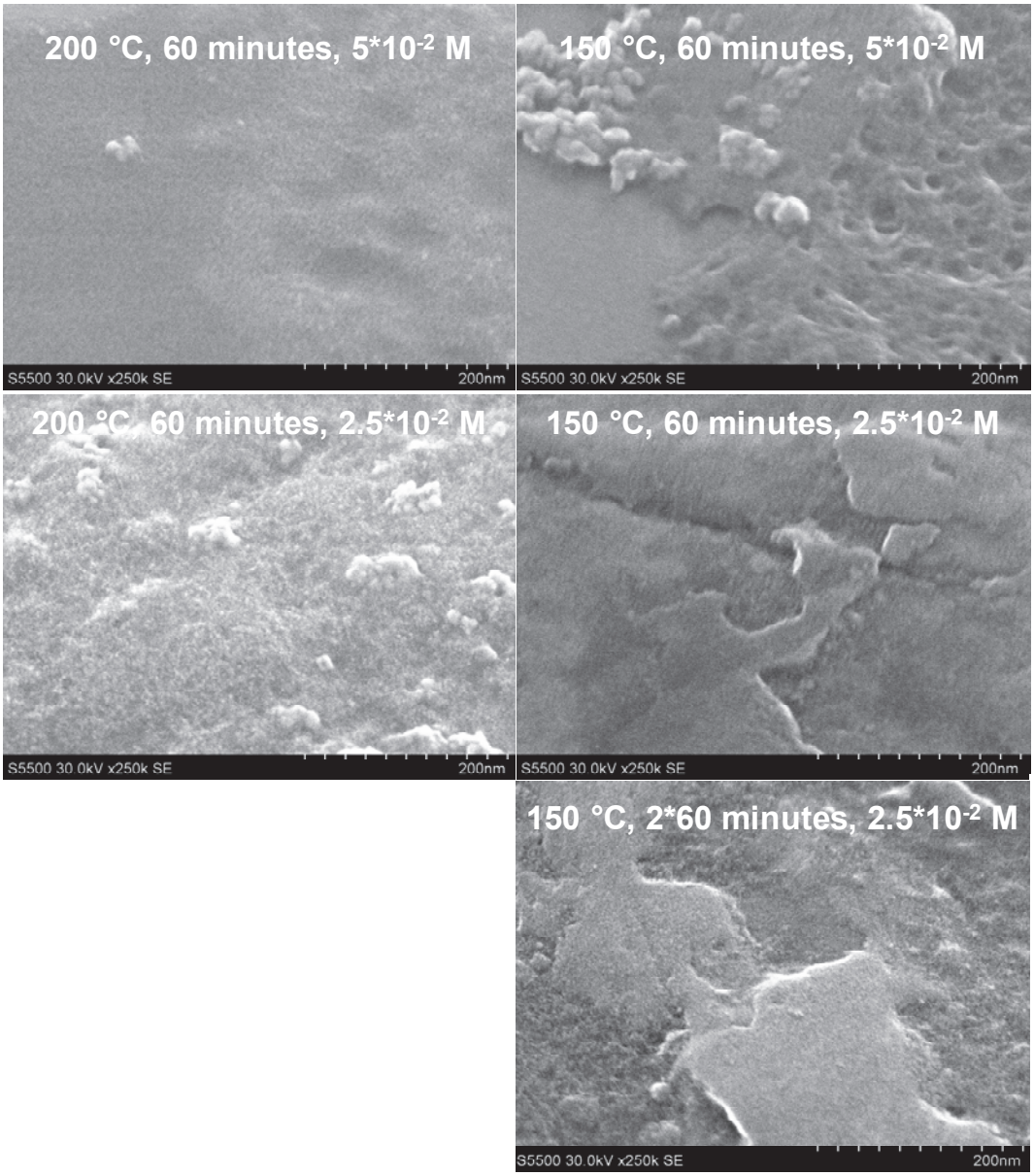

Fig. 3| SEM analysis on Ox3 of suspension of Mn-CuNPs after annealing. Picture tilted at 40 °.

AFM analysis is performed on these different attempts. The attempt realized at 200 °C during 1 h is presented in Figure 4. It is difficult to determine if the peaks observed with $5x10^{-2}$ M is due to IL or NPs, but a more uniform deposit is observed by divided the concentration by a factor of two.

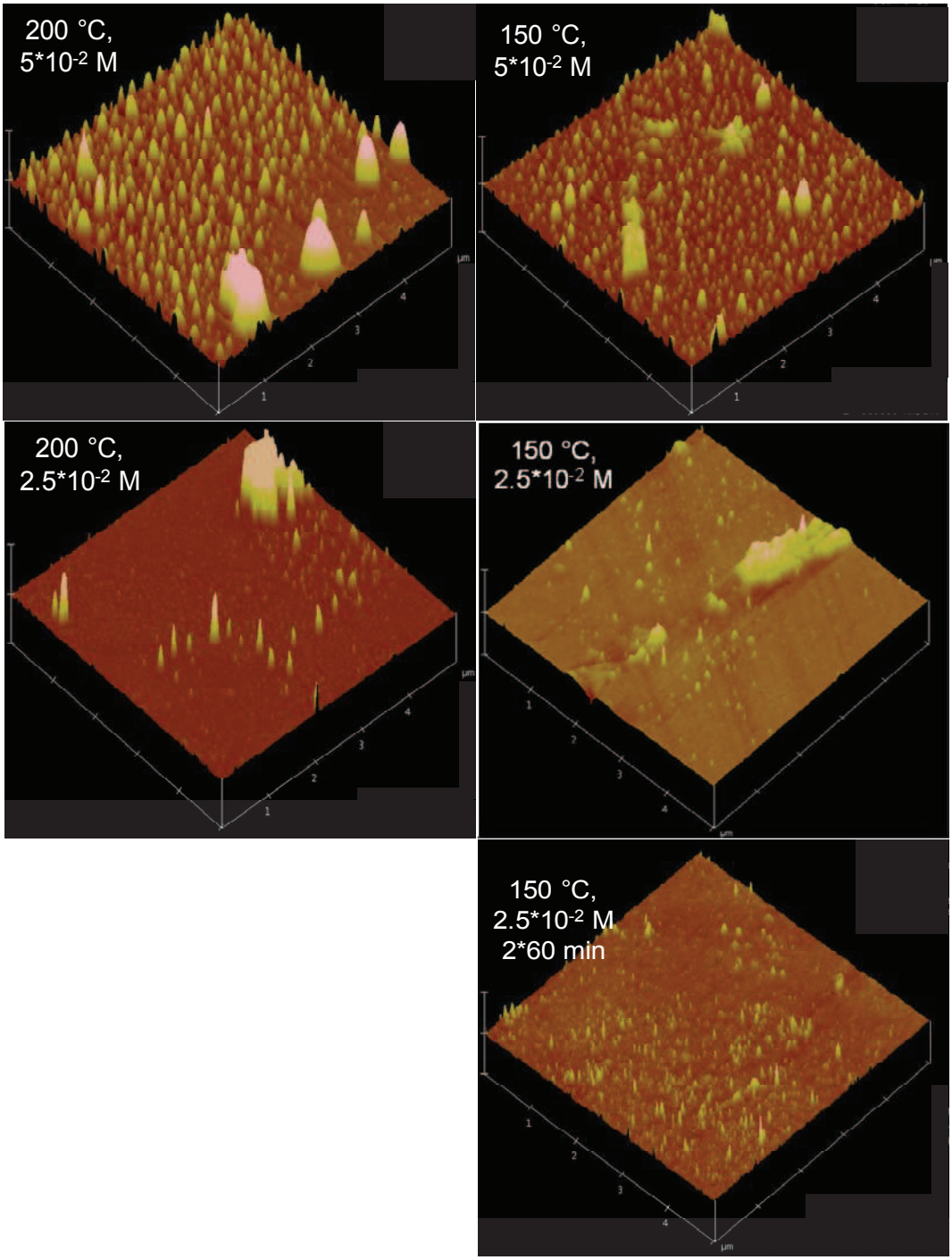

Fig. 4| AFM analysis of deposit obtained on Ox3 by annealing suspension of Mn-CuNPs.

Decreasing the concentration at 150 °C allows decreasing the size of large aggregates present. The deposit seems also to be more uniform. As it was demonstrated before, increasing the duration in this condition enable the formation of more uniform film on the whole surface analyzed.

Table 2| AFM analysis of deposit obtained on Ox3, with solution of Mn-CuNPs in $C_1C_4ImNTf_2$.

Samples	Conc (M)	Temp (°C)	Dur (min)	Ra (nm)	RMS (nm)	Rmax (nm)
Ox3	-	-	-	1.667	2.104	15.606
I	$5x10^{-2}$	200	60	2.942	4.154	41.541
II	$5x10^{-2}$	150	60	2.576	3.771	40.941
III	$2.5x10^{-2}$	200	60	0.705	1.921	54.738
IV	$2.5x10^{-2}$	150	60	0.816	1.577	28.707
V	$2.5x10^{-2}$	150	2x60	0.381	0.661	17.325

The Rmax value could be due to IL microdroplets on the surface but the size obtained is smaller than observed in precedent cases. Decreasing the concentration allows decreasing the roughness and the RMS at the two temperatures. Increasing the duration allows obtaining even more uniform deposit. The roughness of two lasts attempts is even smaller than Ox3 reference.

From these attempts, it could be concluded that a film is performed in all this experiment. It is nevertheless difficult to obtain a uniform film on the whole surface. Annealing in milder conditions (decrease temperature and concentration and increase duration) seems to be a good way to continue to investigate for performing uniform film. Survey of the mechanism of deposition should allow understanding more precisely the NPs deposition and thus with improvement of parameters allow uniform film synthesis.

Appendix 3: Publications

ECS Transactions, 35 (10) 11-16 (2011)
10.1149/1.3640400 ©The Electrochemical Society

Synthesis of Copper and Copper-Ruthenium Nanoparticles in Ionic Liquids for the Metallization of Advanced Interconnect Structures

P. P. Arquillière [a, b], C. C. Santini [b], P.-H. Haumesser [a], M. Aouine [c]

[a] CEA– LETI-Minatec Campus, 17 rue des Martyrs, 38054 Grenoble Cedex 9, France
[b] University of Lyon, C2P2, UMR 5265 CNRS – ESCPE Lyon, 43 Bd du 11 Novembre 1918, 69626 Villeurbanne Cedex, France
[c] IRCELYON, UMR 5256, 2 avenue Albert Einstein, 69626 Villeurbanne Cedex, France

Bimetallic nanoparticles can be used in a variety of applications such as catalysis, in advanced magnetic or optical devices or as starting materials to form continuous metallic layers. In this study, we report the synthesis of bimetallic ruthenium-copper (Ru-Cu) nanoparticles in ionic liquids. For this purpose, solutions of ionic liquids containing a mixture of precursors of Ru and Cu were decomposed under dihydrogen. Small, crystalline and well dispersed Ru-CuNPs (2.5 ± 0.6 nm) were obtained, which are significantly smaller than the pure Ru or pure CuNPs formed under the same conditions. Our analyses suggest that these NPs have a Ru core - Cu shell structure. This structure is expected from thermodynamical and kinetics data. Moreover, this could explain the dramatic size reduction observed when mixing the two metals.

Introduction

In the recent years, research on metallic nanoparticles (NPs) has been extended to the synthesis of bimetallic clusters or nanoalloys. These objects can be used in a variety of applications such as catalysis, or in advanced magnetic or optical devices.(1) Also, these NPs are interesting starting materials to form continuous metallic layers (e.g. by annealing), which are useful for the microelectronics industry.(2) In this study, we report the synthesis of bimetallic ruthenium-copper (Ru-Cu) nanoparticles in ionic liquids.
Ionic liquids are molten salts, generally liquid at room temperature, composed of an organic cation and an inorganic or organic anion. They are thermally and electrochemically stable, non volatile, electrically conductive and exhibit a large degree of self-organization.(3) Therefore, they have gained interest as ideal media for the synthesis of size controlled metallic NPs.(4) Recently, our group has demonstrated that successful synthesis of Ru and Cu NPs can be performed from the decomposition under dihydrogen of solutions containing organometallic precursors. (5, 6)
In this work, we extend this approach and investigate the behavior of solutions containing a mixture of precursors of Ru and Cu. The morphological, structural and chemical characteristics of the bimetallic NPs are examined and compared with the properties of the NPs formed from each individual metal under the same reaction conditions.

Experimental Section

1-butyl-3-methylimidazolium bistriflimide ($C_1C_4ImNTf_2$) was synthesized from commercially available 1-methylimidazole, 1-butylchloride (Sigma Aldrich) and lithium bistriflimide (Solvionic).(7) (η^4-1,5-cyclooctadiene)(η^6-1,3,5-cyclo-

octatriene)ruthenium(0), Ru(COD)(COT), was synthesized from $RuCl_3$-$3H_2O$, 1,5-cyclooctadiene, methanol and zinc powder (Sigma Aldrich).(8) Mesitylcopper (I), (Strem Chemicals), CuMes, was purified twice by recrystallization in toluene.(9)
Each precursor was dissolved in $C_1C_4ImNTf_2$, under inert conditions at $5x10^{-2}$ M. The obtained solution was decomposed under 0.9 MPa of H_2 at 100 °C for 4 hours to form metallic nanoparticles (NPs).(5)
These NPs were observed by Transmission Electron Microscopy (TEM) using a Philips CM120 120 kV and by High Resolution Transmission Electron Microscopy (HRTEM) using a Jeol JEM 2010FEF (field effect gun energy filtering) 200 kV. Their chemical composition was characterized by Electron Dispersive X-Ray (EDX).

Results and Discussion

In these pressure and temperature conditions, well dispersed CuNPs of 5.3 ± 1.1 nm were obtained (Figure 1, 2). By contrast, partially agglomerated RuNPs of 5.5 ± 4.0 nm were formed in the same conditions, (Figure 1, 2). The mean size and dispersion of these RuNPs are significantly larger than reported in the literature.(3) This effect is explained by a higher temperature used in our study.(6) Indeed, our conditions are optimized for the controlled synthesis of CuNPs.(5)

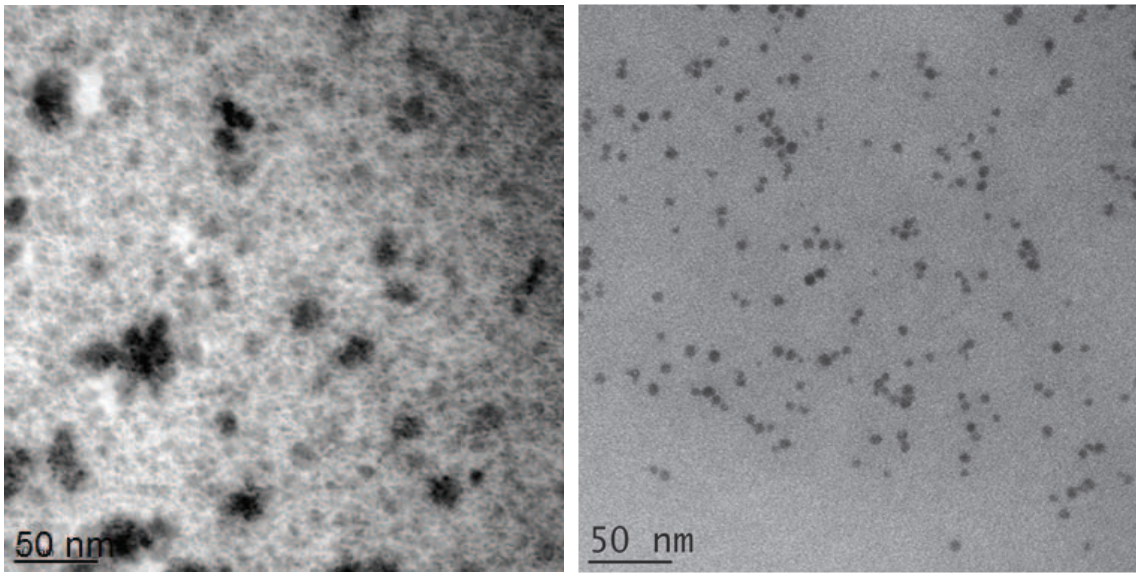

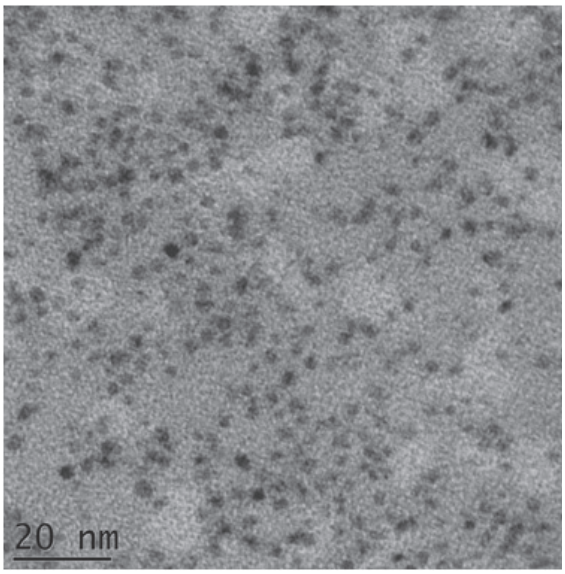

Figure 1. TEM pictures of (top left) RuNPs, (top right) CuNPs and (bottom left) Ru-CuNPs synthesized under 0.9 MPa of H_2 at 100 °C, during 4 hours.

The one step decomposition of a solution containing both organometallic precursors (total concentration $1x10^{-1}$ M, 1:1 ratio) was performed under the same temperature and pressure conditions. After reaction, the solution is black, which is characteristic for the formation of metallic NPs.

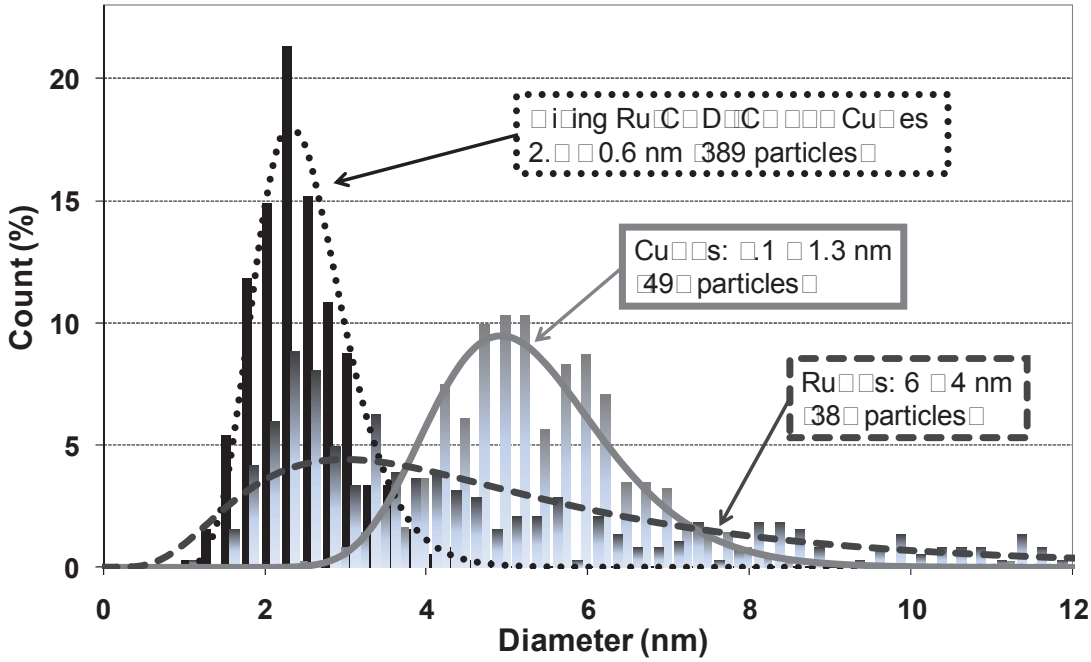

Figure 2. Comparison between size distribution histogram of Ru, Cu and Ru-CuNPs formed in same conditions.

Indeed, Figure 2 clearly shows that homogeneously dispersed NPs are formed. Interestingly enough, their size is merely 2.5 ± 0.6 nm, which is significantly smaller than NPs formed from each individual precursor (Figure 2). Therefore, there is probably some interaction between the two precursors during reaction. To further investigate this effect, EDX spectra and HRTEM pictures were recorded.

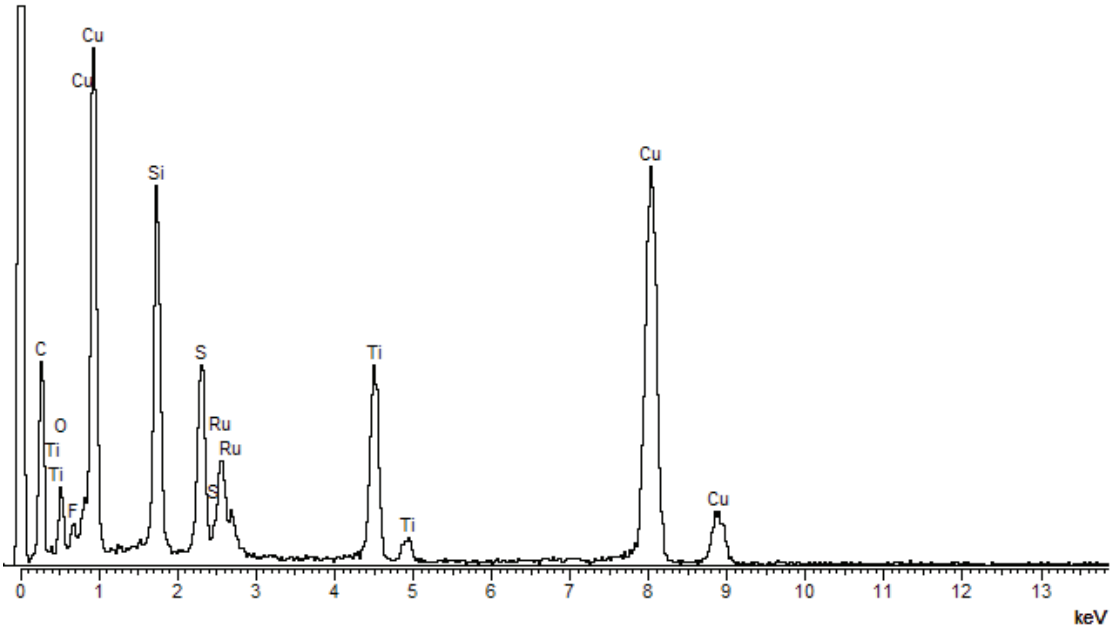

Figure 3. EDX spectrum of an area observed with HRTEM, where NPs formed by simultaneous decomposition of the two precursors are present.

In the EDX spectrum plotted in Figure 3, Cu and Ru are both detected. This is an indication that both precursors have reacted. The other elements, such as C, F, S are related to the presence of ionic liquid traces. Ti comes from TEM grid used. The large peak corresponding to Si could arise from the dissolution of glass during reaction.

The atomic resolution HRTEM pictures (Figure 4) show that the NPs are crystalline. Fourier transform analysis (Figure 4) of these pictures reveals that this crystalline structure corresponds to metallic hexagonal close packed (hcp) Ru (table I).(JCPDS file n°88-1734)

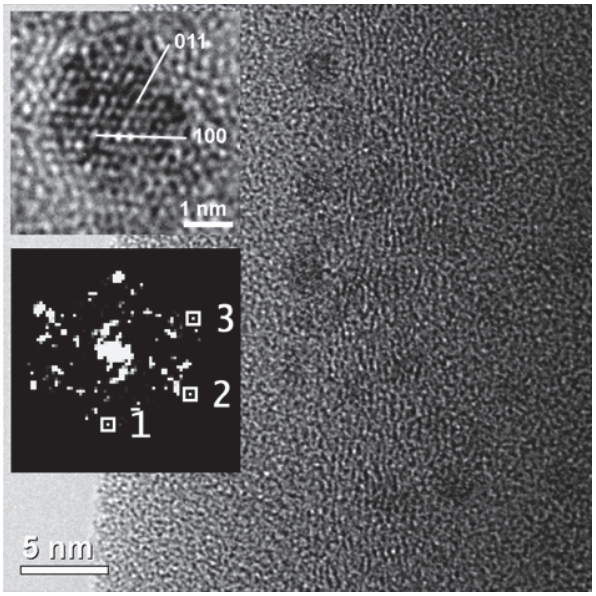

Figure 4. HRTEM pictures and focus on selected area of Ru-CuNPs formed according decomposition of a solution of Ru(COD)(COT) and CuMes, and FID transform of NPs.

TABLE I. Comparison between experimental and hcp metallic crystalline structure.

Spot	hkl	d(exp.)	d(theo)	angle(exp)	angle(theo)
1	100	2.43	2.38	0	0
2	011	2.11	2.08	64.66	64.09
3	$\bar{1}11$	2.08	2.08	115.93	115.91

From these preliminary results, we show that there is a clear interaction between the two precursors during reaction, leading to the formation of smaller, monodispersed NPs. Chemical analysis further suggests that these NPs are bimetallic. However, the structural analysis only reveals Ru crystalline structure. This could be explained if one assumes a core-shell structure of NPs. Indeed, if copper is distributed at the periphery of the NPs, it cannot be detected, since its thickness would be in the order of a monolayer with the 1:1 ratio used. Such a structure is expected from the binary phase diagram of Ru-Cu, which exhibits no solid solution domains.(10) Also, surface energies of both metals are favorable for the formation of a Ru core with a Cu shell (Ru@Cu).(11)

From a chemical standpoint, it is known that kinetic characteristics of the decomposition of each precursor are key to determine the structure of resulting bimetallic NPs.(12, 13) In particular, a large difference in decomposition rates leads to the formation of a core-shell structure, with the fast reacting metal in the core.(14) In our case, Ru(COD)(COT) reacts within a few minutes, whereas CuMes needs several hours. This mechanism-structure relationship would also explain why smaller particles are obtained, with suppression of Ru growth by adsorption and surface organometallic reaction of CuMes.(15) This model is currently under investigation.

Conclusion

The synthesis of ruthenium-copper bimetallic nanoparticles has been performed by decomposition under dihydrogen of organometallic precursors mesitylcopper and η^4-1,5-cyclooctadiene)(η^6-1,3,5-cyclo-octatriene)ruthenium(0) simultaneously in ionic liquid. Small, crystalline and well dispersed Ru-CuNPs (2.5 ± 0.6 nm) were obtained. Our analyses suggest that these NPs have a Ru core - Cu shell structure. This structure is expected from thermodynamical and kinetics data. Moreover, this could explain the dramatic size reduction observed when mixing the two metals.
These Ru@Cu NPs could be a promising starting materials for the elaboration of copper encapsulation or copper seed layers used in microelectronics.

Acknowledgments

The authors wish to thank Dominique Lafond for HRTEM analyses and Inga Steinunn Helgadottir for help and fruitful discussion.

References

1. D. Wang and Y. Li, *Adv. Mater. (Weinheim, Ger.)*, **23**, 1044 (2011).
2. C. Barriere, G. Alcaraz, O. Margeat, P. Fau, J.B. Quoirin, C. Anceau, B. Chaudret, *J. Mater. Chem.*, **18**, 3084 (2008).

3. T. Gutel, C. C. Santini, K. Philippot, A. Padua, K. Pelzer, B. Chaudret, Y. Chauvin, J.-M. Basset, *J. Mater. Chem.*, **19**, 3624 (2009).
4. J. Dupont and J.D. Scholten, *Chem. Soc. Rev.*, **39**, 1780 (2010).
5. P. P. Arquillière, P.-H. Haumesser, C. C. Santini, *Microelectron. Eng.*, under press (2011).
6. T. Gutel, J. Garcia-Anton, K. Pelzer, K. Philippot, C. C. Santini, Y. Chauvin, B. Chaudret, J.-M. Basset, *J. Mater. Chem.*, **17**, 3290 (2007).
7. L. Magna, Y. Chauvin, G. P. Niccolai, J.-M. Basset, *Organometallics*, **22**, 4418 (2003).
8. P. Pertici and G. Vitulli, *Inorg. Synth.* , **22**, 176 (1983).
9. T. Tsuda, K. Watanabe, K. Miyata, H. Yamamoto, T. Saegusa, *Inorg. Chem.*, **20**, 2728 (1981).
10. T.B. Massalski, M.J.L., Bennett and L. H., Baker H., *Binary Alloy Phase Diagrams. Vol. I and II.* , ed. American Society of Metals (1986).
11. C.R. Hammond, *CRC Handbook of Chemistry and Physics 81st edition* (2004).
12. C. Desvaux, P. Lecante, M. Respaud, B. Chaudret, *J. Mater. Chem.*, **20**, 103 (2010).
13. E.V. Shevchenko, D. V. Talapin, H. Schnablegger, A. Kornowski, O. Festin, P. Svedlindh, M. Haase, H. Weller, *J. Am. Chem. Soc.*, **125**, 9090 (2003).
14. N. Atamena, D. Ciuculescu, G. Alcaraz, A. Smekhova, F. Wilhelm, A. Rogalev, B. Chaudret, P. Lecante, R. E. Benfield, C. Amiens, *Chem. Commun. (Cambridge, U. K.)*, **46**, 2453 (2010).
15. Basset, J.-M., A. Baudouin, F. Bayard, J.-P. Candy, C. Coperet, A. De Mallmann, G. Godard, E. Kuntz, F. Lefebvre, C. Lucas, S. Norsic, K. Pelzer, A. Quadrelli, C. Santini, D. Soulivong, F. Stoffelbach, M. Taoufik, C. Thieuleux, J. Thivolle-Cazat, L. Veyre, *Mod. Surf. Organomet. Chem.*, 23 (2009).

Microelectronic Engineering 92 (2012) 149–151

Contents lists available at ScienceDirect

Microelectronic Engineering

journal homepage: www.elsevier.com/locate/mee

Copper nanoparticles generated *in situ* in imidazolium based ionic liquids

P. Arquillière [a,b], P.H. Haumesser [a,*], C.C. Santini [b]

[a] CEA-LETI-MINATEC - 17, rue des Martyrs 38 054 Grenoble Cedex 9, France
[b] Université de Lyon, Institut de Chimie de Lyon, UMR 5265 CNRS-Université de Lyon-ESCPE Lyon, C2P2, Equipe Chimie Organométallique de Surface, ESCPE 43 Boulevard du 11 Novembre 1918, F69616 Villeurbanne, France

ARTICLE INFO

Article history:
Received 24 September 2010
Accepted 23 November 2010
Available online 13 December 2010

Keywords:
Nanoparticles
Ionic liquids
Seed layer
Copper

ABSTRACT

Copper nanoparticles (CuNPs) have been successfully synthesized in imidazolium based ionic liquid (IL) under mild conditions. In this self-ordered medium, particles with narrow size distribution can be formed. No ligand is required to stabilize the suspension, which can be directly used to coat technological substrates. Several parameters are examined: the nature of IL, stirring, dihydrogen pressure and temperature. Under optimal conditions, well dispersed, zero-valent CuNPs of 4.5 nm with narrow size distribution are obtained. These stable suspension of Cu(0)NPs is a promising starting material to form conformal copper seed layers in high aspect ratio interconnect structures.

1. Introduction

In recent years, the synthesis of metallic nanoparticles (MNPs) has become a major challenge, as they are used in a variety of applications such as preparative catalysis, the fabrication of sensors or other nano-structures [1–5]. These MNPs are also of huge interest for the fabrication of advanced interconnecting structures. They can be deposited onto substrates to form conducting layers [6] or initiate the growth of more complex objects such as nanowires or nanotubes [3]. In both instances, an accurate control of the size of these MNPs is mandatory. In particular, a narrow size distribution is key: it will ensure optimal coverage after deposition, or guarantee a uniform size of the nanowires or nanotubes grown from these metallic clusters.

Copper has been adopted as the advanced interconnect material in microelectronic devices. Its use is now extended to the fabrication of Through Silicon Vias (TSVs) in 3D chip stacking approaches. In this metallization scheme, the deposition of a copper seed layer to initiate electroplating becomes more and more challenging. Currently, Cu seed layers are deposited by physical vapor deposition (PVD), which suffers from lack of conformity. Therefore, alternative techniques are investigated such as CVD (chemical vapor deposition) [7] or ALD (atomic layer deposition) [8]. However, these high vacuum techniques do not seem economically adapted for 3D technologies.

A new and efficient silica surface metallization process involving a copper nanoparticle (CuNP) dispersion generated from an organic solution of mesitylcopper is a real breakthrough in the access of thin conductive copper films on silicon substrates [6].

CuNPs are formed by using plasma electrochemical deposition [9], sol gel process [10], or chemical reduction [11–14] from copper salts (Cl^-, NO_3^-, SO_4^{2-}) involving several washing steps and a possible oxidation of the surface of $M^{(0)}$. More recently, thermolysis of coordination complexes [15,16] and decomposition by a reductant of organometallic complexes [6] in the presence of surfactant (ligand) to avoid the aggregation of CuNPs have been described. Finally, the synthesis of CuNPs was obtained by PVD from metallic copper in ionic liquids, leading to spherical particles with a mean diameter of 3 nm [17]. Interestingly, the particles are stabilized by an electrostatic protective layer of ionic liquid (IL). ILs are very stable thermally, non volatile, and exhibit a near-zero surface tension [18]. These media can also be used to electrochemically synthesize copper, and are for instance suitable for performing copper electroplating [19].

It is largely accepted that ILs are media of choice to stabilize MNPs [20]. Indeed, these media are self-organized: for instance, imidazolium based ILs exhibit an extended hydrogen-bond network in the liquid state and a continuous three dimensional network of ionic channels, coexisting with non-polar nano-domains of fixed size created by the grouping of lipophilic alkyl chains [21]. Very recently, a relationship between the size of IL non-polar domains calculated by molecular dynamics simulation and the mean diameter of *in situ* generated ruthenium nanoparticles has been demonstrated [22]. Moreover, the resulting stable RuNPs suspensions have been used to modify Si and TiN surfaces [23,24]. At last, it is important to note that in this case, the synthesis proceeds through the decomposition of organometallic complexes in the presence of H_2, leading to zero-valent MNPs with easy elimination

* Corresponding author. Tel.: +33 4 38 78 57 59; fax: +33 4 38 78 30 34.
E-mail addresses: paul.haumesser@cea.fr (P.H. Haumesser), santini@cpe.fr (C.C. Santini).

0167-9317/$ - see front matter © 2010 Elsevier B.V. All rights reserved.
doi:10.1016/j.mee.2010.11.039

of the by-products, which are inert towards the surface of the MNPs [25].

Consequently, the aim of this work is to use this route to synthesize CuNPs with controlled size *in situ* for subsequent annealing directly in IL media, in order to reduce process steps and cost. Hence, we report herein, the synthesis and characterization of the CuNPs obtained from the reaction of mesitylcopper$^{(I)}$, under dihydrogen in neat 1-alkyl-3-methylimidazolium bis(trifluoromethanesulfonyl) imide, ($C_1C_nImNTf_2$, $n = 4, 6$), in the absence of any ligand.

2. Experimental

The decomposition and the reduction of mesitylcopper by H_2 in IL is of great interest, since the only side product, mesitylene, is easily removed under vacuum. $C_1C_nImNTf_2$ can easily be prepared at a large scale, and is hydrophobic due to the presence of NTf_2 anion.

1-Methylimidazole (>99%), 1-Chlorobutane and 1-Chlorohexane (>99.5%) obtained from Sigma–Aldrich were distilled prior to use. Bis(trifluoromethanesulfonyl)imide lithium salt (>99%) was purchased from Solvionic. These reactants were used to synthesize 1-alkyl-3-methylimidazolium bis(trifluoromethanesulfonyl)imide ($C_1C_nImNTf_2$, $n = 4, 6$) [26]. The products were dried under high vacuum (10^{-3} Pa, 24 h) and stored in a glove box. Mesitylcopper, $[(CH_3)_3C_6H_2]Cu$, (>97%) was received from Strem and used without further purification. All operations were performed in the strict absence of oxygen and water under a purified argon atmosphere using glove box (Jacomex or MBraun).

In a Schlenk tube, a clear yellow solution of (1) (11 mg) in $C_1C_nImNTf_2$ (10 mL) ($[Cu] = 6.10^{-3}$ mol L^{-1}) was prepared by mixing, under stirring, at room temperature. In a typical experiment, under argon, 2 mL of this solution was cannulated into a 10 mL Fischer–Porter bottle or stainless steel autoclave. At this step, the argon atmosphere of autoclaves was evacuated under vacuum, replaced by an atmospheric pressure of H_2. Subsequently, reaction media were warmed to the desired temperature with or without stirring, and the H_2 pressure was adjusted at the desired value.

At the end of the reaction, the resulting dark suspension was evacuated under vacuum to eliminate mesitylene formed and placed under argon in a glove box for storage. Transmission electron microscopy (TEM) experiments were performed directly in the IL media. In a glove box, a thin film of CuNP solution in IL was deposited on a carbon film supported by a copper grid. Conventional TEM micrographs were obtained at the "Centre Technologique des Microstructures", UCBL1, Villeurbanne, France, using a Philips 120 CX electron microscope with acceleration voltage of 120 kV. Size distribution histograms were constructed from the manual measurement with Adobe Photoshop CS3 of at least 100 different nanoparticles assuming a near spherical shape and random orientation. Log normal fits were used to approximate experimental size distribution histograms. High-resolution transmission electron microscopy (HRTEM) images were obtained at IRCELYON using a Jeol 2010 LaB6 instrument at 200 keV with resolution point of 1.9 Å.

3. Results and discussion

3.1. Synthesis of CuNPs

In a first experiment, the influence of the nature of the IL was examined. Two ILs were selected from the $C_1C_nImNTf_2$ family, with $n = 4$ and 6. Synthesis of CuNPs was carried out at 30 °C, under 0.5 MPa H_2 under stirring.

Relatively uniform NPs of 10.1 nm ($\sigma = 1.58$) were obtained in $C_1C_4ImNTf_2$, whereas larger particles with less uniformity were formed in $C_1C_6ImNTf_2$ (14.5 nm, $\sigma = 2.0$). This is clearly attributed to the influence of the length of the alkyl chain [22].

The same experiment was performed in $C_1C_4ImNTf_2$ without stirring. Smaller NPs with narrow size distribution, 7.7 nm ($\sigma = 1.68$) were obtained (Fig. 1). Therefore, $C_1C_4ImNTf_2$ in the absence of stirring was selected for further experiments.

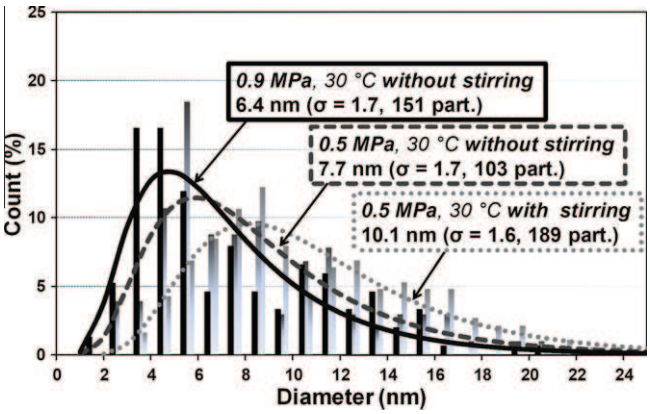

Fig. 1. Size distributions histograms and log-normal fits of CuNPs obtained in $C_1C_4ImNTf_2$ at 30 °C, with and without stirring, under 0.5 MPa of H_2, and without stirring under 0.9 MPa of H_2.

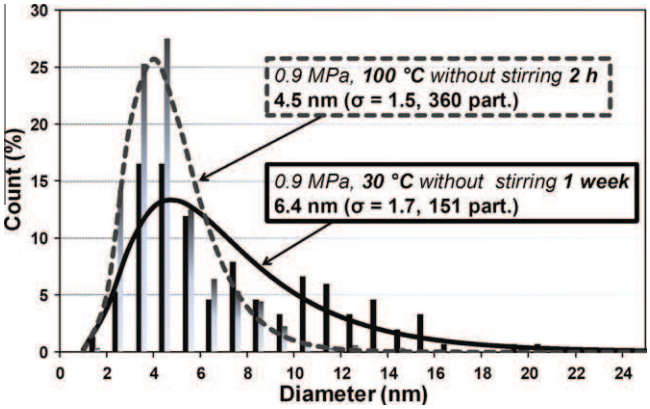

Fig. 2. Size distributions histograms and log-normal fits of CuNPs obtained in $C_1C_4ImNTf_2$ under 0.9 MPa of H_2 without stirring, at 30 °C and at 100 °C.

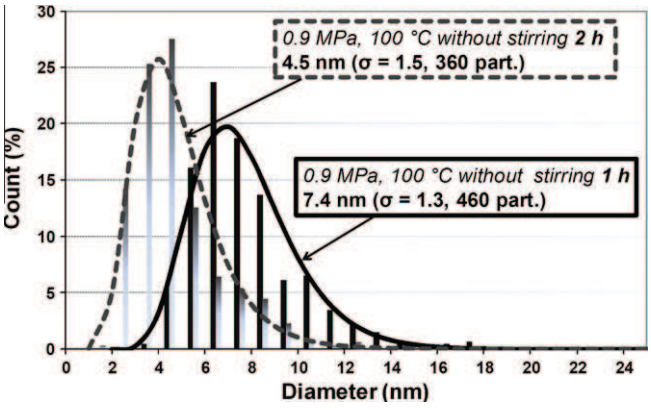

Fig. 3. Size distributions histograms and log-normal fits of CuNPs obtained in $C_1C_4ImNTf_2$ under 0.9 MPa of H_2 without stirring at 100 °C, with reaction durations of 1 and 2 h.

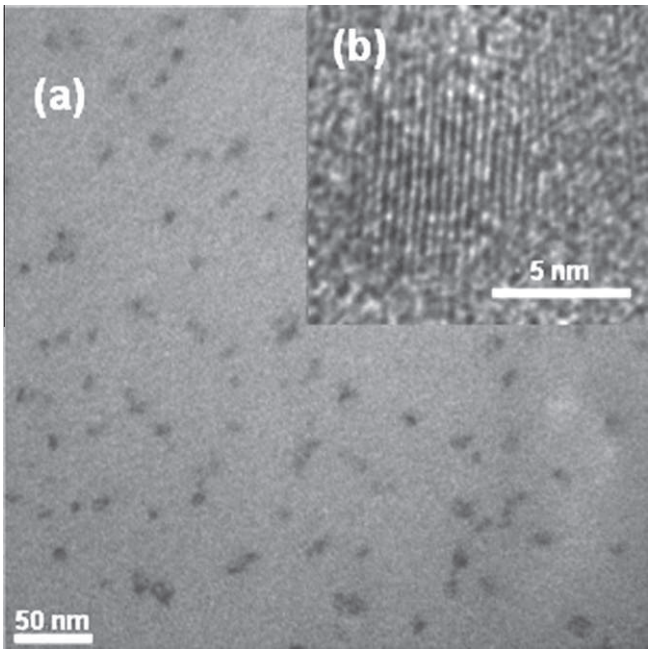

Fig. 4. TEM and HRTEM micrographs of CuNPs obtained in $C_1C_4ImNTf_2$ under 0.9 MPa of H_2 without stirring at 100 °C during 1 h.

In order to improve size control, H_2 pressure was increased to 0.9 MPa. Indeed, it is expected that higher H_2 pressure facilitates the nucleation and consequently the synthesis of smaller nanoparticles [27]. Accordingly, CuNPs of 6.4 nm ($\sigma = 1.72$) were formed (Fig. 1).

However, all the results presented above were obtained after 1 week reaction duration. In order to accelerate the process, temperature was increased to 100 °C. Indeed, an experiment performed at 0.9 MPa in $C_1C_4ImNTf_2$ without stirring led to the formation of NPs of 4.5 nm ($\sigma = 1.45$) after only 2 h (Fig. 2). This is a significant improvement as compared to results obtained at 30 °C. A last attempt was undertaken to further reduce process duration. The same experiment was carried out during 1 h only. Surprisingly, larger NPs were obtained (7.4 nm, $\sigma = 1.93$) (Fig. 3). This could be related to the mechanisms of formation of nuclides [27] and is currently under investigation.

3.2. Structure of CuNPs

The structure of individual particles was investigated using HRTEM. With this technique, the highly crystalline structure of the nanoparticles was revealed. Interestingly enough, the interplanar distance measured from this micrograph is 0.21 nm, which coincides with the (1 1 1) interplanar distance of fcc pure metallic Cu (Fig. 4). This result clearly demonstrates that CuNPs are zero-valent [28].

4. Conclusion

In this study, we have investigated a new route for the synthesis of copper NPs, with controlled size, without contaminating ligands, by a liquid process under mild conditions. CuNPs were successfully synthesized from $[(CH_3)_3C_6H_2]Cu$ in solution $C_1C_nImNTf_2$ with $n = 4$ and 6. Several parameters were examined: the nature of IL, stirring, H_2 pressure and temperature. Under optimal conditions, well dispersed CuNPs of 4.5 nm with narrow size distribution were obtained. HREM observations found a crystalline structure coherent with zero-valent Cu. The resulting stable suspension of $Cu^{(0)}$NPs are a promising starting material to form conformal copper seed layers in high aspect ratio interconnect structures.

Acknowledgements

The authors wish to thank Dr. M. Aouine and Mme L. Burel of IRCELYON for HRTEM analysis. They also are very grateful to Dr. G. Salas-Hernandez and P. Campbell of LCOMS for support and fruitful discussion.

References

[1] M. Valden, X. Lai, D.W. Goodman, Science 281 (1998) 1647.
[2] A.T. Bell, Science 299 (2003) 1688–1691.
[3] G. Schmid, Nanoparticles: From Theory to Application, Wiley-VCH, Weinheim, 2004. pp. 434.
[4] H. Boennemann, K.S. Nagabhushana, Metal nanoclusters: synthesis and strategies for their size control, in: B. Corain, G. Schmid, N. Toshima (Eds.), Metal Nanoclusters in Catalysis and Materials Science. The Issue of Size Contro, Elsevier B.V, Amsterdam, 2008, pp. 21–48.
[5] D. Astruc, Nanoparticles and Catalysis, Wiley-VCH, Weinheim, 2008.
[6] C. Barriere, G. Alcaraz, O. Margeat, P. Fau, J.B. Quoirin, C. Anceau, B. Chaudret, J. Mater. Chem. 18 (26) (2008) 3084–3086.
[7] A. Roule, T.Morel, P.H. Haumesser, O. Pollet, M. Cordeau, S. Maitrejean, J. Klocke, T. Ritzdorf, G. Passemard, Copper metallization of advanced interconnects: strategies for beyond 65 nm, in: D. Erb, P. Ramm, K. Mazu, A. Osaki (Eds.), Advanced Metallization Conference. Materials Research Scoiety (MRS), Warrendale, Pennsylvania, 2004, pp. 341–346.
[8] Z. Li, A. Rahtu, R.G. Gordon, J. Electrochem. Soc. 153 (2006) C787–C794.
[9] M. Brettholle, O. Hoefft, L. Klarhoefer, S. Mathes, W. Maus-Friedrichs, S. Zein El Abedin, S. Krischok, J. Janek, F. Endres, Phys. Chem. Chem. Phys. 12 (8) (2010) 1750–1755.
[10] O.A. Yeshchenko, I.M. Dmitruk, A.M. Dmytruk, A.A. Alexeenko, Mater. Sci. Eng. B 137 (1–3) (2007) 247–254.
[11] P. Christian, M. Bromfield, J. Mater. Chem. 20 (6) (2010) 1135–1139.
[12] V. Engels, F. Benaskar, D.A. Jefferson, B.F.G. Johnson, A.E.H. Wheatley, Dalton Trans. 39 (28) (2010) 6496–6502.
[13] R. Prucek, L. Kvitek, A. Panacek, L. Vancurova, J. Soukupova, D. Jancik, R. Zboril, J. Mater. Chem. 19 (44) (2009) 8463–8469.
[14] L. Yu, H. Sun, J. He, D. Wang, X. Jin, M. Hu, G.Z. Chen, Electrochem. Commun. 9 (6) (2007) 1374–1381.
[15] J. Hambrock, R. Becker, A. Birkner, J. Weiss, A. Fischer Ronland, Chem. Commun. (1) (2002) 68–69.
[16] Y.H. Kim, D.K. Lee, B.G. Jo, J.H. Jeong, Y.S. Kang, Colloids and Surf. A 284–285 (2006) 364–368.
[17] K. Richter, A. Birkner, A.-V. Mudring, Angew. Chem. Int. Ed. 49 (13) (2010) 2431–2435. S2431/1-S2431/9.
[18] P. Wasserscheid, T. Welton, Ionic Liquids in Synthesis, Wiley-VCH, Weinheim, 2008.
[19] S. Schaltin, A. Shkurankov, K. Binnemans, J. Fransaer, ECS Trans. 25 (2010) 119–128.
[20] J. Dupont, J.D. Scholten, Chem. Soc. Rev. 39 (5) (2010) 1780–1804.
[21] A.A.H. Padua, M.F. Costa Gomes, J.N.A. Canongia Lopes, Acc. Chem. Res. 40 (2007) 1087–1096.
[22] T. Gutel, C.C. Santini, K. Philippot, A. Padua, K. Pelzer, B. Chaudret, Y. Chauvin, J.-M. Basset, J. Mater. Chem. 19 (22) (2009) 3624–3631.
[23] C.C. Santini, J.-M. Basset, T. Gutel, P. Campbell, S. Deleonibus, P.H. Haumesser, CEA CNRS, WO 2009-1464 2943850.
[24] C.C. Santini, J.-M. Basset, T. Gutel, P. Campbell, S. Deleonibus, P.H. Haumesser, CEA CNRS, EP 2010-157354 2234115.
[25] K. Philippot, B. Chaudret, C. R. Chim. 6 (8–10) (2003) 1019–1034.
[26] L. Magna, Y. Chauvin, G.P. Niccolai, J.-M. Basset, Organometallics 22 (22) (2003) 4418–4425.
[27] E.V. Shevchenko, D.V. Talapin, H. Schnablegger, A. Kornowski, O. Festin, P. Svedlindh, M. Haase, H. Weller, J. Am. Chem. Soc. 125 (2005) 9092–9101.
[28] K.W. Andrews, D.J. Dyson, S.R. Keown, Interpretation of Electron Diffraction Patterns, second ed., Springer, 1971, p. 239.